

The University of Adelaide  
Faculty of Engineering, Computer and Mathematical Sciences  
School of Civil, Environment and Mining Engineering



**Simulation and Experimental Study on the Effect of  
Acid-fracturing in Carbonaceous Shale**

Mohsen Farrokhrouz  
M.Sc. Petroleum Well Engineering  
B. Sc. Mining Engineering

Thesis submitted in fulfillment of the requirements for the degree of  
Doctor of Philosophy to the School of Civil, Environment and  
Mining Engineering and Adelaide Graduate Centre of the University  
of Adelaide

-July 2022-

## Table of Contents

<b>HDR Thesis Declaration</b> .....	<b>v</b>
<b>Abstract</b> .....	<b>vi</b>
<b>Acknowledgement</b> .....	<b>viii</b>
<b>List of Publications</b> .....	<b>ix</b>
<b>Chapter 1: Introduction</b>	
1. General Background.....	1
2. Literature Review.....	4
2.1. Gas Injection Techniques.....	4
2.2. Water Injection Techniques.....	5
2.3. Chemical Techniques.....	6
2.4. Acid Fracturing History.....	7
3. Research Objectives.....	9
4. Thesis Organisations.....	11
References.....	14
<b>Chapter 2: Reactive Flow Simulation during Acid Fracturing in Carbonaceous Shale</b>	
1. Introduction.....	19
2. Geochemical reactions on the surface of carbonaceous shale.....	20
3. Materials and methods.....	21
3.1. Geochemical simulation.....	21
3.2. Simulation of acid flow through the core.....	24
4. Carbonaceous shale simulation and parametric study.....	24
4.1. Effect of acid concentration.....	24
4.2. Effect of injection rate.....	26
4.3. Effect of temperature.....	27
4.4. Discussion and analysis of simulation results.....	27
5. Conclusion.....	28
References.....	29
<b>Chapter 3: Analytical exact Solution for Co-Current Spontaneous Imbibition in Porous Media Considering Early- and Late-Time Effects</b>	
1. Introduction.....	33

2. Problem formulation.....	34
2.1. Contribution of advection and capillary terms.....	34
2.2. Incentive toward analytical solution.....	35
3. Experimental Setup.....	35
4. Novel solution methodology considering solute transport.....	36
4.1. Mathematical formulation of new method.....	36
5. Model verification and interpretation of results.....	37
5.1. Model validation with numerical solution.....	37
5.2. Model validation with experimental results.....	37
6. Analytical solution in immiscible two-phase flow.....	39
7. Sensitivity analysis.....	42
8. Conclusion.....	42
Appendix A.....	42
Appendix B.....	43
Appendix C.....	43
References.....	44

#### **Chapter 4: Exact Analytical Solution of Counter-Current Imbibition with Both Capillary and Gravity Effects**

1. Introduction.....	48
2. Two-phase flow: theoretical background.....	49
2.1. Continuity equation in two-phase flow.....	49
2.2. Review of conventional COUCSI solution.....	50
3. New solution methodology for fluid phase with components.....	50
3.1. Capillary-dominated spontaneous imbibition.....	51
3.2. Gravity-dominated case.....	52
3.3. Simultaneous contribution of capillary and gravity.....	53
4. Validating the exact solution.....	55
4.1. Capillary-dominated case.....	55
4.2. Gravity-dominated case.....	56
4.3. Simultaneous contribution of both forces.....	56
5. Sensitivity to influencing parameters.....	56
6. Discussion.....	58
7. Conclusion.....	58
References.....	59

## **Chapter 5: Laboratory and analytical study for prediction of porosity changes in carbonaceous shale coupling reactive flow and dissolution**

1. Introduction.....	63
2. Materials and experimental setup.....	64
2.1. Geological features of core samples.....	65
2.2. Sample preparation and experimental setup.....	65
3. Experimental observations and uncertainties.....	66
4. Mathematical modelling: theoretical background.....	68
4.1. Kinetics of HCl reaction.....	68
4.2. Acid dispersion in porous media.....	69
5. Data matching and model validation.....	71
6. Conclusion.....	73
References.....	73

## **Chapter 6: The effect of acidizing propped fracture on productivity optimization: Eagle Ford case study**

Abstract.....	77
1. Introduction.....	77
2. Materials and Methods.....	78
2.5. Properties of Proppants.....	78
2.6. Core Samples.....	78
2.7. Experimental Procedures.....	78
3. Theory of Acidizing in Proppant Pack.....	78
4. Results and Discussion.....	81
4.1. Aid Concentration Effect.....	81
4.2. Effect of Proppant Concentration.....	82
4.3. Effect of Proppant Size.....	82
4.4. Effect of Acid Injection Rate.....	82
4.5. Skin Factor at Constant Confining Pressure.....	83
5. Conclusion.....	84
References.....	85

## **Chapter 7: Conclusions and Recommendations ..... 87**



## **HDR Thesis Declaration**

I certify that this work contains no material which has been accepted for the award of any other degree or diploma in my name, in any university or other tertiary institution and, to the best of my knowledge and belief, contains no material previously published or written by another person, except where due reference has been made in the text. In addition, I certify that no part of this work will, in the future, be used in a submission in my name for any other degree or diploma in any university or other tertiary institution without the prior approval of the University of Adelaide and where applicable, any partner institution responsible for the joint award of this degree.

I acknowledge that the copyright of published works contained within this thesis resides with the copyright holder(s) of those works.

I also give permission for the digital version of my thesis to be made available on the web, via the University's digital research repository, the Library Search and through web search engines, unless permission has been granted by the University to restrict access for a period of time. I acknowledge the support I have received for my research through the provision of an Australian Government Research Training Program Scholarship.

## **Abstract**

Unconventional oil and gas reservoirs have been given a lot of attention due to oil prices in the market. Production costs of these formations are very high due to directional drilling completion and hydraulic fracturing operations. However, the primary recovery factor of these reservoirs is as low as 2% to 8%. Therefore, recent studies have focused on recovery factor improvement.

Some of these methods in conventional reserves are also applicable for unconventional layers like waterflooding, miscible gas injection, and chemical material utilization. Acidizing can also be used to extend the productivity of the reservoir as an improved recovery method. It can be in the form of acid washing, matrix acidizing and acid fracturing. However, acid application in the already propped fracture is a new area that has not been fully investigated.

This study performed a detailed analysis of HCl acidizing in Eagle Ford shale as a typical unconventional oil reservoir. As a first step, a simulation model was created to explore the effect of HCl on fractured medium numerically. The model was firstly validated by an experimental result and then the effects of acid concentration, acid injection rate, and temperature were fully investigated. It was revealed that for each of these parameters there is an optimum condition that makes required water breakthrough into the minimum.

Since non-carbonate content is also present within carbonaceous shale formations, the acid front movement within the formation is not always reactive. Instead, there is a two-phase fluid inside the medium, and saturation changes because of injected fluid. Due to the saturation gradient between the injected fluid and in-situ irreducible wetting phase, there is a spontaneous imbibition

within the porous medium when there is no injection. An exact analytical solution was proposed for co-current and counter-current imbibition of this movement and validated by experimental results. The suggested equational form can be used to present the distribution of injected fluid within the porous medium.

Finally, experimental tests were conducted to monitor the short-term effect of high concentration acid and the long-term impact of low concentration acid. During the short-term contact of acid with carbonaceous shale (Eagle Ford shale sample), the rock samples were confined by in-situ condition (pressure and temperature) and the rock surface was prone to the acid by keeping it open through utilization of proppant, as the permeability of the rock sample was very low. Again, different effects including acid concentration, proppant type and size and acid injection rate were investigated. It was found that 5% HCl acid concentration, injection with 8 ml/min and with proppant size and concentration of 600-700  $\mu\text{m}$  and 0.3 lb/ft<sup>2</sup>, respectively.

For long-term effect of acid on the rock surface, mathematical model as well as experimental setup were constructed. A semi-analytical solution achieved with very good matching with experimental results. Diffusion coefficient of acid into the rock matrix was also measured at different acid concentration and with various brines.

Altogether, analytical, experimental and simulation results of this study are the tools for different production strategies for carbonaceous shale formations as a major unconventional oil and gas resources.

## **Acknowledgement**

First of all, I would like to thank Allah Almighty for providing me a wonderful opportunity to conduct research at one of the finest institution in Australia. Continued support, prayers and encouragement from my family (my parents and my wife) before and during my PhD in Adelaide University was the key factor of my drive to conduct research.

I would like to thank my principal supervisor, Dr Abbas Taheri, for being supportive and encouraging during my research pursuit. Abbas offered his friendship, time, encouragement, dedication and financial support throughout the whole PhD journey and I owe him an enormous debt of gratitude.

I would like to express my appreciation to Dr Alireza Keshavarz, as my co-supervisor and currently as senior Lecturer in Edith Cowan University. Without him and his spiritual dedication and encouragement, I could do nothing in experimental section of my thesis. I wish him the best throughout the rest of his academic life.

I also would like to express special thanks to Prof Stefan Iglauer as a co-author and support for most of my papers and his valuable comments while preparation of the papers and their submissions.

I would also like to acknowledge the School of Engineering in Edith Cowan University, specifically Prof Daryoush Habibi, giving me permission to use the facility and experimental setups in their school. Another special thanks would be offered to the laboratory technicians of Edith Cowan University for technical supports.

## List of Publications

**Paper 1:** *M. Farrokhrouz, A. Taheri, A. Keshavarz*, 2020. Numerical reactive flow transport simulation on core samples during acid fracturing in carbonaceous shale, *Journal of Natural Gas Science and Engineering*, Volume 84, <https://doi.org/10.1016/j.jngse.2020.103615>; (Impact Factor: **5.285**; Q1)

**Paper 2:** *M. Farrokhrouz, A. Taheri, S. Iglauer, A. Keshavarz*, 2021. Analytical Exact Solution for Co-Current Spontaneous Imbibition in Porous Media Considering Early- and Late-Time Effects. *Energy & Fuels*, Vol. 35 (21), 17499-17511. <https://doi.org/10.1021/acs.energyfuels.1c02492>; (Impact Factor: **4.654**; Q1)

**Paper 3:** *M. Farrokhrouz, A. Taheri, S. Iglauer, A. Keshavarz*, 2022. Exact Analytical Solutions of Countercurrent Imbibition with Both Capillary and Gravity Effects. *Energy & Fuels*, Vol. 36 (3), 1457-1469. <https://doi.org/10.1021/acs.energyfuels.1c03868>; (Impact Factor: **4.654**; Q1)

**Paper 4:** *M. Farrokhrouz, A. Taheri, S. Iglauer, A. Keshavarz*, 2022. Experimental Study and Analytical Solution for Prediction of Porosity Changes in Carbonaceous Shale Coupling Reactive Flow and Dissolution, *J. Pet. Sci. & Eng.*, Vol. 215, Part B, 110670. <https://doi.org/10.1016/j.petrol.2022.110670>; (Impact Factor: **5.168**; Q1)

**Paper 5:** *M. Farrokhrouz, A. Taheri, S. Iglauer, A. Keshavarz*, 2022. The effect of acidizing propped fracture on productivity optimization: Eagle Ford case study, *Fuel*, Vol. 329, 125363. <https://doi.org/10.1016/j.fuel.2022.125363>; (Impact Factor: **8.035**; Q1)

# Chapter 1

## Introduction

### 1. General Background

Based on the last update given by the US Energy Information Administration (as of September 2021), shale reservoirs are major unconventional energy resources in North America. Oil and gas in the United States represent 48 and 58 percent of the energy share in this country, respectively, with 65 percent of the produced oil and 86 percent of the produced gas being from unconventional shale reserves (US Energy Outlook 2021). However, production plans are very sensitive to the market price as it is only economical for high oil and gas prices due to high production costs. The oil price peak in 2008 and the consequent energy shock resulted from a steep rise in the oil price that started in 2002. Such a continuous increase in energy price resulted in a huge investment in the development of oil and gas shale in North America. Many companies came into action during those years. Although oil price dropped dramatically in 2009 and 2016 and many of these unconventional reservoirs became uneconomic for a while, the oil and gas price were gradually increasing and reached over \$100 again in early 2022.

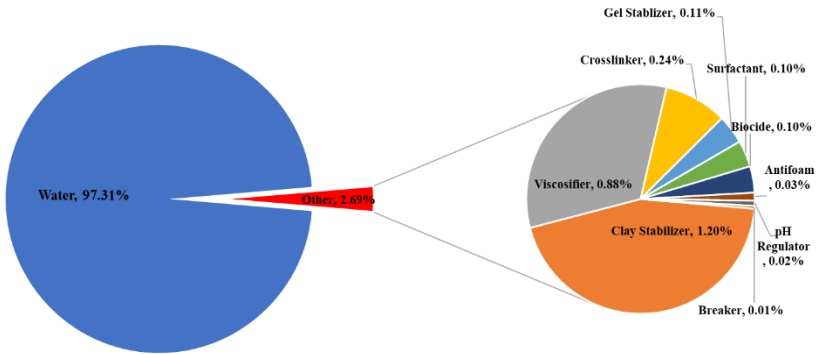
One of the significant drawbacks of unconventional shale resources is their average recovery factor of less than 10% [1]. Therefore, different Enhanced Oil Recovery (EOR) methods and/or productivity improvement approaches are required to increase the efficiency of these resources. Hydraulic fracturing is the most critical stage for long-term and efficient production from unconventional reservoirs. It is also called fracking, hydrofracking, and

hydrofracturing. It is a well stimulation method during which high-pressure fluid is injected into the wellbore and cracks are initiated in the deep-rock formation. Proppants (usually silicate base) are pumped into these induced fractures to keep them open after releasing the fluid pressure. During production, these proppants let the fluids inside the well flow freely into the wellbore and production tanks. However, hydraulic fracturing is a costly operation and it can only increase the maximum recovery up to 15% [2].

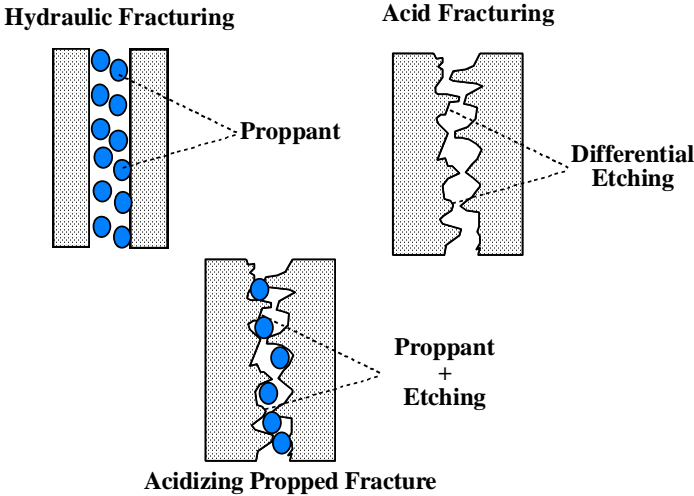
Accordingly, oil and gas companies and academic research centers investigated different strategies to increase the efficiency of hydraulic fracturing operation or new methods other than hydraulic fracturing, which can improve the recovery of unconventional reservoirs. Some studies showed that a large proportion of propped fractures remain unpropped after pressure release despite a significant injection of proppant during hydraulic fracturing [3]. Therefore, some studies focused on new designs of proppant injection into the hydraulic fractures like graded proppant injection [4-6], design of ceramic-based proppants [7, 8], incorporation of micro-proppant in stimulation treatment designs [9], changing the rheology of the injected fluid to prevent back flow into the wellbore [10, 11], etc. All these studies showed some improvements in the ultimate recovery factor of hydraulic fracturing due to improvements in proppant designs. Other studies also concentrated on other EOR methods, such as Huff-n-Puff methods within carbonaceous shale reservoirs, like Eagle Ford [12]. Altogether, these enhancements in hydraulic fracturing highly depend on reservoir conditions and in-situ geological characteristics.

In conventional reservoirs, stimulating processes are known as initial improvement operations before initiating EOR activities. These methods are

the most common and cheapest operations in these fields. In carbonate reservoirs, hydrochloric acid (HCl) can be used in stimulating procedures with different intensities: acid washing, matrix acidizing, and acid fracturing. During hydraulic fracturing, a small portion of the injection fluid is acid, as shown in Figure 1(a). It should be reminded that the ratio of hydraulic fracturing fluid to the proppant is 9 to 1.



(a)



(b)

**Figure 1: a) the components of hydraulic fracturing fluid while injecting into the wellbore; b) the difference between hydraulic fracturing and acid fracturing in terms of characteristics of fracture walls and comparison with application of both methods.**



Acid fracturing is the same in terms of concept and operational process while no proppant is used during that, and the surface of the rock is rather harsh and etching (Figure 1(b)). In fact, after releasing the high pressure from the well, proppants prevent the closure of the fracture in a hydraulic fracturing operation. In contrast, in acid fracturing, the etching surfaces prevent the complete closure of the fracture. This study aims to apply both methods in unconventional reservoirs and perform acidizing through the propped fractures (Figure 1(b)).

Carbonaceous shales are ideal candidates for these operations as a considerable amount of the rock is composed of carbonates. However, acidizing already propped fractures can be a new approach that has not been fully investigated within the literature and is the main objective of this study.

## **2. Literature Review**

Different enhancement methods are conceivable for production through unconventional hydrocarbon reservoirs. These methods will be studied briefly in the following sections.

### **2.1. Gas Injection Techniques**

Injection of gas into the unconventional reservoirs can be in the form of huff-and-puff (water vapor) [13, 14], CO<sub>2</sub> injection [15-17], Nitrogen, lean gas, and methane [18].

Each gas injection method has some advantages and disadvantages. For instance, CO<sub>2</sub> can decrease the viscosity of the oil within the unconventional reservoir, reduction in capillary pressure, oil swelling, and re-pressurization [17]. However, it may cause corrosion within surface facilities, and it is not

always available next to the large fields [15]. The applicability of gases for EOR in unconventional reservoirs is shown in Table 1.

**Table 1: Different gases used in miscible gas injection [17, 19]**

<b>Gases</b>	<b>Minimum Miscible Pressure (MMP)</b>	<b>Sweep Efficiency</b>	<b>Cost</b>	<b>In situ Oil Density</b>
CO <sub>2</sub>	Lowest	Highest	Medium	> 25° API
Methane	Medium	Medium	Highest	> 30° API
N <sub>2</sub>	Highest	Lowest	Lowest	> 40° API

## **2.2. Water Injection Techniques**

Low Salinity Waterflooding (LSW) performed through simulations and experiments for unconventional and tight formations. It is shown that LSW results in wettability alteration, change in interfacial tension [20], clay swelling, and shale cracking [21]. Different unconventional shale reservoirs, including Eagle Ford, Marcellus, Mancos, and Barnett, were studied through experiments [22-24]. These studies showed that LSW in comparison with formation water flooding would lead to a higher ultimate recovery factor. However, in long term, ultimate recovery of huff-and-puff is higher than LSW [15, 25].

In terms of field experiences, a few cases have been reported. The main problem of water injection in the field is the injectivity of water. Apart from this issue, some successful results of water flooding in the field are available in the literature [26]. Still, most of these attempts were unsuccessful , as shown in Table 2.

**Table 2: Field project experiences of water injection**

<b>Field</b>	<b>Performance</b>	<b>Mode</b>	<b>Reference</b>
Bakken + Lower Shaunavan	Oil rate increase	waterflooding	[27]
Bakken in North Dakota	No oil rate increase, Low sweep efficiency	waterflooding	[26]
Bakken in Montana	Water breakthrough	waterflooding	[26]
Bakken in North Dakota	Little or no oil increase, No injectivity issue	Huff-n-puff	[26]
Parshall Field	No oil increase	Huff-n-puff	[28]

### **2.3. Chemical Techniques**

Major chemicals used for EOR are Alkaline, Surfactant, and Polymer (ASP). The objective of using chemicals (i.e., surfactants) in unconventional reservoirs is to change the wettability from oil-wet to water-wet reservoirs and increase the productivity as oil shales are usually oil-wet [29, 30]. Surfactants can also be used as an additive in fracturing fluids [31]. Experimental studies showed that utilization of surfactant in Bakken formation increased oil recovery up to 30-40%, which is a significant number in unconventional reservoirs [32].

Spontaneous imbibition is the primary method for the transfer of these chemicals into the formation. After conducting the experiments, they scaled up the results into the field scale using simulation [19]. Experimental studies were performed on Eagle Ford shale and Bakken formation, and it was revealed that recovery would be higher if salinity is also considered [33]. In other words, at

higher salinities, the surfactant is less capable of interfacial tension reduction and wettability alteration.

Apart from the injection of chemicals into the formations, certain formations can be a good candidate for acidizing and acid fracturing. Since this section is the main objective of this study, it will be discussed separately in another section.

#### **2.4. Acid fracturing history**

Acid fracturing is a production stimulation technique being widely used by the oil industry. During this treatment, acid is injected down the well at rates greater than the flowing rate of pore fluid. Such injection produces a build-up in wellbore pressure in order to overcome compressive and tensile strength. After rock failure, a crack is initiated in the rock and continuous fluid injection increases the fracture length and width. , The reaction of the acid with the formation, makes a flow channel that remains open when the well is put back into production.

Acid fracturing has certain advantages in comparison with proppant fracturing, including:

- a) There is no risk of proppant bridging while injection; proppant bridging occurs due to the flocculation of particles during injection and may cause a sudden increase in pumping pressure.
- b) There is no concern for cleanout problems as gelled residues and proppant crushing are two significant causes of permeability impairment while proppant fracturing.

- c) A good conductivity in each channel and between different channels is generated, making a high permeability value and good productivity.

However, the extent of acid fracturing is also restricted by several factors like:

- a) In fast-reacting formations (carbonates at high temperatures), the length of fracture is short as most of the acid is spent at an immediate distance of the injection point. Heterogeneity of the formation may intensify this problem, and the final efficiency of acid fracturing becomes less than expected.
- b) The conductivity of an acid fracture is far less than infinite conductivity and is usually restricted by formation strength.
- c) For chalk formations, effective stress increases as reservoir depletes, leading to pore collapse and a significant decrease in permeability. Such geomechanical behaviors should be considered during acid fracturing operations.

Considering the drawbacks of acid fracturing, some research was carried out to improve acid efficiency in carbonates. Some studies focused on the rheological characteristics of injected acid [34, 35], while other researchers attempted to find a perfect fracture deformation model [36-38].

While many experimental studies were conducted on acid fracturing, most of them were laboratory tests and were not scaled to field conditions. Hence, acid fracturing conductivity predictions were not able to match actual results [39]. This confirms the requirement for new laboratory facilities to create field conditions as much as possible and develop the model based on etched volume, etched pattern, and fracture strength under closure stress.

Applying in-situ stress conditions for acid fracturing treatment and determining failure mechanisms was regarded by emerging proper laboratory facilities and considering closure stress in conductivity models and experiments. Several acid-fracture conductivity correlations were suggested according to new facilities and modeling software [40-42].

However, most of this research was conducted on carbonate samples (calcite, dolomite, chalk, or a mixture of them). Due to the importance of oil shale and gas shale, new interest appeared just recently to apply acid fracturing treatment in shaly formations. In a study evaluating acid fracturing in the shale formation, samples were made with cuts parallel to bedding to explore the influence of carbonate mineral content, acid fluid types and concentrations, fracture plane roughness, proppant, and confining pressure on shale samples [43]. Their results showed that the previously suggested acid fracture conductivity model [38] is not always valid in carbonaceous shale and some other models need to be considered.

This study attempts to improve the extension of previous studies on acid fracturing and hydraulic fracturing by applying acid on propped fractures. The experimental results of this study are fully applicable for pilot utilization in unconventional shale formations, especially the carbonaceous ones.

### **3. Research Objectives**

The overall aim of this study is to fully investigate the short-term and long-term effects of acid on carbonaceous shale and optimize acidizing operations accordingly. The specific objectives can be categorized as below:

1. To develop an acid fracturing model and optimize acidizing conditions:

- To develop a geochemical model, reaching equilibrium condition before acidizing,
  - To validate the model using with some primary laboratory results and to further develop it to incorporate a complex mixture of minerals within the rock sample,
  - To select the optimum acid concentrations and mixtures based on simulation results and design the most effective operation considering rock mineral composition and pore fluid condition.
2. To investigate the fluid front movement through the porous medium as a result of saturation difference:
- Spontaneous imbibition of fluid inside closed fractures and cracks (counter-current imbibition) and implementing an analytical model;
  - Spontaneous imbibition of low concentration acid within non-reactive medium along connected fractured systems (co-current imbibition) and suggesting the mathematical model;
3. To generate new experimental data and evaluate acid fracturing in carbonaceous shales:
- To operate acid flooding experiments on the conductivity cell while considering previously implemented fracture and study advection mass transfer through injection rate, changes in heterogeneity and reservoir pressure,

- To investigate the effect of different acid concentrations on the efficiency of acid fracturing,
  - To recommend optimum conditions while considering all economic issues, in-situ conditions of the formation, rock mineral composition, and safety and environmental concerns.
4. To study the long-term effect of acid after the injection process:
- To prepare fractured samples within the acid while there are no injection and mass transfers only through dispersivity,
  - To predict long-term effect of acid within the formation and compare experimental results with the simulation model.

#### **4. Thesis Organization**

This study attempts to extend experimental studies for the utilization of acid in carbonaceous shales. Simulation studies and analytical modeling are also conducted to demonstrate the front movement of the fluid within the fractured structure. The flow chart of the thesis is shown in Figure 2.

In **Chapter 1**, a brief description of previous studies and literature review regarding this area of acidizing is covered. The motive towards this study is also described briefly in this section.

In **Chapter 2**, fracture conductivity was modelled through numerical simulation and validated with an experimental work. CMG-STARs as software for simulation of fluid flow in porous media is applied in this study. In contrast, it was mainly used for intact carbonate samples and investigating breakthrough



and wormholing in cores without fracture [44, 45]. Implementing fractured core in CMG-STARS and calibrating with experimental results have not been tested before, and it is a novelty of this work. In this regard, paper No. 1 is published in the Journal of Natural Gas Science and Engineering.

In **Chapter 3 & 4**, the movement of the fluid front within the porous medium was studied. As acid reacts with carbonates only and carbonaceous shales are not completely made of carbonates, injection fluid front moves inside the medium without reacting. In this case, the driving mechanism for fluid displacement is saturation difference within the porous medium. The valid law for fluid movement is continuity equation and it can be in the form of co-current movement (displaced and displacing fluid move in the same direction) or counter-current movement (displaced and displacing fluid move in the opposite direction). To cover these movements, analytical models were suggested and exact solution attained and validated with previously published experimental data. These chapters resulted in two papers as paper No. 2 and No. 3.

**Chapter 5 & 6** was allocated to the experimental part of the thesis. Using rectangular carbonaceous shale core samples with rounded edges would help better simulation of fractures in downhole condition of shaly formations. Applying in-situ stress condition in such experiment, would be something interesting for the industry and can be counted as another significance of this thesis. Experimental tests performed on Eagle Ford shale samples in presence of proppant and optimized condition of acid achieved through a number of tests. Paper No. 5 is related to objective No. 4 and it is under review at the moment with the Journal of Fuel.

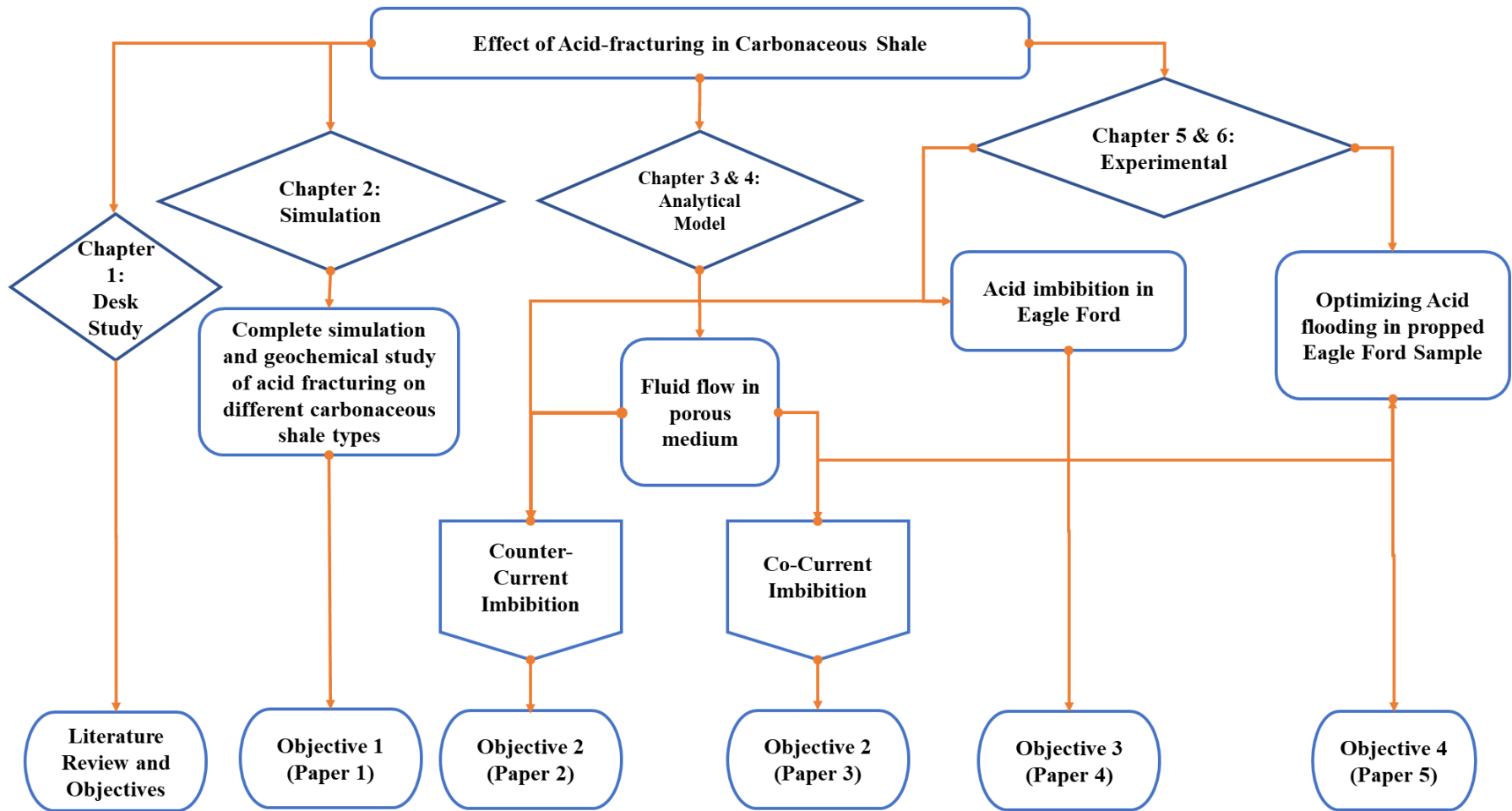


**Figure 2: Flowchart showing the stream of the thesis and published papers in each chapter.**

There are also cases where previously injected acid remains within the porous medium and cannot be displaced into the wellbore. The concentration of the acid in this case is much lower than initially injected acid, but it is in contact with the formation for a longer time. Therefore, its effect needs to be checked. Designing a new experimental setup and preparation of Eagle Ford disks, this effect was investigated for a long time and the results were validated by an analytical model. Both the experiments and the analytical model were the novelty of the work in this area and Paper No. 4 is accepted in the Journal of Petroleum Science and Engineering to fulfill objective No. 3.

## REFERENCES

1. Cronin, M., Emami-Meybodi, H., Johns, R. T., *Unified Theory of Ultimate Hydrocarbon Recovery for Primary and Cyclic Injection Processes in Ultratight Reservoirs*. Scientific reports, 2019. **9**(1): p. 10706-10706.
2. Wang, M., Chen, S., Lin, M., *Enhancing recovery and sensitivity studies in an unconventional tight gas condensate reservoir*. Petroleum science, 2018. **15**(2): p. 305-318.
3. Wu, W., Zhou, J., Kakkar, P., Russell, R., Sharma, M. M., *An Experimental Study on Conductivity of Unproped Fractures in Preserved Shales*. SPE Production & Operations, 2018. **34**(02): p. 280-296.
4. Khanna, A., Keshavarz, A., Mobbs, K., Davis, M., Bedrikovetsky, P., *Stimulation of the natural fracture system by graded proppant injection*. Journal of Petroleum Science and Engineering, 2013. **111**: p. 71-77.
5. Keshavarz, A., Badalyan, A., Carageorgos, T., Bedrikovetsky, P., Johnson, R., *Stimulation of coal seam permeability by micro-sized graded proppant placement using selective fluid properties*. Fuel, 2015. **144**: p. 228-236.
6. Keshavarz, A., Yang, Y., Badalyan, A., Johnson, R., Bedrikovetsky, P., *Laboratory-based mathematical modelling of graded proppant injection in CBM reservoirs*. International Journal of Coal Geology, 2014. **136**: p. 1-16.
7. Li, X. and J. Hao, *Optimization design of low-density and high-strength ceramic proppants by orthogonal experiment*. Advanced Composites Letters, 2020. **29**: p. 2633366X20954875.
8. Schmidt, D., Rankin, P. E., Williams, B., Palisch, T., Kullman, J. *Performance of mixed proppant sizes*. in *SPE Hydraulic Fracturing Technology Conference*. 2014. OnePetro.
9. Calvin, J., Grieser, B., Bachman, T., *Enhancement of Well Production in the SCOOP Woodford Shale through the Application of Microproppant*, in *SPE Hydraulic Fracturing Technology Conference and Exhibition*. 2017. p. D031S008R004.
10. Yarushina, V.M., Bercovici, D., Oristaglio, M. L., *Rock deformation models and fluid leak-off in hydraulic fracturing*. Geophysical Journal International, 2013. **194**(3): p. 1514-1526.

11. Abbasi, J., Raji, B., Riazi, M., Kalantariasl, A., *A simulation investigation of performance of polymer injection in hydraulically fractured heterogeneous reservoirs*. Journal of Petroleum Exploration and Production Technology, 2017. **7**(3): p. 813-820.
12. Umurzakov, Y., *Modeling Huff-n-Puff application in Eagle Ford*, in *Faculty of the Graduate School*. 2020, University of Texas at Austin: Texas. p. 148.
13. Mukhina, E., Cheremisin, A., Khakimova, L., Garipova, A., Dvoretzkaya, E., Zvada, M., Kalacheva, D., Prochukhan, K., Kasyanenko, A., Cheremisin, A., *Enhanced Oil Recovery Method Selection for Shale Oil Based on Numerical Simulations*. ACS Omega, 2021. **6**(37): p. 23731-23741.
14. Wan, T., Sheng, J., Soliman, M. Y., *Evaluation of the EOR Potential in Shale Oil Reservoirs by Cyclic Gas Injection*, in *SPWLA 54th Annual Logging Symposium*. 2013. p. SPWLA-2013-MM.
15. Sheng, J.J., *Enhanced oil recovery in shale reservoirs by gas injection*. Journal of Natural Gas Science and Engineering, 2015. **22**: p. 252-259.
16. Zhang, K., *Experimental and Numerical Investigation of Oil Recovery from Bakken Formation by Miscible CO<sub>2</sub> Injection*, in *SPE Annual Technical Conference and Exhibition*. 2016. p. D023S099R019.
17. Alfarge, D., Wei, M., Bai, B., *Data analysis for CO<sub>2</sub>-EOR in shale-oil reservoirs based on a laboratory database*. Journal of Petroleum Science and Engineering, 2018. **162**: p. 697-711.
18. Elturki, M., Imqam, A., *Application of Enhanced Oil Recovery Methods in Unconventional Reservoirs: A Review and Data Analysis*, in *54th U.S. Rock Mechanics/Geomechanics Symposium*. 2020. p. ARMA-2020-1081.
19. Wang, D., Zhang, J., Butler, R., Olatunji, K., *Scaling Laboratory-Data Surfactant-Imbibition Rates to the Field in Fractured-Shale Formations*. SPE Reservoir Evaluation & Engineering, 2016. **19**(03): p. 440-449.
20. Alfarge, D., Wei, M., Bai, B., , *IOR Methods in Unconventional Reservoirs of North America: Comprehensive Review*, in *SPE Western Regional Meeting*. 2017. p. D031S008R005.
21. Balasubramanian, S., Chen, P., Bose, S., Alzahabi, A., Thakur, G. C., *Recent Advances in Enhanced Oil Recovery Technologies for Unconventional Oil Reservoirs*, in *Offshore Technology Conference*. 2018. p. D021S024R004.
22. Morsy, S., Sheng, J. J., *Effect of Water Salinity on Shale Reservoir Productivity*. Advances in Petroleum Exploration and Development, 2014. **8**: p. 9-14.
23. Morsy, S., Sheng, J. J., Soliman, M. Y., *Waterflooding in the Eagle Ford Shale Formation: Experimental and Simulation Study*, in *SPE Unconventional Resources Conference and Exhibition-Asia Pacific*. 2013. p. SPE-167056-MS.
24. Palyanitsina, A., Tananykhin, D., Masoud, R., *Strategy of Water-Flooding Enhancement for Low-Permeable Polymictic Reservoirs*. Procedia Environmental Science, Engineering and Management, 2020. **7**(4): p. 649-661.
25. Yu, Y., Li, L., Sheng, J. J., *A comparative experimental study of gas injection in shale plugs by flooding and huff-n-puff processes*. Journal of Natural Gas Science and Engineering, 2017. **38**: p. 195-202.
26. Todd, H.B., Evans, J. G., *Improved Oil Recovery IOR Pilot Projects in the Bakken Formation*, in *SPE Low Perm Symposium*. 2016. p. SPE-180270-MS.
27. Thomas, A., Kumar, A., Rodrigues, K., Sinclair, R., Lackie, C., Galipeault, A., Blair, M., *Understanding Water Flood Response in Tight Oil Formations: A Case Study of the Lower Shaunavon*, in *SPE/CSUR Unconventional Resources Conference – Canada*. 2014. p. D011S004R001.

28. Sorensen, J.A., Hamling, J. A., *Historical bakken test data provide critical insights on EOR in tight oil plays*. The American Oil & Gas Reporter, 2016. **59**(2): p. 55-61.
29. Phillips, Z.D., Halverson, R. J., Strauss, S. R., Layman, J., Green, T. W., *A Case Study in the Bakken Formation: Changes to Hydraulic Fracture Stimulation Treatments Result in Improved Oil Production and Reduced Treatment Costs*, in *Rocky Mountain Oil & Gas Technology Symposium*. 2007. p. SPE-108045-MS.
30. Wang, D., Butler, R., Liu, H., Ahmed, S., *Flow-Rate Behavior and Imbibition in Shale*. SPE Reservoir Evaluation & Engineering, 2011. **14**(04): p. 505-512.
31. Sheng, J.J., *Critical review of field EOR projects in shale and tight reservoirs*. Journal of Petroleum Science and Engineering, 2017. **159**: p. 654-665.
32. Dawson, M., Nguyen, D., Champion, N., Li, H., *Designing an Optimized Surfactant Flood in the Bakken*, in *SPE/CSUR Unconventional Resources Conference*. 2015. p. D011S004R003.
33. Nguyen, D., Wang, D., Oladapo, A., Zhang, J., Sickorez, J., Butler, R., Mueller, B., *Evaluation of Surfactants for Oil Recovery Potential in Shale Reservoirs*, in *SPE Improved Oil Recovery Symposium*. 2014. p. SPE-169085-MS.
34. Crowe, C.W., Hutchinson, B. H., Trittipio, B. L., *Fluid-Loss Control: The Key to Successful Acid Fracturing*. SPE Production Engineering, 1989. **4**(02): p. 215-220.
35. White, D.J., Holms, B. A., Hoover, R. S., *Using a Unique Acid-Fracturing Fluid To Control Fluid Loss Improves Stimulation Results in Carbonate Formations*, in *Permian Basin Oil and Gas Recovery Conference*. 1992. p. SPE-24009-MS.
36. Gangi, A.F., *Variation of whole and fractured porous rock permeability with confining pressure*. International Journal of Rock Mechanics and Mining Sciences & Geomechanics Abstracts, 1978. **15**(5): p. 249-257.
37. Nierode, D.E., Kruk, K. F., *An Evaluation of Acid Fluid Loss Additives Retarded Acids, and Acidized Fracture Conductivity*, in *Fall Meeting of the Society of Petroleum Engineers of AIME*. 1973. p. SPE-4549-MS.
38. Tsang, Y.W., Witherspoon, P. A., *Hydromechanical behavior of a deformable rock fracture subject to normal stress*. Journal of Geophysical Research, 1981. **86**: p. 9287-9298.
39. Pournik, M., *Laboratory-scale fracture conductivity created by acid etching*, in *Petroleum Engineering Department*. 2008, Texas A&M University: Texas. p. 181.
40. Deng, J., Mou, J., Hill, A. D. D., Zhu, D., *A New Correlation of Acid-Fracture Conductivity Subject to Closure Stress*. SPE Production & Operations, 2012. **27**(02): p. 158-169.
41. Pournik, M., Li, L., Smith, B., Nasr-El-Din, H. A. A., *Effect of Acid Spending on Etching and Acid-Fracture Conductivity*. SPE Production & Operations, 2013. **28**(01): p. 46-54.
42. Al-Momin, A., Zhu, D., Hill, A. D., *The Effects of Initial Condition of Fracture Surfaces, Acid Spending and Acid Type on Conductivity of Acid Fracture*, in *Offshore Technology Conference-Asia*. 2014. p. OTC-24895-MS.
43. Guo, T., Li, Y., Ding, Y., Qu, Z., Gai, N., Rui, Z., *Evaluation of Acid Fracturing Treatments in Shale Formation*. Energy & Fuels, 2017. **31**(10): p. 10479-10489.
44. Almarri, H. *Analysis of Critical Parameters Affecting the Formation of Wormholes in Acid Stimulation of Carbonate Formations*. 2015.
45. Maheshwari, P., Ratnakar, R. R., Kalia, N., Balakotaiah, V., *3-D simulation and analysis of reactive dissolution and wormhole formation in carbonate rocks*. Chemical Engineering Science, 2013. **90**: p. 258-274.

**Chapter 2:**  
**Reactive Flow Simulation during Acid Fracturing in  
Carbonaceous Shale**

# Statement of Authorship

Title of Paper	Numerical Reactive Flow Transport Simulation on Core Samples during Acid Fracturing in Carbonaceous Shale
Publication Status	<input checked="" type="checkbox"/> Published <input type="checkbox"/> Accepted for Publication <input type="checkbox"/> Submitted for Publication <input type="checkbox"/> Unpublished and Unsubmitted work written in manuscript style
Publication Details	Journal of Natural Gas Science and Engineering Volume 84, December 2020, 103615 <a href="https://doi.org/10.1016/j.jngse.2020.103615">https://doi.org/10.1016/j.jngse.2020.103615</a>

## Principal Author

Name of Principal Author (Candidate)	Mohsen Farrokhrouz			
Contribution to the Paper	Conception, Acquiring Data, Model Simulation, Experimental data matching with the model Knowledge, Analysis, Drafting			
Overall percentage (%)	70%			
Certification:	This paper reports on original research I conducted during the period of my Higher Degree by Research candidature and is not subject to any obligations or contractual agreements with a third party that would constrain its inclusion in this thesis. I am the primary author of this paper.			
Signature	<table border="1" style="width: 100%;"> <tr> <td style="width: 60%;"></td> <td style="width: 20%; text-align: center;">Date</td> <td style="width: 20%;">15/04/2020</td> </tr> </table>		Date	15/04/2020
	Date	15/04/2020		

## Co-Author Contributions

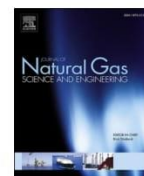
By signing the Statement of Authorship, each author certifies that:

- i. the candidate's stated contribution to the publication is accurate (as detailed above);
- ii. permission is granted for the candidate to include the publication in the thesis; and
- iii. the sum of all co-author contributions is equal to 100% less the candidate's stated contribution.

Name of Co-Author	Dr Abbas Taheri			
Contribution to the Paper	Conception, Analysis, Drafting			
Signature	<table border="1" style="width: 100%;"> <tr> <td style="width: 60%;"></td> <td style="width: 20%; text-align: center;">Date</td> <td style="width: 20%;">15/04/2020</td> </tr> </table>		Date	15/04/2020
	Date	15/04/2020		

Name of Co-Author	Dr Alireza Keshavarz			
Contribution to the Paper	Conception, Analysis, Drafting			
Signature	<table border="1" style="width: 100%;"> <tr> <td style="width: 60%;"></td> <td style="width: 20%; text-align: center;">Date</td> <td style="width: 20%;">15/04/2020</td> </tr> </table>		Date	15/04/2020
	Date	15/04/2020		

Please cut and paste additional co-author panels here as required.



## Numerical reactive flow transport simulation on core samples during acid fracturing in carbonaceous shale

Mohsen Farrokhrouz<sup>a</sup>, Abbas Taheri<sup>a</sup>, Alireza Keshavarz<sup>b,\*</sup>

<sup>a</sup> The University of Adelaide, Adelaide, SA, Australia

<sup>b</sup> School of Engineering, Edith Cowan University, Joondalup, WA, Australia

### ARTICLE INFO

#### Keywords:

Carbonaceous shale  
Simulation  
Geochemical model  
Ion activity  
pH

### ABSTRACT

Acid fracturing also referred to as fracture acidising, is an application of hydraulic fracturing in which fluid is mixed with an acid. Recently, special attention has been paid to carbonaceous shale reservoirs as new unconventional energy resources. In this study, geochemical and hydraulic behaviour of the fracture acidising was investigated through numerical simulations. A geochemical model was constructed based on the rock composition and the simulated initial state of the formation before acid fracturing. Then, changes in the pH versus time in the form of pore volume injected (PVI) was modelled using an explicit finite difference algorithm.

For the hydraulic phase, a fractured core sample model was built and calibrated using the experimental results for a carbonate sample with the same characteristics. Then the model was modified for a carbonaceous shale sample, and the results were examined considering influential parameters such as injection rate, acid concentration, and temperature. For fractured samples, lower injection rate decreases the required pore volume injected (PVI). Simulation results also showed that an increase in acid content reduces breakthrough PVI up to a certain acid concentration. The temperature of injected fluid did not affect acidising efficiency to a great extent. Finally, statistical analysis was carried out to amend some implications and indirect measurements for experiments. The results of this benchmark simulation can be used to improve acid fracturing design for field case studies and to optimise effective parameters to enhance the productivity in unconventional carbonaceous shale reservoirs.

### 1. Introduction

Stimulating reservoir rocks is commonly used to enhance oil and gas recovery. New acid and proppant fracturing techniques have been applied to create a conductive flow channel lengthening into a formation in order to increase the contact area with the reservoir to deplete it as much as possible (Khanna et al., 2013; Keshavarz et al., 2014a,b, 2015, 2016). In naturally fractured reservoirs, which hold a significant portion of confirmed hydrocarbon reserves in the world (Aguilera, 1980; van Golf-Racht, 1982; Nelson, 1985), inducing new fractures can create more complex networks to drain the remaining hydrocarbons in the formation (Bedrikovetsky et al., 2012; Keshavarz et al., 2014c; Akhondzadeh et al., 2018, 2020; Mahesar et al., 2020).

A number of additives have been added to acid fracturing fluids, including polymers, buffers, and cross-linkers to generate sufficient viscosity during fracturing (HF Asl et al., 2020a,b; Bahraminejad et al., 2019; Najimi et al., 2019). The fluids also contain some breakers such as oxidisers (at temperatures below 250 °F) or bromates (at temperatures

above 250 °F) (Al-Muntasheri, 2014; Almubarak et al., 2015) to lower their viscosity at the end of treatment. In addition to viscosity regulators, a compatible acid and additive combination are required to create etching patterns to prevent sludge formation or asphaltene precipitation when they contact the rock. However, the carrier fluid is still essential, and many field examples have used freshwater, raw seawater, or produced water (Li et al., 2016; Almubarak et al., 2016).

Fracturing in horizontal wells requires a large volume of injection fluid at a very high pressure, while vertical wells require lower fluid volumes and pumping pressures (Rafie et al., 2014). The ultimate objective of acid fracturing is to enhance well productivity and reservoir sweep efficiency for a higher recovery factor. The design of applied fracture stages and perforation techniques are used to determine whether the completion type is open hole or cased hole (Aviles et al., 2015). The technique of acid fracturing can also be used for low-carbonate reservoirs providing that complete reaction between the acid and carbonate content takes place.

Most available literature concerning shale reservoirs has mainly

\* Corresponding author.

E-mail address: [a.keshavarz@ecu.edu.au](mailto:a.keshavarz@ecu.edu.au) (A. Keshavarz).

<https://doi.org/10.1016/j.jngse.2020.103615>

Received 15 April 2020; Received in revised form 9 September 2020; Accepted 9 September 2020

Available online 20 September 2020

1875-5100/© 2020 Elsevier B.V. All rights reserved.



focused on geochemical and mineralogical studies and their potential for hydrocarbon production (Temraz, 2005; Hanneman, 2014; Makoundi, 2016; Daymond, 2017; Meng et al., 2017; Memon et al., 2020; Aslan-nezhad et al., 2020; Ali et al., 2020). Experimental studies dedicated to acid fracturing are mostly limited to carbonates (Reda, 2014; Sohn, 2018). To the best of our knowledge, there are only a few studies on fractured carbonate core samples (He, 2015; Nawik et al., 2016). Furthermore, simulation software and models have only recently focused on the acidising process and acid fracturing (Maheshwari et al., 2013; Almari, 2015) for wormhole modelling and the prediction of optimum injection rates. On the other hand, acidisation on carbonaceous shale to remove carbonate content and increase the productivity of unconventional shale reservoirs is a novel topic. Besides, acidising can be applied to those shale reservoirs which has been already fractured hydraulically. Simulation on such models and investigating acid behaviour would be very interesting for oil and gas companies and researchers in this area.

This research gap motivated us to perform a numerical simulation study using commercial software CMG\_STARS to simulate geochemical and hydraulic behaviour of the fracture acidising in carbonaceous shales. The model is a carbonaceous shale with a fracture along the axis of cylinder-like core. The model was first validated by a fractured carbonate core and then modified for different typical carbonaceous shales. The mineral compositions of these samples were determined according to previous geochemical and mineralogical studies, which will be explained in the following section. Then, applying different activation energies and frequency factors to different samples based on the mineral composition, the acid flow rate through fractured cores was simulated. Finally, parametric and statistical studies on the simulated models were performed to determine effective factors that influence the efficiency of acidising till minimizing pressure drop across the core.

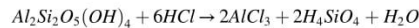
This study is the first simulation study to simulate geochemical and hydraulic behaviour of the fracture acidising in carbonaceous shales. On the other hand, significance of initial in-situ geochemical condition and

- i. The transport of hydrogen cations ( $H^+$ ) from the injected fluid to the surface of the carbonate;
- ii. The reaction of  $H^+$  with carbonate at the surface of the rock;
- iii. The transport of products from the surface toward the bulk solution.

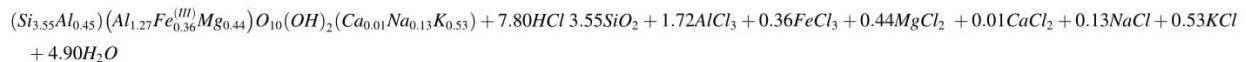
Two constraints restrict the surface reactions of carbonates with acids: mass transfer and surface reactions. The slowest rate determines the rate of the overall reaction. If the slowest rate is the adsorption or desorption of reactants and products to and from the rock surface, this reaction is considered as mass-transfer-limited and products cannot be transported as fast as the frequency of reactions occurrence. If the slowest rate is the reaction rate on the surface of the rock, then the reaction is surface-reaction-limited, and products can easily transfer from the surface of the rock, but the reaction does not occur at the same speed.

Experiments performed by Lund et al. (1975) showed that the reaction of calcite with HCl is mass transfer limited at ambient conditions (25 °C), and at -15.6 °C, both mass transfer and surface reaction rates limit the dissolution rate. For dolomite, Lund et al. (1973) showed that the reaction of dolomite with HCl at 25 °C was surface-reaction limited and as the temperature increased to 100 °C, this reaction was limited by mass-transfer.

For carbonaceous shale samples containing a certain amount of organic matter, there are always minor amounts of carbonates in the form of dolomite and calcite (Dayal, 2017). The reaction of hydrochloric acid with calcite and dolomite is similar to the above reactions. However, reactions with clay minerals are different due to the complex compositions and distribution of clay minerals on the surface of the rock. Kaolinite is a simple clay mineral, and its reaction with acid is more straightforward than other clay minerals:



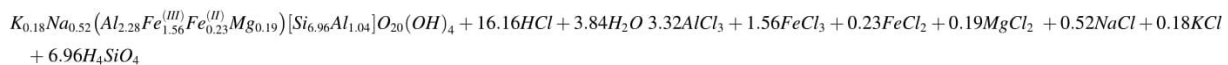
Illite hydrolysis reaction with an acid (as reported by Vieillard (2000)) proceeds as below:



applying it within the simulation has been rarely performed in previous modelling studies.

## 2. Geochemical reactions on the surface of carbonaceous shale

Assuming appropriate contact between the acid and the rock surface, the reaction between HCl and calcite is:



A similar reaction occurs when an acid contacts the surface of dolomite:



Lund et al. (1973) stated that the reaction between acids and carbonates occurs in three steps:

Because of the presence of different metallic elements like lithium, magnesium, and aluminium surrounded by silicon tetrahedral, up to 8 diverse representative chemical formulae have been proposed for smectite (or montmorillonite) (Alekseyev, 2007). The reaction of a typical smectite molecule with hydrochloric acid proceeds as:

The dissolution of minerals within an acid is defined through the Arrhenius equation, which describes the temperature dependency of reaction rates at a constant pH (Laidler, 1987):

$$Rate = A \cdot \exp\left(\frac{-E_a}{R \cdot T}\right) \quad (1)$$

**Table 1**  
Reported activation energy values for carbonates and clay minerals.

Rock Type	$E_a$ (kJ/mol)	Experimental Condition	Reference
Calcite	25	Rotating disk, marble	King and Liu (1933)
	35	Ground sample, $8 < \text{pH} < 10$	Sjoberg (1976)
	8.4	Ground sample, $\text{pH} < 3.5$	Plummer et al. (1978)
	16.7	Ground sample, $\text{pH} < 5$	Chan and Rochelle (1982)
	$19 \pm 4$	Rotating disk, $1 < \text{pH} < 3$	Alkattan et al. (1998)
	8–60	Review (calcite)	Morse and Arvidson (2002)
	$21 \pm 1$	Calcite powder, $\text{pH} < 6.5$	Gledhill and Morse (2006)
	30/21	Presence/absence of sulphide, $\text{pH} = 5.5$	Xiang et al. (2009)
Dolomite	62	Ground sample of finely crystalline sample	Lund et al. (1973)
	32	Stirring at high revolution rate	Herman and White (1985)
	15/40	$\text{pH}_{\text{surf}} = 5/\text{pH}_{\text{surf}} = 1, 25^\circ\text{C} < T < 80^\circ\text{C}$	Gautelier et al. (1999)
	32	Ground sample, at $20^\circ\text{C}$	Yildirim (2008)
Clay Minerals	104.5	Metakaolin (kaolin heated up to $732^\circ\text{C}$ ), ground sample, $\text{pH} = 0.5, T = 60^\circ\text{C}$	Hulbert and Huff (1970)
	56	Kaolinite, $2 < \text{pH} < 5$	Carroll and Walther (1990)
	29	Kaolinite, $\text{pH} = 4, T = 80^\circ\text{C}$	Ganor et al. (1995)
	46	Illite, $4 < \text{pH} < 7, 5^\circ\text{C} < T < 50^\circ\text{C}$	Köhler et al. (2003)
	71	Montmorillonite, $1 < \text{pH} < 4, 25^\circ\text{C} < T < 70^\circ\text{C}$	Amram and Gangor (2005)
	39	Montmorillonite, $1 < \text{pH} < 14, T = 80^\circ\text{C}$ , with some modification in Arrhenius Equation	Alekseyev (2007)
	46	Illite, $1.4 < \text{pH} < 12.4, 5^\circ\text{C} < T < 50^\circ\text{C}$ , with some modification in Arrhenius Equation	Alekseyev (2007)
	71	Chlorite, $1 < \text{pH} < 5, 5^\circ\text{C} < T < 50^\circ\text{C}$ , with some modification in Arrhenius Equation	Alekseyev (2007)
	38–77	Mixed clay minerals from soil samples in NSW	Bibi (2012)
	91	Metakaolin, spherical particles, $T = 70^\circ\text{C}$	Lima et al. (2017)

$A$  ( $\text{mol}/\text{m}^2 \text{ s}$ ) is a pre-exponential factor known as the frequency factor,  $E_a$  ( $\text{J}/\text{mol}$ ) is the apparent activation energy,  $R$  is the gas constant ( $8.3145 \text{ J}/\text{K} \cdot \text{mol}$ ), and  $T$  ( $\text{K}$ ) is the temperature. The activation energy is the minimum energy molecules must possess to react and to form products. The frequency factor is the frequency of reactions and the likelihood of correct molecular orientation. The typical values of activation energy for different carbonates and clay minerals are given in Table 1.

Generally speaking, the equation representing the acid solution in different silicates is more complex than in carbonates. For instance, Amram and Gangor (2005) noted the dependence of the montmorillonite dissolution rate on temperature ( $25\text{--}70^\circ\text{C}$ ) and pH (1–4) according to the Langmuir equation as follows:

$$r = A \cdot \exp\left(\frac{-E_a}{RT}\right) \left[ \frac{K \exp\left(-\frac{\Delta H^0}{RT}\right) a_{\text{H}^+}}{1 + K \exp\left(-\frac{\Delta H^0}{RT}\right) a_{\text{H}^+}} \right] \quad (2)$$

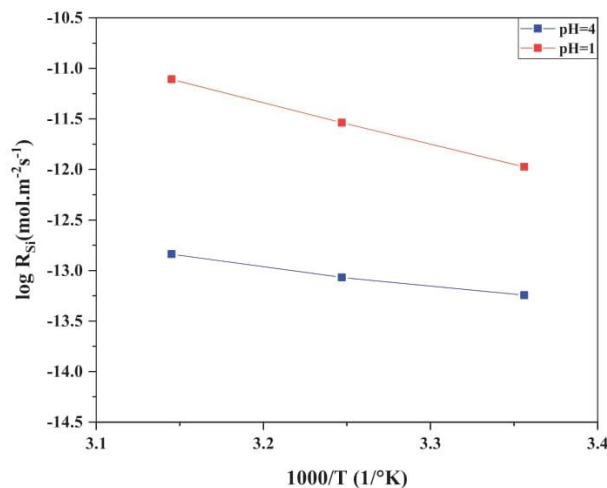


Fig. 1. Variation in clay dissolution rate shown as  $\log \text{Rate}$  ( $\text{mol}/\text{m}^2 \text{ s}$ ) versus  $1000/T$  ( $1/^\circ\text{K}$ ) at different pH values. Simple linear regression equation exists at different pH values ( $R^2 > 0.99$ ): at  $\text{pH} = 1$   $\log \text{Rate} = 3.996x + 1.472$ , and at  $\text{pH} = 4$   $\log \text{Rate} = -1.959x - 6.656$  (Bibi, 2012) (clay samples obtained from cores of Bottle Bend lagoon in southwestern New South Wales, Australia).

$\Delta H^0$  is the enthalpy of adsorption and  $a_{\text{H}^+}$  is the activity of hydrogen in the solution (the solution pH). In this equation, it is assumed that the rate of dissolution is proportional to the concentration of protons adsorbed on the surface of the mineral. However, the equation is only valid for acidic conditions, and additional equations were proposed for neutral and alkaline conditions (Bauer and Berger, 1998; Huertas et al., 2001; Sato et al., 2005) which are not discussed in this paper. Alekseyev (2007) suggested a master reaction equation for montmorillonite for a full pH range with a U-shape reaction dependency on the pH of the solution:

$$r = \exp\left(\frac{-E_a}{RT}\right) [A_{\text{H}^+} a_{\text{H}^+}^m + A_{\text{H}_2\text{O}} + A_{\text{OH}^-} a_{\text{OH}^-}^n] \quad (3)$$

The term within the rightmost parentheses describes the dominant solution mechanism of acidic, neutral, or alkaline conditions. Based on 150 experimental results, Alekseyev (2007) recommended some values for the constants of Equation (3)  $A_{\text{H}^+} = 1.08 \times 10^{-4}$ ,  $m = 0.764$ ,  $A_{\text{H}_2\text{O}} = 1.86 \times 10^{-8}$ ,  $A_{\text{OH}^-} = 1.08 \times 10^{-5}$  and  $n = 0.422$ .

However, since the range of pH changes in our simulation was in an acidic state, Equation (2) is preferable. Additionally, keeping in mind that the right-hand side of Equation (2) in acidic range (data are given in Table 1) is very close to unity, acidising clay minerals can be approximated by the Arrhenius equation (Equation (1)). A typical Arrhenius plot was obtained by plotting the logarithm of the reaction rate versus the inverse of temperature. The slope of the Arrhenius equation at two different pH values for clay minerals is shown in Fig. 1.

### 3. Materials and methods

According to the nature of the work, two-step simulations with two different software are required: geochemical simulation in order to implement the effect of different minerals on the initial property of the formation and hydraulic simulation to investigate formation behaviour during acidising. A descriptive explanation of the models and the link between them is explained in this section.

#### 3.1. Geochemical simulation

Carbonaceous shale contains large amounts of carbonised organic matter, ranging from 3 to 15% (Liang et al., 2012; Farrokhrouz and Asef, 2013) and is black to grey in colour. The major carbonaceous shale



**Table 2**

Mineral composition of typical carbonaceous shale samples used in this study (all values given in percent).

	Cooper Basin (Australia)	Eagle Ford (USA)	Sargelu Formation (Iran)	Gulf Coast (USA)	Lower Bakken (USA)	McArthur Basin (Australia)
Sample Code	#3	#5	G5	#1	#11	R007
Quartz	44.02	3.9	26	57.88	48.08	34
Illite	28.37	6.4	5	0.95	20.63	52
Kaolinite	14.32	2.1	–	2.02	16.00	–
Montmorillonite	–	–	–	3.90	–	6
Chlorite	–	–	–	4.56	–	1
K-Feldspar	4.54	2.3	4	8.18	3.20	6
Siderite	5.35	18.1	–	–	–	–
Pyrite	0.02	–	–	–	4.58	–
Albite	–	0.1	–	16.80	4.05	–
Calcite	–	42.8	55	2.72	0.45	1
Dolomite	–	10.9	5	–	0.74	–
Anhydrite	–	1.9	–	–	–	–
Apatite	–	4.5	–	–	–	–
Organic (Non-mineral) Content	2.49	3	4.66	3	2.27	5
Reference	Ahmad (2014)	Tripathi and Pournik (2014)	Shabani et al. (2018)	Zhang et al. (2012)	Liu et al. (2018)	Frichot et al. (2017)

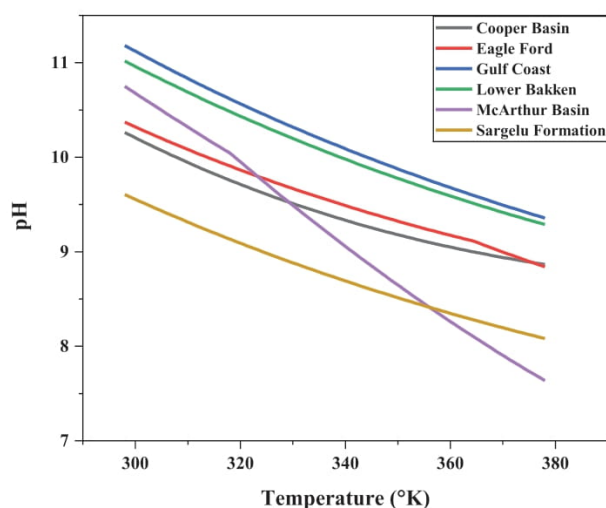


Fig. 2. Simulation of initial pH for shale samples given in Table 1 as a function of temperature.

formations in North America are located in Barnett, Woodford, Ordovician, Eagle Ford, and Haynesville plays, and the Kimmeridge formation in the North Sea. Various values of total organic content (TOC) have been reported in different formations, as low as 0.5 wt% in Haynesville (Kale, 2009) up to 55 wt% in Kimmeridge (Kumar et al., 2012). The petrophysical properties of carbonaceous shale, including the porosity, mineralogy, and acoustic wave velocities are available in the literature (Sondhi, 2011; Gupta, 2012; Sarkar, 2008). Various amounts of other minerals are also present in carbonaceous shale. For instance, the Eagle Ford formation is primarily a clay-rich carbonate with low quartz and feldspar contents (Kumar et al., 2012).

In order to provide an overview of *in-situ* conditions, the mineral compositions of six typical shale formations were selected as in Table 2. Knowing the burial history and initial temperature of these formations, a geochemical simulation in PHREEQC Code (Parkhurst, 1995) was run to model the equilibrium state of these formations. This code is a computer program for simulating chemical reactions and transport processes in natural or polluted water. The program is run based on the equilibrium chemistry of aqueous solutions interacting with minerals, gases, solid solutions, exchangers, and sorption surfaces. The 1D transport includes

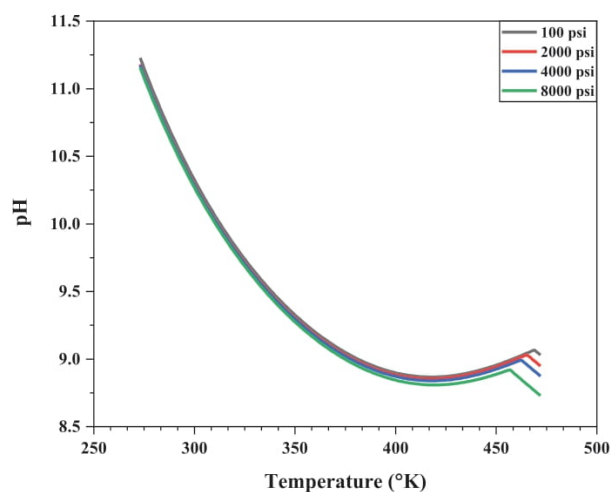


Fig. 3. Simulation of the initial pH of shale samples as a function of pressure and temperature (Cooper Basin sample).

dispersion, diffusion, and various options for single and dual-porosity media through an explicit finite difference algorithm.

Fig. 2 shows the simulated changes in equilibrium pH as a function of temperature for the samples shown in Table 2. A similar simulation was already performed on carbonates containing shale inter-beds (Farrokhrouz and Asef, 2010). As observed, the initial pH of samples with a higher clay content was higher than those with a higher carbonate content. Based on studies performed by Aksulu et al. (2012) and Aghaeifar et al. (2015), the exchange of  $\text{Ca}^{2+}$  by  $\text{H}^+$  on clay surface is a slow process that determines the initial pH of formation brine. Clay mineral desorbs calcium cations and adsorbs hydrogen cations. As the concentration of  $\text{H}^+$  decreases within the fluid, its pH increases. Therefore, samples with a higher clay mineral content should have a higher initial pH. Fig. 2 confirms this assumption, as the highest initial pH was found for the Gulf Coast sample, which had the highest amount of clay minerals (i.e. montmorillonite, illite, kaolinite, chlorite).

Fig. 3 examines the effects of confining pressure on the initial pH of the samples as a function of temperature (from 0 to 200 °C). Organic matter is modelled as methane gas within the simulation to investigate the effect of the pressure. However, the modelling results show that a confining pressure of up to 8000 psi has a negligible impact on the pH

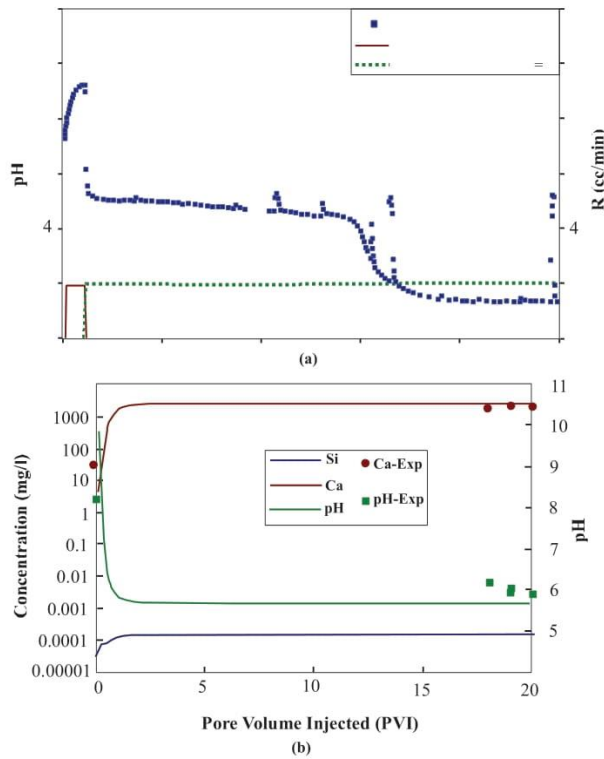


Fig. 4. pH changes at the effluent during core flooding with pH = 1 acid a) pH changes at the effluent while acid flooding with HCl (R = Injection Rate), (Benson, 2007); b) PHREEQC simulation results (solid line) versus experimental results (squares) during HCl (C = Concentration, mg/l) flooding (Bacci, 2011).

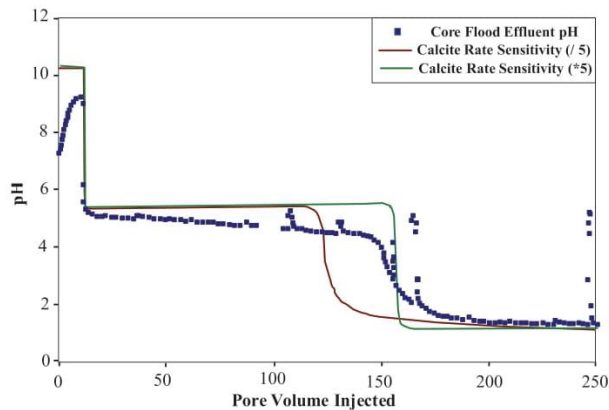


Fig. 5. Effluent pH for 5 times higher and 5 times lower calcite reaction rate constants (Benson, 2007).

value, and it can be said that pH is only a function of temperature and rock composition.

When acid flows through a fracture (channel), the fluid front moves forward and gradually affects the pH and at each point on the fracture wall. Using an injection point as a reference point, the equilibrium pH is reached before acid injection. Upon HCl injection, the pH of the same point decreases due to mixing with the highly acidic fluid. The pH measurements at the core effluent fluid confirm this behaviour, and some examples can be seen in Fig. 4 (Benson, 2007; Bacci, 2011). Further investigation by Benson (2007) showed that the ultimate pH

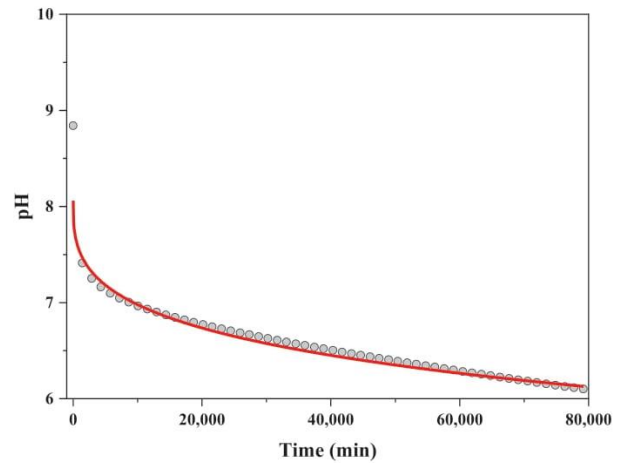


Fig. 6. pH as a function of time for the Eagle Ford shale sample; statistical data available in Table 3.

Table 3  
Statistical results of the correlation of pH changes as a function of time for different carbonaceous shale samples; the equation is in the form of,  $pH = \frac{1}{(a + bt^c)}$

Sample Core	a	b	c	R-square
Cooper Basin	0.12405	$8.43261 \times 10^{-4}$	0.34017	0.98337
Eagle Ford	0.12405	$8.18245 \times 10^{-4}$	0.34289	0.98465
Sargelu Formation	0.1301	$2.13021 \times 10^{-4}$	0.44727	0.99491
Gulf Coast	0.12076	0.00145	0.29957	0.97107
Lower Bakken	0.12102	0.00136	0.30445	0.97401
McArthur Basin	0.13375	$5.58433 \times 10^{-5}$	0.55677	0.99738

value is the same at different reaction rates of calcite with acid and a decrease in pH is mainly a function of time (Fig. 5). Therefore, the pH during the acidising period was simulated in PHREEQC for the samples in Table 2. Then, pH as a function of time was plotted, and a sample for Eagle ford shale is shown in Fig. 6. Afterwards, correlations between pH changes as a function of time were appraised on all shale samples in Table 2. The results showed that such a correlation is strong enough, and the functions have correlation coefficients near unity in all cases (Table 3).

Table 4  
Properties of the model and parameters used in the simulation (laboratory units in simulation).

Model	3-Dimensional Cartesian
No. of grids	$25 \times 15 \times 47$
Core dimensions	1.5 in. $\times$ 6 in.
Core porosity	0.144
Core permeability (md)	6.8
Fracture permeability (Darcy)	11.2
Porosity-Permeability Relationship, (Carmen-Kozeny type formula)	5.25
Chemical peaction rate per unit time (Frequency of Reaction)	7500
Core saturation (%)	95
Injection rate (cc/min)	5
Core confining pressure (psi)	1500
Core pore pressure (psi)	1000
HCl concentration (%)	15
Core temperature (°F)	250



### 3.2. Simulation of acid flow through the core

The hydraulic behaviour of acid flowing through the core is another significant feature of the simulation. Carbonaceous shale formation as a porous media with some fluid inside the pores must be simulated with specialised software for porous media. CMG-STARs performs simulation on multi component fluids up to three different phases. Flow through fractures can be simulated using four different models: dual porosity (DP), dual permeability (DK), multiple interacting continua (MINC), or vertical refinement (VR) - depending on the process or mechanisms to be studied. A numerical scheme in CMG-STARs can be run in fully implicit and adaptive implicit modes.

Using STARs software developed by CMG satisfies this requirement and can model chemical reactions in the fluid phase. A core model with a fracture along the height of a cylindrical shape was generated in CMG-STARs, and the injection of HCl across it was simulated. A primary model was calibrated by the experimental results of He (2015) for acidising on fractured Indiana limestone core sample (containing more than 99% calcite).

The simulation model was built by assuming the values in the literature for unavailable input data. Some parameters were defined within the laboratory experiment conducted by He (2015) (i.e. injection rate, acid concentration, and reservoir pressure), while other parameters were not defined (i.e. porosity-permeability relation, heterogeneity magnitude, reaction rate, activation energy, frequency factor, and degree of mineral solubility) as these parameters were not within the scope of his work. Referring to the literature data and some previous logical approaches in simulation, a range of input data for some parameters was selected (Lund et al., 1975; Plummer et al., 1978; Alekseyev, 2007; Yildirim, 2008) and are summarised in Table 4. The results of the pressure drop simulation across the core and simulated pH values at the core effluent calibrated with the experimental results are shown in Fig. 7 and Fig. 8, respectively.

During the simulation, the pressure at the core outlet is equal to 1000 psi to create a constant pore pressure. While injecting acid with pressure higher than pore pressure, acid flows through the fracture and the matrix, and it takes some time for the complete performance of acid as the reaction between the rock surface, and HCl is mass transfer limited. Accordingly, inlet pressure increases gradually until the breakthrough. Afterwards, the pressure difference across the core decreases as the products of the reaction can be expelled from the core outlet with a higher rate (Fig. 7).

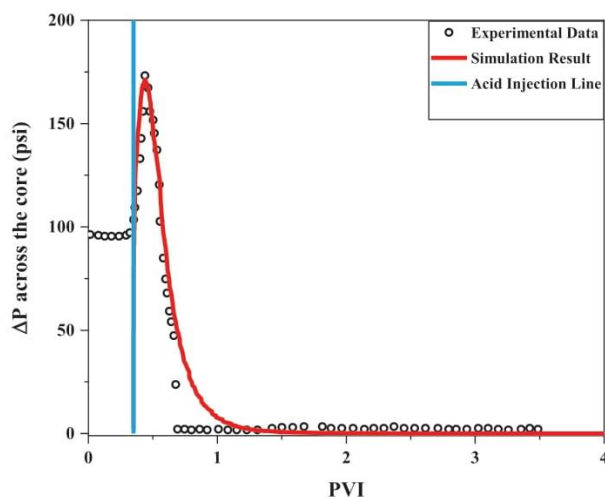


Fig. 7. Simulation results showing the pressure drop across the fractured core versus the experimental data obtained from He (2015) (PVI: pore volume injected).

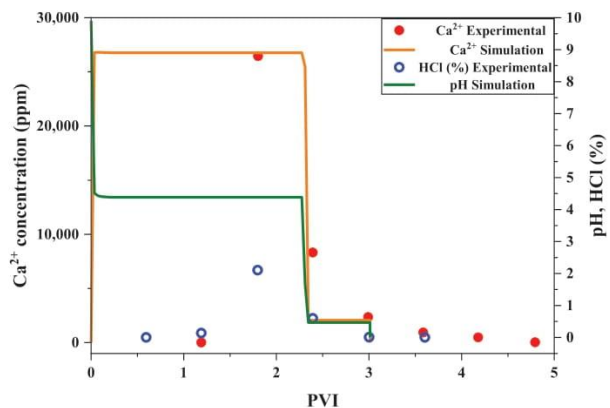


Fig. 8. Simulation results versus experimental data on fractured sample showing calcium cation and pH in the effluent (experimental data obtained from He (2015)). Note that HCl content in the effluent disappeared after 3 PVI and simulation did not perform after that).

A similar trend is expected for the concentration of  $\text{Ca}^{2+}$  at the effluent. The concentration of calcium cation is low at the beginning as a small mass of reaction products are transferred to the end of fracture. But after breakthrough, a huge amount of cation is expelled all of a sudden and then decreases gradually as carbonate content on the rock surface decreases. Fig. 8 shows the results of geochemical simulation versus experimental measurements until the end of acidising. Comparing these simulation results (hydraulic and geochemical) with experimental data measured in the laboratory showed very good agreement and validated the accuracy of simulation to a great extent.

### 4. Carbonaceous shale simulation and parametric study

After calibrating the model with experimental data for calcite, acidising on fractured core samples was simulated for the different shale formations presented in Table 2. Acidising is more efficient in samples with higher carbonate contents due to the fast reaction rate with HCl. As mentioned earlier, there are different activation energy values available for carbonates and clay minerals (Table 1). The values proposed in the simulation are also cited in the same table. The reaction of HCl with different silicates (including quartz, illite, montmorillonite, chlorite, kaolinite, feldspar, and siderite) is much slower than the reaction with carbonates, which can be understood by the smaller frequency factors and larger activation energies. The frequency factor will change on a rock surface with a higher silicate content compared with carbonates, and this point was considered in the simulation of shale samples.

#### 4.1. Effect of acid concentration

Fig. 9 presents the impact of HCl concentration on the acidising efficiency, which is shown as the pressure difference between the injection and production point ( $\Delta P$ ) versus injected pore volume (PV). In terms of acid concentration, as expected, a lower acid content resulted in longer reaction time, and increasing the acid concentration was followed by a rise in the number of reactions per unit time. However, this increase in acid concentration did not always result in lower breakthrough pore volume for all rock types. Meaning that a higher HCl concentration in the injected fluid did not affect the breakthrough pore volume after a certain time. The number of reactions that occur on the rock surface of calcite is mass-transfer-limited; meaning that products cannot transfer from the environment with the same rate as reaction rate. Therefore, there is an accumulation of the products on the surface that prevents acid reaction with the fresh surface of the rock. Accordingly, increasing the acid content can help up to a certain value. Beyond that, HCl cannot

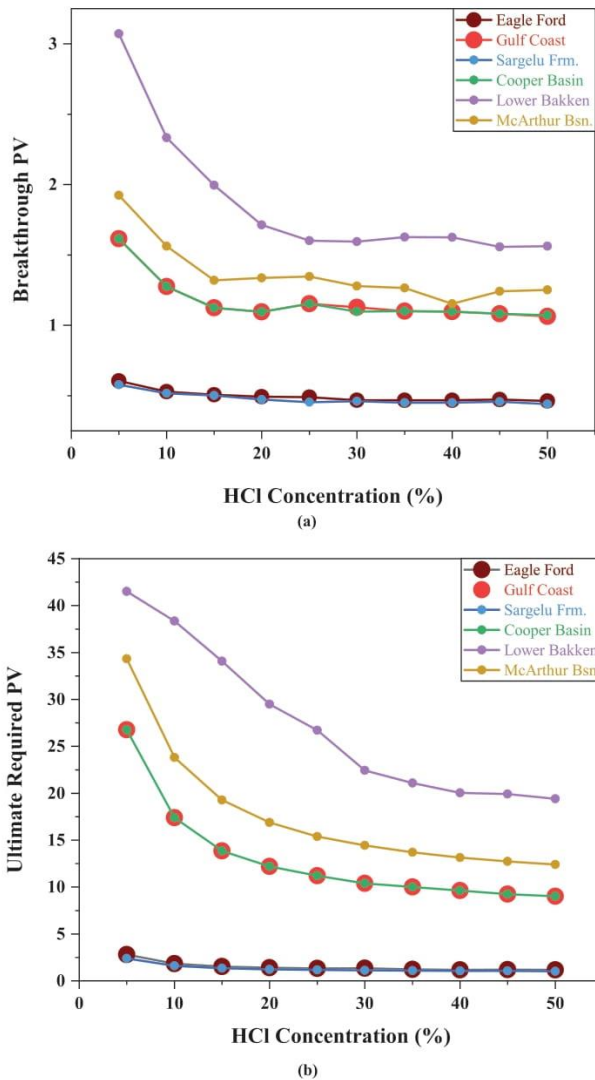


Fig. 9. Effect of different acid concentrations on fractured carbonaceous shale samples a) breakthrough pore volume; b) required pore volume when  $\Delta P \approx 0$ .

reach the fresh rock surface and practically no further reaction occurs until all products are transferred.

Based on the work by Daccord et al. (1993), keeping all other parameters constant, wormhole growth is directly proportional to acid concentration. They also mentioned that the injection rate must be modified based on the acid concentration, i.e., a higher acid concentration requires a higher injection rate and vice versa. In dimensionless models, the effect of acid concentration is determined by an “acid capacity number”, which is a constant that is defined as the dissolved solid volume per unit volume of acid:

$$N_{ac} = \frac{\alpha C_0}{\rho_s} \quad (4)$$

$N_{ac}$  is the acid capacity number,  $C_0$  is the inlet acid concentration,  $\rho_s$  is the density of the solid phase, and  $\alpha$  is the dissolving power of the acid. Panga et al. (2005) showed that the breakthrough pore volume is inversely proportional to the acid capacity number.

Fig. 10 demonstrates that there is an optimum acid concentration for intact core samples. At concentrations higher than this optimal

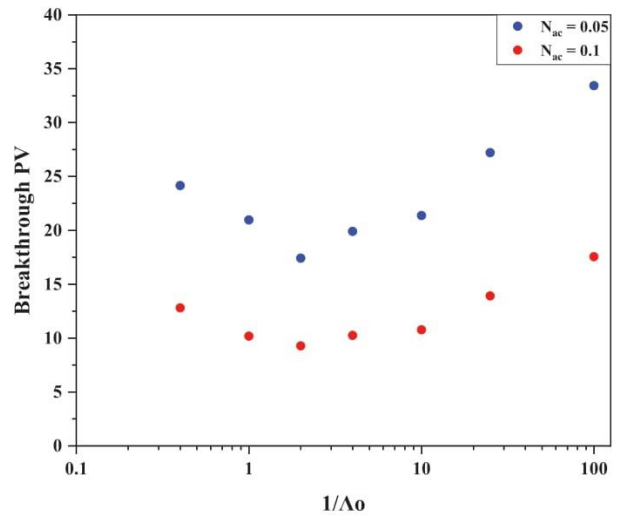


Fig. 10. Pore volume required for a breakthrough at different acid capacity numbers for intact (un-fractured) sample;  $N_{ac}$ : acid capacity number,  $\Lambda_0$ : effective Damkohler number (Panga et al., 2005).

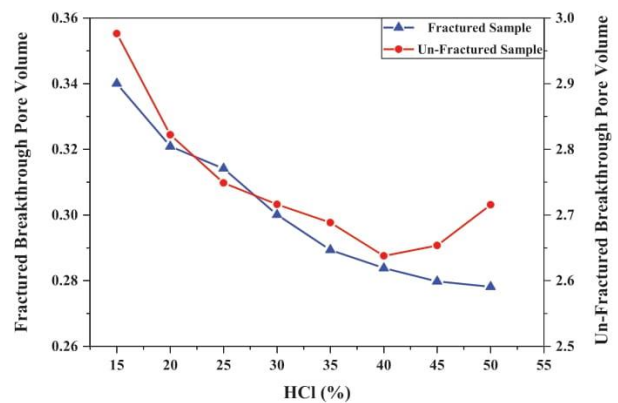


Fig. 11. Simulation results for fractured and un-fractured core samples at different acid concentration. Simulation performed on Indiana limestone with given characteristics as in Table 4.

condition, face dissolution is the main mechanism of the reaction, while at a lower HCl concentration, uniform dissolution predominates, and both cases are counterproductive. Therefore, there is an optimum acid concentration (shown by the reverse of Damkohler number) with minimum breakthrough pore volume.

For fractured cores in our simulation models (Fig. 9), contrary to Fig. 10, there is no minimum breakthrough pore volume at different acid concentrations. At a constant injection rate, increasing the acid concentration (higher than 20% for most of the samples) did not affect acidising recovery, as the reaction products could not be transferred at that rate. Increasing the injection rate at higher acid concentrations may enhance acidising efficiency. For samples with high carbonate contents (i.e. Eagle Ford and Sargelu), an acid concentration as low as 10% led to breakthrough at smaller pore volumes. Defining the distribution patterns of carbonate on the surface of the fracture using CT scanning can be very helpful to optimise the acid concentration.

We performed another validation on the simulation model and plotted pressure drop across the fractured sample (e.g. Fig. 7) versus acid concentration and compared the result with un-fractured sample. That was the only simulation on intact rock sample in this study. As it is



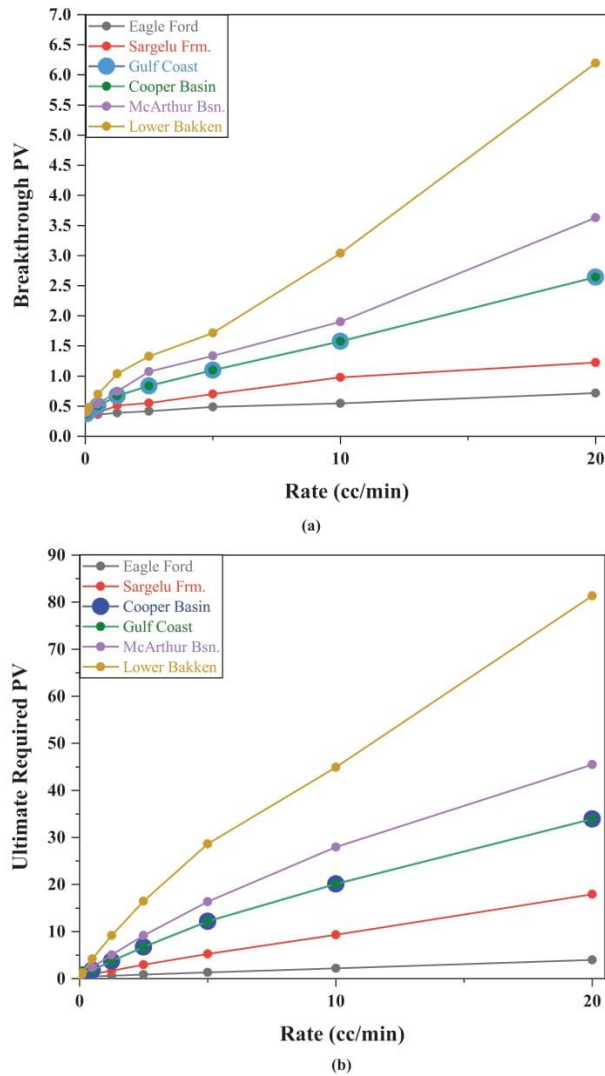


Fig. 12. Effect of injection rate on different fractured carbonaceous shale samples: a) breakthrough pore volume; b) required pore volume when  $\Delta P \approx 0$ .

shown in Fig. 11, there is an optimum acid concentration within the injected fluid leading to a minimum breakthrough. This result is consistent with previous studies, as in Fig. 10. On the other hand, for the fractured sample, a decreasing trend is observed at different acid concentrations. Comparing the decreasing trend in Fig. 9 (shale samples) with Fig. 11 (Indiana limestone), it is construed that such trend is expected in any fractured sample regardless of the rock type.

#### 4.2. Effect of injection rate

Many believe that the highest possible injection rate (without fracturing) would lead to a perfect acidising operation when using a highly reactive acid like hydrochloric acid (e.g. Williams et al., 1979; Paccaloni and Tambini, 1990). However, Daccord et al. (1989) proposed a procedure for optimizing the acid volume with a low injection rate. Such conflicting results were followed by a study by Wang et al. (1993), who found that there is an optimum injection rate for any acid treatment through cores. A similar optimum condition was achieved in other core flooding experiments (Panga et al., 2005; McDuff et al., 2010; Almarri,

2015).

Fig. 12 shows the effect of injection rate on the studied carbonaceous shale samples in Table 1. The results show that in the case of acid flowing through a fractured core, the breakthrough pore volume decreased at very low injection rates. At higher injection rates, higher pore volumes were required for the breakthrough pore volume and in the case of no pressure drop across the core. This was mainly because at high acid flux, the reaction time was much shorter than the acid residence time inside the pore spaces, and the acid moved upwards and downwards into new pores and increased the effective radius of wormholes. Therefore, higher pore volumes were required to provide enough reaction time for the acid and rock. On the other hand, at lower injection rates, there was enough time for the reaction between acid and rock, and the acid could move through the highly-permeable fracture. Subsequently, smaller pore volumes were required for the breakthrough. Furthermore, Fig. 12 reveals that for samples with a high calcite content at different injection rates, the breakthrough occurred almost in the same injected pore volume which confirms the significance of carbonate

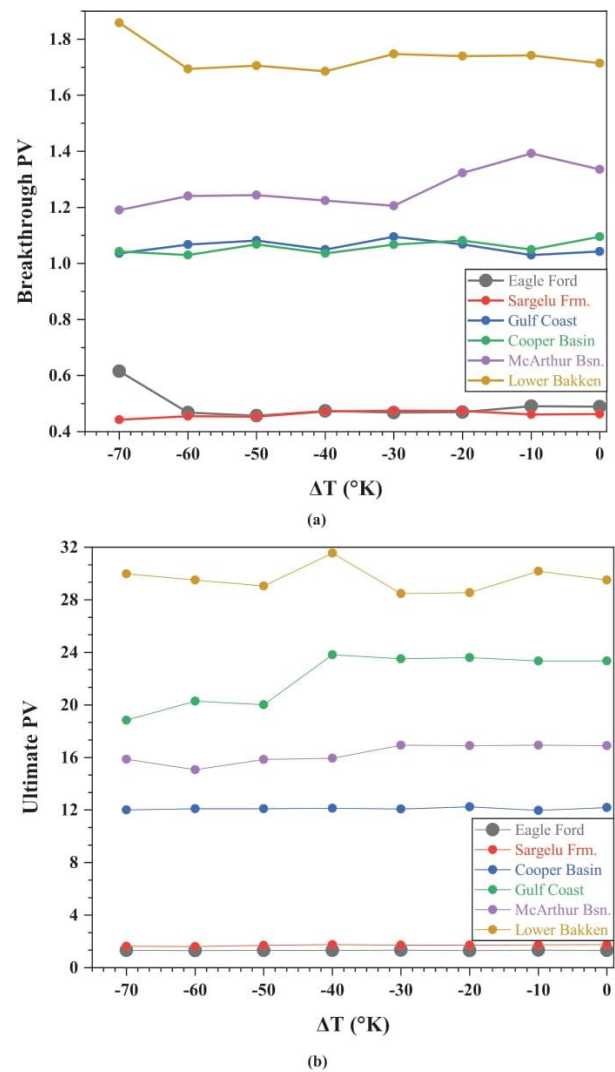


Fig. 13. Effect of the temperature difference between the injected pore fluid of various fractured samples ( $T_{res} = 120$   $^{\circ}C$ , and the injected fluid was cooler than the reservoir temperature): a) breakthrough pore volume; b) required pore volume when  $\Delta P \approx 0$ .

**Table 5**

An inverse function of equations in Table 3 in the general form of  $f^{-1}(pH) = a \left( \frac{1}{t} - b' \right)^{c'}$

Sample Core	a'	b'	c'
Cooper Basin	$1.08835 \times 10^9$	0.12405	2.9397
Eagle Ford	$1.00746 \times 10^9$	0.12405	2.9164
Sargelu Formation	$1.61756 \times 10^8$	0.13010	2.2358
Gulf Coast	$2.99012 \times 10^9$	0.12076	3.3381
Lower Bakken	$2.60143 \times 10^9$	0.12102	3.2846
McArthur Formation	$4.35265 \times 10^7$	0.13375	1.7961

content during acid fracturing of carbonaceous shales.

4.3. Effect of temperature

The reservoir temperature is usually higher than the heat of the injected fluid. The same condition was simulated in our model and the experimental results used for calibration (the experiment performed by He (2015) was conducted at 120 °C, and we selected the same temperature as reservoir temperature of shale cores). For a negative temperature difference ( $T_{inj} < T_{res}$ ), the surface reaction rate was lower, while the viscosity, density, and diffusivity of the acid increased. Experiments on intact cores showed that wormholes with higher densities were created when  $T_{inj} < T_{res}$ . If a certain permeability after acidising is targeted, it is necessary to investigate the temperature difference (Kalia and Glasbergen, 2009).

Fig. 13 displays the temperature effect on different shale samples in this study. The role of temperature for the fractured core is not as important as in intact cores. In a study by Wang et al. (1993), increasing the temperature for both limestone and dolomite increased the optimum HCl injection rates. However, they also stated that under isothermal conditions, fluid was primarily driven by increased permeability, and for non-isothermal conditions, both permeability and viscosity were effective.

During the simulation in this study, the viscosity of the pore fluid before acid injection was lower than water and acid (the hydrocarbon within the reservoir was considered to be a gas or a very low viscosity oil). At the start of injection, the mobility of the acid is lower because of higher viscosity than the pore fluid, and the hydrocarbon penetrates into the highly-permeable region because of lower viscosity. Therefore, permeability is the most effective parameter. Since there is a high-permeability fracture in this model, temperature changes did not significantly affect acidising efficiency, and Fig. 13 also conveys the same concept.

4.4. Discussion and analysis of simulation results

After investigating the effects of different parameters on the acid fracturing efficiency, it is beneficial to use the calibrated model to predict other parameters with operational restrictions. Pressure drop measurement across the core is carried out by installing two gauges in the model at the inlet and outlet of the core. For any arbitrary point between the inlet and outlet, another gauge may be fitted around the

**Table 6**

Correlation of the pressure drop across the core versus time before the breakthrough. The general equation form is  $\Delta p = g(t) = m + n \cdot t^q$

Sample Core	m	N	Q	R-square
Cooper Basin	38.5411	328.49098	0.53001	0.97839
Eagle Ford	0.000	326.2911	0.26231	0.99547
Sargelu Formation	0.000	320.6698	0.25129	0.99126
Gulf Coast	42.0494	347.6319	0.60013	0.9859
Lower Bakken	46.12002	282.26152	0.66155	0.97302
McArthur Formation	40.69524	321.41618	0.57059	0.98444

**Table 7**

Correlation of pressure drop across the core versus time after breakthrough. The general equation form is  $\Delta p = h(t) = y_0 + w \cdot \exp\left(-\frac{t}{z_0}\right)$

Sample Core	$y_0$	W	$z_0$	R-square
Cooper Basin	0.00134	397.2087	4.19063	0.99773
Eagle Ford	-4.5543	325.1742	0.4169	0.99634
Sargelu Formation	-0.02126	331.93693	0.30915	0.997
Gulf Coast	0.57577	412.78352	3.7273	0.99873
Lower Bakken	-2.15484	435.3205	9.525	0.99799
McArthur Formation	-3.30118	406.32957	5.83141	0.99791

**Table 8**

Inverse function for correlations in Table 6. The general equation form is  $g^{-1}(\Delta p) = m'(t - n')^q$

Sample Core	m'	n'	q'
Cooper Basin	$1.78621 \times 10^{-5}$	38.5411	1.88676
Eagle Ford	$2.61472 \times 10^{-10}$	0	3.81228
Sargelu Formation	$1.0647 \times 10^{-10}$	0	3.97947
Gulf Coast	$5.83066 \times 10^{-5}$	42.0494	1.66631
Lower Bakken	$1.97511 \times 10^{-4}$	46.12	1.51160
McArthur Formation	$4.03816 \times 10^{-4}$	40.6952	1.75257

core on that point to measure the circumferential pressure.

Another interesting parameter during acidising operation is the determination of instantaneous ion activity (pH) of the acid on the fluid displacement front. At the core outlet, pH measurements can be easily performed on the effluent fluid, but at any point across the core between the inlet and outlet, direct measurements are not possible. The approach in this paper is to identify the relationship between the pressure drop and pH changes across the core inlet and outlet and then adapt it to any arbitrary point in between. As shown in Figs. 7 and 8, it was experimentally found that the pressure drop and pH are both functions of time:

$$\begin{cases} pH = f(t) \rightarrow t = f^{-1}(pH) \\ \Delta p = g(t) \rightarrow t = g^{-1}(\Delta p) \end{cases} \Rightarrow g^{-1}(\Delta p) = f^{-1}(pH) \quad (5)$$

Table 3 shows the pH functions of different carbonaceous shale samples, and Table 5 presents the inverse functions of these correlations. In terms of calculus, an inverse function can only be defined for a monotonic function (entirely increasing or decreasing). Bearing this in mind, the pressure drop across the core does not always have monotonic behaviour. Thus, it was decided to identify an inverse pressure drop function before and after the maximum value (breakthrough).

This methodology requires characterisation of the pressure drop function before ( $\Delta p = g(t)$ ) and after breakthrough ( $\Delta p = h(t)$ ). These functions and their inverses are shown in Tables 6–9. All correlations showed a similar general form of the equation with a very high value of correlation coefficient. Data of correlations were obtained from simulation results, which were already calibrated by the experimental results of one special case. Fig. 14 shows the equity of the inverse functions using the concept of bisector in xy plane (Farrokhrrouz and Asef, 2012, 2017):  $g^{-1}(\Delta p) = f^{-1}(pH)$  and  $h^{-1}(\Delta p) = f^{-1}(pH)$ .

The core setup was designed based on the pressure gauge at the injection point and the outlet, plus any arbitrary point between these two

**Table 9**

Inverse function for the correlations in Table 7. The general equation form is  $h^{-1}(\Delta p) = y_0' \ln(w'(t + z_0'))$

Sample Core	$y_0'$	w'	$z_0'$
Cooper Basin	-4.19063	$2.51757 \times 10^{-3}$	-0.00134
Eagle Ford	-0.4169	$3.07527 \times 10^{-3}$	4.5543
Sargelu Formation	-0.30915	$3.01262 \times 10^{-3}$	0.02126
Gulf Coast	-3.7273	$2.42258 \times 10^{-3}$	-0.57577
Lower Bakken	-9.525	$2.29716 \times 10^{-3}$	2.15484
McArthur Formation	-5.83141	$2.46106 \times 10^{-3}$	3.30118



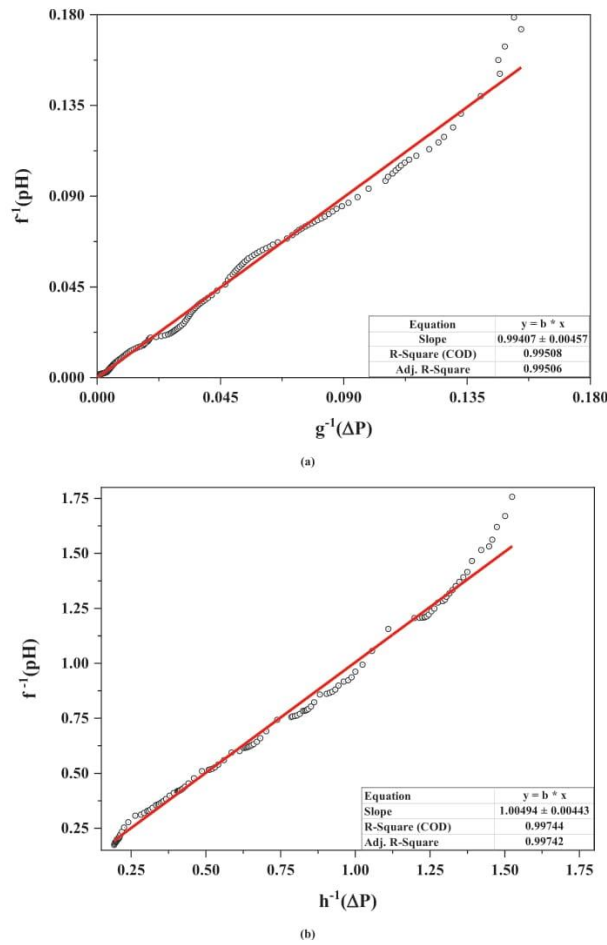


Fig. 14. Equity of inverse functions: a) before breakthrough, b) after breakthrough.

boundaries. The pressure drop functions can be correlated based on continuous real-time measurements. Knowing the definition of a derivative for inverse functions as follows:

$$(F^{-1})'(x) = \frac{1}{F'(F^{-1}(x))} \tag{6}$$

For the inverse function of pressure drop before the breakthrough, this definition is:

$$(g^{-1})'(\Delta p) = \frac{1}{g'(g^{-1}(\Delta p))} \tag{7}$$

As  $g^{-1}(\Delta p) = f^{-1}(pH)$  based on Equation (5), it can be replaced in Equation (7) in order to define  $g^{-1}(pH)$ :

$$(g^{-1})'(\Delta p) = \frac{1}{g'(f^{-1}(pH))} \Rightarrow g'(f^{-1}(pH)) = \frac{1}{(g^{-1})'(\Delta p)} \tag{8}$$

Integrating from both sides:

$$g(f^{-1}(pH)) = \int_0^{T_{BT}} \frac{1}{(g^{-1})'(\Delta p)} dt + C \tag{9}$$

We also know that:

$$(F^{-1} \circ F)(x) = x \tag{10}$$

Accordingly, the inverse function for ion activity ( $f^{-1}(pH)$ ) is obtained:

$$f^{-1}(pH) = g^{-1} \left[ \int_0^{T_{BT}} \frac{1}{(g^{-1})'(\Delta p)} dt + C \right] \tag{11}$$

Finding this function is very useful and essential in cases with no breakthrough and pH changes on the acid front is required. Suppose that we are looking for pH changes on the fluid front before the breakthrough. It is not possible to implement an effluent point in the middle of the core to gather fluid sample (it would be another effluent point). Still, we can apply a pressure measurement point anywhere between the inlet and the outlet to define the pressure drop function versus time. Then, using Equation (11), the inverse function of pH will be obtained. The same methodology is also applied on the field scale as an *in-situ* measurement of ion activity is still very costly, and finding an indirect technique would be attractive for companies operating in the acid fracturing field.

### 5. Conclusion

In this paper, an acid fracturing simulation is conducted on fractured shale samples. Geochemical numerical simulation on typical carbonaceous shale samples was conducted. The results showed a monotonic exponential decrease in pH versus time. Results of the geochemical section were validated by experimental measurements and showed very good agreement.

During parametric studies on the numerical hydraulic model, the most effective parameters and optimal conditions were determined. Then, statistical analyses were performed in order to make use of simulation results to understand the effect of ion activity on fluid front displacement. The following conclusions can be drawn:

- For intact core samples, there is an optimum injection rate at which the required breakthrough pore volume is minimised. For fractured cores, the lower the injection rate, the lower breakthrough pore volume is required.
- Increasing the HCl concentration within the injection fluid reduced the required breakthrough pore volume. However, after a particular acid concentration, increasing the HCl concentration has no effect on acidising efficiency.
- Considering the low viscosity of hydrocarbon (gas), as a pore fluid in carbonaceous shale formations, temperature changes do not affect the acidising efficiency as the injecting fluid is more viscous.

Altogether, geochemical and hydraulic simulation results made a complete framework for acidising in carbonaceous shale samples and a prototype for further studies in the future.

### Credit author statement

Mohsen Farrokhrouz proposed the idea and Abbas Taheri made a general framework for that in order to be applicable. Alireza Keshavarz Software and recommended the general tactics of numerical simulation.

Mohsen Farrokhrouz made the model and verified it by experimental data and performed parametric study on that and all these steps were conducted with supervision of Abbas Taheri and Alireza Keshavarz.

### Declaration of competing interest

The authors declare that they have no known competing financial interests or personal relationships that could have appeared to influence the work reported in this paper.

### Appendix A. Supplementary data

Supplementary data to this article can be found online at <https://doi.org/10.1016/j.jngse.2020.103615>.

### References

- Aghaeifar, Z., et al., 2015. Adsorption/desorption of  $\text{Ca}^{2+}$  and  $\text{Mg}^{2+}$  To/from Kaolinite Clay in Relation to the Low Salinity EOR Effect. IOR 2015-18th European Symposium on Improved Oil Recovery. European Association of Geoscientists & Engineers.
- Aguilera, R., 1980. Naturally Fractured Reservoirs. Petroleum Publishing Co., Tulsa, OK; None.
- Ahmad, M., 2014. Petrophysical and Mineralogical Evaluation of Shale Gas Reservoirs: a Cooper Basin Case Study. Australian School of Petroleum. Australia, University of Adelaide, p. 214.
- Akhondzadeh, Hamed, et al., 2018. Investigating the relative impact of key reservoir parameters on performance of coalbed methane reservoirs by an efficient statistical approach. *J. Nat. Gas Sci. Eng.* 53, 416–428.
- Akhondzadeh, Hamed, et al., 2020. Pore-scale analysis of coal cleat network evolution through liquid nitrogen treatment: A Micro-Computed Tomography investigation. *Int. J. Coal Geol.* 219, 103370.
- Aksulu, H., et al., 2012. Evaluation of low-salinity enhanced oil recovery effects in sandstone: effects of the temperature and pH gradient. *Energy Fuels* 26 (6), 3497–3503.
- Alekseyev, V.A., 2007. Equations for the dissolution reaction rates of montmorillonite, illite, and chlorite. *Geochem. Int.* 45 (8), 770–780.
- Ali, Muhammad, et al., 2020. Nanomaterial-based drilling fluids for exploitation of unconventional reservoirs: a review. *Energies* 13 (13), 3417.
- Alkattan, M., et al., 1998. An experimental study of calcite and limestone dissolution rates as a function of pH from –1 to 3 and temperature from 25 to 80 C. *Chem. Geol.* 151 (1–4), 199–214.
- Almarri, H., 2015. Analysis of critical parameters affecting the formation of wormholes in acid stimulation of carbonate formations. In: *Energy and Mineral Engineering. The Pennsylvania State University. Msc Thesis*, p. 154.
- AlMubarak, T., et al., 2016. Design and application of high temperature seawater based fracturing fluids in Saudi arabia. In: *Offshore Technology Conference Asia*, vol. 24. Offshore Technology Conference, Kuala Lumpur, Malaysia.
- AlMubarak, T.A., et al., 2015. Insights on potential formation damage mechanisms associated with hydraulic fracturing. In: *International Petroleum Technology Conference*. Doha, Qatar, International Petroleum Technology Conference, p. 20.
- Al-Muntasheri, G.A., 2014. A critical review of hydraulic fracturing fluids over the last decade. In: *SPE Western North American and Rocky Mountain Joint Meeting*, vol. 25. Society of Petroleum Engineers, Denver, Colorado.
- Amram, K., Ganor, J., 2005. The combined effect of pH and temperature on smectite dissolution rate under acidic conditions. *Geochem. Cosmochim. Acta* 69, 2535–2546.
- Asl Hamed, Foroughi, et al., 2020a. Effect of SiO<sub>2</sub> nanoparticles on the performance of L-Arg and L-Cys surfactants for enhanced oil recovery in carbonate porous media. *J. Mol. Liq.* 300, 112290.
- Asl Hamed, Foroughi, et al., 2020b. Experimental investigation into l-Arg and l-Cys eco-friendly surfactants in enhanced oil recovery by considering IFT reduction and wettability alteration. *Petrol. Sci.* 17 (1), 105–117.
- Aslamezhad, M., et al., 2020. Evaluation of mechanical, chemical, and thermal effects on wellbore stability using different rock failure criteria. *J. Nat. Gas Sci. Eng.* 103276.
- Aviles, I., et al., 2015. Infinite plug and perf - the value of a full bore degradable system. In: *Abu Dhabi International Petroleum Exhibition and Conference*, vol. 10. UAE, Society of Petroleum Engineers, Abu Dhabi.
- Bacci, G., 2011. An experimental and numerical investigation into permeability and injectivity changes during CO<sub>2</sub> storage in saline aquifers. In: *Earth Science and Engineering*. Imperial College London. Doctor of Philosophy (PhD).
- Bahraminejad, Hossein, et al., 2019. CuO/TiO<sub>2</sub>/PAM as a novel introduced hybrid agent for water–oil interfacial tension and wettability optimization in chemical enhanced oil recovery. *Energy Fuels* 33 (11), 10547–10560.
- Bauer, A., Berger, G., 1998. Kaolinite and smectite dissolution rate in high molar KOH solutions at 35° and 80°C. *Appl. Geochem.* 13 (7), 905–916.
- Bedrikovetsky, P.G., et al., 2012. Stimulation of natural cleats for gas production from coal beds by graded proppant injection. In: *SPE Asia Pacific Oil and Gas Conference and Exhibition*. Society of Petroleum Engineers.
- Benson, I.P., 2007. Numerical Simulation of pH-Sensitive Polymer Injection as a Conformance Control Method. Faculty of Graduate School, University of Texas at Austin. Master of Science, p. 229.
- Bibi, I., 2012. Mineralogy and Acid Neutralisation Mechanisms in Inland Acid Sulfate Environments. Faculty of Agriculture and Environment. University of Sydney. PhD Thesis, Sydney, p. 258.
- Carroll, S.A.W., J. V., 1990. Kaolinite dissolution at 25 degrees , 60 degrees , and 80 degrees C. *Am. J. Sci.* 290, 797–810.
- Chan, P.K., Rochelle, G.T., 1982. Limestone Dissolution: Effects of pH, CO<sub>2</sub>, and Buffers Modeled by Mass Transfer. ACS Publications.
- Daccord, G., et al., 1993. Chemical dissolution of a porous medium by a reactive fluid—I. Model for the “wormholing” phenomenon. *Chem. Eng. Sci.* 48 (1), 169–178.
- Daccord, G., et al., 1989. Carbonate acidizing: toward a quantitative model of the wormholing phenomenon. *SPE Prod. Eng.* 4 (1), 63–68.
- Dayal, A.M., Dayal, A.M., Mani, D., 2017. Chapter 2 - Deposition and Diagenesis. *Shale Gas*. Elsevier, pp. 13–23.
- Daymond, P.A., 2017. Analysis of Mudrock Lithofacies and Hydrocarbon-Source Potential of the Middle Ordovician Athens Shale, Alabama Fold and Thrust Belt. Auburn University. Msc Thesis, p. 125.
- Farrokhrouz, M., Asef, M.R., 2010. “Simulating model to reduce detrimental acidizing in Tabnak gas field.” SPE-131986-MS. In: *SPE Deep Gas Conference and Exhibition*, vols. 24–26. Manama, Bahrain.
- Farrokhrouz, M., Asef, M.R., 2012. “Evaluation of empirical correlations for Biot’s coefficient prediction. In: Presented at 15<sup>th</sup> International Workshop on Seismic Anisotropy. Manama, Bahain.
- Farrokhrouz, M., Asef, M.R., 2013. *Shale Engineering: Mechanics and Mechanisms*. Taylor and Francis, CRC Press, London.
- Farrokhrouz, M., Asef, M.R., 2017. Experimental investigation for predicting compressive strength of sandstone. *J. Nat. Gas Sci. Eng.* 43, 222–229.
- Frichot, L., et al., 2017. The Vaughton Siltstone of the Northern McArthur Basin: Preliminary Data and Issues Related to Assessing its Potential as a Petroleum Source Rock.
- Ganor, J., et al., 1995. The effect of pH on kaolinite dissolution rates and on activation energy. *Geochem. Cosmochim. Acta* 59 (6), 1037–1052.
- Gautelier, M., et al., 1999. An experimental study of dolomite dissolution rates as a function of pH from –0.5 to 5 and temperature from 25 to 80°C. *Chem. Geol.* 157 (1), 13–26.
- Gledhill, D.K., Morse, J.W., 2006. Calcite dissolution kinetics in Na–Ca–Mg–Cl brines. *Geochem. Cosmochim. Acta* 70 (23), 5802–5813.
- Gupta, N., 2012. Multi-scal Characterization of the Woodford Shale in West- Central Oklahoma: from Scanning Electron Microscope to 3D Seismic. University of Oklahoma. PhD Thesis, Norman, Oklahoma, USA.
- Hanneman, H., 2014. Mineralogy and Geochemistry of Carbonaceous Mudstone as a Vector to Ore: a Case Study at the Lagunas Norte High-Sulfidation Gold Deposit. Colorado School of Mines. PhD, Peru, p. 152.
- He, J., 2015. An Innovative Closed Fracture Acidizing Technique for Deep Carbonate Reservoirs Using GLDA. Texas A&M University, PhD Thesis, p. 115.
- Herman, J.S., White, W.B., 1985. Dissolution kinetics of dolomite: effects of lithology and fluid flow velocity. *Geochem. Cosmochim. Acta* 49 (10), 2017–2026.
- Huertara, F., et al., 2001. Kinetics of montmorillonite dissolution in granitic solutions. *Applied Geochemistry - APPL GEOCHEM* 16, 397–407.
- Hulbert, S.F., Huff, D.E., 1970. Kinetics of alumina removal from a calcined kaolin with nitric, sulphuric and hydrochloric acids. *Clay Miner.* 8 (3), 337–345.
- Kale, S., 2009. Petrophysical Characterization of Barnett Shale. Mewbourne School of Petroleum and Geological Engineering, The University of Oklahoma. Msc Thesis.
- Kalia, N., Glasbergen, G., 2009. Wormhole formation in carbonates under varying temperature conditions. In: *8th European Formation Damage Conference*, vol. 19. Society of Petroleum Engineers, Scheveningen, The Netherlands.
- Keshavarz, A., et al., 2014a. Laboratory-based mathematical modelling of graded proppant injection in CBM reservoirs. *Int. J. Coal Geol.* 136, 1–16.
- Keshavarz, A., et al., 2014b. Stimulation of unconventional naturally fractured reservoirs by graded proppant injection: experimental study and mathematical model. In: *SPE/EAGE European Unconventional Resources Conference and Exhibition*, vol. 2014. European Association of Geoscientists & Engineers, pp. 1–12.
- Keshavarz, A., et al., 2014c. Enhancement of CBM well fracturing through stimulation of cleat permeability by ultra-fine particle injection. *The APPEA Journal* 54 (1), 155–166.
- Keshavarz, A., et al., 2015. Stimulation of coal seam permeability by micro-sized graded proppant placement using selective fluid properties. *Fuel* 144, 228–236.
- Keshavarz, A., et al., 2016. Productivity enhancement by stimulation of natural fractures around a hydraulic fracture using micro-sized proppant placement. *J. Nat. Gas Sci. Eng.* 33, 1010–1024.
- Khanna, A., et al., 2013. Stimulation of the natural fracture system by graded proppant injection. *J. Petrol. Sci. Eng.* 111, 71–77.
- King, C.V., Liu, C.L., 1933. The rate of solution of marble in dilute acids. *J. Am. Chem. Soc.* 55 (5), 1928–1940.
- Köhler, S.J., et al., 2003. An experimental study of illite dissolution kinetics as a function of pH from 1.4 to 12.4 and temperature from 5 to 50°C. *Geochem. Cosmochim. Acta* 67 (19), 3583–3594.
- Kumar, V., et al., 2012. Nano to macro mechanical characterization of shale. In: *SPE Annual Technical Conference and Exhibition*, vol. 23. Society of Petroleum Engineers, San Antonio, Texas, USA.
- Laidler, K.J., 1987. *Chemical Kinetics*. Harper & Row, New York.
- Li, L., et al., 2016. A review of crosslinked fracturing fluids prepared with produced water. *Petroleum* 2 (4), 313–323.



- Liang, C., et al., 2012. Shale lithofacies and reservoir space of the wufeng-longmaxi formation, sichuan basin, China. *Petrol. Explor. Dev.* 39 (6), 736–743.
- Lima, P.E.A., et al., 2017. Dissolution kinetics of Amazonian metakaolin in hydrochloric acid. *Clay Miner.* 52 (1), 75–82.
- Liu, Y., et al., 2018. Pore structure characterization and the controlling factors of the bakken formation. *Energies* 11 (11).
- Lund, K., et al., 1973. Acidization—I. The dissolution of dolomite in hydrochloric acid. *Chem. Eng. Sci.* 28 (3), 691–IN691.
- Lund, K., et al., 1975. Acidization—II. The dissolution of calcite in hydrochloric acid. *Chem. Eng. Sci.* 30 (8), 825–835.
- Mahesar, Aftab Ahmed, et al., 2020. Morphological and petro physical estimation of eocene tight carbonate formation cracking by cryogenic liquid nitrogen; a case study of Lower Indus basin, Pakistan. *J. Petrol. Sci. Eng.* 107318.
- Maheshwari, P., et al., 2013. 3-D simulation and analysis of reactive dissolution and wormhole formation in carbonate rocks. *Chem. Eng. Sci.* 90, 258–274.
- Makoundi, C., 2016. Geochemistry of Phanerozoic Carbonaceous Black Shales, Sandstones and Cherts in Malaysia: Insights into Gold Source Rock Potential. University of Tasmania. PhD, p. 383.
- McDuff, D., et al., 2010. Understanding wormholes in carbonates: unprecedented experimental scale and 3D visualization. *J. Petrol. Technol.* 62 (10), 78–81.
- Memon, K.R., et al., 2020. Influence of cryogenic liquid nitrogen on petro-physical characteristics of mancos shale: an experimental investigation. *Energy Fuels* 34 (2), 2160–2168.
- Meng, Q., Sachsenhofer, Reinhard F., Liu, ZhaoJun, Sun, PingChang, Hu, Fei, Zhou, RenJie, Wang, KeBing, 2017. Mineralogy and geochemistry of fine-grained clastic rocks in the Eocene Huadian Basin (NE China): implications for sediment provenance, paleoclimate and depositional environment. *Austrian Journal of Earth Sciences* 10 (2).
- Morse, J.W., Arvidson, R.S., 2002. The dissolution kinetics of major sedimentary carbonate minerals. *Earth Sci. Rev.* 58 (1–2), 51–84.
- Najimi, Siamak, et al., 2019. Investigating the effect of [C 8 Py][Cl] and [C 18 Py][Cl] ionic liquids on the water/oil interfacial tension by considering Taguchi method. *Journal of Petroleum Exploration and Production Technology* 9 (4), 2933–2941.
- Nawik, A., et al., 2016. An Environmentally Friendly Alternative for the Conventional Acids Used in Acid Fracturing of Carbonate Reservoirs.
- Nelson, R.A., 1985. *Geologic Analysis of Naturally Fractured Reservoirs*. Gulf Publishing Co., Houston, TX, None.
- Pacchaloni, G., Tambini, M., 1990. *Advances in Matrix Stimulation Technology* (New Orleans).
- Panga, M.K.R., et al., 2005. Two-scale continuum model for simulation of wormholes in carbonate acidization. *AIChE J.* 51 (12), 3231–3248.
- Parkhurst, D.L., 1995. User's Guide to PHREEQC, a Computer Program for Speciation, Reaction-Path, Advective-Transport, and Inverse Geochemical Calculations. *Water-Resources Investigations Report*.
- Plummer, L., et al., 1978. The kinetics of calcite dissolution in CO<sub>2</sub>-water systems at 5 degrees to 60 degrees C and 0.0 to 1.0 atm CO<sub>2</sub>. *Am. J. Sci.* 278 (2), 179–216.
- Rafie, M., et al., 2014. The first successful multistage acid frac of an oil producer in Saudi arabia. In: *SPE Saudi Arabia Section Technical Symposium and Exhibition*, vol. 15. Al-Khobar, Saudi Arabia, Society of Petroleum Engineers.
- Reda, A.S., 2014. *Tracer Fluid Flow through Porous Media: Theory Applied to Acid Stimulation Treatments in Carbonate Rocks*. Texas A& M University. PhD Thesis, p. 186.
- Sarkar, M., 2008. *Petrophysical Study of Shales under High Temperature and Pressure*. University of Oklahoma. Msc Thesis, Norman, USA.
- Sato, T., Kuroda, M., Yokoyama, S., et al., 2005. Dissolution kinetics of smectite under alkaline condition. In: *Clays in Natural and Engineering Barriers for Radioactive Waste Confinement*. International Meeting, Tours, France, pp. 19–20.
- Shabani, M., et al., 2018. Methane sorption and storage characteristics of organic-rich carbonaceous rocks, Lurestan province, southwest Iran. *Int. J. Coal Geol.* 186, 51–64.
- Sjöberg, E.L., 1976. A fundamental equation for calcite dissolution kinetics. *Geochem. Cosmochim. Acta* 40 (4), 441–447.
- Sohn, Y.S., 2018. *Experimental and Simulated Investigation on the Effect of Chemically Retarded Acid Systems in Carbonates*. Texas A& M University. Msc Thesis, p. 136.
- Sondhi, N., 2011. *Petrophysical Characterisation of Eagle Ford Shale*. University of Oklahoma. Msc Thesis, Norman, Oklahoma, USA.
- Temraz, M.G., 2005. *Mineralogical and Geochemical Studies of Carbonaceous Shale Deposits from Egypt*. Technical University of Berlin. PhD, p. 124.
- Tripathi, D., Pournik, M., 2014. Effect of acid on productivity of fractured shale reservoirs. In: *SPE/AAPG/SEG Unconventional Resources Technology Conference*, vol. 13. Unconventional Resources Technology Conference, Denver, Colorado, USA.
- van Golf-Racht, T.D., 1982. *Developments in Petroleum Science*. In: *Fundamentals of Fractured Reservoir Engineering*, vol. 12. Elsevier/North-Holland Inc., New York, NY; None.
- Vieillard, P., 2000. A new method for the prediction of gibbs free energies of formation of hydrated clay minerals based on the electronegativity scale. *Clay Clay Miner.* 48 (4), 459–473.
- Wang, Y., Hill, A., Schechter, R., 1993. *The Optimum Injection Rate for Matrix Acidizing of Carbonate Formations* (Houston, TX).
- Williams, B., Gidley, J., Schechter, R., 1979. *Monograph series*. In: *Acidizing Fundamentals* TX. SPE.
- Xiang, G., et al., 2009. Dissolution rate of limestone for wet flue gas desulfurization in the presence of sulfite. *J. Hazard Mater.* 168 (2–3), 1059–1064.
- Yildirim, M., 2008. Dissolution kinetics of icel-aydincik dolomite in hydrochloric acid. *S. Afr. J. Chem.* 61.
- Zhang, R., et al., 2012. *A Fully Coupled Model of Nonisothermal Multiphase Flow Solute Transport and Reactive Chemistry in Porous Media*.

**Chapter 3:**  
**Analytical Exact Solution for Co-Current Spontaneous  
Imbibition in Porous Media Considering Early and Late-  
Time Effects**

# Statement of Authorship

Title of Paper	Analytical exact Solution for Co-Current Spontaneous Imbibition in Porous Media Considering Early- and Late-Time Effects
Publication Status	<input checked="" type="checkbox"/> Published <input type="checkbox"/> Accepted for Publication <input type="checkbox"/> Submitted for Publication <input type="checkbox"/> Unpublished and Unsubmitted work written in manuscript style
Publication Details	Journal of Energy & Fuels 2021, 35, 21, 17499–17511 <a href="https://doi.org/10.1021/acs.energyfuels.1c02492">https://doi.org/10.1021/acs.energyfuels.1c02492</a>

## Principal Author

Name of Principal Author (Candidate)	Mohsen Farrokhrouz		
Contribution to the Paper	Conception, Acquiring Data, Model Simulation, Experimental data matching with the model Knowledge, Analysis		
Overall percentage (%)	70%		
Certification:	This paper reports on original research I conducted during the period of my Higher Degree by Research candidature and is not subject to any obligations or contractual agreements with a third party that would constrain its inclusion in this thesis. I am the primary author of this paper.		
Signature		Date	22/07/2021

## Co-Author Contributions

By signing the Statement of Authorship, each author certifies that:

- i. the candidate's stated contribution to the publication is accurate (as detailed above);
- ii. permission is granted for the candidate to include the publication in the thesis; and
- iii. the sum of all co-author contributions is equal to 100% less the candidate's stated contribution.

Name of Co-Author	Dr Abbas Taheri		
Contribution to the Paper	Knowledge, Analysis, Drafting		
Signature		Date	22/07/2021
Name of Co-Author	Dr Alireza Keshavarz		
Contribution to the Paper	Knowledge, Analysis, Drafting		
Signature		Date	22/07/2021
Name of Co-Author	Prof Stefan Iglauer		
Contribution to the Paper	Knowledge, Analysis, Drafting		
Signature		Date	22/07/2021

Please cut and paste additional co-author panels here as required.

# Analytical Exact Solution for Co-Current Spontaneous Imbibition in Porous Media Considering Early- and Late-Time Effects

Mohsen Farrokhrrouz,\* Abbas Taheri, Stefan Iglauer, and Alireza Keshavarz



Cite This: <https://doi.org/10.1021/acs.energyfuels.1c02492>



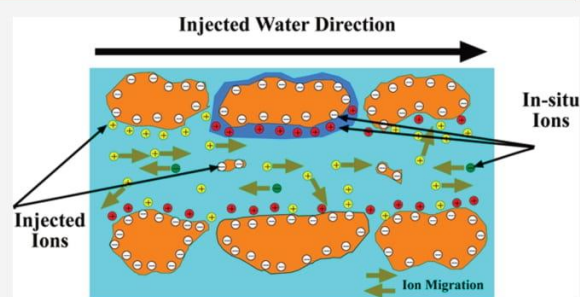
Read Online

ACCESS |

Metrics & More

Article Recommendations

**ABSTRACT:** Spontaneous imbibition (SI) of the wetting phase through the porous medium to displace the nonwetting phase is determined by capillary diffusion and injection fluid advection. This system is described using a transport equation of involved mechanisms and a pressure equation. The Buckley–Leverett solution is a particular case when capillary pressure is negligible. There are also analytical solutions available for cases with capillary diffusion as the dominant involved mechanism. In this study, a new mathematical model is developed to consider how both effects are significant. The model proposes an exact valid solution for both early-time (until the saturation front reaches effluent) and late-time imbibition. The accuracy of the model has been validated by comparing the suggested analytical model with numerical and experimental data. One of the advantages of the developed model is that despite the previous models, the injection rate does not need to be proportional to the square root of time, and other functional forms can be applied. Furthermore, the suggested analytical scheme is valid for strongly water-wet (SWW), weakly water-wet (WWW), and mixed-wet (MW) rock surfaces.



## 1. INTRODUCTION

Simultaneous flow of two immiscible fluids in porous media has long been of awareness in different earth science systems. When two phases are present in porous media, the displacement direction of each phase turns out to be significant. Two types of imbibition are defined, considering the displacement direction of each phase with respect to the other phase. Counter-current imbibition is a spontaneous process of wetting phase invasion into the medium and displacing the nonwetting phase in the opposite direction. This phenomenon appears to be significant in the recovery of fractured oil reservoirs where water moves rapidly within the fractures and surrounds the lower permeability matrix. Oil displacement in a low-permeability medium is mainly controlled by counter-current imbibition. There are a lot of studies focusing on experimental, theoretical, and numerical measurements of counter-current imbibition.<sup>1–5</sup>

There are also cases when wetting-phase displacement is parallel to nonwetting-phase displacement. This process is known as co-current spontaneous imbibition (SI), which is the focus of this study. In this process, the faces of the cores are coated, the wetting phase is flowed from one end, and the nonwetting phase is expelled from the other end. There are certain experimental studies dedicated to this type of imbibition.<sup>6–9</sup>

Both counter-current and co-current SI influence production recovery in fractured reservoirs. In a very specialized experimental study on Berea and chalk matrix blocks,<sup>10</sup> it was

usually observed that injected water did not fill the fracture channels around the matrix blocks rapidly. During this time, the recovery mechanism was mainly co-current imbibition. Once the wetting phase surrounded the matrix block, the oil recovery decreased to a great extent as the recovery mechanism changes to counter-current imbibition. Accordingly, investigation of both mechanisms is vital for recovery optimization in porous media, especially in fractured reservoirs.

On the other hand, the viscous flow of two different phases in porous media is also of interest for soil and groundwater contamination studies, as organic contaminant material penetrates lower soil layers as a solute of nonwetting agents (like gasoline or chlorinated solvents). This is still an active area of research, and many scholars proposed numerical and semianalytical solutions for co-current spontaneous imbibition.<sup>11–14</sup>

Due to the importance of this topic, apart from outlining governing equations, proposition of new solutions is still interesting. The objective of this study is to apply a new

Received: July 22, 2021

Revised: October 7, 2021



**Table 1.** Proposed Approaches for Saturation Solution at Counter-Current SI (CF: Solution along with Characteristic Function; MW: Mixed Wet; BC: Boundary Condition)

additional assumption	dimensionless time	reference
$\mu_n \ll \mu_w$	$T \propto \frac{\sigma r}{2L_c^2 \mu_w} t$	19, 20
$\mu_n \ll \mu_w$	$T \propto \frac{\sigma}{L_c^2 \mu_w} \cdot \sqrt{\frac{K}{\phi}} t$	21, 22
$\mu_n \approx \mu_w$	$T \propto \frac{\sigma}{L_c^2 \sqrt{\mu_w \mu_n}} \cdot \sqrt{\frac{K}{\phi}} t$	23
$\left(\frac{\lambda_w \lambda_n}{\lambda_t}\right)(S_w) \approx \left(\frac{\lambda_w \lambda_n}{\lambda_t}\right)_{CF}$	$T \propto \frac{\sigma}{L_c^2} \cdot \sqrt{\frac{K}{\phi}} \left(\frac{\lambda_w \lambda_n}{\lambda_t}\right)_{CF} \cdot t$	24
$MW: \lambda_w \ll \lambda_n$	$T \propto \frac{\sigma}{L_c^2} \cdot \sqrt{\frac{K}{\phi}} (\lambda_w)_{CF} \cdot t$	25
$F(x, t) = \frac{q_w(x_{CF}, t)}{q_w(0, t)}$	$T \propto \frac{\sigma}{L_c^2} \cdot \sqrt{\frac{K}{\phi}} \left(\frac{\lambda_w \lambda_n}{\lambda_t}\right)_{CF} \cdot J_{CF} \cdot (S_{BC} - S_0) \cdot t$	4
	$T \propto \left(\frac{2A}{\phi L_c}\right)^2 \cdot t$	6

methodology that does not have the shortcomings of previous approaches. This new methodology resulted in an exact analytical solution, and an explicit functional form of saturation front. This equational solution can be used for early-time imbibition (before wetting-phase breakthrough in the effluent) and predicting late-time saturation profile with modification of dimensionless time. Furthermore, contrary to previous studies, injection rate is not only the function of the square root of time, but other dependencies on time are also considered. Besides, the proposed solution function is examined by experimental and numerical measurements to highlight the accuracy and validity of the proposed method. Finally, the application of a new methodology in determining the breakthrough concentration of the solute in chemical flooding (surfactants, polymers, foams, etc.) or tracer will be presented with an exact solution.

## 2. PROBLEM FORMULATION

The partial differential equation stating the horizontal flow of two immiscible and incompressible fluids in one dimension has been derived by many authors since a long time ago.<sup>15–18</sup> The volume flux of the wetting phase is expressed as

$$q_w = f_w \cdot q_t - D(S_w) \frac{\partial S_w}{\partial x} \quad (1)$$

where  $q_w$  is the wetting phase flow,  $f_w$  is the fractional flow function,  $q_t$  is the total flux,  $D$  is the diffusivity coefficient,  $S_w$  is the water saturation, and  $x$  is the displacement. The capillary and hydraulic properties of two phases in the medium are reflected through functions of  $f_w$  and  $D(S_w)$ , respectively

$$f_w(S_w) = \frac{\frac{k_{rw}}{\mu_w}}{\frac{k_{rw}}{\mu_w} + \frac{k_{ro}}{\mu_o}} \quad (2)$$

$$D(S_w) = -\frac{k_{ro}}{\mu_o} \cdot f_w \cdot \frac{dp_c}{dS_w} \quad (3)$$

For two-phase immiscible, incompressible, isotherm flow through a rigid porous medium, the wetting phase  $w$  satisfies  $P = \rho_w q_w$  and eq 1 becomes

$$\phi \frac{\partial(\rho_w S_w)}{\partial t} = -\nabla \cdot (\rho_w q_w) \quad (4)$$

where  $w$  refers to the wetting fluid phase, which is usually water. Applying eqs 1 and 3 into eq 4 results in (constant  $\rho_w$ )

$$\phi \frac{\partial S_w}{\partial t} + q_t \frac{df_w}{dS_w} \frac{\partial S_w}{\partial x} = \frac{\partial}{\partial x} \left( \frac{k_{ro}}{\mu_o} \cdot f_w \cdot \frac{dp_c}{dS_w} \frac{\partial S_w}{\partial x} \right) \quad (5)$$

With the following initial and boundary conditions

$$S_w(\infty, t) = S_w(x, 0) = S_{wi}; \quad S_w(0, t) = 1 - S_{or} \quad (6)$$

where  $S_{wi}$  is initial water saturation and  $S_{or}$  is the residual oil saturation. It should be noted that eq 4 is a law meaning that it can be derived from the first principles. However, eq 1 is an assumption and cannot be derived from the first principles.

### 2.1. Contribution of Advection and Capillary Terms.

Total flow,  $q_t$  is the sum of the wetting-phase and nonwetting-phase fluxes. As the fluids are incompressible,  $q_t$  is not a function of  $x$ . For co-current displacements,  $q_t > 0$  is always valid, while for counter-current flows,  $q_t = 0$  since wetting phase and nonwetting phase flow in opposite direction ( $q_n = -q_w$ ).

Concerning eq 1, wetting phase flux is the sum of hydraulic and capillary terms, as stated before. Since  $q_t$  is space-invariant, the term  $f_w \cdot q_t$  is determined by injection rate on the boundary through Darcy's law (and the term  $k_{rw}/\mu_w$  which controls fractional flow function,  $f_w$ ). The term  $D(S_w)\partial S_w/\partial x$  is an additional force because of the capillary pressure gradient. The latter term was ignored by Buckley and Leverett<sup>15</sup> because of the large  $q_t$  and solved partial differential equations (PDE) by the method of characteristics. There were also further attempts of the Buckley–Leverett analogue with additional conditions.<sup>17</sup>

There were also cases that ignore the hydraulic term, and the capillary term is the only driving force (counter-current imbibition). Derivation of analytical solutions for this case has been investigated by many researchers over the last decades with several proposed solutions (see Table 1). The reason for such interest is clear: like Buckley–Leverett, analytical solution gives an overview of involved parameters for flow process control.

The third type of analytical solution is for the case that both hydraulic and capillary terms in eq 5 are considered. Most of these solution methodologies considered horizontal flow. The first exact analytic solution was proposed by Yortsos and Fokas<sup>18</sup> with constant  $q_t$  and predefined function for diffusivity coefficient as  $D = (\beta S_w + \gamma)^{-2}$  and derivative of fractional flow function  $df_w/dS_w = \alpha D$ , where  $\alpha$ ,  $\beta$ , and  $\gamma$  are arbitrary constants. Although such predetermined functions of  $D(S_w)$  and  $f_w(S_w)$  lead to the exact analytical solution, it is not suitable for most real cases in porous media. Earlier, Knight and Philip<sup>26</sup> declared that using the form of  $D = (\beta S_w + \gamma)^{-2}$  is the only function resulting in the exactly linearized solution of eq 7, providing that  $f_w = 0$ .

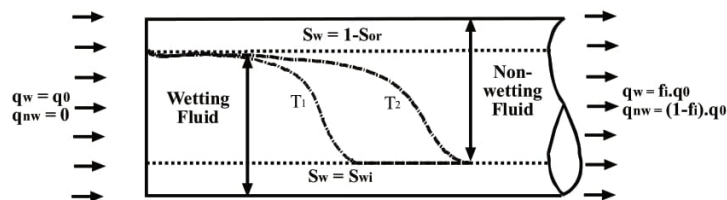


Figure 1. One-dimensional (1D) unidirectional spontaneous imbibition (modified from McWhorter and Sunada<sup>27</sup>).

**2.2. Incentive toward Analytical Solution.** Applying the concept of fractional flow function, an exact quasi-analytical solution for eq 5 was established.<sup>16</sup> As shown in eq 2, the ratio of wetting phase flow to total flow is defined as a fractional flow function. In this research,<sup>16</sup> it was proved that  $f_w$  can be a function of  $S_w$  only if a total flow ( $q_t$ ) is proportional to  $t^{-1/2}$ . A similar approach was proposed for the imbibition of wetting phase in the presence of inviscid air.<sup>26</sup>

The key exact integral solution for two-phase flow in porous media considering both hydraulic and capillary terms was later suggested.<sup>27</sup> In this methodology, in addition to eq 6, they proposed another boundary condition

$$q_0 = q_w(0, t) = At^{-1/2} \quad (7)$$

where  $A$  is a constant and  $t$  denotes time. For every prescribed value of  $A$ , there is a constant value of  $S_w(0, t)$  and calculation of dependence of  $(1 - S_{or})$  on  $A$  is a significant part of experimental work. During the experiment, the pump should be positive displacement and the discharge rate needs to be proportional to  $t^{-1/2}$ . A schematic of co-current displacement by injecting the wetting phase to the core is shown in Figure 1.

A brief explanation of this solution approach is presented in Appendix A. Detailed methodology of integration and deriving the exact value of  $A$  can be found in the same reference. The final value of  $F$  is attained by iteration and after using the first guess (which is usually  $F = 1$ ). There are also some modified proposed methods for faster convergence.<sup>28,29</sup> For counter-current displacement, the same approach is still valid, and as  $R = 0$ ,  $f_n$  in eq A7 will be zero, and it will be removed from eq A9. As it is found, no function is portrayed for  $F$  and the function is made as a continuous estimation of points at each saturation value.

A fundamental shortcoming of this solution methodology is that the injection rate should be proportional to  $t^{-1/2}$ . According to Hu et al.,<sup>30,31</sup> imbibition into rocks is a function of pore connectivity and imbibition front does not always move with the square root of time. The first model for front imbibition in the porous medium was introduced by Lucas<sup>19</sup> and Washburn,<sup>20</sup> and this model is known as the Lucas–Washburn equation (LWE). Most of the researchers focused on LWE due to its simplicity and attempted to promote it to some extent,<sup>32,33</sup> but still some deviations existed with experimental results. They pointed out that irregular structure and complicated pathway of the pores inside the porous medium are the main reasons for this deviation. Some other researchers attempted to define and measure these parameters including roughness, specific surface area, effective capillary force,<sup>34</sup> and apparent contact angle<sup>35</sup> and acclaimed that they all play roles in imbibition. While these proposed models still did not match completely with LWE, Dimitrov et al.<sup>36</sup> modified the Lucas–Washburn equation using molecular dynamics evidence for coarse-grained models (i.e., roughness). Considering nanostructured roughness, Girardo et al.<sup>37</sup> and Kusumaatmaja et al.<sup>38</sup> employed lattice Boltzmann and

molecular kinetics model, respectively. Their experimental data showed good agreement with modified LWE and not the conventional LWE. Liu et al.<sup>39</sup> showed that model fitting of experimental data for simplistic but long-accepted LWE is valid when the mass of liquid imbibed is very low and capillary pressure at nano- and microscale is very much higher than gravity effect.

Considering all of these studies, the proposed approach by McWhorter and Sunada<sup>27</sup> cannot cover all of the ranges of fluid imbibition functions, and a more precise analytical solution is required. Figure 2 shows the plot of experimental measurements

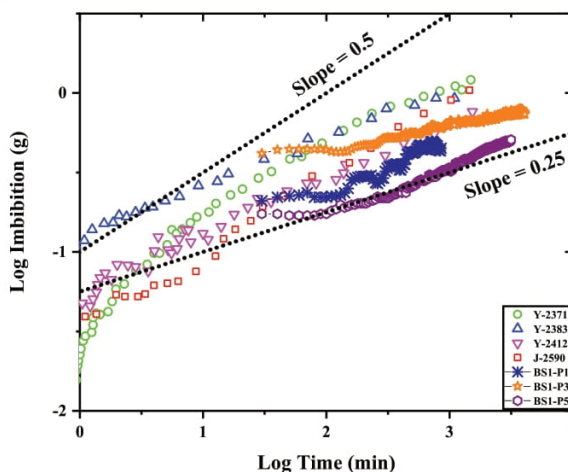


Figure 2. Effect of pore connectivity on imbibition behavior. The data were obtained from Yang et al.<sup>40</sup> for different Chinese shale samples, and Berea sandstones results are obtained from the experimental data in this study (BSI-P1, P3, and P5).

of imbibition front movement versus time. As it can be observed, saturation front within the porous media may imbibe at different time functions depending on the pore connectivity of the medium.

### 3. EXPERIMENTAL SETUP

Three core samples of Berea sandstone were prepared for the co-current imbibition test. Porosity and permeability of the samples were measured using the helium porosimeter facility provided by the CoreLab standard porosimeter. The rock–fluid interaction parameters (including relative permeability curves and capillary pressure entry values) for nitrogen as a nonwetting phase and 2% KCl brine as a wetting phase for Berea sandstone samples were obtained from the literature.<sup>41</sup> The core samples were clean experimental ones using as intact laboratory samples. To create a co-current fluid displacement, the circumferential areas of the core samples were covered with epoxy to prevent any imbibition in radial direction, and imbibition takes place in a one-dimensional order across the cylinder height and perpendicular to the cylinder base. Then, the core sample was suspended from a balance



(FZ-iW500 Series) and the weight of the submerged sample was recorded continuously using WinCT software provided by the producer (Figure 3). The brine used in the experiments was 2% KCl

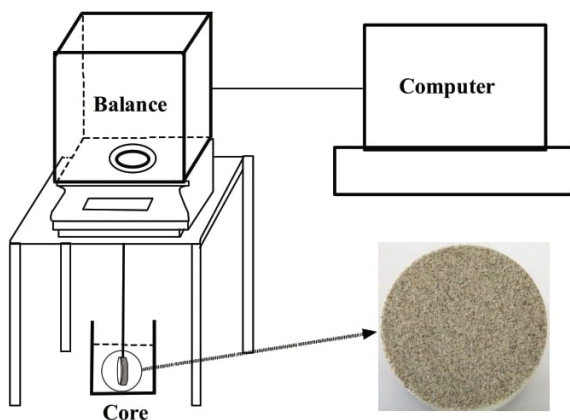


Figure 3. Schematic of the test setup used for co-current spontaneous imbibition (COCSI) of Berea sandstone samples.

solution. The nonwetting phase in these experiments was air. The tests were repeated for all four samples, and the results obtained are shown in Figure 6.

Combining eq 7 and A3 with the definition of  $R$  ( $R = 1$  for co-current imbibition) as well as a self-similar variable  $\lambda = x \cdot t^{-1/2}$ , the value of "A" can be determined<sup>27</sup>

$$q_0 = - \left. \frac{D(S_{w,BC})}{1 - f(S_{w,BC})R} \frac{dS_w}{d\lambda} \right|_{\lambda=0} t^{-1/2} = At^{-1/2} \quad (8)$$

#### 4. NOVEL SOLUTION METHODOLOGY CONSIDERING SOLUTE TRANSPORT

As described in the above section, previously proposed analytical solutions for two-phase flow in porous media were confined by specific functions of some involved parameters or additional assumptions. Although these solutions are still valid for a range of practical circumstances, they are still considered as restrictions for a general solution.

**4.1. Mathematical Formulation of New Method.** To overcome some of these restrictions and present a more general solution, a new approach was selected. As the wetting phase is injected into the medium, two continuity equations would be valid due to the difference in two parameters: one for saturation and the other for the concentration of the particles. These particles might be salinity, polymer, surfactant, or tracer. The set of equations is

$$\begin{cases} \phi \frac{\partial S_w}{\partial t} + \frac{\partial q_w}{\partial x} = 0 \\ \phi S_w \frac{\partial c}{\partial t} + q_w \frac{\partial c}{\partial x} = 0 \end{cases} \quad (9)$$

Definition of Leverett J-function<sup>42</sup>

$$J(S_w) = \frac{P_c(S_w)}{\sigma \cos \theta \sqrt{K}} \quad (10)$$

The form of imbibition equation for horizontal displacement (neglecting gravity effect) and introducing J-function changes eq 1 to

$$q_w = f_w q_t + \frac{\sigma \cos \theta \sqrt{K\phi}}{\mu_o} [f_w(S_w) \cdot k_{ro}(S_w) \cdot J'(S_w)] \frac{\partial S_w}{\partial x} \quad (11)$$

Therefore, the set of eq 9 will be  $(\Phi(S_w) = f_w(S_w) \cdot k_{ro}(S_w) \cdot J'(S_w))$

$$\begin{cases} \phi \frac{\partial S_w}{\partial t} = - \frac{\partial}{\partial x} \left[ f_w \cdot q_t + \frac{\sigma \cos \theta \sqrt{K\phi}}{\mu_o} \cdot \Phi(S_w) \cdot \frac{\partial S_w}{\partial x} \right] \\ \phi S_w \frac{\partial c}{\partial t} = - \left[ f_w \cdot q_t + \frac{\sigma \cos \theta \sqrt{K\phi}}{\mu_o} \cdot \Phi(S_w) \cdot \frac{\partial S_w}{\partial x} \right] \frac{\partial c}{\partial x} \end{cases} \quad (12)$$

Bringing in mind that as in Figure 2, imbibition front may flow with different functions of time ( $q_0 = q_w(0,t) = At^{-1/m}$ ,  $2 < m < 4$ ), both sides are divided over  $q_t$

$$\begin{cases} \frac{\phi \sqrt[m]{t} \partial S_w}{A \partial t} = - \frac{\partial}{\partial x} \left[ f_w + \frac{\sigma \cos \theta \sqrt[m]{t} \cdot \sqrt{K\phi}}{A \cdot \mu_o} \cdot \Phi(S_w) \cdot \frac{\partial S_w}{\partial x} \right] \\ \frac{\phi \sqrt[m]{t} S_w \partial c}{A \partial t} = - \left[ f_w + \frac{\sigma \cos \theta \sqrt[m]{t} \cdot \sqrt{K\phi}}{A \cdot \mu_o} \cdot \Phi(S_w) \cdot \frac{\partial S_w}{\partial x} \right] \frac{\partial c}{\partial x} \end{cases} \quad (13)$$

It should be reminded that the unit of A depends on the order of time with regard to the pore connectivity concept as proposed by Hu et al.<sup>30,43</sup> The unit of the total flow in the inlet for 1D displacement,  $q_0$ , is

$$\begin{aligned} q_t = q_0 = At^{-1/m} &\Rightarrow [LT^{-1}] = [A][T^{-1/m}] \\ \Rightarrow [A] &= \frac{[LT^{-1}]}{[T^{-1/m}]} = \frac{[L]}{[T^{1-1/m}]} \end{aligned} \quad (14)$$

A parameter  $\varepsilon$  is identified like below with the dimension of

$$[\varepsilon] = \left[ \frac{\sigma \cos \theta \sqrt[m]{t} \cdot \sqrt{K\phi}}{A \cdot \mu_o} \right] = \frac{[MT^{-2}][T^{1/m}][L]}{[LT^{-1+1/m}][ML^{-1}T^{-1}]} = [L] \quad (15)$$

We brand a new parameter like this

$$\tau = \frac{m}{m-1} \cdot \frac{A}{\varphi \cdot L} \cdot t^{1-1/m} \rightarrow \partial \tau = \frac{A}{\varphi L \sqrt[m]{t}} \partial t \quad (16)$$

The dimension of this new parameter is

$$\tau = \frac{m}{m-1} \frac{A}{\varphi L} t^{1-1/m} \rightarrow [\tau] = \frac{[LT^{-1+1/m}][T^{1-1/m}]}{[L]} = 1 \quad (17)$$

And with dimensionless length defined as  $X = x/L$ , after replacing in eq 13

$$\begin{cases} \frac{\partial S_w}{\partial \tau} = - \frac{\partial}{\partial X} \left[ f_w + \left( \frac{\varepsilon}{L} \right) \cdot \Phi(S_w) \cdot \frac{\partial S_w}{\partial X} \right] \\ S_w \frac{\partial c}{\partial \tau} = - \left[ f_w + \left( \frac{\varepsilon}{L} \right) \cdot \Phi(S_w) \cdot \frac{\partial S_w}{\partial X} \right] \frac{\partial c}{\partial X} \end{cases} \quad (18)$$

reminding that all of the terms of  $[\varepsilon/L]$ ,  $[\tau]$ , and  $[X]$  are dimensionless parameters. The solution methodology is presented in Appendix B. The final equation form proposed for the  $\zeta$  function is like eq B15. The integral solution results in definite equation form based on selected capillary pressure

function and nonwetting relative permeability function. However, there is not a universal functional form for capillary J-function and relative permeability curves.<sup>44,45</sup>

For example, the following equations have been recommended for capillary pressure and nonwetting phase relative permeability<sup>46</sup>

$$k_{ro} = k_{ro}^0(1 - S)^{n_0} \quad (19)$$

$$P_c = -B \ln(S) \quad (20)$$

In eqs 19 and 20, the parameters  $k_{ro}^0$ ,  $n_0$ , and  $B$  are constant values and  $S$  is the normalized saturation as the following equity

$$S = \frac{S_w - S_{wi}}{1 - S_{or} - S_{wi}} \quad (21)$$

According to the definition of J-function as in eq 10, eq 20 changes to

$$J'(S_w) = -B \frac{\sqrt{K}}{\sigma \cos \theta \sqrt{\varphi}} \frac{1}{S_w} \quad (22)$$

Introducing the integration interval using eq B15 and functional forms of eqs 19 and 22 and constant values reported by Pooladi-Darvish and Firoozabadi<sup>46</sup> ( $n_0 = 4.0$ ,  $B = 10$  kPa,  $k_{ro}^0 = 0.75$ ), we have

$$\begin{aligned} \zeta &= \left( \frac{k_{ro}^0 \cdot \varepsilon \cdot B \cdot \sqrt{K}}{L \cdot \tau \cdot \sigma \cos \theta \cdot \sqrt{\varphi}} \right) \int_0^1 \left[ \frac{(1 - S)^4}{S} - C_2 \right] dS + C_3 \\ \Rightarrow \zeta &= \left( \frac{k_{ro}^0 \cdot \varepsilon \cdot B \cdot \sqrt{K}}{L \cdot \tau \cdot \sigma \cos \theta \cdot \sqrt{\varphi}} \right) \left[ \ln(S) + \frac{S^4}{4} - \frac{4S^3}{3} + 3S^2 \right. \\ &\quad \left. - (4 + C_2)S \right] \quad (23) \end{aligned}$$

The value of  $C_3$  is equal to zero using the initial condition, and the value of  $C_2$  is determined based on boundary conditions at different  $X$  values considering eq B15. For instance, at late times, the derivative of  $dS_w/d\zeta$  is close to zero and the value of  $C_2$  can be considered as zero. For early times, this value is very important as the slope of  $S_w$  in  $\zeta$  domain is very large.

As it is observed, in comparison with previous analytical solutions, there is a clear functional form available for  $\zeta$ , and the saturation changes can be predicted at any time and place, accordingly. For instance, at the core outlet,  $X = 1 \rightarrow \zeta = 1/\tau$  and eq 23 may be used for plotting saturation profile versus time. This form of equation for saturation front has been proposed for the first time. It should be reminded again that different correlations have been suggested for relative permeability and capillary pressure functions, and other equational forms will result in various explicit forms of the  $\zeta$  function. Therefore, there would be no unique equational form of solution due to such variety in relative permeability correlations. Furthermore, the solution must be proposed for both early and late times; this was suggested in recent studies and will be discussed in the next section

## 5. MODEL VERIFICATION AND INTERPRETATION OF RESULTS

Apart from complex mathematical solutions, it is crucial to validate the cogency of the mathematical model with other approaches and experimental results. The most common approach selected by industrial companies and practical

researchers is the numerical calculation of partial differential equations (PDE) through numerical math methods. However, it is still necessary to have a benchmark for numerical methods. This benchmark is usually derived for one-dimensional model, and it can be validated with experimental results. We selected the same methodology for our exact mathematical solution.

**5.1. Model Validation with Numerical Solution.** In the view of a semianalytical method proposed by McWhorter and Sunada,<sup>27</sup> a numerical scheme was proposed by Schmid<sup>6</sup> as a fast and straightforward method for calculation of fractional flow function ( $F$ ). In their numerical approach, an approximate value for  $F''$  is estimated, and for a continuous range of saturation,  $F(S_w)$  is determined. Since  $F$  also depends on the constant  $A$ , iteration for estimation of  $A$  is required. As  $F = 1$  at the core inlet (at maximum water saturation), iteration on estimation of  $A$  is repeated until  $F(x = 0, t) = 1$ . Detailed numerical scheme calculated by Schmid<sup>6</sup> is presented in Appendix C.

This numerical scheme is a practical and straightforward utilization of the previously suggested semianalytical method.<sup>27</sup> As explained, still some presumptions and initial guess are required for solution. However, according to data in Table 2, the

**Table 2. Input Parameters for the Numerical Scheme and Exact Analytical Solution Considering Co-Current Imbibition with Mixed Wettability (Data Provided by Schmid<sup>6</sup>)**

rock wettability	mixed-wet case
initial water saturation	0.2
residual oil/water saturation	0.2
$k_{rw \max}$	0.5
$k_{ro \max}$	0.8
entry capillary pressure (Pa)	12 000
maximum capillary pressure (Pa)	400 000
water viscosity (Pa·s)	0.001
oil viscosity (Pa·s)	0.003
permeability (mD)	300
porosity	0.2
interfacial tension (N/m)	0.050

result of the exact solution proposed in this study and the numerical scheme suggested by Schmid<sup>6</sup> are in very good agreement (Figure 4). It is worth mentioning that in their model, they considered injected water influx proportional to the square root of time. Therefore, in Figure 4, the square root of time is shown for the  $x$ -axis.

**5.2. Model Validation with Experimental Results.** A suitable analytic model should also cover the scatter of experimental results with an acceptable error range. Utilization of experimental co-current spontaneous imbibition (COCSI) requires rock–fluid interaction data, including capillary pressure curves as well as wetting and nonwetting relative permeability curves. Data obtained from the experimental section were selected to plot against the mathematical model. Additionally, experimental results provided by Mirzaei-Paiaman et al.<sup>47</sup> were included for data matching. In their study, they applied a history matching-based computation technique to determine relative permeability and capillary pressure functions. Initially, this method was recommended for counter-current spontaneous imbibition (COUCSI). Then, they changed boundary conditions and used this method for one-dimensional COCSI.<sup>47</sup> Corresponding relative permeability curves and capillary pressure of experiments are given as well. The residual oil



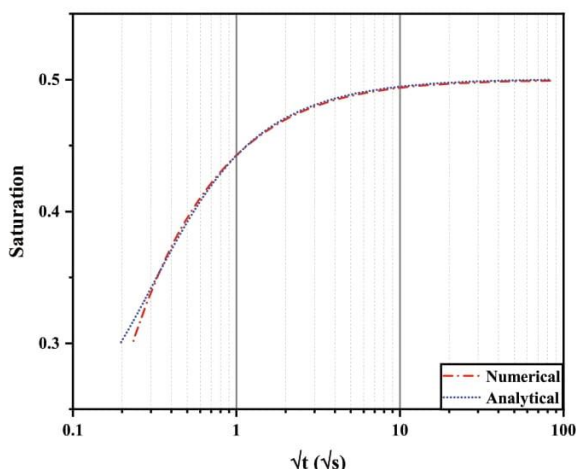


**Figure 4.** Numerical and analytical exact solutions for co-current imbibition showing saturation versus self-similar function (data in Table 2).

saturation in this series of tests was independent of wetting-phase viscosity, which was confirming previous experimental results.<sup>48,49</sup>

The effect of boundary conditions was also considered for matching the experimental data. In COUCSI, those faces permeable to flow are surrounded by wetting phase in a porous medium. As a result, each flowing face has a respective no-flow boundary.<sup>50</sup> The situation for COCSI process is rather complex. First, a part of the permeable face is in front of the wetting phase, and the remaining is in contact with the nonwetting phase. Second, in COCSI, different faces are chosen as no-flow boundaries or flow boundaries. Considering rock–fluid properties and reservoir rock data,<sup>47,51,52</sup> different boundary conditions (Figure 5) resulted in experimental matching with the mathematical model given in Figure 6 using the matching procedure as already applied.<sup>53–55</sup> As the experimental matching in Figure 6 confirms, boundary condition and direction of flow have no effect on the accuracy of the mathematical solution presented in this study, and it is another positive point of this methodology. Because the solution approach does not depend

on these parameters, and they are only affected by fluid–rock interaction functions.

There is another significant feature of the mathematical model to be emphasized in Figure 6. The mathematical solution matches the experimental data points in some of the experiments (i.e., MP2–MP9, EH1–EH2, EH9–EH10) properly and within a 5% error range. For some of the experimental data points, it matches early-time data values, and for the rest of the data points, the error range exceeds 5%.

The reasoning behind this observation is already discussed.<sup>13,14</sup> According to these studies, two terms of advection and capillary diffusion are competing inside the porous medium. At early times (till the front reaches the effluent), both capillary and advection terms contribute to front displacement within the rock. The proposed mathematical exact solution in this study, fully covers such behavior as it includes these terms inside the equation.

The time when the front reaches effluent is determined as critical time.<sup>13,14</sup> After this time, the solution changes to the Buckley–Leverett profile as the injected fluid displaces continuously inside the medium and displaces at the effluent. The following equation can calculate this critical time

$$t_c = \frac{\sqrt{\frac{\phi}{K}} L^2 \left[ \frac{1}{\lambda_r^*} + \frac{1}{\lambda_o(S_{wr})} \right]}{2\sigma f'_w [J_{S_{wr}} - \Delta J^*]} \quad (24)$$

However, there are some studies in the literature showing that at some critical rates (depending on the rock type, fluid viscosity, and wettability characteristics), relative permeability curves may not be obtained.<sup>56</sup> There are also some other minor parameters<sup>57,58</sup> that can be easily ignored as the extent of their effect is negligible.

The Buckley–Leverett profile can also be dissolved from eq 18. Ignoring the capillary term in this equation is equal to assuming  $\varepsilon \approx 0$ . Then, this equation reduces to

$$\begin{cases} \frac{\partial S_w}{\partial \tau} = -\frac{df_w}{dS_w} \frac{\partial S_w}{\partial X} \\ S_w \frac{\partial c}{\partial \tau} = -f_w \frac{dc}{dS_w} \frac{\partial S_w}{\partial X} \end{cases} \quad (25)$$

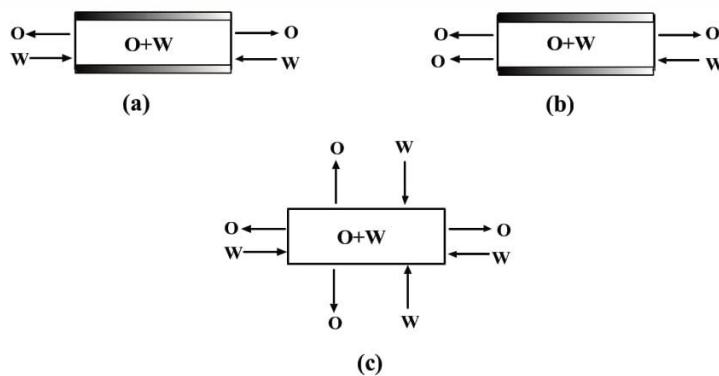


**Figure 5.** Schematic of COCSI types in this study: (a) one-dimensional, (b) two-dimensional, (c) multidimensional; the direction of wetting phase (W) imbibition into the medium and the direction of nonwetting (O) phase expelled from the medium determine the dimension of each imbibition mechanism.

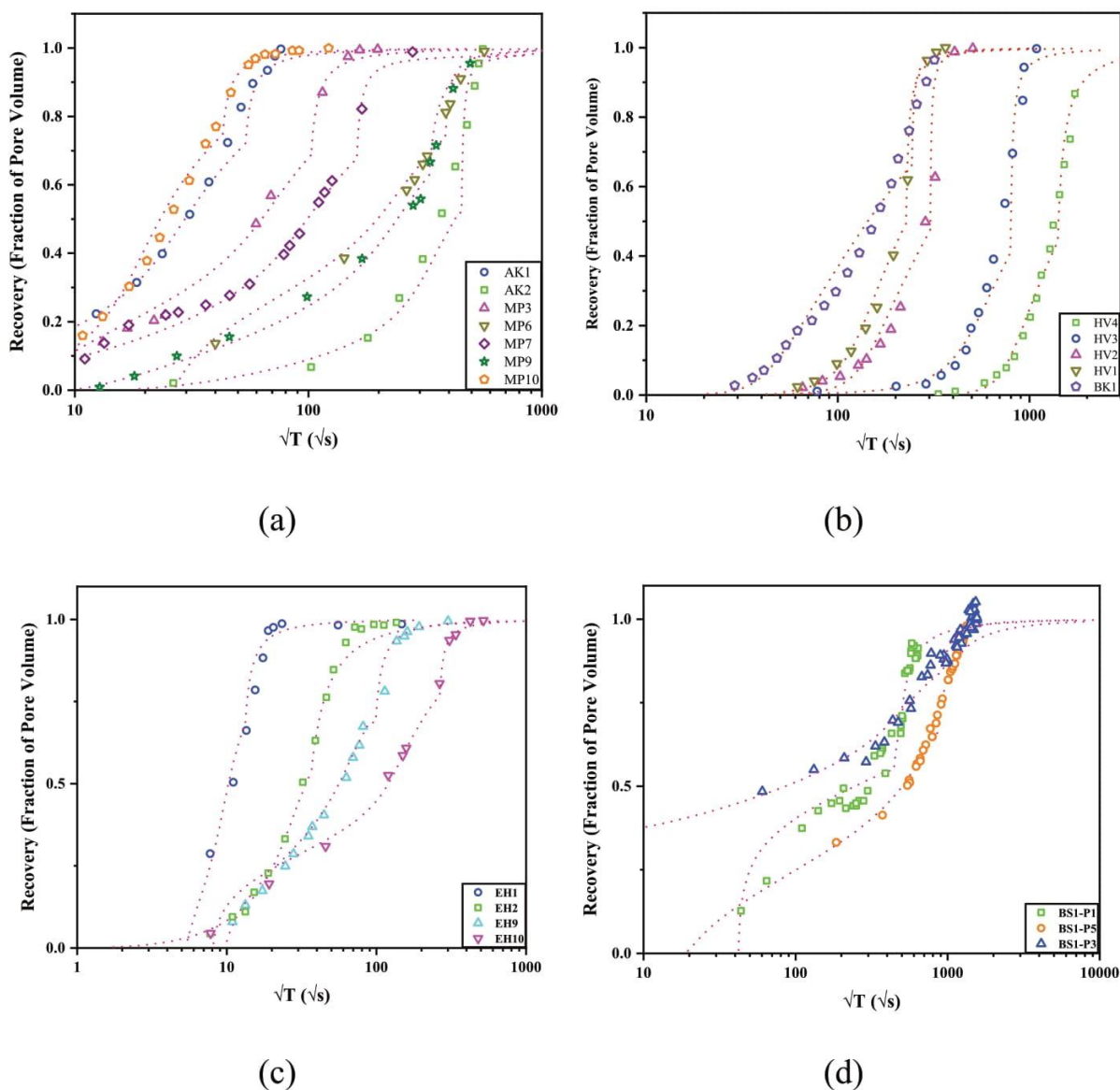


**Figure 6.** Matching experimental and analytical exact solutions for co-current imbibition showing saturation versus square root of time for data in Table 3: (a) one-dimensional, (b) two-dimensional, (c) multidimensional, and (d) author's data.

Applying self-similar function in any arbitrary form  $\psi(X, \tau) = f(X, \tau)$

$$\begin{cases} \frac{\partial S_w}{\partial \psi} \left( \frac{d\psi}{d\tau} + \frac{df_w}{dS_w} \frac{d\psi}{dX} \right) = 0 \\ S_w \frac{\partial c}{\partial \psi} \frac{d\psi}{d\tau} = -f_w \frac{\partial c}{\partial \psi} \frac{d\psi}{dX} \end{cases} \quad (26)$$

Replacing eqs 26.b in 26.a

$$\frac{\partial S_w}{\partial \psi} \left( -\frac{f_w}{S_w} \frac{d\psi}{dX} + \frac{df_w}{dS_w} \frac{d\psi}{dX} \right) = 0 \Rightarrow \frac{df_w}{dS_w} = \frac{f_w}{S_w} \quad (27)$$

The result obtained from eq 27 reveals that saturation front breakthrough is at the point where the derivative of fractional flow function ( $f'$ ) is equal to the ratio of fractional flow function over the saturation ( $f/S_w$ ) at the same point. This is a great finding of this study in comparison to similar researches and makes a great promotion in this area. Furthermore, applying this method shows good agreement with experimental data points as in Figure 6.

## 6. ANALYTICAL SOLUTION FOR SOLUTE TRANSPORT IN IMMISCIBLE TWO-PHASE FLOW

There are cases that flooding fluid contains dissolved material, and displacement of nonwetting phase by wetting phase is followed by transport of solute materials. Examples of these cases are polymer flooding, surfactant injection, foams, and/or

Table 3. Experimental Data for Strongly Water-Wet Core Samples Presented by Different References Given in the Table

reference	wettability	test code	imbibition type	$S_{wi}$	$L$ (m)	$K$ ( $m^2$ )	$\phi$	$\mu_{nw}^*$ (Pa·s)	$\mu_{nw}$ (Pa·s)	$\sigma$ (N/m)	end point $k_{rw}$	end point $k_{nw}$	max. $P_c$ (rPa)	$A$ ( $m/\sqrt{s}$ )
47, 51	strongly water-wet sandstone	MP3	ID	0.00	0.03830	$1.1202 \times 10^{-12}$	0.2278	0.0180	0.00113	0.049	1.00	0.088	14.59	$2.6 \times 10^{-5}$
		MP6	ID	0.00	0.06075	$5.1336 \times 10^{-13}$	0.1936	0.0180	0.00113	0.049	1.00	0.16	14.93	$7.0 \times 10^{-6}$
		MP7	ID	0.00	0.04924	$3.1400 \times 10^{-14}$	0.1351	0.0010	0.00113	0.049	1.00	0.235	20.56	$9.0 \times 10^{-6}$
		MP9	ID	0.00	0.04924	$3.1400 \times 10^{-14}$	0.1351	0.0010	0.00113	0.049	1.00	0.235	20.56	$3.0 \times 10^{-6}$
		MP10	ID	0.00	0.05119	$1.9683 \times 10^{-13}$	0.2451	0.0010	0.00113	0.049	1.00	0.195	24.47	$6.8 \times 10^{-5}$
		EH1	MD	0.00	0.01700	$1.1202 \times 10^{-12}$	0.2278	0.0010	0.00113	0.049	1.00	0.088	14.59	$8.8 \times 10^{-5}$
		EH2	MD	0.00	0.01700	$5.1336 \times 10^{-13}$	0.1936	0.0010	0.00113	0.049	1.00	0.16	14.93	$2.8 \times 10^{-5}$
		EH9	MD	0.00	0.01700	$1.9683 \times 10^{-13}$	0.2451	0.0033	0.00113	0.049	1.00	0.195	24.47	$4.2 \times 10^{-5}$
		EH10	MD	0.00	0.01700	$1.9683 \times 10^{-13}$	0.2451	0.0180	0.00113	0.049	1.00	0.195	24.47	$1.2 \times 10^{-5}$
		59	strongly water-wet chalk	AK1	ID	0.00	0.095	$7.0 \times 10^{-15}$	0.69	0.001	0.0000182	0.072	1.00	0.09
AK2	ID			0.00	0.095	$7.0 \times 10^{-15}$	0.69	0.001	0.00084	0.0514	1.00	0.15	200.4	$4.6 \times 10^{-5}$
8	weakly water-wet strongly water-wet	BK1	2D	0.39	0.29	$1.37 \times 10^{-13}$	0.23	0.0012	0.0015	0.035	0.47	0.06	12.5	$2.6 \times 10^{-5}$
		HV1	2D	0.35	0.097	$1.8 \times 10^{-15}$	0.27	0.001	0.0115	0.049	0.98	0.14	480.1	$9.5 \times 10^{-6}$
7	strongly water-wet	HV2	2D	0.35	0.199	$2.0 \times 10^{-15}$	0.28	0.001	0.0115	0.049	0.97	0.12	461.2	$1.7 \times 10^{-5}$
		HV3	2D	0.36	0.498	$2.0 \times 10^{-15}$	0.277	0.001	0.0115	0.049	0.95	0.10	458.5	$2.0 \times 10^{-5}$
this study	mixed-wet sandstone	HV4	2D	0.36	0.848	$1.6 \times 10^{-15}$	0.274	0.001	0.0115	0.049	0.95	0.12	512.8	$1.7 \times 10^{-5}$
		BS-P1	2D	0.00	0.0052	$1.48 \times 10^{-15}$	0.2646	0.001	0.000019	0.070	0.95	0.12	295.6	$7.2 \times 10^{-5}$
		BS-P3	2D	0.00	0.0044	$1.48 \times 10^{-15}$	0.2830	0.001	0.000019	0.070	0.95	0.12	295.6	$4.7 \times 10^{-5}$
		BS-P5	2D	0.00	0.0047	$1.48 \times 10^{-15}$	0.2915	0.001	0.000019	0.070	0.95	0.12	295.6	$8.4 \times 10^{-4}$



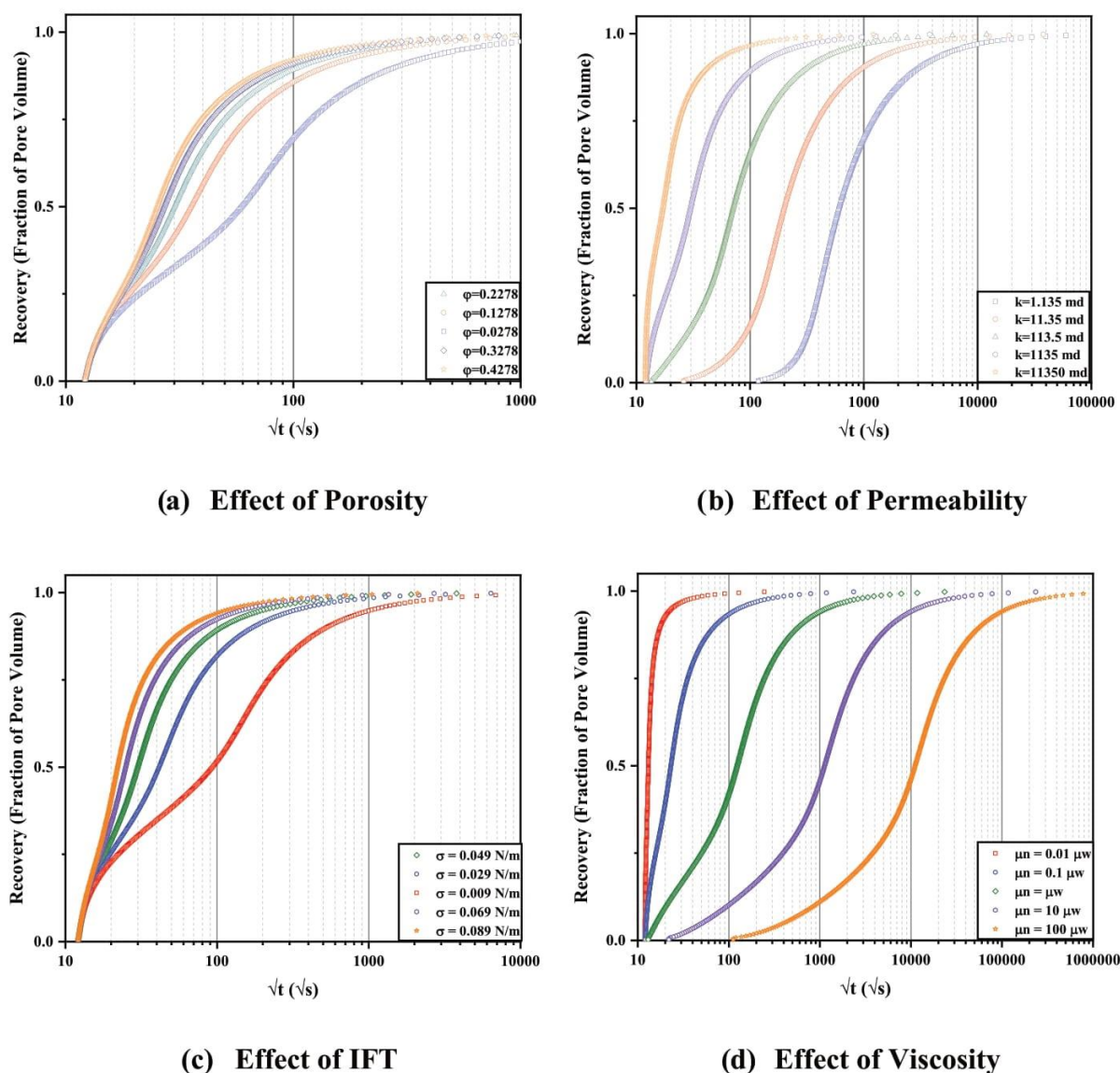


Figure 7. Effect of different parameters on the saturation front recovery factor.

tracers. During such operations, dissolved material affects the viscosity of the wetting phase and, as a result, its relative permeability and fractional flow function (eq 2). The assumptions for such components are like below:

- i. They do not alter the porous medium (through chemical reactions);
- ii. They are not partitioning into the other phase;
- iii. Solute mass flux due to hydrodynamic dispersion within a phase is described by the Fickian model;
- iv. The volume fraction of the components is small compared to that of the wetting phase.
- v. The only chemical interaction between the rock and the components should be classified into equilibrium adsorption.<sup>60</sup>

Considering the set of equations as in eq 18, solution for concentration is obtained using the second term

$$S_w \frac{dc}{d\zeta} \left( -\frac{\zeta}{\tau} \right) = - \left[ f_w + \left( \frac{\varepsilon}{L} \right) \cdot \Phi(S_w) \cdot \frac{dS_w}{d\zeta} \right] \frac{dc}{d\zeta} \frac{1}{\tau}$$

$$\Rightarrow \frac{dc}{d\zeta} \left[ -\zeta S_w + f_w + \left( \frac{\varepsilon}{\tau \cdot L} \right) \cdot \Phi(S_w) \cdot \frac{dS_w}{d\zeta} \right] = 0 \quad (28)$$

A solution is a case that  $dc/d\zeta = 0$  was not considered for our case. The other solution is the case when the value within the bracket is zero. The term  $dS_w/d\zeta$  from eq B14 is  $\omega = \frac{dS_w}{d\zeta} = \frac{L \cdot \tau}{\varepsilon \cdot \Pi(S_w)} + C_2$ , and applying this value in eq 28 results in

$$\zeta = \frac{f_w}{S_w} + \left( \frac{\varepsilon}{\tau \cdot L} \right) \cdot \frac{\Phi(S_w)}{S_w} \cdot \left( \frac{\tau \cdot L}{\varepsilon} \right) \cdot \left[ \frac{1}{\Pi(S_w)} + \frac{\varepsilon \cdot C_2}{\tau \cdot L} \right] \Rightarrow \zeta$$

$$= \frac{f_w}{S_w} \left( 1 + \frac{\varepsilon \cdot C_2}{\tau \cdot L} \right) \quad (29)$$

The value of  $C_2$  is determined according to boundary conditions (eq 9c). The final equivalent for  $\zeta$  in eq 29 is consistent with simpler results of polymer flooding introduced by Pope<sup>57</sup> for the Buckley–Leverett<sup>15</sup> solution approach and Schmid<sup>6</sup> for both convective and capillary solution forms.

## 7. SENSITIVITY ANALYSIS

Careful consideration of eq B15 in Appendix B reveals that the term  $\varepsilon/(L \cdot \tau)$  controls the value of  $\zeta$  and consequently  $X$  and  $T$ . Again, this term is reminded as

$$\frac{\varepsilon}{L \cdot \tau} = \frac{(m-1)\sigma \cos \theta (\sqrt{K\phi^3})(\sqrt{\tau})}{m A^2 \mu_0 \cdot (t^{1-1/m})} \quad (30)$$

Referring to eq 17, it can be concluded that the term  $(L \cdot \tau)$  is independent of the length, meaning that as far as the gravity is negligible (horizontal medium), the length of the core has no effect on the continuity equation. The term in eq 30 also contains time and, for example, for  $m = 2$ , time can be removed. The remaining parameters are rock–fluid interaction parameters, comprising as interfacial tension, contact angle, porosity, permeability, nonwetting fluid viscosity, and parameter  $A$ . The competing parameter in this ratio is the capillary diffusion term to the advection term. The higher the numerator, capillary behavior is dominant, and the higher the denominator, the advection term is dominant.

Technically speaking, lower porosity and permeability imply a slower movement of the saturation front within the porous medium, as the pore throats are smaller and less in comparison with a highly permeable medium. Accordingly, for a lower porous and permeable medium, a longer time is required for the saturation front to displace all nonwetting phase already within the medium. This simple hypothesis can be easily seen in Figure 7a,b.

Secondly, the interfacial tension is between the wetting phase and the walls of the pores. High interfacial tension (IFT) means a higher tendency of the fluid to settle on the pore surface. It can also be interpreted as a lower wettability angle. Therefore, nonwetting phase can be evacuated from the medium easily and maximum recovery factor is attained at earlier times. For lower IFT values, the wetting and nonwetting phases might be mixed inside the pores as the tension between the fluid phase and solid surface is not high enough (Figure 7c,d). Subsequently, complete transposition of the nonwetting phase requires higher injected pore volumes and longer time for maximum recovery factor.

The effect of nonwetting phase viscosity is also like the interfacial tension effect. When the nonwetting viscosity is very low, it can be easily removed from the pore volume, and the recovery factor sharply increases to a maximum value. For the very viscous nonwetting phase, the recovery factor is lower at a certain time, meaning that it takes a longer time to reach maximum recovery during flooding.

## 8. CONCLUSIONS

The newly proposed exact solution in this study used a new approach that resulted in a functional form of solution front

profile within the porous medium. Compared with previously proposed methods, this method is a fully analytical solution, and an explicit functional form can be achieved. Application of the analytical scheme with experimental results showed good agreement at early times. For late times (when saturation front reaches the effluent), another simple and sensible solution methodology was suggested with an outstanding agreement with experimental results. This approach is also applicable for the estimation of the concentration front within the medium. Besides, the analytical model proposed is valid for one-dimensional, two-dimensional, and multidimensional co-current spontaneous imbibition.

Sensitivity analysis of the effective parameters also showed that recovery factor reaches a maximum at higher porosity, permeability, wetting phase viscosity, and interfacial tension of the wetting phase and rock surface.

## APPENDIX A

Exact quasi-analytical solution can be achieved by defining a fractional flow function like below<sup>16</sup>

$$F(x, t) = \frac{q_w/q_0 - f_i R}{1 - f_i R} \quad (A1)$$

$R = q_t/q_0$  defines the direction of movement for two phases: for co-current displacement,  $q_t = q_0$  and  $R = 1$ . For counter-current displacement,  $q_t = 0$  and  $R = 0$ . The fraction of total efflux is defined by  $f_i = f(S_{wi})$ . Using eq 4 with definition of  $q_w$  from eq A1, we have

$$A \cdot t^{-1/2} (1 - f_i R) \frac{\partial F}{\partial x} = -\varphi \frac{\partial S_w}{\partial t} \quad (A2)$$

Utilizing self-similar equation in the form of  $\lambda = x \cdot t^{-1/2}$ , eq A2 turns to

$$\frac{2A(1 - f_i R)}{\varphi} \frac{dF}{dS_w} = \lambda(S_w) \quad (A3)$$

Initial and boundary conditions in (6) changes to

$$F(S_w = S_{wi}) = 0; \quad F(S_w = 1 - S_{or}) = 0 \quad (A4)$$

Derivative of eq A3 will be

$$\frac{2A(1 - f_i R)}{\varphi} \frac{d^2 F}{dS_w^2} = \frac{d\lambda}{dS_w} \quad (A5)$$

On the other hand, with  $q_t = R \cdot A \cdot t^{-1/2}$  and self-similar equation of  $\lambda = x \cdot t^{-1/2}$  in eq 1

$$\frac{d\lambda}{dS_w} = \frac{1}{A(1 - f_i R)} \frac{D}{F - f_n} \quad (A6)$$

with  $f_n$  defined as

$$f_n = \frac{(f - f_i)R}{1 - f_i R} \quad (A7)$$

Equating eqs A5 and A6

$$\frac{d^2 F}{dS_w^2} = -\frac{\varphi}{2A^2(1 - f_i R)^2} \frac{D}{F - f_n} \quad (A8)$$

Equation 8 is an ordinary differential equation (ODE), function of  $F$  only. The solution for that is obtained by integrating twice and applying initial and boundary conditions as in eq A4:

$$F(S_w) = 1 - \frac{\int_{S_w}^{1-S_{or}} \frac{(\beta - S_w)D}{F - f_n} d\beta}{\int_{S_i}^{1-S_{or}} \frac{(S_w - S_i)D}{F - f_n} dS_w} \quad (\text{A9})$$

## APPENDIX B

Introducing the self-similar function

$$\zeta = \frac{X}{\tau}, \quad \frac{\partial \zeta}{\partial X} = \frac{1}{\tau}, \quad \frac{\partial \zeta}{\partial \tau} = -\frac{X}{\tau^2} = -\frac{\zeta}{\tau} \quad (\text{B1})$$

results in the form of equations as

$$\begin{cases} \zeta \frac{\partial S_w}{\partial \zeta} = \frac{\partial}{\partial \zeta} \left[ f_w + \left( \frac{\varepsilon}{L \cdot \tau} \right) \cdot \Phi(S_w) \cdot \frac{\partial S_w}{\partial \zeta} \right] \\ \zeta S_w \frac{\partial c}{\partial \zeta} = \left[ f_w + \left( \frac{\varepsilon}{L \cdot \tau} \right) \cdot \Phi(S_w) \cdot \frac{\partial S_w}{\partial \zeta} \right] \frac{\partial c}{\partial \zeta} \end{cases} \quad (\text{B2})$$

Dividing both sides of eqs B2 over each other gives

$$\frac{\zeta \frac{dS_w}{d\zeta}}{\zeta S_w \frac{dc}{d\zeta}} = \frac{\frac{df_w}{dS_w} \frac{dS_w}{d\zeta} + \left( \frac{\varepsilon}{L \cdot \tau} \right) \cdot \frac{d}{d\zeta} \left[ \Phi(S_w) \cdot \frac{dS_w}{d\zeta} \right]}{\left[ f_w + \left( \frac{\varepsilon}{L \cdot \tau} \right) \cdot \Phi(S_w) \cdot \frac{dS_w}{d\zeta} \right] \frac{dc}{d\zeta}} \quad (\text{B3})$$

Provided that  $\frac{dc}{d\zeta} \neq 0$ , it can be removed from both sides, and the final equation form would be

$$\begin{aligned} \left( \frac{1}{S_w} \right) \cdot \left[ f_w + \left( \frac{\varepsilon}{L \cdot \tau} \right) \cdot \Phi(S_w) \cdot \frac{dS_w}{d\zeta} \right] \frac{dS_w}{d\zeta} \\ = \frac{df_w}{dS_w} \frac{dS_w}{d\zeta} + \left( \frac{\varepsilon}{L \cdot \tau} \right) \cdot \frac{d}{d\zeta} \left[ \Phi(S_w) \cdot \frac{dS_w}{d\zeta} \right] \end{aligned} \quad (\text{B4})$$

Introducing  $\omega = \frac{dS_w}{d\zeta}$  and using the chain rule gives

$$\begin{aligned} \frac{d\Phi(S_w)}{d\zeta} &= \frac{d\Phi(S_w)}{dS_w} \frac{dS_w}{d\zeta} \\ \frac{d}{d\zeta} \left( \frac{dS_w}{d\zeta} \right) &= \frac{d}{dS} \frac{dS_w}{d\zeta} \left( \frac{dS_w}{d\zeta} \right) = \frac{dS_w}{d\zeta} \cdot \frac{d}{dS} \left( \frac{dS_w}{d\zeta} \right) \end{aligned} \quad (\text{B5})$$

Equation A4 changes to

$$\begin{aligned} \frac{f_w}{S_w} + \left( \frac{\varepsilon}{L \cdot \tau} \right) \cdot \frac{\Phi(S_w)}{S_w} \cdot \omega \\ = f'_w(S_w) + \left( \frac{\varepsilon}{L \cdot \tau} \right) \cdot \Phi'(S_w) \cdot \omega + \left( \frac{\varepsilon}{L \cdot \tau} \right) \cdot \Phi(S_w) \cdot \omega' \end{aligned} \quad (\text{B6})$$

and dividing by  $\left( \frac{\varepsilon}{L \cdot \tau} \right) \cdot \Phi(S_w)$  gives

$$\frac{\left[ \frac{f_w}{S_w} - f'_w(S_w) \right]}{\left( \frac{\varepsilon}{L \cdot \tau} \right) \cdot \Phi(S_w)} + \left[ \frac{1}{S_w} - \frac{\Phi'(S_w)}{\Phi(S_w)} \right] \cdot \omega = \omega' \quad (\text{B7})$$

Keeping in mind that the term  $\left( \frac{\varepsilon}{L \cdot \tau} \right)$  is given by

$$\frac{\varepsilon}{L \cdot \tau} = \frac{(m-1)\sigma \cos \theta (\sqrt{K\rho^3})(\mathcal{R}/\bar{r})}{m A^2 \mu_b \cdot (t^{1-1/m})} \quad (\text{B8})$$

and is a dimensionless term,

$$\left[ \frac{\varepsilon}{L \cdot \tau} \right] = \frac{[MT^{-2}][L][T^{1/m}]}{[L^2 \cdot T^{-2+2/m}][ML^{-1}T^{-1}][T^{1-1/m}]} = 1 \quad (\text{B9})$$

Equation B7 in a general form is like a first-order ordinary differential equation:

$$\begin{aligned} \frac{d\omega}{dS_w} + \left[ \frac{\Phi'(S_w)}{\Phi(S_w)} - \frac{1}{S_w} \right] \omega &= \frac{\left( \frac{f_w}{S_w} - f'_w(S_w) \right)}{\left( \frac{\varepsilon}{L \cdot \tau} \right) \Phi(S_w)} \\ &= \frac{d\omega}{dS_w} + P(S_w) \cdot \omega = H(S_w) \end{aligned} \quad (\text{B10})$$

The solution of this ODE is

$$\omega(S_w) = \frac{1}{e^{\int P(S_w) dS_w}} \int e^{\int P(S_w) dS_w} H(S_w) dS_w + C_2 \quad (\text{B11})$$

where

$$\int P(S_w) dS_w = \int \left[ \frac{\Phi'(S_w)}{\Phi(S_w)} - \frac{1}{S_w} \right] dS_w = \ln \left( \frac{C_1 \cdot \Phi(S_w)}{S_w} \right) \quad (\text{B12})$$

Therefore

$$e^{\int P(S_w) dS_w} = e^{\ln \left[ \frac{C_1 \cdot \Phi(S_w)}{S_w} \right]} = \frac{C_1 \cdot \Phi(S_w)}{S_w} \quad (\text{B13})$$

Consequently, integral in eq B11 would be

$$\begin{aligned} \omega(S_w) &= \left( \frac{L \cdot \tau}{\varepsilon} \right) \cdot \frac{S_w}{\Phi(S_w)} \int \frac{[f_w - S_w f'_w(S_w)]}{S_w^2} dS_w + C_2 \\ \Rightarrow \omega(S_w) &= \left( \frac{L \cdot \tau}{\varepsilon} \right) \cdot \frac{S_w}{\Phi(S_w)} \int -\frac{d}{dS_w} \left( \frac{f_w}{S_w} \right) dS_w + C_2 \\ \Rightarrow \omega(S_w) &= -\left( \frac{L \cdot \tau}{\varepsilon} \right) \cdot \frac{S_w}{\Phi(S_w)} \cdot \left( \frac{f_w}{S_w} \right) + C_2 = -\frac{L \cdot \tau}{\varepsilon \cdot \Pi(S_w)} + C_2 \end{aligned} \quad (\text{B14})$$

The last term  $\Pi(S_w)$  is equal to  $k_{\tau o}(S_w) \cdot J'(S_w)$ . Returning to definition of  $\omega(S_w)$

$$\begin{aligned} \frac{dS_w}{d\zeta} &= -\frac{L \cdot \tau}{\varepsilon \cdot \Pi(S_w)} + C_2 \Rightarrow \frac{d\zeta}{dS_w} = -\left( \frac{\varepsilon}{L \cdot \tau} \right) \cdot \Pi(S_w) + C_2 \\ \Rightarrow \int_0^{+\infty} d\zeta &= -\int_{S_{wi}}^{1-S_{or}} \left[ \left( \frac{\varepsilon}{L \cdot \tau} \right) \cdot \Pi(S_w) - C_2 \right] dS_w \\ \Rightarrow \zeta &= -\left( \frac{\varepsilon}{L \cdot \tau} \right) \int_{S_{wi}}^{1-S_{or}} [\Pi(S_w) - C_2] dS_w + C_3 \end{aligned} \quad (\text{B15})$$

## APPENDIX C

The backward approximate derivative of  $F''$  is

$$F''(S_w) \approx \frac{F(S_w + 2\Delta S_w) - 2F(S_w + \Delta S_w) + F(S_w)}{\Delta S_w^2} \quad (\text{C1})$$

Checking eq A8 again and using the definition given in eq C1, the numerical method for calculation of  $F(S_w)$  will be



$$\begin{aligned}
 F(S_w) = & [F(S_w + \Delta S_w) - 0.5F(S_w + 2\Delta S_w) + 0.5f_w(S_w)] \\
 & + \left( 0.25[F(S_w + 2\Delta S_w) - 2F(S_w + \Delta S_w) - f_w(S_w)]^2 \right. \\
 & - \left. \left\{ f_w(S_w)[F(S_w + 2\Delta S_w) - 2F(S_w + \Delta S_w)] \right. \right. \\
 & \left. \left. + \left( \frac{\varphi}{2A^2} \right) D(S_w) \Delta S_w^2 \right\} \right)^{1/2} \quad (C2)
 \end{aligned}$$

Using the numerical form as in C2, an approximation of  $F(S_w)$  is achieved providing that  $F(S_w + \Delta S_w)$  and  $F(S_w + 2\Delta S_w)$  have been defined already, based on some starting value of  $F(S_{w,start})$ . The value of  $F(x = 0, t) = 1$  is considered as that starting value. Another required value of  $F(S_{w,max} - \Delta S_w)$  is obtained using an approximation of the Taylor series

$$F(S_{w,max} - \Delta S_w) = \frac{F(S_{w,max})}{=1} - \frac{\Delta S_w \cdot F'(S_{w,max})}{=0} = 1 \quad (C3)$$

It is assumed that maximum saturation is not exchanged towards the medium and consequently  $F'(S_{w,max}) = 0$ . Convergence of  $F$  is achieved applying two criteria: firstly, as  $F$  is a fractional flow function and we have no flow at irreducible water saturation ( $S_{wir}$ ), then  $F(S_{wir}) = 0$ ; secondly, due to mass balance law, the integrated saturation curve must equal the total imbibed pore volume; e.g.

$$\int_{S_{wir}}^{S_{w,max}} x(S_w, t) dS_w = \frac{Q_w(t)}{\varphi} = \frac{2A\sqrt{t}}{\varphi} \quad (C4)$$

## AUTHOR INFORMATION

### Corresponding Author

**Mohsen Farrokhrouz** – School of Civil, Environment and Mining Engineering, The University of Adelaide, Adelaide 5005, Australia; Petroleum Engineering Research Group, School of Engineering, Edith Cowan University, Joondalup 6027 WA, Australia; [orcid.org/0000-0001-5169-6894](https://orcid.org/0000-0001-5169-6894); Email: mohsen.farrokhrouz@adelaide.edu.au

### Authors

**Abbas Taheri** – School of Civil, Environment and Mining Engineering, The University of Adelaide, Adelaide 5005, Australia; The Robert M. Buchan Department of Mining, Queen's University, Kingston, Ontario K7L 3N6, Canada  
**Stefan Iglauer** – Petroleum Engineering Research Group, School of Engineering, Edith Cowan University, Joondalup 6027 WA, Australia; [orcid.org/0000-0002-8080-1590](https://orcid.org/0000-0002-8080-1590)  
**Alireza Keshavarz** – Petroleum Engineering Research Group, School of Engineering, Edith Cowan University, Joondalup 6027 WA, Australia; [orcid.org/0000-0002-8091-961X](https://orcid.org/0000-0002-8091-961X)

Complete contact information is available at:  
<https://pubs.acs.org/10.1021/acs.energyfuels.1c02492>

### Notes

The authors declare no competing financial interest.

## LIST OF ABBREVIATIONS

### English Symbols

$A$  = proportionality constant, m/ $\sqrt{s}$   
 $c$  = concentration of solvent, fraction

$D$  = diffusivity coefficient, m<sup>2</sup>/s  
 $f$  = fractional flow function, fraction  
 $J$  = Leverett J-Function, dimensionless  
 $K$  = permeability, m<sup>2</sup>  
 $k_r$  = relative permeability, fraction  
 $L$  = length, m  
 $p$  = pressure, Pa  
 $q$  = 1D phase flow, m/s  
 $S$  = saturation, fraction  
 $t$  = time, s  
 $x$  = displacement, m  
 $X$  = displacement, dimensionless

### Greek Symbols

$\beta, \gamma$  = function constants  
 $\tau$  = time, dimensionless  
 $\mu$  = phase viscosity, kg/m·s  
 $\lambda$  = mobility ratio, kg·m/s  
 $\theta$  = contact angle, degree  
 $\phi$  = porosity, fraction  
 $\sigma$  = interfacial tension, N/m

### Subscripts

$c$  = capillary  
 $i$  = initial  
 $n, o$  = nonwetting  
 $r$  = residual  
 $t$  = total  
 $w$  = wetting

## REFERENCES

- (1) Chen, Z.-X. et al. *A New Formulation for One-Dimensional Horizontal Imbibition in Unsaturated Porous Media*, University of California, 1990.
- (2) Cil, M.; Reis, J. C. A multi-dimensional, analytical model for counter-current water imbibition into gas-saturated matrix blocks. *J. Pet. Sci. Eng.* **1996**, *16*, 61–69.
- (3) Civan, F.; Rasmussen, M. Asymptotic Analytical Solutions for Imbibition Waterfloods in Fractured Reservoirs. *SPE J* **2001**, *6*, 171–181.
- (4) Li, K.; Horne, R. N. Generalized Scaling Approach for Spontaneous Imbibition: An Analytical Model. *SPE Reservoir Eval. Eng.* **2006**, *9*, 251–258.
- (5) Mirzaei-Paiaman, A.; Masihi, M.; Standnes, D. An Analytic Solution for the Frontal Flow Period in 1D Counter-Current Spontaneous Imbibition into Fractured Porous Media Including Gravity and Wettability Effects. *Transp. Porous Media* **2011**, *89*, 49–62.
- (6) Schmid, K. S. *Mathematical Analysis, Scaling and Simulation of Flow and Transport During Immiscible Two-phase Flow*. Doctoral Theses, Heriot Watt University, 2012.
- (7) Hamon, G.; Vidal, J. Scaling-Up the Capillary Imbibition Process From Laboratory Experiments on Homogeneous and Heterogeneous Samples, European Petroleum Conference, Society of Petroleum Engineers, London, United Kingdom, 1986; p 12.
- (8) Bourbiaux, B. J.; Kalaydjian, F. J. Experimental Study of Cocurrent and Countercurrent Flows in Natural Porous Media. *SPE Reservoir Eng.* **1990**, *5*, 361–368.
- (9) Pooladi-Darvish, M.; Firoozabadi, A. Experiments and Modelling of Water Injection in Water-wet Fractured Porous Media. *J. Can. Pet. Technol.* **2000**, *393*, 31–42 DOI: 10.2118/00-03-02.
- (10) Pooladi-Darvish, M.; Firoozabadi, A. Experiments And Modelling of Water Injection in Water-wet Fractured Porous Media. *J. Can. Pet. Technol.* **2000**, *3903* DOI: 10.2118/00-03-02.
- (11) Meng, Q.; et al. Effect of Wetting-Phase Viscosity on Cocurrent Spontaneous Imbibition. *Energy Fuels* **2016**, *30*, 835–843.
- (12) Andersen, P. Ø.; Qiao, Y.; Standnes, D. C.; Evje, S. Cocurrent Spontaneous Imbibition In Porous Media With the Dynamics of

- Viscous Coupling and Capillary Backpressure. *SPE J.* **2019**, *24*, 158–177.
- (13) Andersen, P. Ø. Early- and Late-Time Analytical Solutions for Cocurrent Spontaneous Imbibition and Generalized Scaling. *SPE J.* **2021**, *26*, 220–240.
- (14) Andersen, P. Ø.; Ahmed, S. Simulation study of wettability alteration enhanced oil recovery during co-current spontaneous imbibition. *J. Pet. Sci. Eng.* **2021**, *196*, No. 107954.
- (15) Buckley, S. E.; Leverett, M. Mechanism of fluid displacement in sands. *Trans AIME* **1942**, *146*, 107–116.
- (16) McWhorter, D. B. Infiltration Affected by Flow of Air. In *Hydrology Papers*, Colorado State University, 1971, no. 49.
- (17) Morel-Seytoux, H. J.; Khanji, J. Prediction of Imbibition in a Horizontal Column. *Soil Sci. Soc. Am. J.* **1975**, *39*, 613–617.
- (18) Yortsos, Y.; Fokas, A. An analytical solution for linear waterflood including the effects of capillary pressure. *Soc. Pet. Eng. J.* **1983**, *23*, 115–124.
- (19) Lucas, R. Ueber das Zeitgesetz des kapillaren Aufstiegs von Flüssigkeiten. *Kolloid-Z.* **1918**, *23*, 15–22.
- (20) Washburn, E. W. The dynamics of capillary flow. *Phys. Rev.* **1921**, *17*, 273–283.
- (21) Rapoport, L. A. Scaling laws for use in design and operation of water-oil flow models. *Trans. AIME* **1955**, *204*, 143–150.
- (22) Mattax, C. C.; Kyte, J. R. Imbibition Oil Recovery from Fractured, Water-Drive Reservoir. *Soc. Pet. Eng. J.* **1962**, *2*, 177–184.
- (23) Shouxiang, M.; Morrow, N. R.; Zhang, X. Generalized scaling of spontaneous imbibition data for strongly water-wet systems. *J. Pet. Sci. Eng.* **1997**, *18*, 165–178.
- (24) Zhou, D.; et al. Scaling of counter-current imbibition processes in low-permeability porous media. *J. Pet. Sci. Eng.* **2002**, *33*, 61–74.
- (25) Behbahani, H.; Blunt, M. J. Analysis of Imbibition in Mixed-Wet Rocks Using Pore-Scale Modeling. *SPE J.* **2005**, *10*, 466–474.
- (26) Knight, J.; Philip, J. Exact solutions in nonlinear diffusion. *J. Eng. Math.* **1974**, *8*, 219–227.
- (27) McWhorter, D. B.; Sunada, D. K. Exact integral solutions for two-phase flow. *Water Resour. Res.* **1990**, *26*, 399–413.
- (28) Fučík, R.; et al. Multidimensional self-similar analytical solutions of two-phase flow in porous media. *Adv. Water Resour.* **2016**, *90*, 51–56.
- (29) Fučík, R.; et al. An improved semi-analytical solution for verification of numerical models of two-phase flow in porous media. *Vadose Zone J.* **2007**, *6*, 93–104.
- (30) Hu, Q.; et al. Low pore connectivity in natural rock. *J. Contam. Hydrol.* **2012**, *133*, 76–83.
- (31) Hu, Q.; et al. Low nanopore connectivity limits gas production in Barnett formation. *J. Geophys. Res.: Solid Earth* **2015**, *120*, 8073–8087.
- (32) Hammecker, C.; Jeannette, D. Modelling the capillary imbibition kinetics in sedimentary rocks: Role of petrographical features. *Transp. Porous Media* **1994**, *17*, 285–303.
- (33) Leventis, A.; Verganelakis, D. A.; Halse, M. R.; Webber, J. B.; Strange, J. H. Capillary Imbibition and Pore Characterisation in Cement Pastes. *Transp. Porous Media* **2000**, *39*, 143–157.
- (34) Li, K. More general capillary pressure and relative permeability models from fractal geometry. *J. Contam. Hydrol.* **2010**, *111*, 13–24.
- (35) Onda, T.; Shibuichi, S.; Satoh, N.; Tsujii, K. Super-Water-Repellent Fractal Surfaces. *Langmuir* **1996**, *12*, 2125–2127.
- (36) Dimitrov, D. I.; Milchev, A.; Binder, K. Capillary Rise in Nanopores: Molecular Dynamics Evidence for the Lucas-Washburn Equation. *Phys. Rev. Lett.* **2007**, *99*, No. 054501.
- (37) Girardo, S.; Palpacelli, S.; De Maio, A.; Cingolani, R.; Succi, S.; Pisignano, D. Interplay between Shape and Roughness in Early-Stage Microcapillary Imbibition. *Langmuir* **2012**, *28*, 2596–2603.
- (38) Kusumaatmaja, H.; Yeomans, J. M. Modeling Contact Angle Hysteresis on Chemically Patterned and Superhydrophobic Surfaces. *Langmuir* **2007**, *23*, 6019–6032.
- (39) Liu, G.; Zhang, M.; Ridgway, C.; Gane, P. Spontaneous Inertial Imbibition in Porous Media Using a Fractal Representation of Pore Wall Rugosity. *Transp. Porous Media* **2014**, *104*, 231–251.
- (40) Yang, R.; et al. Experimental investigations on the geometry and connectivity of pore space in organic-rich Wufeng and Longmaxi shales. *Mar. Pet. Geol.* **2017**, *84*, 225–242.
- (41) Pini, R.; Benson, S. M. Simultaneous determination of capillary pressure and relative permeability curves from core-flooding experiments with various fluid pairs. *Water Resour. Res.* **2013**, *49*, 3516–3530.
- (42) Leverett, M. Capillary behavior in porous solids. *Trans. AIME* **1941**, *142*, 152–169.
- (43) Hu, Q.-H. et al. *Pore Connectivity, Episodic Flow, and Unsaturated Diffusion in Fractured Tuff*, Proceedings of the 11th International High Level Radioactive Waste Management Conference, IHLRWM, 2006.
- (44) Naik, S.; You, Z.; Bedrikovetsky, P. Productivity index enhancement by wettability alteration in two-phase compressible flows. *J. Nat. Gas Sci. Eng.* **2018**, *50*, 101–114.
- (45) Al-Sarhi, A.; You, Z.; Behr, A.; Genolet, L.; Kowolik, P.; Zeinijahromi, A.; Bedrikovetsky, P. Admissible Parameters for Two-Phase Coreflood and Welge–JBN Method. *Transp. Porous Media* **2020**, *131*, 831–871.
- (46) Pooladi-Darvish, M.; Firoozabadi, A. Cocurrent and Counter-current Imbibition in a Water-Wet Matrix Block. *SPE J.* **2000**, *5*, 3–11.
- (47) Mirzaei-Paiaman, A.; et al. Scaling one- and multi-dimensional co-current spontaneous imbibition processes in fractured reservoirs. *Fuel* **2017**, *196*, 458–472.
- (48) Fischer, H.; Morrow, N. R. Scaling of oil recovery by spontaneous imbibition for wide variation in aqueous phase viscosity with glycerol as the viscosifying agent. *J. Pet. Sci. Eng.* **2006**, *52*, 35–53.
- (49) Fischer, H.; et al. Modeling the Effect of Viscosity Ratio on Spontaneous Imbibition. *SPE Reservoir Eval. Eng.* **2008**, *11*, 577–589.
- (50) Abbasi, J.; et al. Discussion on Similarity of Recovery Curves in Scaling of Imbibition Process in Fractured Porous Media. *J. Nat. Gas Sci. Eng.* **2016**, *36*, 617–629.
- (51) Hamidpour, E.; et al. Experimental study of some important factors on nonwetting phase recovery by co-current spontaneous imbibition. *J. Nat. Gas Sci. Eng.* **2015**, *27*, 1213–1228.
- (52) Mirzaei-Paiaman, A.; Masihi, M. Scaling of Recovery by Co-current Spontaneous Imbibition in Fractured Petroleum Reservoirs. *Energy Technol.* **2014**, *2*, 166–175.
- (53) Farrokhrrouz, M.; Asef, M. R. *Simulating Model to Reduce Detrimental Acidizing in Tabnak Gas Field*, SPE Deep Gas Conference and Exhibition, OnePetro, 2010.
- (54) Farrokhrrouz, M.; Asef, M. R. Evaluation of Empirical Correlations for Biot's Coefficient Prediction, The 15th International Workshop on Seismic Anisotropy, Manama, Bahrain, 2012.
- (55) Farrokhrrouz, M.; Taheri, A.; Keshavarz, A. Numerical reactive flow transport simulation on core samples during acid fracturing in carbonaceous shale. *J. Nat. Gas Sci. Eng.* **2020**, *84*, No. 103615.
- (56) Alizadeh, Amir Hossein.; Keshavarz, Alireza.; Haghghi, Manouchehr. *Flow Rate Effect on Two-Phase Relative Permeability in Iranian Carbonate Rocks*, Paper presented at the SPE Middle East Oil and Gas Show and Conference, Manama, Bahrain, 2007.
- (57) Awan, F. U. R.; Al-Yaseri, A.; Akhondzadeh, H.; Iglauer, S.; Keshavarz, A. Influence of mineralogy and surfactant concentration on zeta potential in intact sandstone at high pressure. *J. Colloid Interface Sci.* **2022**, *607*, 401–411.
- (58) Akhondzadeh, H.; Keshavarz, A.; Awan, F. U. R.; Ali, M.; Al-Yaseri, A.; Liu, C.; Lebedev, M. Liquid nitrogen fracturing efficiency as a function of coal rank: A multi-scale tomographic study. *J. Nat. Gas Sci. Eng.* **2021**, *95*, No. 104177.
- (59) Akin, S.; et al. Spontaneous imbibition characteristics of diatomite. *J. Pet. Sci. Eng.* **2000**, *25*, 149–165.
- (60) Pope, G. A. The Application of Fractional Flow Theory to Enhanced Oil Recovery. *Soc. Pet. Eng. J.* **1980**, *20*, 191–205.

**Chapter 4:**  
**Exact Analytical Solution of Counter-Current Imbibition**  
**with Both Capillary and Gravity Effects**



# Statement of Authorship

Title of Paper	Exact Analytical Solutions of Counter-current Imbibition with Both Capillary and Gravity Effects
Publication Status	<input checked="" type="checkbox"/> Published <input type="checkbox"/> Accepted for Publication <input type="checkbox"/> Submitted for Publication <input type="checkbox"/> Unpublished and Unsubmitted work written in manuscript style
Publication Details	Journal of Energy & Fuels 2022, 36, 3, 1457–1469 <a href="https://doi.org/10.1021/acs.energyfuels.1c03868">https://doi.org/10.1021/acs.energyfuels.1c03868</a>

## Principal Author

Name of Principal Author (Candidate)	Mohsen Farrokhrouz		
Contribution to the Paper	Conception, Acquiring Data, Model Simulation, Experimental data matching with the model Knowledge, Analysis, Drafting		
Overall percentage (%)	80%		
Certification:	This paper reports on original research I conducted during the period of my Higher Degree by Research candidature and is not subject to any obligations or contractual agreements with a third party that would constrain its inclusion in this thesis. I am the primary author of this paper.		
Signature		Date	23/12/2021

## Co-Author Contributions

By signing the Statement of Authorship, each author certifies that:

- i. the candidate's stated contribution to the publication is accurate (as detailed above);
- ii. permission is granted for the candidate to include the publication in the thesis; and
- iii. the sum of all co-author contributions is equal to 100% less the candidate's stated contribution.

Name of Co-Author	Dr Abbas Taheri		
Contribution to the Paper	Knowledge, Conception, Drafting		
Signature		Date	23/12/2021
Name of Co-Author	Dr Alireza Keshavarz		
Contribution to the Paper	Knowledge, Conception, Drafting		
Signature		Date	23/12/2021
Name of Co-Author	Prof Stefan Iglauer		
Contribution to the Paper	Knowledge, Conception, Drafting		
Signature		Date	23/12/2021

Please cut and paste additional co-author panels here as required.

# Exact Analytical Solutions of Countercurrent Imbibition with Both Capillary and Gravity Effects

Mohsen Farrokrouz,\* Abbas Taheri, Stefan Iglauer, and Alireza Keshavarz



Cite This: *Energy Fuels* 2022, 36, 1457–1469



Read Online

ACCESS |



Metrics & More

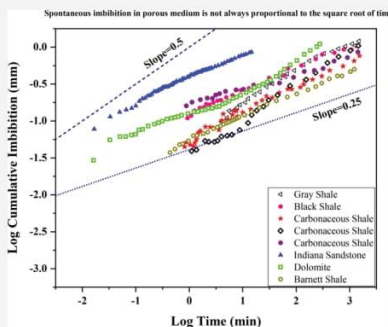


Article Recommendations



Supporting Information

**ABSTRACT:** Spontaneous imbibition (SI) is a key mechanism for hydrocarbon recovery within the matrix system in fractured reservoirs. The production of SI is primarily achieved through the countercurrent imbibition of water, which displaces the hydrocarbon. Various analytical and semianalytical methods have been suggested for the prediction of this process. However, as claimed by further studies, most of these analytical solutions are valid only for rather restrictive and/or unrealistic functions of capillary pressure and relative permeabilities. Some other semianalytical solutions assumed a specific form of inlet boundary condition. Thus, in this paper, a new analytical solution is proposed that does not possess these limitations, fully based on the physics and mathematics of two-phase flow in porous media. In the proposed model, imbibition front movement through the porous medium is termed the pore connectivity concept, which was not considered in any previous studies to date. Pore connectivity, tortuosity, shape factor, and permeability as interconnected parameters have been used in this study, where the relationship between these parameters assisted in the development of the mathematical model. Accordingly, this model has relaxed some of the limitations of previously proposed analytical solutions. Capillary and gravity forces and their relative contributions have been considered, and exact solutions were derived. These analytical solutions were then verified with experimental results, where they showed an acceptable match. A sensitivity analysis of contributing parameters was also performed to identify the most significant parameters and their contributing effect on final recovery. Previous studies showed that displacement efficiency has been shown to be independent of density difference, initial water saturation, and residual oil saturation. These findings were confirmed by previous experimental results. Applying this novel methodology improves the prediction of fluid saturations, reservoir recovery, and hydrocarbon production strategies.



## 1. INTRODUCTION

Spontaneous imbibition (SI) has received significant attention in reservoir engineering due to its importance in oil and gas

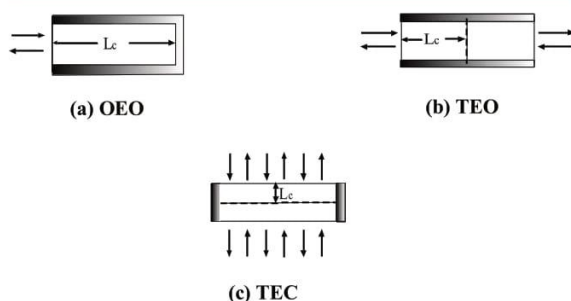


**Figure 1.** Different boundary conditions occur in countercurrent SI with a characteristic length ( $L_c$ ): (a) one end open (OEO) with a small effect of gravity, (b) two ends open (TEO) with a small effect of gravity, and (c) two ends closed (TEC) with considerable effect of gravity. In all of these figures, one-dimensional (1D) displacement is significant and considered.

recovery. Most of the hydrocarbon within the fractures and/or high-permeable matrix can be produced at the early stages of a reservoir life span. However, oil and gas in the low-permeable matrix or dead-end fractures take a longer time to flow into wellbores through spontaneous imbibition (SI). During spontaneous imbibition, the wetting phase dwells into the fractures initially and then imbibe into the matrix where most of the oil is contained. This form of imbibition can occur countercurrently based on the distance of the production point from the water level, distribution of the fractures, and the fracture continuity.<sup>1</sup> During countercurrent imbibition, water and oil flow in opposite directions, as schematically presented in Figure 1. In this figure, the medium is filled with nonwetting phase (usually oil) and wetting phase (usually water) displaces it.

Received: November 14, 2021

Revised: December 29, 2021

Published: January 21, 2022



Reservoir displacement efficiency depends on the imbibition mechanism. When matrix blocks are delimited by water, displacement efficiency reduces dramatically due to the increased significance of countercurrent imbibition. This has been confirmed by numerous experimental and numerical studies.<sup>2,3</sup> A complete analytical description of SI requires differentiation between cocurrent and countercurrent SI as well as physical properties and reservoir characteristics.<sup>4</sup> Countercurrent SI (COUCSI) is related to the cases where vertical or horizontal imbibition of wetting and nonwetting phases occurs from the same side. This movement from one side only is dictated to the porous medium by boundary conditions (e.g., faults, cap rocks, or low-permeable layers).

There have been many attempts by researchers to obtain analytical solutions to spontaneous imbibition.<sup>1,5–8</sup> The reason for this large number of studies relates to a strong underlying nonlinearity and significant mathematical difficulties for analytical solutions due to the nature of the capillary pressure mechanism. Additional assumptions, such as specific relative permeability functions,<sup>9</sup> steady-state flow,<sup>10</sup> or horizontal flow direction to remove gravity effect,<sup>7</sup> have resulted in specific theoretical solutions based on the properties of two phases in porous media. In studies by McWhorter and Sunada,<sup>11,12</sup> restrictions on boundary conditions were considered, and as claimed by ref 10, this approach indicates another specific case. Accordingly, the solution that is formed is valid only for early times. Further, as can be observed, all of these presumptions limit the extent of solution applicability.

Contrary to the Buckley–Leverett analytical solution, there is no unique theoretical solution (without any restrictions) for capillary-dominated imbibition. The objective of the current study is to propose an exact solution for saturation profile within a porous medium when capillary imbibition is the only dominant parameter, by applying a novel methodology as compared with previously suggested solution models. Another important aspect of this study is that its exact solution was suggested for capillary effect alone and gravity imbibition alone, whereby the solution was modified when both forces (imbibition and gravity) are active. Further, the proposed methodology suggests that front flow in spontaneous imbibition is not always proportional to the square root of time, where it is based on experimental results of different imbibition front behaviors in previous studies. Moreover, the exact mathematical solution of this study has been validated with previous experimental results, validating the goodness of saturation front estimations using this solution methodology.

## 2. TWO-PHASE FLOW: THEORETICAL BACKGROUND

Two-phase flow refers to the communicating flow of two fluid phases (either liquid or gas) with an interface between these two different phases. This type of flow may exist in a single-component or multicomponent system. In porous media, the flow of these two phases is governed by Darcy's law and controlled by capillary pressure and gravity.

**2.1. Continuity Equation in Two-Phase Flow.** The derivation of a continuity equation for two-phase flow in a porous medium is given in Appendix A. The general form of saturation continuity equation is

**Table 1. Proposed Approaches and Defined Dimensionless Times for the Solution of Countercurrent SI<sup>a</sup>**

additional assumption	dimensionless time	reference
$\mu_n \ll \mu_w$	$T \propto \frac{\sigma r}{2L_c^2 \mu_w} t$	20, 21
$\mu_n = \mu_w$	$T \propto \frac{\sigma}{L_c^2 \mu_w} \sqrt{\frac{K}{\phi}} t$	22
$\mu_n \approx \mu_w$	$T \propto \frac{\sigma}{L_c^2 \sqrt{\mu_w \mu_n}} \sqrt{\frac{K}{\phi}} t$	23
$F(x, t) = \frac{q_w(\alpha_{CF}, t)}{q_w(0, t)}$	$T \propto \frac{\sigma}{L_c^2} \sqrt{\frac{K}{\phi}} \left( \frac{\lambda_w \lambda_n}{\lambda_t} \right)_{CF} J_{CF} \cdot (S_{BC} - S_0) \cdot t$	18
	$T \propto \left( \frac{2A}{\phi L_c} \right)^2 \cdot t$	11

<sup>a</sup>Capillary-dominated case.

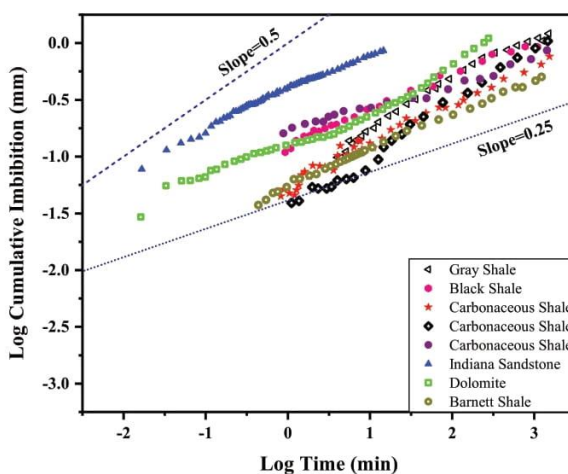


**Figure 2.** Effect of pore connectivity on imbibition behavior. The data was obtained from different experimental studies: dolomite and Indiana sandstone,<sup>30</sup> carbonaceous, gray and black shale samples,<sup>31</sup> and Barnett shale samples.<sup>32</sup>

$$\phi \frac{\partial S_w}{\partial t} + q_t \frac{df}{dS_w} \frac{\partial S_w}{\partial x} + \frac{\partial}{\partial x} \left( D(S_w) \frac{\partial S_w}{\partial x} \right) = 0$$

$$D(S_w) = K \frac{\lambda_w \lambda_n}{\lambda_t} \frac{dP_c}{dS_w} \quad (1)$$

Wetting and nonwetting relative permeability functions depend on saturation ( $S_w$ ) only, where some correlations have already been proposed for them.<sup>13–15</sup> Three scenarios of spontaneous imbibition (SI) that are usually investigated in this area are:

- (a) Viscous flow dominates (the capillary term is ignored). Equation 1 then is simplified to

$$\phi \frac{\partial S_w}{\partial t} = -q_t \frac{df}{dS_w} \frac{\partial S_w}{\partial x} \quad (2)$$

Solution of eq 4 is known as the Buckley–Leverett solution.<sup>16</sup>

- (b) Flow is capillary-dominated, and eq 1 can be simplified to

$$\phi \frac{\partial S_w}{\partial t} = \frac{\partial}{\partial x} \left( D(S_w) \frac{dP_c}{dS_w} \frac{\partial S_w}{\partial x} \right) \quad (3)$$



Derivation of the analytical solution for this case has been investigated by many researchers over recent decades, with several proposed solutions (Table 1).

- (c) Flow is governed by countercurrent spontaneous imbibition (COUCSI), while gravity is still significant. Thus, eq 1 changes to

$$\phi \frac{\partial S_w}{\partial t} = -\frac{\partial}{\partial x} \left[ K \frac{\lambda_w \lambda_o}{\lambda_t} \left( \frac{dP_c}{dS_w} + (\rho_{nw} - \rho_w)g \right) \frac{\partial S_w}{\partial x} \right] \quad (4)$$

For the horizontal direction of imbibition, gravity is not that important for the short length of the medium while it decelerates imbibition for long medium lengths. For vertical media, depending on the direction of displacement, imbibition can be gravity-resistant or gravity-assisted. Many researchers<sup>6,17–19</sup> have also investigated this case by introducing two dimensionless parameters like below

$$R = -\frac{gH(\rho_w - \rho_{nw})\sqrt{\frac{K}{\phi}}}{2S^*J'_{S=S^*}\sigma(1 - S_{nwr} - S_{wi})} \quad (5)$$

$$\alpha = -\frac{\sigma}{H^2} \sqrt{\frac{K}{\phi}} \left( \frac{\lambda_w \lambda_{nw}}{\lambda_w + \lambda_{nw}} J' \right)_{S=S^*} \quad (6)$$

The general approach for analytically solving the saturation continuity equation for capillary-dominated flow (ignoring gravity effects) considers scaling groups. As shown in Table 1, solutions can be divided into two main categories. In the first, additional assumptions are used for eq 3 while introducing dimensionless time. For instance, a specific functional form of  $D(S_w)$  is defined or similar viscosities for wetting and nonwetting phases are assumed.

For the second category of solutions (e.g., McWhorter and Sunada<sup>11</sup>), the inflow rate needs to be proportional to the square root of time. As the similarity variable is in the form of  $x/\sqrt{t}$ , inflow rate can be defined as  $A/\sqrt{t}$ . The initial and boundary conditions for eq 3 in all solution methodologies are

$$\begin{cases} S_w(x=0, t) = S_{w,max} = 1 - S_o \\ S_w(x, t=0) = S_w(\infty, t) = S_{wi} \end{cases} \quad (7)$$

where  $S_{wi}$  is the initial water saturation in the reservoir and  $S_{or}$  is the residual oil saturation. It has been shown by ref 8 that the boundary condition for spontaneous imbibition (SI) for countercurrent imbibition is redundant. While this statement was explicitly mentioned in their study, Pooladi-Darvish and Firoozabadi<sup>2</sup> have previously stated the same thing implicitly and Mirzaei-Paiaman et al.<sup>24</sup> have confirmed this, too.

Returning to eq 1, the flow direction of both phases determines the solution methodology. For countercurrent imbibition, the two phases move in opposite directions, and the total velocity is zero (Figure 1a), i.e.,  $q_w = -q_n$ .

Based on the integral solution derived by McWhorter and Sunada<sup>11</sup> for eq 1, an additional initial condition is required, where  $A$  is a constant that cannot be chosen freely and depends on fluid and porous media characteristics.

This solution by McWhorter and Sunada<sup>11</sup> is based on a modified fractional flow function (eqn B3), providing the plot of a self-similar parameter ( $\omega = x/\sqrt{t}$ ) versus saturation (see Appendix B for a detailed solution methodology).

The computation of  $F(S_w)$  from integral (B-10) can be accomplished by iteration.<sup>11</sup> A first trial  $F$  is used to evaluate the

integrals on the right-hand side, resulting in a second estimate for  $F$ . This second estimate can be used again to evaluate the right side. This process can be repeated until  $F$  converges. Usually, the first estimate is  $F(S_w) = 1$ .

**2.2. Review of Conventional COUCSI Solutions.** Most of the previously proposed solutions for countercurrent spontaneous imbibition (COUCSI) are restricted by additional assumptions. As evident in Table 1, these limitations are related to the viscosity of the wetting and nonwetting phases or predetermined initial and/or boundary conditions. From this, it may appear evident that the solution proposed by McWhorter and Sunada<sup>11</sup> does not have limitations. However, this solution methodology does not present a functional form as an analytical solution; rather, it provides a solution based on implicit integral values point by point and with a lot of iterations to converge.

It is assumed that fluid imbibition into the porous medium is proportional to the square root of time according to the Lucas<sup>20</sup> and Washburn<sup>21</sup> model. However, several studies showed the deviation of Lucas–Washburn equation (LWE) from experimental results and some of them proposed a modified form for this equation.<sup>25–29</sup> They suggested different reasons for this deviation such as irregular pore pathways, surface roughness, specific surface area, effective capillary force, and apparent contact angle.

Experimentally, as can be observed in Figure 2, in a log–log diagram, the results of spontaneous imbibition (SI) versus time do not always fall on the line with 0.5 slope (which represents front movement with respect to the square root of time). Rather, it falls with different slopes from 0.25 up to 0.5. This implies that the imbibition front can move with functions other than the square root of time. Consequently, the methodology proposed by McWhorter and Sunada<sup>11</sup> does not cover all behaviors of imbibition front movement, where a more precise analytical solution is required. In applying this approach, this study proposes a new mathematical exact solution that relaxes this presumption, leading to a universal solution for countercurrent spontaneous imbibition (COUCSI).

### 3. NEW SOLUTION METHODOLOGY FOR FLUID PHASE WITH COMPONENTS

Equation A9 illustrates a simultaneous continuity equation for saturation and chemical components. If the dissolved components are considered to be zero, the final equation form would be like eq 1, which has not occurred in our case. The wetting fluid at *in situ* conditions also contains some chemical components (i.e., ions, tracer, salinity, polymer). Initial water saturation in the reservoir ( $S_{wir}$ ) contains a certain concentration of chemical component, while water flux at  $x = 0$  ( $q_0$ ) contains the same chemical composition but with a different concentration. A good example of this is salinity. Formation brine is usually high salinity water, whereas injected water into a wellbore is often low salinity water. Differences in saturation and concentration can result in water movement from higher saturation and concentration toward lower saturation and concentration. This water movement is covered by the continuity equation.

A detailed explanation of this is given in Figure 3. The porous medium consists of rock particles (brown blocks), where the surface is mainly covered by negative ions (white color anions). At the same time, initial water saturation exists in this porous medium (dark blue color) mostly containing positive ions (red color cations). The imbibition front also contains positive ions (yellow color cations) and negative ions (green color anions).

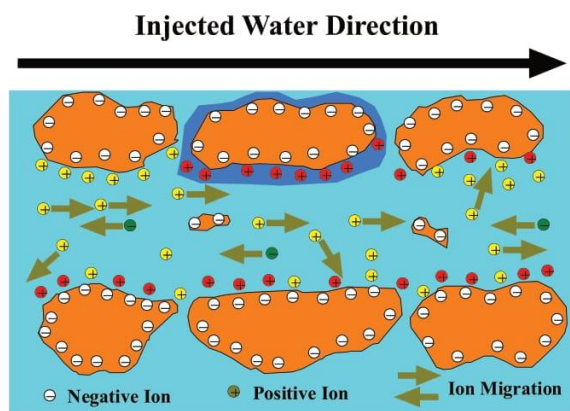


**Figure 3.** Schematic illustration of continuity equations for saturation and ion concentration in a porous medium (eq 12). A detailed explanation is given within the text (reproduced from ref 4. Copyright 2021 American Chemical Society).

The continuity equation exists between imbibed water (turquoise color) and *in situ* saturation (dark blue color) as well as continuity equation between involved anions and cations. As water moves from higher saturation toward lower saturation, ions also move from higher concentration toward lower concentration. It is worth noting here that this is not a presumption for the mathematical solution but rather it just clarifies the physics behind the imbibition. For a one-dimensional equation form, it appears as

$$\left\{ \begin{array}{l} \phi \frac{\partial S_w}{\partial t} + \frac{\partial q_w}{\partial x} = 0 \\ \phi S_w \frac{\partial c}{\partial t} + q_w \frac{\partial c}{\partial x} = 0 \end{array} \right. \quad (8)$$

Introducing a gravitational term changes  $q_w$  to (see Appendix A)

$$\begin{aligned} q_w &= f q_t - D(S_w) \frac{\partial S_w}{\partial x} \\ &= \frac{\lambda_w}{\lambda_t} q_t + K \frac{\lambda_w \lambda_n}{\lambda_t} \frac{dP_c}{dS_w} \frac{\partial S_w}{\partial x} + K \frac{\lambda_w \lambda_n}{\lambda_t} \Delta \rho \cdot g \end{aligned} \quad (9)$$

where the additional definition of the Leverett J-function<sup>16</sup> is

$$P_c(S_w) = \frac{\sigma \cos \theta}{\sqrt{\frac{K}{\phi}}} J(S_w) \quad (10)$$

The term  $\sqrt{k/\phi}$  in eq 10 expresses the dependency of imbibition to shape factor and pore connectivity.<sup>33</sup> Inserting eq 9 into eq 8 for countercurrent imbibition, i.e.,  $q_t = 0$ , it follows

$$\begin{aligned} q_w &= \frac{\lambda_w}{\lambda_t} \left( \frac{k_{ro} \sigma \cos \theta \sqrt{K\phi}}{\mu_0} \cdot \frac{dJ}{dS_w} \cdot \frac{\partial S_w}{\partial x} + \frac{k_{ro} K \Delta \rho}{\mu_0} \cdot g \right) \\ \Rightarrow q_w &= \Phi(S_w) \cdot \frac{\partial S_w}{\partial x} \cdot \varepsilon_c + \Pi(S_w) \cdot \varepsilon_g \\ \rightarrow \Phi(S_w) &= k_{ro} \cdot \frac{\lambda_w}{\lambda_t} \cdot J'; \quad \Pi(S_w) = k_{ro} \cdot \frac{\lambda_w}{\lambda_t} \end{aligned} \quad (11)$$

Note that the dimensions of the capillary and gravity terms are

$$\left\{ \begin{array}{l} [\varepsilon_c] = \left[ \frac{\sigma \cos \theta \sqrt{K\phi}}{\mu_0} \right] = \frac{[M \cdot T^{-2}] \sqrt{[L^2]}}{[M \cdot L^{-1} \cdot T^{-1}]} = \left[ \frac{L^2}{T} \right] \\ [\varepsilon_g] = \left[ \frac{K \Delta \rho}{\mu_0} \cdot g \right] = \frac{[L^2] \cdot [M \cdot L^{-3}] \cdot [L \cdot T^{-2}]}{[M \cdot L^{-1} \cdot T^{-1}]} = \left[ \frac{L}{T} \right] \end{array} \right. \quad (12)$$

$\varepsilon_c$  and  $\varepsilon_g$  are the constants quantifying the dominance of capillary and gravity terms, respectively. In the following sections, the exact solution of eq 8 with predetermined initial and boundary conditions will be presented. Accordingly, these dimensionless terms will be used throughout this paper (dimensionless distance, dimensionless time, and dimensionless concentration and saturation)

$$\begin{aligned} X &= \frac{x}{L}; \quad T_1 = \frac{\varepsilon_c \cdot t}{\phi \cdot L^2}; \quad T_2 = \frac{\varepsilon_g \cdot t}{\phi \cdot L}; \quad C = \frac{c}{c_0}; \quad S \\ &= \frac{S_w - S_{wi}}{1 - S_{wi}} \end{aligned} \quad (13)$$

### 3.1. Capillary-Dominated Spontaneous Imbibition.

For the horizontal flow of two immiscible and incompressible fluids,  $\varepsilon_g \approx 0$  and eq 11 is simplified to

$$q_w = \varepsilon_c \cdot \Phi(S) \cdot \frac{\partial S}{\partial X} \quad (14)$$

And the dimensionless form of eq 8 is

$$\left\{ \begin{array}{l} \frac{\partial S}{\partial T_1} = -\frac{1}{\varepsilon_c} \frac{\partial}{\partial X} \left[ \varepsilon_c \cdot \Phi(S) \cdot \frac{\partial S}{\partial X} \right] \\ \frac{\partial C}{\partial T_1} = -\frac{1}{\varepsilon_c \cdot S} \left[ \varepsilon_c \cdot \Phi(S) \cdot \frac{\partial S}{\partial X} \right] \frac{\partial C}{\partial X} \end{array} \right. \quad (15)$$

With the following initial and boundary conditions

$$\left\{ \begin{array}{l} S(X=0, T_1) = 1 \\ S(X=1, T_1) = S(X, T_1=0) = 0 \end{array} \right. \quad \left\{ \begin{array}{l} C(X=0, T_1) = 1 \\ C(X, T_1=0) = 0 \end{array} \right. \quad (16)$$

Dividing both terms in eq 15 and using any self-similar function results in

$$\begin{aligned} \frac{\frac{\partial S}{\partial X} \frac{\partial \Psi}{\partial T_1}}{\frac{\partial C}{\partial X} \frac{\partial \Psi}{\partial T_1}} &= \frac{\frac{\partial}{\partial X} \frac{\partial \Psi}{\partial X} \left[ \Phi(S) \cdot \frac{\partial S}{\partial X} \frac{\partial \Psi}{\partial X} \right]}{\frac{1}{S} \left[ \Phi(S) \cdot \frac{\partial S}{\partial X} \frac{\partial \Psi}{\partial X} \right] \frac{\partial C}{\partial X} \frac{\partial \Psi}{\partial X}} \end{aligned} \quad (17)$$

It can be re-emphasized here that according to Figure 2, the self-similar function ( $\Psi$ ) can be a different function of time (square root, cube root, or quad root of time) in eq 17. The reason for this is that in this equation derivatives can be easily simplified from the numerator and the denominator. Accordingly, the solution methodology does not depend on the specific inflow rate function, as noted by McWhorter and Sunada,<sup>11</sup> who defined inflow rate to be  $A/\sqrt{t}$ , while in eq 17,  $\Psi$  can be any function of  $X$  and  $T$ . The reason is that the terms  $\partial \Psi / \partial T_1$  and  $\partial \Psi / \partial X$  can be removed from nominator and denominator, independent of the functional form of  $\Psi$ . While any function of



$X$  and  $T$  can be selected, the effect of pore connectivity on imbibition can also be included by different functions of time in selected self-similar functions.

Simplifying algebraic expressions leads to

$$\frac{dS}{d\Psi} = \frac{d}{d\Psi} \left[ \Phi(S) \cdot \frac{dS}{d\Psi} \right]$$

$$\frac{dC}{d\Psi} = \frac{1}{S} \left[ \Phi(S) \cdot \frac{dS}{d\Psi} \right] \frac{dC}{d\Psi} \quad (18)$$

As difference exists in the concentration of the chemical component of formation fluid and wellbore fluid,  $\frac{dC}{d\Psi}$  cannot be zero. Considering the chain rule for derivatives, the following occurs

$$\frac{d\Phi(S)}{d\Psi} = \frac{d\Phi(S)}{dS} \cdot \frac{dS}{d\Psi};$$

$$\frac{d^2S}{d\Psi^2} = \frac{d}{d\Psi} \left( \frac{dS}{d\Psi} \right) = \frac{d}{dS} \frac{dS}{d\Psi} \left( \frac{dS}{d\Psi} \right) \quad (19)$$

And considering  $W = \frac{dS}{d\Psi}$ , this changes eq 18 to

$$\frac{dW}{W} = \left[ \frac{1}{S} - \frac{\Phi'(S)}{\Phi(S)} \right] dS \quad (20)$$

Integration of eq 20 and using the definition of “ $W$ ” result in

$$\frac{dS}{d\Psi} = \frac{C_1 S}{\Phi(S)} \Rightarrow \Psi = \int_{S_0}^{S_1} \frac{\Phi(S)}{C_1 S} dS + C_2 \quad (21)$$

At  $X = 0$ ,  $\Psi$  is zero, and as  $S_1 = S_0$ , the integral in eq 21 is also zero. Therefore,  $C_2$  is zero. In contrast,  $C_1$  depends on the saturation gradient at any certain point as  $\frac{d\Psi}{dS}$  is the tangent of saturation profile, which varies as the saturation front displaces inside the porous medium but remains constant at any time along the saturation profile. For example, if the saturation profile is desired at  $X = 1$ , then  $\Psi = 1/T_1$  for the functional form of  $\Psi = X/T_1$  and  $C_1$  would be the slope of the line from  $S_0$  tangential to the fractional flow function curve at each specific saturation value.

Using the functional form suggested by Pooladi-Darvish and Firoozabadi<sup>3</sup> for capillary pressure and nonwetting relative permeability function as below (the constant values are reported in the same paper)

$$k_{ro} = k_{ro}^0 (1 - S)^{n_0} \quad (22)$$

$$P_c = -B \ln(S) \quad (23)$$

And the simple form of fractional flow function submitted by Brevedo et al.<sup>34</sup> according to the linear Brooks–Corey model will be like below

$$f_w(S) = \frac{S}{2 - S} \quad (24)$$

Altogether, the integral form in eq 21 turns to

$$\Psi = \frac{1}{C_1} \int_{S_0}^{S_1} \frac{\Phi(S)}{S} dS$$

$$= \frac{B \cdot \sqrt{K} \cdot k_{ro}^0}{C_1 \cdot \sqrt{\varphi} \cdot \sigma \cos \theta} \int_{S_0}^{S_1} \frac{(1 - S)^4}{2S - S^2} dS$$

$$\Rightarrow \Psi = \frac{B \cdot \sqrt{K} \cdot k_{ro}^0}{C_1 \cdot \sqrt{\varphi} \cdot \sigma \cos \theta} \left[ \ln \left( \sqrt{\frac{S}{S - 2}} \right) - \frac{S^3}{3} + S^2 - 2S \right]_{S_0}^{S_1} \quad (25)$$

As it is seen in eq 25, a fully functional form is achieved for the self-similar function of  $\Psi$ . For self-similar function as  $\Psi = X/T_1$  (or other similar forms), the value of  $S$  can be calculated at any arbitrary  $X$  and  $T_1$ .

Moreover, the concentration profile is also determined using the term inside the denominator of eq 18, which leads to

$$\frac{dC}{d\Psi} \left[ 1 - \frac{1}{S} \left( \Phi(S) \cdot \frac{dS}{d\Psi} \right) \right] = 0 \quad (26)$$

Equation 26 determines two values for concentration gradient: a case when  $\frac{dC}{d\Psi} = 0$  (that is not considered for our case) and another solution when the value within the bracket is zero, which leads to a solution form similar to eq 21 but for concentration front. Note that the concentration value at each saturation is a constant value. Based on the correlations that are selected for capillary J-function, nonwetting relative permeability, and fractional flow function, the integral in eqs 21 and 26 can be solved.

**3.2. Gravity-Dominated Case.** For the vertical flow of two immiscible and incompressible fluids,  $\varepsilon_c \approx 0$  and eq 11 changes to

$$q_w = \varepsilon_g \cdot \Pi(S) \quad (27)$$

where its dimensionless form is

$$\left\{ \begin{array}{l} \frac{\partial S}{\partial T_2} = -\frac{1}{\varepsilon_g} \frac{\partial}{\partial X} [\varepsilon_g \cdot \Pi(S)] \\ \rightarrow \frac{\partial S}{\partial T_2} + \frac{d(\Pi(S))}{dS} \frac{\partial S}{\partial X} \\ = 0 \text{ (a)} \\ \frac{\partial C}{\partial T_2} = -\frac{1}{\varepsilon_g \cdot S} [\varepsilon_g \cdot \Pi(S)] \frac{\partial C}{\partial X} \\ \rightarrow \frac{\partial C}{\partial T_2} + \frac{\Pi(S)}{S} \frac{\partial C}{\partial X} \\ = 0 \text{ (b)} \end{array} \right. \quad (28)$$

Equation 28a is a first-order quasi-linear equation, and eq 26 is a first-order linear partial differential equation (PDE). Again, initial and boundary conditions are like in eq 16. The solution to eq 28 is analogous to the Buckley–Leverett equation, using the self-similar function  $\Psi = X/T_2$

$$S(\Psi) = \left\{ \begin{array}{l} 1 \quad 0 < \Psi < \frac{d(\Pi(1))}{dS} \\ \Psi = \frac{d(\Pi(S))}{dS} \quad \frac{d(\Pi(1))}{dS} < \Psi < \frac{\Pi(S_c)}{S_c} \\ 0 \quad \frac{\Pi(S_c)}{S_c} < \Psi < \infty \end{array} \right\} \quad (29)$$

$S_c$  is found from the contact discontinuity condition and is equal to  $\Pi(S_c)/S_c$ . Depending on the function  $\Pi(S)$ , the solution may contain a shock, a rarefaction, or a combination of both. However, there are a few studies<sup>35</sup> showing that at some critical rates (depending on the rock type, fluid viscosity, and wettability characteristics), relative permeability curves may not be obtained. The detailed solution of this system can be found in Lake.<sup>36</sup> In the case of a discontinuous solution (shock wave), the relationship between both sides of the discontinuity can be defined by Rankine–Hugoniot conditions.

**3.3. Simultaneous Contribution of Capillarity and Gravity.** If both capillary and gravity terms ( $\varepsilon_c$  and  $\varepsilon_g$ ) are not zero, the term  $q_w$  is the general form like eq 11. The dimensionless groups are defined as  $S$ ,  $T_1$ ,  $C$ , and  $X$  (see eq 13), and the dimensionless set of equations is then

$$\left\{ \begin{array}{l} \frac{\partial S}{\partial T_1} = -\frac{\partial}{\partial X} \left[ \Phi(S) \cdot \frac{\partial S}{\partial X} + \Pi(S) \cdot \kappa \right] \\ \frac{\partial C}{\partial T_1} = -\frac{1}{\varepsilon_c \cdot S} \left[ \Phi(S) \cdot \frac{\partial S}{\partial X} + \Pi(S) \cdot \kappa \right] \frac{\partial C}{\partial X} \end{array} \right\} \quad (30)$$

With the term  $\kappa$  being (this term is dimensionless)

$$\kappa = \frac{\varepsilon_g \cdot L}{\varepsilon_c (1 - S_{or} - S_{wi})} = \frac{\frac{\kappa \cdot \Delta \rho}{\mu_b} \cdot g \cdot L}{(1 - S_{or} - S_{wi}) \frac{\sigma \cos \theta \sqrt{K \varphi}}{\mu_b}} \\ = \frac{\sqrt{K} \cdot \Delta \rho \cdot g \cdot L}{(1 - S_{or} - S_{wi}) \sigma \cos \theta \sqrt{\varphi}} \quad (31)$$

At a laboratory scale, gravity is less critical because of the short length of the sample. However, for long samples or at field scale where  $L$  is considerable, the gravity effect is the dominant case.

At the intermediate range, for instance, at the proximity of the well, contributions of both capillary and gravity effects are substantial, where the capillary term ( $\varepsilon_c$ ) and gravity term ( $\varepsilon_g$ ) in eq 30 need to be considered simultaneously. Besides, the gravity term may compete with the capillary effect for gravity-resistant displacement or can improve displacement efficiency for the gravity-assisting case.

Using the self-similar equation  $\Lambda = \frac{X}{\sqrt{T_1}}$  in eq 30

$$\left\{ \begin{array}{l} \frac{\partial S}{\partial \Lambda} \left( -\frac{\Lambda}{2T_1} \right) = -\frac{\partial}{\partial \Lambda} \left( \frac{1}{\sqrt{T_1}} \right) \left( \Pi(S) \cdot \left( \frac{dJ}{dS} \cdot \frac{\partial S}{\partial \Lambda} \left( \frac{1}{\sqrt{T_1}} \right) + \kappa \right) \right) \\ \frac{\partial C}{\partial \Lambda} \left( -\frac{\Lambda}{2T_1} \right) = -\left( \frac{1}{S} \right) \left[ \Pi(S) \cdot \left( \frac{dJ}{dS} \cdot \frac{\partial S}{\partial \Lambda} \left( \frac{1}{\sqrt{T_1}} \right) + \kappa \right) \right] \frac{\partial C}{\partial \Lambda} \cdot \left( \frac{1}{\sqrt{T_1}} \right) \end{array} \right\} \quad (32)$$

Equation 32 at any arbitrary position (at  $X = a$  and  $\sqrt{T_1} = \frac{a}{\Lambda}$ ) yields

$$\left( \frac{dS}{d\Lambda} \right) \cdot \Pi(S) \cdot J' - S \cdot \left( \frac{dS}{d\Lambda} \right) \cdot \left\{ \Pi'(S) \cdot J' + \Pi(S) \cdot J'' \right\} \\ = \kappa \frac{a}{\Lambda} \left[ S \cdot \Pi'(S) - \Pi(S) \right] + \kappa \cdot S \cdot \Pi(S) \cdot \frac{d}{dS} \left( \frac{a}{\Lambda} \right) \\ + S \cdot \Pi(S) \cdot J' \cdot \frac{d}{dS} \left( \frac{dS}{d\Lambda} \right) \quad (33)$$

Using the derivative law as  $\frac{1}{\frac{dS}{d\Lambda}} = \frac{d\Lambda}{dS} = \Lambda'(S)$  and removing similar parameters from both sides

$$\left( \frac{1}{S} - \frac{\Pi'(S)}{\Pi(S)} - \frac{J''}{J'} \right) \\ = \frac{\kappa \cdot a}{J'} \cdot \frac{\Lambda'(S)}{\Lambda(S)} \left[ \frac{\Pi'(S)}{\Pi(S)} - \frac{1}{S} - \frac{\Lambda'(S)}{\Lambda(S)} \right] + \frac{d}{dS} \left( \frac{dS}{d\Lambda} \right) \quad (34)$$

Applying the logarithmic rules and integration from both sides in respect to  $S$

$$\ln \left( \frac{C_1 \cdot S}{\Pi(S) \cdot J' \cdot \left( \frac{dS}{d\Lambda} \right)} \right) = \kappa \cdot a \cdot \left\{ \left( \frac{1}{J'} \right) \cdot \ln \left( \frac{\Pi(S)}{S} \right) + \Omega(S) \right\} \\ \rightarrow \Omega(S) = \int \ln \left( \frac{\Pi(S)}{S} \right) \cdot \left( \frac{J''}{J'^2} \right) dS \quad (35)$$

The last integral consists of “ $S^n$ ” functions only, which are usually determined by empirical relations already given.<sup>13–15</sup> Further algebraic simplifications and removing logarithm functions include

$$\frac{\Pi(S) \cdot J' \cdot \left( \frac{\Pi(S) \cdot e^{\Omega(S) \cdot J'} }{S} \right)^{(\kappa \cdot a / J')}}{C_1 \cdot S} dS = d\Lambda \\ \Rightarrow \Lambda = \left( \frac{1}{C_1} \right) \int_0^1 \left( \frac{\Pi(S)}{S} \right)^{1 + \left( \frac{\kappa \cdot a}{J'} \right)} \cdot J' \cdot \left( e^{\Omega(S) \cdot J'} \right)^{(\kappa \cdot a / J')} dS \quad (36)$$

In accordance with eq 36,  $C_1$  depends on the slope of saturation gradient at any specific point. For the determination of changes

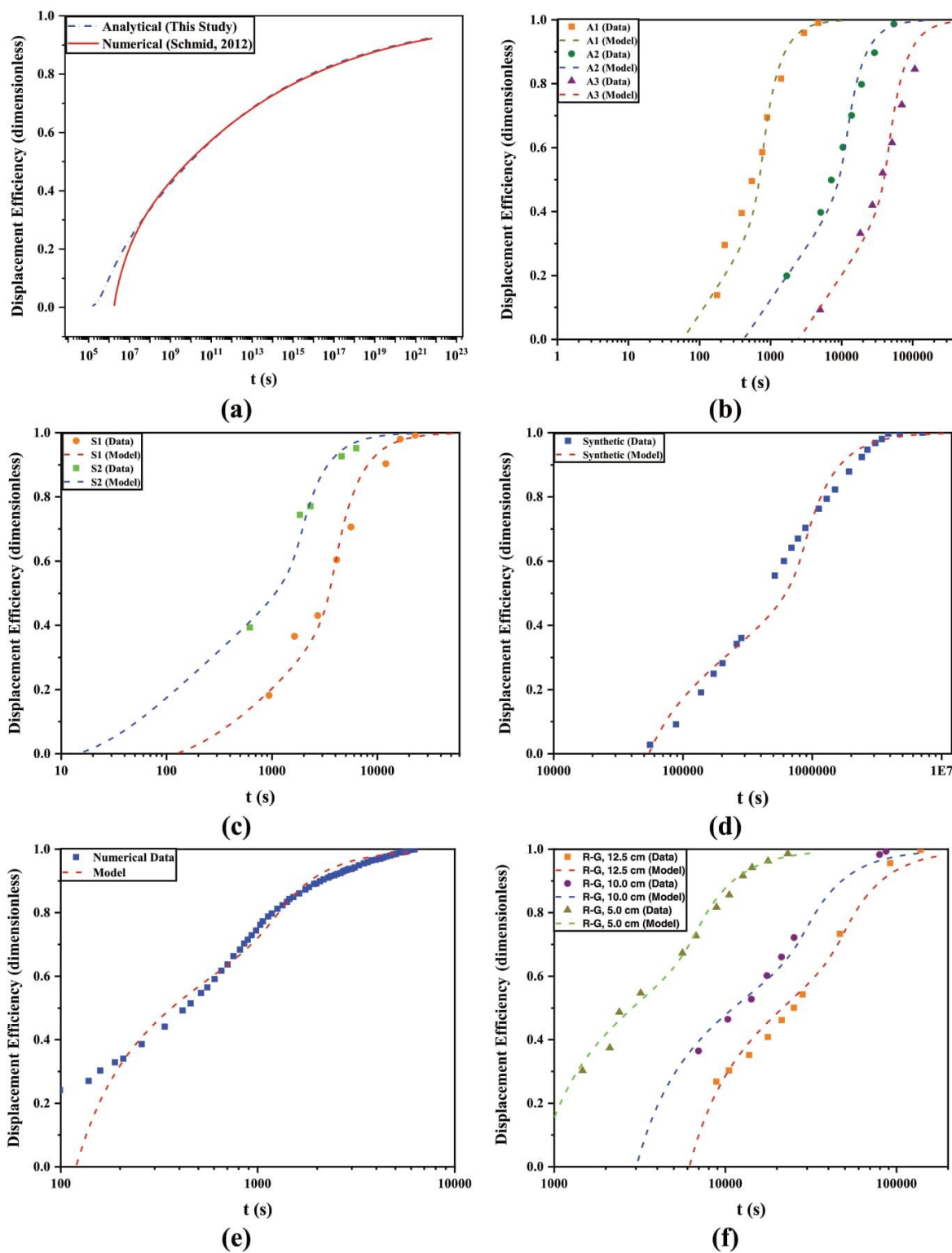


**Figure 4.** (a) Numerical and exact analytical solutions for counter-current imbibition (data in Table 2). Experimental and analytical exact solutions for counter-current imbibition showing saturation versus time for data in Table 3: (b) alundum sample;<sup>22</sup> (c) Weiler sandstone;<sup>22</sup> (d) synthetic sample;<sup>38</sup> (e) numerical model data;<sup>2</sup> and (f) G-R samples.<sup>3</sup>



in saturation at any arbitrary location ( $X = a$ ) as a function of time, we use  $\Lambda = \frac{a}{\sqrt{T}}$

$$T = \left[ \frac{a}{\int_0^1 \left( \frac{1}{C_1} \right) \left( \frac{\Pi(S)}{S} \right)^{1+\left(\frac{\kappa}{\bar{r}}\right)} \cdot J' \cdot \left( e^{\Omega(S) \cdot J'} \right)^{(\kappa \cdot a / J')} dS} \right]^2 \quad (37)$$

For the case that capillary term is dominant and gravity term is ignored ( $\varepsilon_g \approx 0$ ), the value of  $\kappa$  tends to zero ( $\kappa \approx 0$ ), and considering this situation in eq 37 and at an effluent ( $a = 1$ ), the integral changes to

$$\begin{aligned} \Lambda &= \frac{1}{\sqrt{T}} = \left( \frac{1}{C_1} \right) \int_0^1 \left( \frac{\Pi(S)}{S} \right) \cdot J' dS \\ &= \left( \frac{1}{C_1} \right) \int_0^1 \left( \frac{\Phi(S)}{S} \right) dS \end{aligned} \quad (38)$$

which is equal to eq 21 and proves the accuracy of the analytical approach.

#### 4. VALIDATING THE EXACT SOLUTION WITH NUMERICAL AND EXPERIMENTAL DATA

Every analytical solution needs to be confirmed with experimental results to validate the accuracy of the solution methodology. In cases

**Table 2. Input Parameters for the Numerical Scheme and Exact Analytical Solution Considering a Mixed-Wet System<sup>a</sup>**

initial water saturation (fraction)	0.2
residual oil/water saturation (fraction)	0.1
$k_{rwmax}$ (fraction)	0.6
$k_{romax}$ (fraction)	0.8
entry capillary pressure (Pa)	12 000
maximum capillary pressure (Pa)	400 000
water viscosity (Pa·s)	0.001
oil viscosity (Pa·s)	0.003
permeability (mD)	300
porosity (fraction)	0.2
interfacial tension (N/m)	0.05

<sup>a</sup>Data provided by ref 37.

where experimental values are not available, high-resolution and fine-grid numerical simulation may be used to verify an analytical solution. In this section, the newly proposed analytical solution will be validated with the available data from the literature.

**4.1. Capillary-Dominated Case.** Governing eq 15 with boundary conditions in eq 16 may be verified with numerical results, as proposed by ref 37. In their work, an approximation of fractional flow function ( $F$ )

**Table 3. Experimental Data for Core Samples with Different Wettability and Different Countercurrent Displacement Mechanisms (as in Figure 1)**

reference	rock type	sample length (m)	sample permeability (m <sup>2</sup> )	porosity (fraction)	oil viscosity (Pa·s)	water viscosity (Pa·s)	interfacial tension (N/m)	initial water saturation
22	Alundum	0.1105	$1.525 \times 10^{-12}$	0.289	0.0085	0.0009	0.035	0.243
	Weiler sandstone	0.0523	$1.184 \times 10^{-13}$	0.181	0.158	0.0009	0.035	0.243
38	synthetic sample (aluminum silicate)	0.847	$2.961 \times 10^{-12}$	0.478	0.0115	0.001	0.052	0.164
2	base-case numerical model	0.2	$1.974 \times 10^{-14}$	0.300	0.001	0.001	0.025	0.001
3	G-R-1	0.125	$2.36 \times 10^{-14}$	0.300	0.001	0.001	0.025	0.01
	G-R-2	0.1008	$2.36 \times 10^{-14}$	0.300	0.001	0.001	0.025	0.01
	G-R-3	0.0502	$2.36 \times 10^{-14}$	0.300	0.001	0.001	0.025	0.01

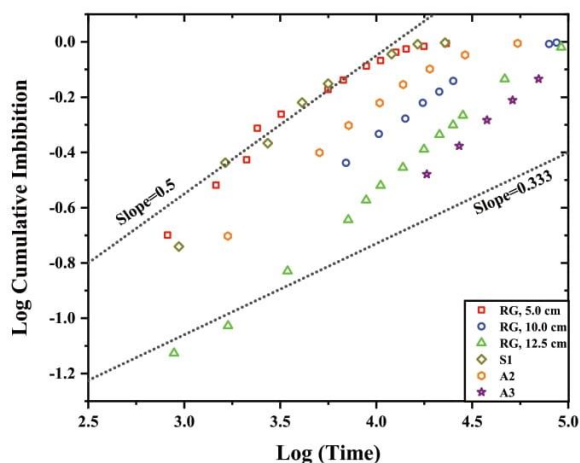


**Figure 5.** Data points from Figure 4b–d in the log–log plot. Scatter of data points shows that imbibition is proportional to the square root of time for some of the data points, while for the rest of the data points, imbibition is proportional to the function of time between the square and cube roots of time.

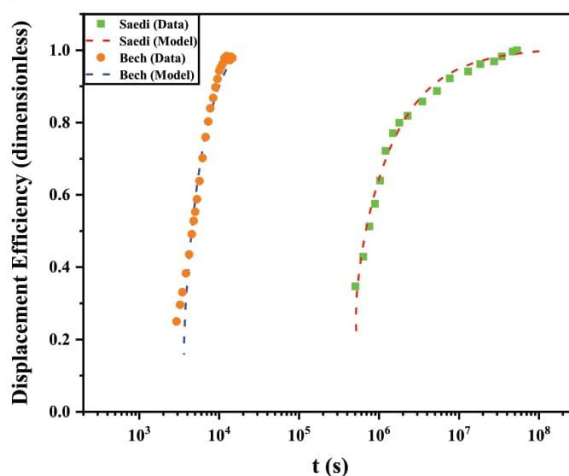


**Figure 6.** Simulation result and exact analytical solution for gravity-dominated imbibition showing saturation versus time for data in Table 4.

with an arbitrary accuracy of  $A$  was suggested. Then,  $F$  was approximated to obtain  $F(S_w)$  for the continuous range of  $S_w$ , with distance  $\Delta S_w$  between residual and maximum water saturation. The



Table 4. Experimental Data for Models of Gravity Dominance<sup>40,41</sup>

reference	reservoir pressure (MPa)	sample length (m)	sample permeability (m <sup>2</sup> )	porosity (fraction)	nonwetting viscosity (Pa·s)	wetting viscosity (Pa·s)	initial water saturation
40	0.5	0.6	$5.92 \times 10^{-13}$	0.4	0.0025	0.001	0.0
41	31	8	$9.87 \times 10^{-16}$	0.29	0.0033	0.00035	0.2

Table 5. Experimental Data for Core Samples Researched by Zhang et al.<sup>42</sup>

rock type	sample length (m)	sample permeability (m <sup>2</sup> )	porosity (fraction)	gas viscosity (Pa·s)	water viscosity (Pa·s)	interfacial tension (N/m)	initial water saturation
Bakken-1 (Shale)	0.0212	$4.84 \times 10^{-16}$	0.084	0.000018	0.000896	0.035	0.0
Bakken-4 (Shale)	0.0429	$1.28 \times 10^{-16}$	0.049	0.000018	0.000896	0.05	0.0
Berea-3 (Sand)	0.0455	$1.06 \times 10^{-14}$	0.231	0.000018	0.000896	0.05	0.0

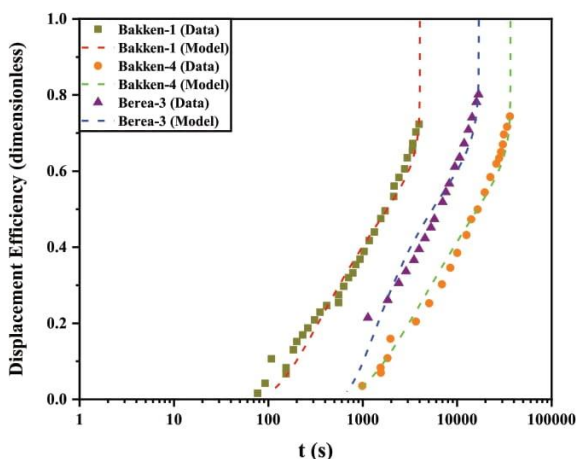


Figure 7. Experimental and analytical exact solutions for counter-current imbibition showing saturation versus time for data in Table 5.

detailed numerical scheme they applied is presented in Appendix C. This numerical pattern has been completed by ref 37.

Although the proposed scheme appears straightforward and applicable, it is still numerical, where analytical validation is required. The exact solution proposed in this study (eq 21) can be verified by this method, with results shown in Figure 4a (using the data listed in Table 2). The analytical and numerical solutions are in very good agreement.

There is also available experimental data relating to countercurrent imbibition on different rock cores. The very first available data was presented by Mattax and Kyte<sup>22</sup> who performed a linear imbibition test (OEO) on cylindrical alundum and Weiler sandstone samples encased in a plastic container. Their experimental data has been referred to in many studies.<sup>6,23,37</sup> Another essential set of experiments was performed by Hamon and Vidal<sup>38</sup> on synthetic samples made of aluminum silicate. The properties of these samples are shown in Table 3, and the plot of experimental data versus analytical solution is shown in Figure 4. It can be observed that very good agreement forms between the exact analytical solution and laboratory data.

The importance of pore connectivity theorem and deviation from LWE can be observed in Figure 5. In this figure, the experimental data in Figure 4 was plotted in the log–log diagram to represent the effect of pore connectivity. Accepting the imbibition front movement in respect to the square root of time, all experimental data points should lie on the line with the slope equal to 0.5. It is seen that some of the points follow this theory. However, the rest of data points do not show the same behavior and front imbibes with a function of time between the square and the cube roots of time. This confirms that the self-similar function in eq 19 does not need to be necessarily proportional to the square root of time. Rather, other dependencies of front imbibition in respect to the time are also plausible. Interestingly, the methodology used to solve this

equation permits the application of any functional form in respect to time and space.

**4.2. Gravity-Dominated Case.** Semiempirical and approximate analytical solutions already exist for gravity-dominated scenarios,<sup>17,18</sup> where multiple scaling groups were derived for them.<sup>1,17,18</sup> Related to this, two dimensionless parameters have been suggested within the literature ( $R$  and  $\alpha$  as explained in eqs 5 and 6) and used for the derivation of analytical and semianalytical solutions of gravity-dominated imbibition.<sup>6,7,18,19</sup>

If capillary forces are sufficiently small, gravity segregation can make a significant contribution to the oil displacement. These conditions are mostly observed within fractures or EOR methods, such as steam-assisted gravity drainage (SAGD). Under these circumstances, initial water saturation has a significant influence on the rate of oil recovery.<sup>39</sup>

Creating an experimental setup with no capillary pressure and gravity as the dominant mechanism is difficult in a laboratory environment. However, a few simulations and experiments have been conducted, where gravity was dominant, while capillary forces were considered negligible.<sup>40</sup> Figure 6 shows the plot of simulation data versus the analytical solution achieved in this study (eq 29), where modeling data is listed in Table 4.

**4.3. Simultaneous Contribution of Capillary and Gravity Forces.** There are very few experimental results for cases when both capillary pressure and gravity force are active. A very recent laboratory study was performed by Zhang et al.,<sup>42</sup> who measured these effects on low-permeability and high-permeability samples of Bakken shale and Berea sandstone. The experimental data for their tests are presented in Table 5 and Figure 7, showing an experimental recovery of imbibition versus time compared with the analytical approach presented in this study (Section 3.3 and eq 37). There is also good agreement between the experimental and analytical results in this figure.

## 5. SENSITIVITY TO INFLUENCING PARAMETERS

Careful consideration of solution methodology, as evident in Section 4.3, reveals that the most significant parameter influencing the contribution of gravity or capillary force is  $\kappa$ . This value is estimated by eq 31, which is the ratio of gravity to capillary coefficients ( $\epsilon_g$  and  $\epsilon_c$  respectively). Therefore, sensitivity analysis should be performed on this parameter. In turn, this parameter is affected by reservoir parameters like the length of the reservoir, initial water saturation, residual oil saturation, density difference of fluid phases, interfacial tension, porosity, and permeability.

Figure 8 shows the effect of density changes, reservoir length, initial water saturation, and residual oil saturation on the displacement efficiency of the reservoir when both capillary and gravity forces are contributing. For the plot of experimental points versus the model, the methodology of Farrokhrouz and Asef<sup>43</sup> was applied.

The density difference between the wetting and nonwetting phases is translated as gravity segregation. Two phases in Figure 8a indicate how water and air play roles in the wetting phase. At

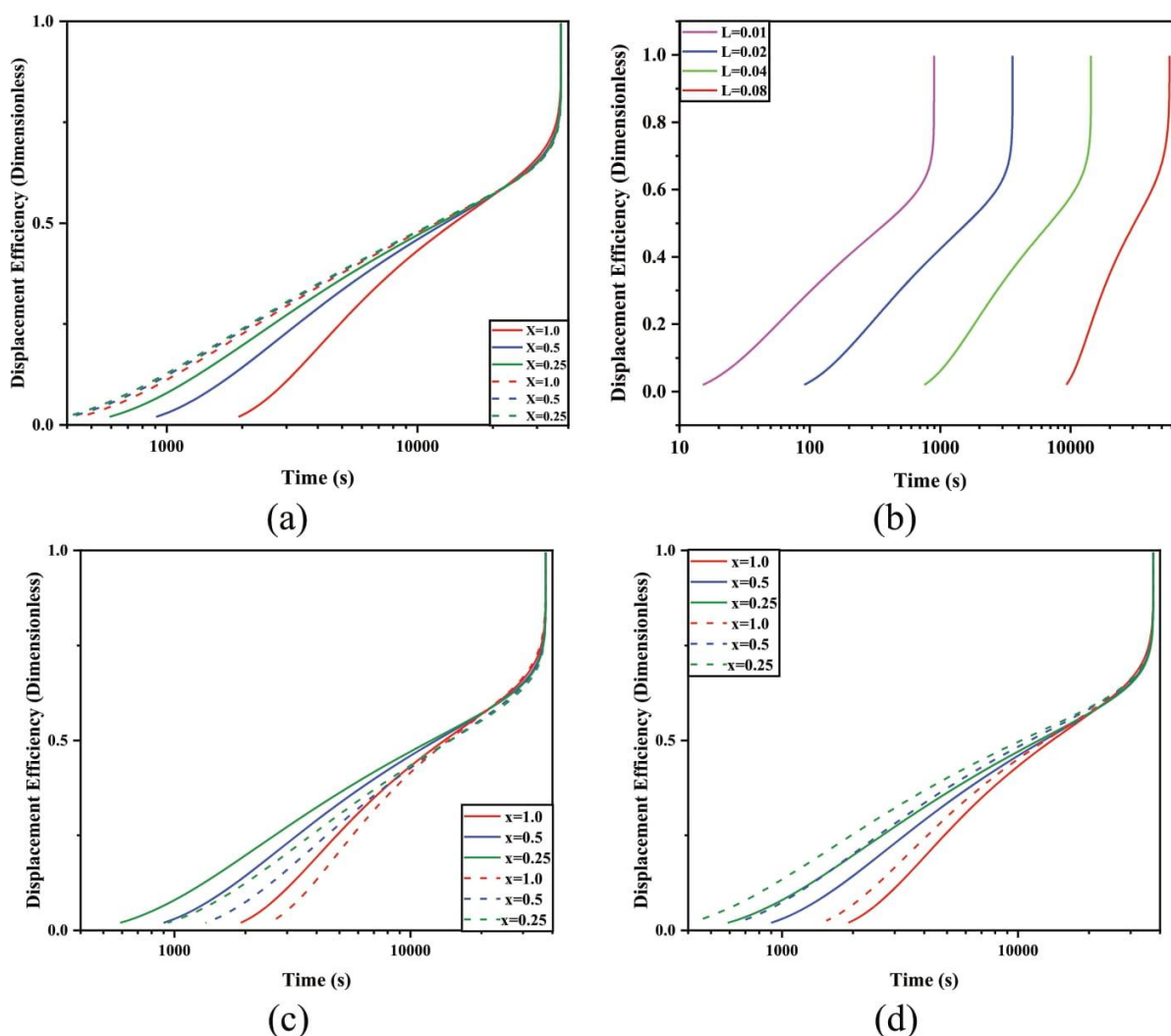


**Figure 8.** Effect of (a) density difference, (b) core length, (c) initial water saturation, and (d) residual oil saturation on the displacement efficiency of the core sample. Data taken from the Bakken-4 Shale sample in Table 5. Solid lines in panels (a), (c), and (d) show the initial condition ( $\Delta\rho = 1000 \text{ kg/m}^3$ ,  $S_{wi} = 0.0$  and  $S_{or} = 0.2$ ), and dashed lines show the second condition case ( $\Delta\rho = 100 \text{ kg/m}^3$ ,  $S_{wi} = 0.2$ , and  $S_{or} = 0.0$ ).

early distances from the injection point, gravity force cannot be greatly promoted, and the curves of low ( $\Delta\rho = 100 \text{ kg/m}^3$ ) and high ( $\Delta\rho = 1000 \text{ kg/m}^3$ ) density differences are very close to each other as capillary force is the dominant parameter (solid and dashed green lines at  $X = 0.25$ ). As fluid front moves along with the core, displacement efficiency becomes higher in lower  $X$  values for  $\Delta\rho = 100 \text{ kg/m}^3$  at a certain time. However, at later times and by giving enough time for imbibition, displacement efficiency for  $\Delta\rho = 1000 \text{ kg/m}^3$  surpasses a little of the core in respect to  $\Delta\rho = 100 \text{ kg/m}^3$ . This is due to the complete segregation of denser fluid as a gravity-assisting case, as evident in Figure 8a. It is expected that the result would be reversed for gravity-opposing drainage.

Longer core samples show a higher effect of gravity (Figure 8b), where this is shown in a sharper trend of the efficiency for  $L = 0.08 \text{ m}$  compared with that for  $L = 0.01 \text{ m}$ . This is also predictable, where at longer lengths, the gravity force is the dominant parameter and capillary force cannot contribute to

displacement efficiency to a great extent. At smaller core lengths, there are two distinct regions of recovery: the lower slope region showing the capillary-dominant case and the sharp slope region showing the gravity-dominant case.

At a certain time, displacement efficiency is always higher at  $S_{wi} = 0$  in comparison with that at  $S_{wi} = 0.2$  (Figure 8c). Initial water saturation within the core depends on the *in situ* rock properties, especially tortuosity and pore size distribution. Considering the methodology approach selected for this core sample,<sup>42</sup> further interpretations require more accurate measurement (using NMR, for instance) and further descriptive data about the pore distribution through the core samples (scanning electron microscopy, SEM, or X-ray analyses), which falls outside the scope of this study. The same interpretation can be concluded for residual oil saturation, as seen in Figure 8d. In cases of low residual oil saturation, displacement efficiency is higher, while for  $S_{or} = 0.2$ , it is lower at a certain distance from the injection point and for the same time. Again, at late times,



displacement efficiency is independent of time and distance due to gravity.

## 6. DISCUSSION

The new analytical solution proposed in this paper has been accurately validated against the numerical and experimental results available in the literature. Previous analytical solutions of countercurrent SI have been mainly dedicated to horizontal flows or solutions with certain assumptions about the viscosity of phases. McWhorter and Sunada<sup>11</sup> have assumed that spontaneous imbibition (SI) always changes with the square root of time, while Hu et al.<sup>30</sup>—through experimental measurements—have shown later that SI is a function of pore connectivity and may deviate from classical behavior. Those studies that challenged LWE (as in Section 2.2) also proved that this front movement relative to the square root of time is not always accurate. In conclusion, the methodology proposed by McWhorter and Sunada<sup>1</sup> is not valid in all instances.

The characteristics of this new approach make it independent of similar presumptions. This can also be utilized for vertical flows (considering the gravity effect) and at the same time with capillary imbibition. In addition, the function of fluid imbibition through the rock can be selected arbitrarily. Furthermore, analytical data matches with experimental measurements in the acceptable 10% error band. Deviation in error ranges may be due to various correlations proposed for relative permeability functions. A list of proposed correlations for relative permeability functions and fractional flow functions can be found in the literature.<sup>13,14,15</sup>

In actual cases, one of these two forces (gravity and capillary) is usually dominant in the field or experiment. For tight and low-permeable formations (e.g., oil shale or tight sand), gravity cannot be effective as fluid would not move freely within the media. Instead, imbibition develops through the pores but very slowly due to high capillary pressure. Contrastingly, for vertical movement of the fluid (e.g., gravity drainage), gravity can play an important role as fluid flows due to gravity. Capillary imbibition also exists but with a small contribution to the total recovery of the hydrocarbon.

There are also cases where reasonable influence of both gravity and capillary forces occur (e.g., dual-porosity or dual permeability media). For the high-permeable zone, fluid flows freely through the channels and fractures, and gravity is dominant in this case. For the low-permeability zone, the capillary surpasses gravity force. For cases where fractures surround the matrix, the remaining oil/gas within the matrix would only be expelled over a long time by capillary imbibition. In the intermediate state, both capillary and gravity forces can contribute, where nonwetting phase displacement occurs as a result of these two mechanisms. In these cases, the analytical approach in Section 3.3 is valid and perfectly matches with the experimental data (Figure 7).

## 7. CONCLUSIONS

A new exact solution methodology has been suggested in this paper for the countercurrent spontaneous imbibition of wetting phase, effectively displacing the nonwetting phase porous medium, while most of the assumptions in previously proposed models have been relaxed to give a more general solution. The most important of these has been the front movement, which has only been considered proportional to the square root of time in

previous studies. Other experimental studies have shown that this is not the only functional form of front movement.

The analytical model has been adapted for the case of dominant capillary force, dominant gravity force, and simultaneous capillary and gravity presence. Matching of experimental results (all data obtained from the literature) with the theoretical model shows accuracy of the analytical solution and appropriate consistency.

Sensitivity analyses of the involved parameters have shown that most of the effective parameters behave similarly at late times, while at early times, density difference,  $S_{wir}$  and  $S_{or}$  play significant roles.

## ■ ASSOCIATED CONTENT

### Supporting Information

The Supporting Information is available free of charge at <https://pubs.acs.org/doi/10.1021/acs.energyfuels.1c03868>.

Detailed derivation of the equations and references for Appendices A–C (PDF)

## ■ AUTHOR INFORMATION

### Corresponding Author

**Mohsen Farrokhrouz** — School of Civil, Environment and Mining Engineering, The University of Adelaide, Adelaide, South Australia 5005, Australia; School of Engineering, Edith Cowan University, Joondalup, Western Australia 6027, Australia; Centre for Sustainable Energy and Resources, Edith Cowan University, Perth 6027, Australia; [orcid.org/0000-0001-5169-6894](https://orcid.org/0000-0001-5169-6894); Email: [mohsen.farrokhrouz@adelaide.edu.au](mailto:mohsen.farrokhrouz@adelaide.edu.au)

### Authors

**Abbas Taheri** — School of Civil, Environment and Mining Engineering, The University of Adelaide, Adelaide, South Australia 5005, Australia; The Robert M. Buchan Department of Mining, Queen's University, Kingston, Ontario K7L 3N6, Canada

**Stefan Iglauer** — School of Engineering, Edith Cowan University, Joondalup, Western Australia 6027, Australia; Centre for Sustainable Energy and Resources, Edith Cowan University, Perth 6027, Australia; [orcid.org/0000-0002-8080-1590](https://orcid.org/0000-0002-8080-1590)

**Alireza Keshavarz** — School of Engineering, Edith Cowan University, Joondalup, Western Australia 6027, Australia; Centre for Sustainable Energy and Resources, Edith Cowan University, Perth 6027, Australia; [orcid.org/0000-0002-8091-961X](https://orcid.org/0000-0002-8091-961X)

Complete contact information is available at:

<https://pubs.acs.org/doi/10.1021/acs.energyfuels.1c03868>

### Notes

The authors declare no competing financial interest.

## ■ LIST OF NOMENCLATURES

### Roman Symbols

$A$  = constant rate,  $m/\sqrt{s}$

$B$  = surface area,  $m^2$

$c_t$  = total compressibility,  $m^2/N$

$C$  = adsorption,  $m^3/kg$

$c$  = ion concentration, dimensionless

$D$  = hydrodynamic dispersion,  $m^2/s$

$F, f$  = fractional flow function, dimensionless

$g$  = gravity acceleration,  $m/s^2$

$k_r$  = relative permeability, dimensionless  
 $J$  = Leverett J-function, dimensionless  
 $q$  = 1D flow, velocity, m/s  
 $R$  = total flow to water flux ratio, dimensionless  
 $S$  = saturation, dimensionless  
 $t$  = time, s  
 $K$  = permeability,  $m^2$   
 $L_c$  = characteristic length, m  
 $p$  = pressure,  $N/m^2$   
 $r$  = pore radius, m  
 $x$  = distance, m  
 $V$  = volume,  $m^3$

## ■ GREEK SYMBOLS

$\varepsilon$  = constant, dimensionless  
 $\kappa$  = constant, dimensionless  
 $\lambda$  = mobility ratio  
 $\mu$  = phase viscosity, Pa·s  
 $\rho$  = density,  $kg/m^3$   
 $\sigma$  = interfacial tension, N/m  
 $\tau$  = tortuosity  
 $\varphi$  = porosity  
 $\Psi$  = self-similar function

## ■ SUBSCRIPTS

b = bulk  
 c = capillary  
 g = gravity  
 n = nonwetting phase  
 w = wetting phase  
 t = total  
 o = oil  
 g = gas  
 r = rock  
 w = water  
 $\alpha$  = fluid phase

## ■ REFERENCES

- Mirzaei-Paiaman, A.; Masihi, M.; Standnes, D. An Analytic Solution for the Frontal Flow Period in 1D Counter-Current Spontaneous Imbibition into Fractured Porous Media Including Gravity and Wettability Effects. *Transp. Porous Media* **2011**, *89*, 49–62.
- Pooladi-Darvish, M.; Firoozabadi, A. Cocurrent and Counter-current Imbibition in a Water-Wet Matrix Block. *SPE J.* **2000**, *5*, 3–11.
- Pooladi-Darvish, M.; Firoozabadi, A. Experiments and Modelling of Water Injection in Water-wet Fractured Porous Media. *Journal of Canadian Petroleum Technology* **2000**, *39*, No. 2.
- Farrokhrouz, M.; Taheri, A.; Iglauer, S.; Keshavarz, A. Analytical Exact Solution for Co-Current Spontaneous Imbibition in Porous Media Considering Early- and Late-Time Effects. *Energy Fuels* **2021**, *35*, 17499–17511.
- Civan, F.; Rasmussen, M. Asymptotic Analytical Solutions for Imbibition Waterfloods in Fractured Reservoirs. *SPE J.* **2001**, *6*, 171–181.
- Tavassoli, Z.; Zimmerman, R.; Blunt, M. Analytic Analysis for Oil Recovery During Counter-Current Imbibition in Strongly Water-Wet Systems. *Transp. Porous Media* **2005a**, *58*, 173–189.
- Tavassoli, Z.; Zimmerman, R. W.; Blunt, M. J. Analysis of counter-current imbibition with gravity in weakly water-wet systems. *J. Pet. Sci. Eng.* **2005**, *48*, 94–104.
- Schmid, K.; Geiger, S. Universal scaling of spontaneous imbibition for water-wet systems. *Water Resour. Res.* **2012**, *48*, No. 3507.
- Yortsos, Y. C.; Fokas, A. S. An Analytical Solution for Linear Waterflood Including the Effects of Capillary Pressure. *Soc. Pet. Eng. J.* **1983**, *23*, 115–124.
- Kashchiev, D.; Firoozabadi, A. Analytical Solutions for 1D Counter-current Imbibition in Water-Wet Media. *SPE J.* **2003**, *8*, 401–408.
- McWhorter, D. B.; Sunada, D. K. Exact integral solutions for two-phase flow. *Water Resour. Res.* **1990**, *26*, 399–413.
- McWhorter, D. B.; Sunada, D. K. Reply [to ‘Comment on ‘Exact integral solutions for two-phase flow’ by David B. McWhorter and Daniel K. Sunada’]. *Water Resour. Res.* **1992**, *28*, 1479.
- Corey, A. T. The interrelation between gas and oil relative permeabilities. *Prod. Mon.* **1954**, *19*, 38–41.
- Brooks, R. H.; Corey, A. T. *Hydraulic Properties of Porous Media*; Hydrology papers (Colorado State University), 1964; Vol. 3.
- Fourar, M.; Lenormand, R. In *A Viscous Coupling Model for Relative Permeabilities in Fractures*, SPE Annual Technical Conference and Exhibition; Society of Petroleum Engineers, 1998.
- Buckley, S. E.; Leverett, M. Mechanism of fluid displacement in sands. *Trans. AIME* **1942**, *146*, 107–116.
- Morrow, N. R.; Xie, X. Oil recovery by spontaneous imbibition from weakly water-wet rocks. *Petrophysics* **2001**, *42*, No. v42n4a1.
- Li, K.; Horne, R. N. Generalized Scaling Approach for Spontaneous Imbibition: An Analytical Model. *SPE Reservoir Eval. Eng.* **2006**, *9*, 251–258.
- Mirzaei-Paiaman, A. Analysis of counter-current spontaneous imbibition in presence of resistive gravity forces: Displacement characteristics and scaling. *J. Unconv. Oil Gas Resour.* **2015**, *12*, 68–86.
- Lucas, R. Ueber das Zeitgesetz des kapillaren Aufstiegs von Flüssigkeiten. *Kolloid-Z.* **1918**, *23*, 15–22.
- Washburn, E. W. The dynamics of capillary flow. *Phys. Rev.* **1921**, *17*, No. 273.
- Mattax, C. C.; Kyte, J. R. Imbibition Oil Recovery from Fractured, Water-Drive Reservoir. *Soc. Pet. Eng. J.* **1962**, *2*, 177–184.
- Shouxiang, M.; Morrow, N. R.; Zhang, X. Generalized scaling of spontaneous imbibition data for strongly water-wet systems. *J. Pet. Sci. Eng.* **1997**, *18*, 165–178.
- Mirzaei-Paiaman, A.; Masihi, M.; Roghanian, R. A Review on Analytical Scaling Equations for Counter-Current Spontaneous Imbibition in Naturally Fractured Oil Reservoirs. *J. Pet. Res.* **2020**, *30*, 21–33.
- Hammecker, C.; Jeannette, D. Modelling the capillary imbibition kinetics in sedimentary rocks: Role of petrographical features. *Transp. Porous Media* **1994**, *17*, 285–303.
- Onda, T.; Shibuichi, S.; Satoh, N.; Tsujii, K. Super-Water-Repellent Fractal Surfaces. *Langmuir* **1996**, *12*, 2125–2127.
- Leventis, A.; Verganelakis, D. A.; Halse, M. R.; Webber, J. B.; Strange, J. H. Capillary Imbibition and Pore Characterisation in Cement Pastes. *Transp. Porous Media* **2000**, *39*, 143–157.
- Dimitrov, D. I.; Milchev, A.; Binder, K. Capillary Rise in Nanopores: Molecular Dynamics Evidence for the Lucas-Washburn Equation. *Phys. Rev. Lett.* **2007**, *99*, No. 054501.
- Stukan, M. R.; Ligneul, P.; Crawshaw, J. P.; Boek, E. S. Spontaneous Imbibition in Nanopores of Different Roughness and Wettability. *Langmuir* **2010**, *26*, 13342–13352.
- Hu, Q.; Ewing, R. P.; Dultz, S. Low pore connectivity in natural rock. *J. Contam. Hydrol.* **2012**, *133*, 76–83.
- Yang, R.; Hao, F.; He, S.; He, C.; Guo, X.; Yi, J.; Hu, H.; Zhang, S.; Hu, Q. Experimental investigations on the geometry and connectivity of pore space in organic-rich Wufeng and Longmaxi shales. *Mar. Pet. Geol.* **2017**, *84*, 225–242.
- Hu, Q.; Ewing, R. P.; Rowe, H. D. Low nanopore connectivity limits gas production in Barnett formation. *J. Geophys. Res.: Solid Earth* **2015**, *120*, 8073–8087.
- Mirzaei-Paiaman, A.; Ostadhassan, M.; Rezaee, R.; Saboorian-Jooybari, H.; Chen, Z. A new approach in petrophysical rock typing. *J. Pet. Sci. Eng.* **2018**, *166*, 445–464.
- Brevdo, L.; et al. Permanent Fronts in Two-Phase Flows in a Porous Medium. *Transp. Porous Media* **2001**, *44*, 507–537.
- Alizadeh, A. H.; Keshavarz, A.; Haghghi, M. In *Flow Rate Effect on Two-Phase Relative Permeability In Iranian Carbonate Rocks*, SPE-104828-MS, SPE Middle East Oil and Gas Show and Conference, 2007.



(36) Lake, L. W. *Enhanced Oil Recovery*; Prentice Hall: Englewood Cliffs, NJ, 1989; p 550.

(37) Schmid, K. S.; Alyafei, N.; Geiger, S.; Blunt, M. J. Analytical Solutions for Spontaneous Imbibition: Fractional-Flow Theory and Experimental Analysis. *SPE J.* **2016**, *21*, 2308–2316.

(38) Hamon, G.; Vidal, J. In *Scaling-Up the Capillary Imbibition Process From Laboratory Experiments on Homogeneous and Heterogeneous Samples*, European Petroleum Conference; Society of Petroleum Engineers: London, United Kingdom, 1986; p 12.

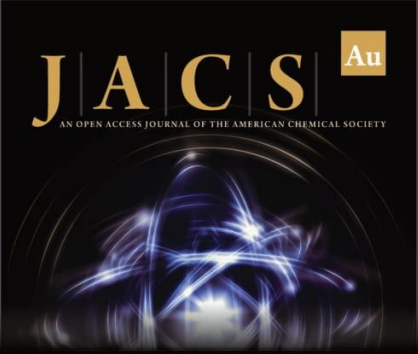
(39) Mirzaei-Paiaman, A.; Masihi, M. Scaling equations for oil/gas recovery from fractured porous media by counter-current spontaneous imbibition: from development to application. *Energy Fuels* **2013**, *27*, 4662–4676.

(40) Saedi, B.; Ayatollahi, S.; Masihi, M. Free fall and controlled gravity drainage processes in fractured porous media: Laboratory and modelling investigation. *Can. J. Chem. Eng.* **2015**, *93*, 2286–2297.

(41) Bech, N.; Jensen, O. K.; Nielsen, B. Modeling of Gravity-Imbibition and Gravity-Drainage Processes: Analytic and Numerical Solutions. *SPE Reservoir Eng.* **1991**, *6*, 129–136.


(42) Zhang, S.; Pu, H.; Zhao, J. X. Experimental and numerical studies of spontaneous imbibition with different boundary conditions: case studies of middle bakken and berea cores. *Energy Fuels* **2019**, *33*, 5135–5146.


(43) Farokhrouz, M.; Asef, M. R. In *Evaluation of Empirical Correlations for Biot's Coefficient Prediction*, The 15th International Workshop on Seismic Anisotropy, Manama, Bahrain, 2012.



**JACS** Au  
AN OPEN ACCESS JOURNAL OF THE AMERICAN CHEMICAL SOCIETY

Editor-in-Chief  
**Prof. Christopher W. Jones**  
Georgia Institute of Technology, USA

**Open for Submissions** 

pubs.acs.org/jacsau  ACS Publications  
Most Trusted. Most Cited. Most Read.

**Chapter 5:**  
**Experimental and Analytical Study of Acid Effect on  
Eagle Ford Shale Sample Considering Short-Term and  
Long-Term Effect**

# Statement of Authorship

Title of Paper	Laboratorial and analytical study for prediction of porosity changes in carbonaceous shale coupling reactive flow and dissolution
Publication Status	<input checked="" type="checkbox"/> Published <input type="checkbox"/> Accepted for Publication <input type="checkbox"/> Submitted for Publication <input type="checkbox"/> Unpublished and Unsubmitted work written in manuscript style
Publication Details	Journal of Petroleum Science and Engineering Volume 215, Part B, 110670 <a href="https://doi.org/10.1016/j.petrol.2022.110670">https://doi.org/10.1016/j.petrol.2022.110670</a>

## Principal Author

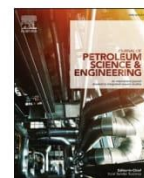
Name of Principal Author (Candidate)	Mohsen Farrokhrouz		
Contribution to the Paper	Designing the setup, Running the experiments, Acquiring Data, Experimental data matching with Analytical model, Knowledge, Analysis, Drafting		
Overall percentage (%)	80%		
Certification:	This paper reports on original research I conducted during the period of my Higher Degree by Research candidature and is not subject to any obligations or contractual agreements with a third party that would constrain its inclusion in this thesis. I am the primary author of this paper.		
Signature		Date	05/01/2022

## Co-Author Contributions

By signing the Statement of Authorship, each author certifies that:

- i. the candidate's stated contribution to the publication is accurate (as detailed above);
- ii. permission is granted for the candidate to include the publication in the thesis; and
- iii. the sum of all co-author contributions is equal to 100% less the candidate's stated contribution.

Name of Co-Author	Dr Abbas Taheri		
Contribution to the Paper	Knowledge, Conception, Drafting		
Signature		Date	05/01/2022
Name of Co-Author	Dr Alireza Keshavarz		
Contribution to the Paper	Knowledge, Conception, Drafting		
Signature		Date	05/01/2022
Name of Co-Author	Prof Stefan Iglauer		
Contribution to the Paper	Knowledge, Conception, Drafting		
Signature		Date	05/01/2022



## Laboratorial and analytical study for prediction of porosity changes in carbonaceous shale coupling reactive flow and dissolution

M. Farrokhrouz<sup>a,b,c,\*</sup>, A. Taheri<sup>a,d</sup>, S. Iglauer<sup>b,c</sup>, A. Keshavarz<sup>b,c</sup>

<sup>a</sup> School of Civil, Environment and Mining Engineering, The University of Adelaide, Adelaide, Australia

<sup>b</sup> School of Engineering, Edith Cowan University, Perth, Australia

<sup>c</sup> Centre for Sustainable Energy and Resources, Edith Cowan University, Perth, Australia

<sup>d</sup> The Robert M. Buchan Department of Mining, Queen's University, Kingston, Ontario, Canada

### ARTICLE INFO

#### Keywords:

Diffusion coefficient  
Reactive dissolution  
Residual acid  
Mathematical modeling  
Analytical solution

### ABSTRACT

Molecular diffusion of acid into a porous carbonate medium is usually referred to as acid imbibition. Accurate prediction of acid penetration into a formation and reaction with rock is not possible without a comprehensive understanding of the acid diffusion process and associated parameters.

This work aimed to derive an analytical solution for mineral-dissolution reactive diffusion when acid imbibes into a rock surface and where there is no flow condition under laboratory conditions. For the experimental part of the study, different disk samples of Eagle Ford shale were selected, and the effect of acid diffusion on the rock surface was fully investigated. Digital microscopic images confirm that with differing concentrations of consumed acid and saturation front movement, varying degrees of reactivity are conceivable, including surface reaction, surface dissolution, matrix acidizing, and induced fracturing.

For the mathematical modeling section, a continuity equation without an advection term and only a diffusion term was considered. An analytical solution was found for the dissolution of minerals as a result of reactive imbibition in a porous medium with porosity variations. The final form of the equation and the analytical solution is proposed here for the first time. Additional experiments were performed on Indiana limestone samples as control tests, with all experimental results matching perfectly with the developed analytical solution. Data from the literature relating to different temperatures also matched appropriately with the mathematical solution, effectively affirming the validity of the suggested solution. The proposed approach can be used as a predictive tool to verify the reactive models leading to porosity creation in the field scale.

### Credit author statement

The contribution of the authors can be listed like below: M. Farrokhrouz: Creation and development of the models, conducting the experiments, analysing the data gathered, draft preparation. Dr A. Taheri: Conceptualization, financial support, supervision, review, and editing. Dr A. Keshavarz: Provision of study materials and laboratory samples, supervision, review, and Editing. Dr S. Iglauer: Supervision, review and editing, team management.

### 1. Introduction

According to the statistics released by Annual Energy Outlook (2021) (EIA, 2021), US natural gas production by 2050 will account for more

than 80% from tight reservoirs and shale gas as unconventional resources of energy. Thus, a long-term plan for production management from these energy resources is needed. Unlike conventional oil and gas reservoirs, production from unconventional resources is more pricey. Stimulation operations like hydraulic fracturing, horizontal well technology or acid fracturing are very time-consuming and expensive jobs (Bedrikovetsky et al., 2012; Keshavarz et al., 2014, 2018; Akhondzadeh et al., 2021). Moreover, such operations cannot significantly increase oil recovery from unconventional resources. The typical oil recovery from low permeability reserves after hydraulic fracturing is less than 10% (Mukhina et al., 2021; Sheng, 2015).

Accordingly, incentives toward improving recovery from tight formations have started in the last decade. Some studies have suggested the utilization of surfactant and gas injection (Li et al., 2016; Alfarge et al.,

\* Corresponding author. School of Civil, Environment and Mining Engineering, The University of Adelaide, Adelaide, Australia.

E-mail addresses: [mohsen.farrokhrouz@adelaide.edu.au](mailto:mohsen.farrokhrouz@adelaide.edu.au), [m.farrokhrouz@ecu.edu.au](mailto:m.farrokhrouz@ecu.edu.au) (M. Farrokhrouz), [a.keshavarz@ecu.edu.au](mailto:a.keshavarz@ecu.edu.au) (A. Keshavarz).

<https://doi.org/10.1016/j.petrol.2022.110670>

Received 5 January 2022; Received in revised form 10 May 2022; Accepted 18 May 2022

Available online 6 June 2022

0920-4105/© 2022 Elsevier B.V. All rights reserved.



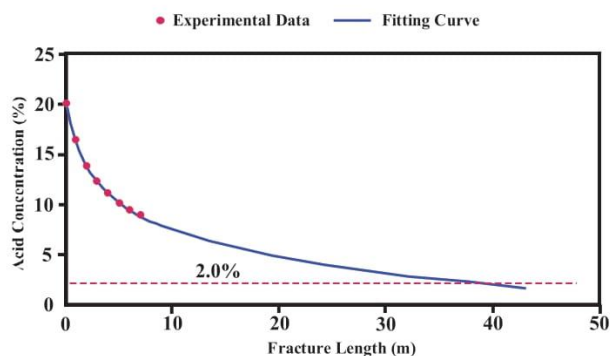


Fig. 1. Fracture length versus acid concentration self-diversion (adapted from (Liu et al., 2021)).

2018; Sanaei et al., 2018; Teklu et al., 2014) and acid treatment (Morsy et al., 2013, 2015; Sheng et al., 2014; Tripathi and Pournik, 2014; Suleimenova, 2015) to improve the ultimate recovery of the tight formations. Analogous to these studies, some researchers have focused on modeling and numerical studies to improve the understanding of fluid flow within fractured unconventional reservoirs. However, the key issue in this area is handling fracture-matrix interactions under different conditions (Farah, 2016). To solve this, various approaches have been used to characterize fluid flow in shaly reservoirs using analytical models or commercial simulators (Wu et al., 2013; Rubin, 2010; Li et al., 2011; Yan et al., 2013; Farrokhrouz et al., 2020), whilst others have focused on the nanopore modeling and molecular diffusion that makes the connection between the matrix and the fractures (Alharthy et al., 2016; Santiago and Kantzas, 2020).

In terms of experimental studies, different aspects of unconventional reservoirs were covered. Examples of recent studies include the experimental transport of fluid flow within complex fractures (Peng et al., 2022), the impact of micro-reactions on the production of unconventional (Deng et al., 2012) and experimental studies on low-velocity seepage within such reservoirs (Li et al., 2020).

Stimulation with acid is one of the oldest techniques used for production enhancement. Acid affects reservoir rock by increasing the matrix permeability (Economides, 2013; Abass et al., 2006; Cash et al., 2016) or altering the wettability (Saneifar, 2012; Alvarez and Schechter, 2017; Wang et al., 2012) of the formation surface. The acidizing procedure is usually initiated by the injection of a pre-flush fluid (e.g., gasoil), followed by acid injection and then over-displacing the acid with post-flush brine (Williams et al., 1979). During acidizing, the injected acid flows through the preferential pathways, i.e., through the fractures as a high permeability medium. Consequently, the oil-rich zones in the

low permeability matrix will be bypassed (Sang et al., 2014). Due to the heterogeneity of the formation, some methods are applied to divert injected acid inside the formation. Mechanical diverting methods (MaGee et al., 1997) or chemical diverting technology (Gomaa and Nasr-El-Din, 2010; Samuel et al., 1997; Talabani and Islam, 1999) are applied during the acid injection process to divert acid into the lower permeability layers and enable better distribution of acid within the reservoir rock.

The flowback fluid contains an oil-and-water mixture, solid plugs, products of the acid reaction with rock, diverting agents and residual acid (Mohammadzadeh Shirazi et al., 2019). There are always some acids that cannot flow back and, depending on the constituents, can effectively reduce the permeability of the reservoir instead of increasing it (Nasr-El-Din et al., 2002; Farrokhrouz and Asef, 2010a; Farrokhrouz and Asef, 2010b). Appropriate management of the residual acid can improve the efficiency of the acidizing process. It should be considered that the concentration of acid across the formation (matrix or fracture) does not remain the same. Liu et al. (2021) conducted experiments and showed that when acid concentration is 20% at the inlet, it decreases exponentially inside the formation in such a way that after 20 m from the injection point, it is less than 5% (Fig. 1) and flow-back of acid from this depth on penetration is less likely.

This study aimed to propose the effect of low concentration (residual) acid as a long-term permeability improvement procedure for unconventional reservoirs and tight formation. A series of acidizing experimental tests on Indiana limestone disk samples were conducted as a base acid and carbonate reaction study. These were performed under ambient pressure and temperature conditions in a laboratory environment. A mathematical model was implemented for porosity alteration due to acid diffusion, and an analytical solution was achieved. Furthermore, an acid diffusion coefficient was also determined based on this test. Experimental studies were expanded to Eagle Ford rock samples as a major type of unconventional carbonaceous shale. The mathematical model was in good agreement with the shale samples' experimental results and validated the model's accuracy. The findings of this research will help advise on a long-term acidizing process on carbonaceous shale as well as provide a theoretical model to predict porosity variations because of the acidizing operation.

## 2. Materials and experimental setup

The experimental setup of this study was designed to examine the validity of the proposed mathematical model and exact solution. First, a brief geological explanation of the samples is provided.

Table 1

Specifications of the samples used in the experimental setups (EF: Eagle Ford, IL: Indiana Limestone, ACT: acid concentration test, RT: repeatability test). The ultimate porosity of the limestone samples could not be determined due to the severe deformation of the rock surface.

Sample ID	Solution Utilized	Test Type	Thickness (mm)	Diameter (mm)	Weight (g)	Initial Porosity (%)	Pore Volume (cc)	Ultimate Porosity (%)
EF2-P1	1.5% HCl	ACT	5.5	37.64	15.87	1.961	0.120	43.219
EF2-P3	3.0% HCl	ACT	10.71	37.62	31.14	3.259	0.388	36.514
EF2-P4	5.0% HCl	ACT	14.23	37.64	39.78	1.977	0.313	35.026
EF3-P2	1.5% HCl, 2.0% KCl	RT	9.60	37.70	27.93	5.795	0.621	23.610
EF3-P3	4.0% HCl	ACT	10.50	37.63	30.23	6.791	0.793	43.307
EF3-P4	1.5% HCl	RT	9.54	37.67	27.53	6.226	0.662	34.688
EF3-P5	5.0% NaCl	RT	9.59	37.66	27.48	5.301	0.558	33.617
EF3-P6		RT	8.60	37.68	24.90	4.755	0.456	38.446
IL-P1	1.0% HCl	RT	7.75	37.88	19.52	22.956	2.005	–
IL-P2	3.0% HCl	ACT	10.16	37.90	24.92	26.906	3.084	–
IL-P3	5.0% HCl	ACT	10.10	37.90	25.53	33.228	3.786	–
IL-P4	2.0% HCl	ACT	10.16	37.92	25.37	20.987	2.408	–
IL-P5	1.0% HCl	ACT	6.62	37.92	16.78	14.353	1.073	–

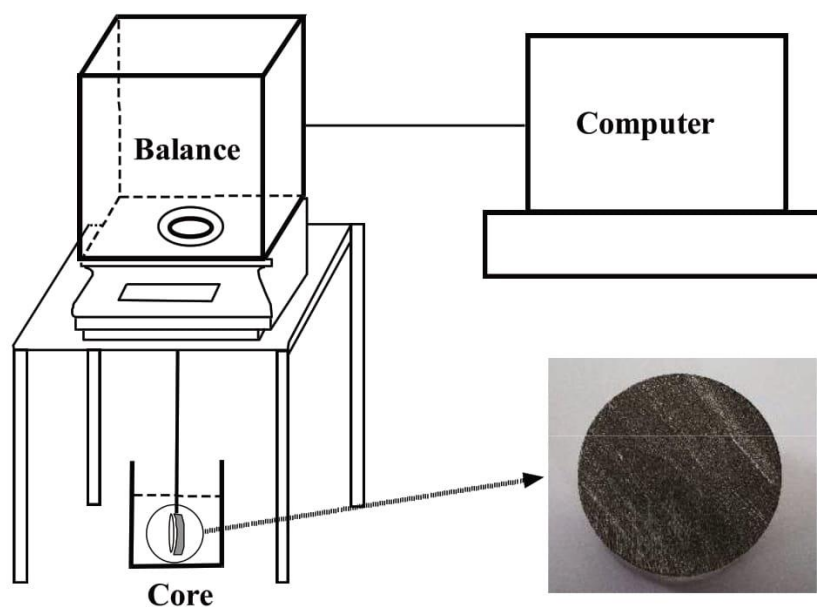


Fig. 2. Schematic of the test setup; the sample shown is Eagle Ford shale sample. The circumference of the rock disk is covered with epoxy to avoid radial diffusion of the sample, and the acid front moves in 1D only.

### 2.1. Geological features of core samples

Indiana limestone, alternatively known as Salem limestone and Bedford limestone, is a middle Mississippian oolitic rock covering the top portion of the Sanders Group (Gray, 1979). Indiana limestone is renowned as a homogenous carbonate in terms of its grain size and texture. This buff-colored strong rock can be found throughout the Illinois Basin and contains several types of marine organisms. Indiana limestone contains more than 97% pure calcium carbonate, which can be used as a reference carbonate rock in laboratory studies (Shaffer, 2020).

Eagle Ford is a well-known late Cretaceous marl (or carbonaceous shale) sample that features in Texas next to the Gulf of Mexico, where it is stratigraphically laid between two chalks. Its hole formation can be

divided into upper and lower sub-layers, and they have high carbonate contents averaging between 60 and 70%. The total organic content (TOC) in this formation is in the range of 3–10 wt% for the lower member and 2–7 wt% for the upper member. These ranges of organic matter indicate Eagle Ford as a kind of unconventional oil and gas reservoir (Driskill et al., 2013).

### 2.2. Sample preparation and experimental setup

Four Indiana limestone core samples were prepared for control testing of HCl acid in relation to matrix acidizing and to investigate the effect of acid concentration. The samples were unsaturated laboratory core samples and were cut into thin core samples. The circumferential areas of the cores were then covered in epoxy in order to remove the radial movement of the acid and to render them into a linear 1D acid dispersion. The physical properties of the core samples are provided in Table 1, where it can be seen that the limestone samples were subjected to varying percentages of HCl. The percentage of the acid used in these experiments was selected by considering the typical residual acid concentration according to Fig. 1.

For the second series of experiments, six Eagle Ford shale core samples of similar shape and diameter were selected and placed into differing acid solutions. The porosity of the samples was then measured using Standard CoreLab porosimeter facilities. Helium gas with an initial pressure of 200 psi was used as the pore fluid to expand into an accurately known chamber containing each core sample, after which the pressure was then reduced to 80 psi. Based on Boyle's law, the pore volume of the rock sample (porosity) was determined.

After measuring the porosity of the samples, the cores were submerged in different acid solutions of HCl diluted with distilled water. For some of the tests, dilution was accomplished by using 5% NaCl brine. All the tests were conducted at ambient temperature. A detailed explanation of the solutions used for the differing rock types and the effects of acid on the disk samples are also given in Table 1. The ultimate Helium porosity of the samples was measured after acidizing and the results can be seen in the same table. It is worth noting here that Indiana limestone disk samples were affected by the acid to such an extent that they could not be placed in the porosity measurement system after acidizing.

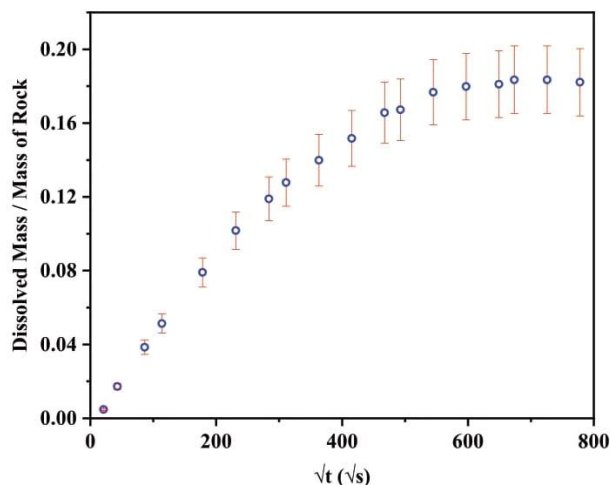


Fig. 3. Repeatability test of acid diffusion test with 1.5% HCl and 5% NaCl solution on Eagle Ford shale samples. The tests were repeated 4 times (as in Table 1) and error bands show 10% accuracy and repeatability of the tests.



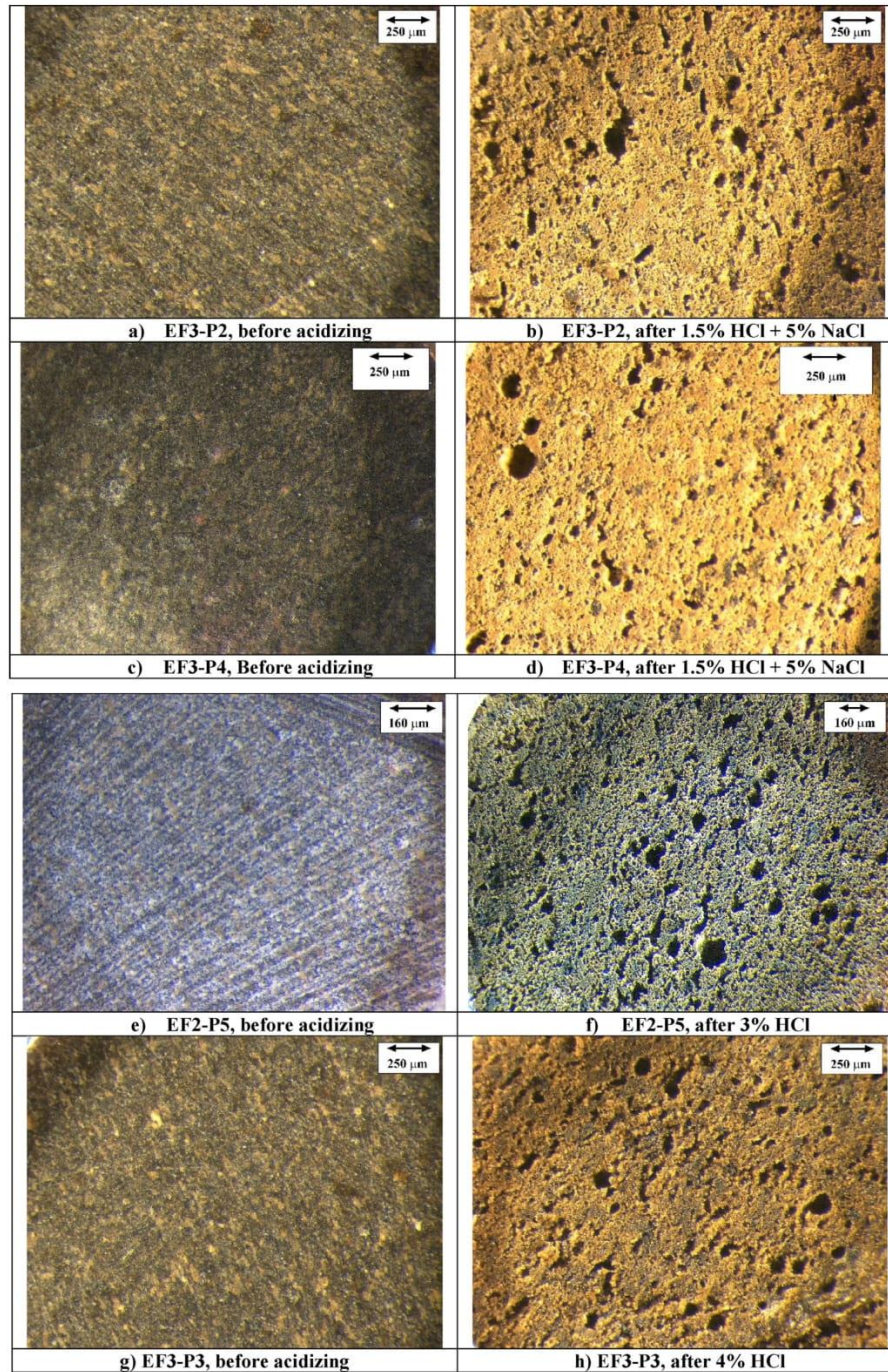


Fig. 4. Effect of acid percentage on the rock surface by creating holes on the surface representing porosity increase. The qualitative trend of acid percentage on porosity increase can be observed completely.

Due to the reaction of the acid on the rock surfaces, the weight of the samples changed and these changes were recorded continuously with a weight-based imbibition setup, as shown in Fig. 2. In all these tests, the volume of diluted acid solution was 400 mL, where variations in sample weights were recorded until a stable condition was reached.

### 3. Experimental observations and uncertainties

After performing the experiments, the study required the quantification of results into a uniform functional form using a mathematical model. Indiana limestone disks were shown to have higher porosity and permeability in comparison to Eagle Ford disks. Therefore, for the limestone samples, an increase in weight occurred due to saturation,



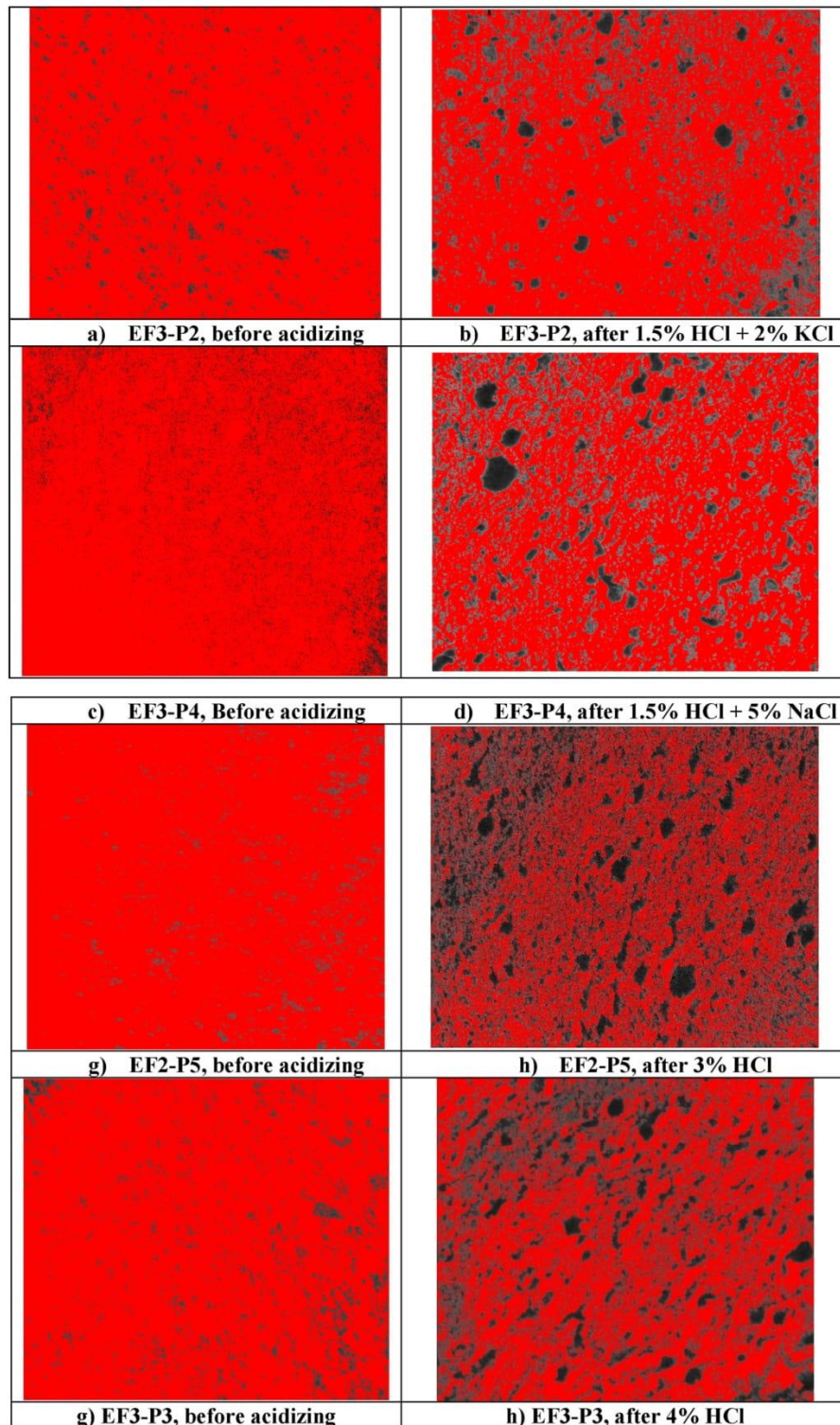


**Fig. 5.** Image analysis and pore segmentation on the rock surface of different samples as a function of acid percentage and brine salinity. Red area displays matrix and black area characterizes the pores initiated by acid. Quantitative analysis of these images are presented in [Table 2](#). (For interpretation of the references to color in this figure legend, the reader is referred to the Web version of this article.)



**Table 2**  
Quantitative porosity increase as a function of acid percentage, calculated using ImageJ opensource image segmentation software.

Sample ID	HCl (%)	Brine Type	Matrix Content (%)	Initial Porosity (%)	Ultimate Porosity (%)	$\Delta\phi$ (%)
				Before Acidizing	After Acidizing	
EF3-P2	1.5	2% KCl	94.6	5.4	22.7	17.3
EF3-P4	1.5	5% NaCl	92.2	7.8	28.7	20.9
EF2-P5	3	Water	96.2	3.8	37.3	33.5
EF3-P3	4	DI Water	92.4	7.6	31.2	23.6

whereas a decrease in weight occurred as a result of a reaction with the acid. Due to the very low permeability of the Eagle Ford shale samples, it was not possible to saturate them during the experiments. Therefore, the weight loss occurred only due to the surface dissolution of the rock.

An essential feature of acidizing efficiency is the repeatability of experiments. Accordingly, in this study, Eagle Ford shale samples were suspended in 1.5% HCl acid with 5% NaCl to avoid clay mineral swelling on the rock samples. Fig. 3 shows a corresponding diagram with error bands, where test results confirm that all experiments were within a 10% error range, which is an acceptable error band in engineering studies.

Fig. 4 shows the surfaces of the core (disk) samples both before and after acidizing. The effects of acid on the Eagle Ford samples can be distinguished as micro-scale holes, indicating a porosity increase in rock samples. As observed in these images, increasing the percentage of the acid results in larger holes (i.e., porosity increase). Apart from this qualitative description of porosity increase, image analysis and segmentation of the pores as a function of acid percentage were performed using opensource ImageJ software and the results are presented in Fig. 5 and Table 2. Another effect of an increase in acid percentage is the formation of additional connections between induced micropores, leading to the generation of micro-fractures on the rock surface (Fig. 6).

For Indiana Limestone samples, some parts of the rock were removed after acid exposure, where carbonate constituents could be defined on microscopic images (Fig. 7). The severity of this disintegration depended entirely on the acid concentration. For low HCl concentrations, the cement between grains was partially removed (compare Fig. 7 (a) and (b)). Increasing the acid percentage to 2% obliterated the carbonate cement (compare Fig. 7 (c) and (d)); however, the silicate cement and the cement on the contact points could not be removed due to the low efficiency of the acid. For 3% acid concentration, cementation was completely removed, with some carbonates on grain-to-grain contacts also removed (see Fig. 7 (d) and (f)). With higher concentrations of HCl, the images before and after acidizing cannot be compared due to the

high acidizing efficiency. For the same reason, quantitative analysis and segmentation of the rock surfaces were not attainable. The components of the rock samples that remain following cement removal are small silicate cement and minor dolomite within the rock frame. Another important finding is that acid diffusion in Indiana Limestone does not lead to acid fracturing, as it is made up of more than 97% calcite and the acid removes everything after the reaction. In contrast, for Eagle Ford variants, the acid dissolved the calcite mineral vein within the sample.

#### 4. Mathematical modeling: theoretical background

Appropriate modeling of acid reactions on the rock surface requires a comprehensive understanding of the physics and mathematical theory behind this phenomenon. A chemical definition can be interpreted as the kinetics of the reaction, where the mathematical model can be directed through the utilization of continuity equations between reacting components. Using these two mechanisms together, we constructed a mathematical model and applied a unique solution methodology, whereby we can propose a new mathematical solution for HCl acid reaction on carbonate surfaces where transverse dispersion is dominant.

##### 4.1. Kinetics of HCl reaction

The kinetics of acid on rock (calcite in this study) is defined based on the dissolution rate of the rock surface, the reaction rate constant, order of the reaction, activation energy, and diffusion coefficient. Some studies on acid-rock reaction rates have been conducted via a Rotating Disk Apparatus (RDA). In these tests, a rotating assembly is employed to give rotational motion to the sample up to 1800 rpm. During rotation, the acid is then exposed to the surface of the rock sample under the desired pressure and temperature. This measurement methodology, however, is not applicable in this study since the residual acid within the formation and diffusion is considered the only driving mechanism.

The reaction on the surface of the carbonate occurs in three steps (Lund et al., 1973):

- 1) Diffusion of the liquid towards the fluid-rock interface;
- 2) The reaction between the carbonate and acid at the same interface;
- 3) Diffusion of the produced liquids outwards of the interface.

The rate and type of reaction can then be determined by the slowest rate of these three mechanisms. If the first and/or the third mechanisms dominate, the reaction is limited to mass transfer. In contrast, if the second mechanism possesses the slowest rate, it is known as a surface reaction-limited (Taylor and Nasr-El-Din, 2009).

In RDA studies, typical curves can be demonstrated versus the square root of time as it can be assumed that acid front imbibition moves with the functionality of time. If a curve has a positive slope, the reaction is

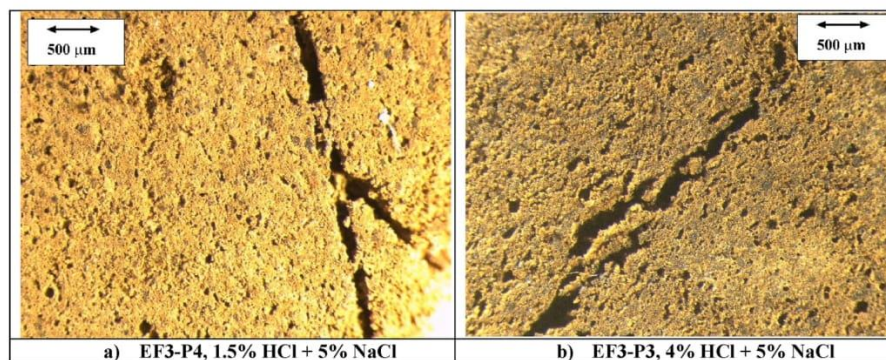


Fig. 6. Effect of acid percentage on induced fracture initiation on Eagle Ford shale samples; higher percentage acid causes wider and longer fractures.



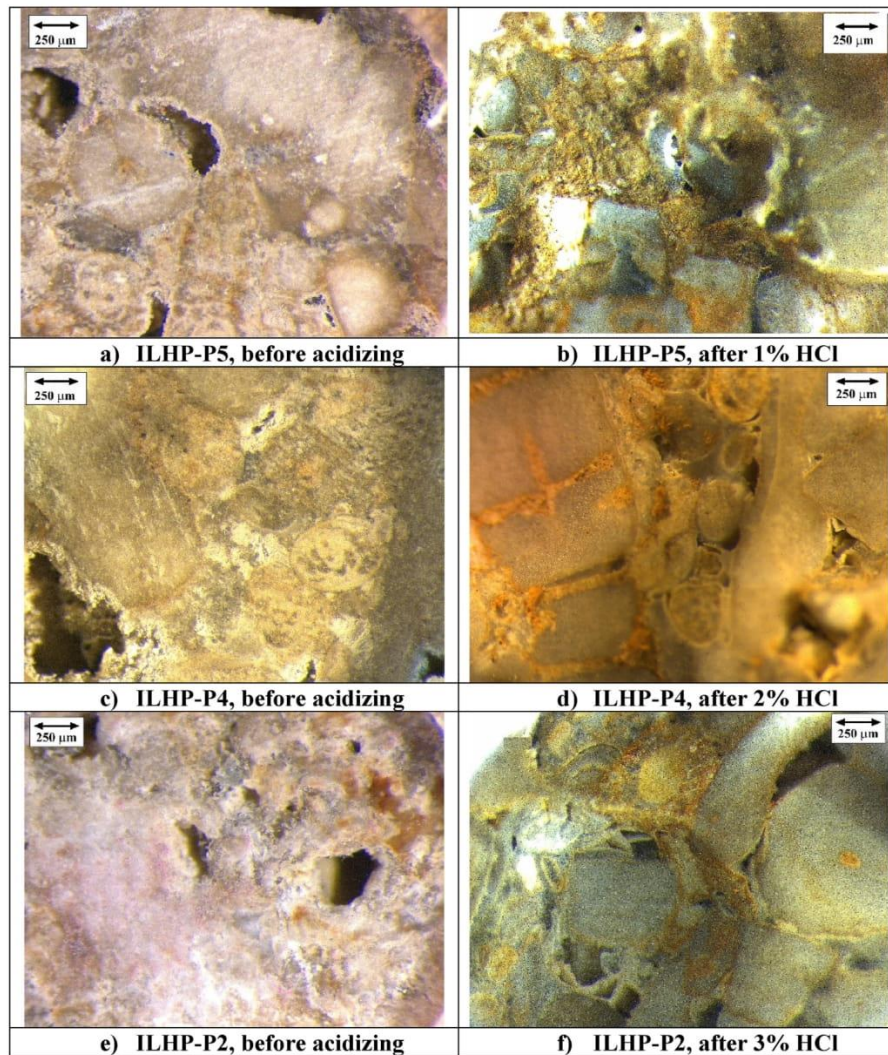


Fig. 7. Effect of acid concentration on the acidizing efficiency for Indiana Limestone disk samples.

known as mass transfer limited. When the slope approaches zero, it is referred to as surface reaction limited (Boomer et al., 1972).

4.2. Acid dispersion in porous media

The creation of acid channels in the form of wormhole, conical, or surface dissolution depends on the relative magnitude of convection and dispersion forces inside a medium. In the case of dominant transverse dispersion, the acid reaction leads to conical and/or face dissolution. In cases where convective transport is more dominant, the concentration of acid and acid dissolution pattern can be expected to be uniform.

In addition, acid displacement inside a porous medium follows Darcy’s law. Acid is diluted with the water and then the solution is in contact with the rock surface. After the reaction of the acid with the rock surface, the products (i.e., CaCl<sub>2</sub>, CO<sub>2</sub> and H<sub>2</sub>O) are displaced from the rock surface, exposing the fresh rock surface to become in contact with the acid. Accordingly, a system of equations is presented below at the Darcy scale and the 1D equations of the model are (Panga et al., 2005):

$$\begin{cases}
 a) \frac{\partial \varphi}{\partial t} + \frac{\partial u}{\partial x} = 0 \\
 b) \frac{\partial(c\varphi)}{\partial t} + \frac{\partial(cu)}{\partial x} = \frac{\partial}{\partial x} \left( \varphi D \frac{\partial c}{\partial x} \right) - k_c \cdot a_v \cdot (c - c_e) \\
 c) k_c \cdot a_v \cdot (c - c_e) = R(c_e) \\
 d) \frac{\partial \varphi}{\partial t} = \frac{R(c_e) a_v \cdot \alpha}{\rho}
 \end{cases}
 \tag{1}$$

The terms (a) and (b) in Eq. (1), like any other continuity equation, contribute to the accumulation, convection and dispersion of the acid phase. Applying Eq. (1.c) and (1. d) into (1. b) results in:

$$\frac{\partial[\varphi(c - 1)]}{\partial t} + \frac{\partial(cu)}{\partial x} = \frac{\partial}{\partial x} \left( \varphi D \frac{\partial c}{\partial x} \right)
 \tag{2}$$

Eq. (1.c) represents the transfer of acid from the fluid phase towards the acid-rock interface on the rock surface. For the case of dominance of transverse dispersion, this equation becomes:

$$\frac{\partial[\varphi(c - 1)]}{\partial t} = \frac{\partial}{\partial x} \left( \varphi D \frac{\partial c}{\partial x} \right)
 \tag{3}$$

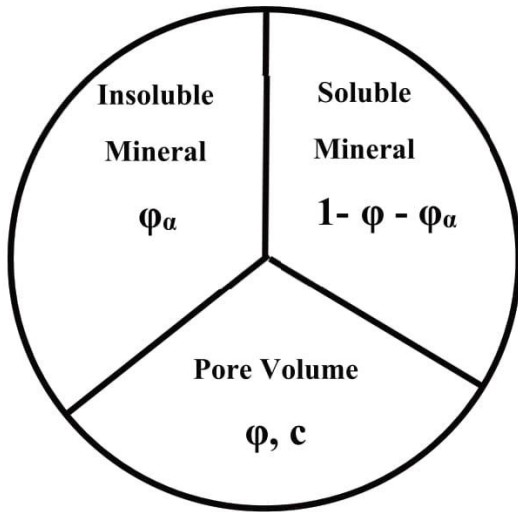


Fig. 8. Schematic of a porous medium constituent in pore-scale.

whilst the kinetics of the reaction is achieved by utilization of Eq. (1. c) and (1. d):

$$\frac{\partial \varphi}{\partial t} = \frac{a_v^2 \cdot \alpha \cdot k_c}{\rho} (c - c_e) = \tau (c - c_e) \quad (4)$$

The porous medium consists of three components: a rock component that can be dissolved in acid (for example, calcite, dolomite and/or different carbonates), another rock component that cannot be dissolved in the acid (like quartz, feldspar, or other silicates), and pore volume (or porosity). The pore volume is filled with fluid into which the solid constituent of the rock can partially dissolve before the addition of acid into the system. As a result, pore fluid contains ions and cations (Ca<sup>2+</sup>, Na<sup>+</sup>, Cl<sup>-</sup>, CO<sub>3</sub><sup>2-</sup>, etc.). Fig. 8 is a schematic of this porous medium.

In contrast, when these ions are removed from a rock surface, the solid volume is decreased, and additional volume is added to the pore volume. This leads the change in porosity and kinetics of reactions to be based on Eq. (4). The magnitude of this change depends on the rate of two mechanisms: the number of reactions taking place in a unit of time, and the rate of mass transfer from the acid-rock interface to the bulk fluid.

For prolonged reaction rates (e.g., the reaction of HCl on the dolomite surface), the transfer of the reaction products occurs very fast and the concentration gradient is negligible. This type of reaction is referred to as a 'kinetically controlled regime', where a single concentration variable is enough to characterize the reaction. Alternatively, for fast reaction rates (e.g., the reaction of HCl on calcite surface), the transfer of the products is not accomplished at the same rate and is referred to as a 'mass transfer controlled regime'. In this case, the concentration gradient is meaningful, where corresponding variables are 'c' and 'c<sub>e</sub>' in the model.

$$T = \left(\frac{2A}{\varphi_0 L}\right)^2 t; X = \frac{x}{L} \quad (5)$$

It is important to note that a description of parameter 'A' should be given here. In accordance with previous studies that have introduced this constant value into dimensionless groups (McWhorter and Sunada, 1990), it can be concluded that this constant highly depends on the porosity, permeability, and viscosity of the wetting phase when compared with similar dimensionless groups. A detailed explanation and derivation of these dependencies are outside the scope of this paper. Interested readers are referred to other studies in this area (Ma et al., 1997; Li and Horne, 2006; Schmid et al., 2016; Farrokhrouz et al., 2021, 2022).

Accordingly, the continuity Eq. (3) turns into:

$$\frac{\partial}{\partial T} [\varphi(c-1)] = \left(\frac{\varphi_0}{2A}\right)^2 \frac{\partial}{\partial X} \left(\varphi D \frac{\partial c}{\partial X}\right) \quad (6)$$

For the first-order solution kinetics, Eq. (4) converts to:

$$c = c_e - \left(\frac{2A}{\varphi_0 L}\right)^2 \tau \frac{\partial \varphi}{\partial T} \quad (7)$$

Applying Eq. (7) into Eq. (6) and integrating them once with respect to time:

$$\varphi \left( c_e - \tau \cdot \left(\frac{2A}{\varphi_0 L}\right)^2 \frac{\partial \varphi}{\partial T} - 1 \right) = -\tau \cdot \left(\frac{\varphi_0}{L}\right)^2 \cdot \varphi D \frac{\partial}{\partial X} \left(\frac{\partial \varphi}{\partial X}\right) + C_1 \quad (8)$$

The initial and boundary conditions in dimensionless form would be:

$$\begin{cases} T = 0 : \varphi = \varphi_0, c = c_e \\ X = 0 : c = 0, \frac{\partial \varphi}{\partial T} = \frac{c_e}{\tau} \left(\frac{\varphi_0 L}{2A}\right)^2 \end{cases} \quad (9)$$

The value of C<sub>1</sub> in Eq. (8) can be calculated using the initial condition in Eq. (9). Now, defining the following parameters:

$$\gamma = \left(\frac{2A}{\varphi_0}\right)^2 \delta = \frac{\tau \cdot \varphi_0^2}{L^2} \quad (10)$$

simplifies the equation as:

$$\frac{\partial \varphi}{\partial T} = \frac{D}{\gamma} \frac{\partial}{\partial X} \left(\frac{\partial \varphi}{\partial X}\right) - \frac{\varphi(c_e - 1) + \varphi_0}{\varphi \delta \cdot \gamma} \quad (11)$$

Introducing the travelling wave form:

$$\begin{aligned} \varphi(X, T) &= \omega(X - sT) \\ \Rightarrow \frac{\partial \varphi}{\partial T} &= -s\omega'; \frac{\partial \varphi}{\partial X} = \omega'; \frac{\partial^2 \varphi}{\partial X^2} = \omega'' \end{aligned} \quad (12)$$

Making another rearrangement for the Equation form of (11):

$$-s\omega' = \frac{D}{\gamma} \omega'' - \frac{(c_e - 1)}{\delta \gamma} - \frac{\varphi_0}{\varphi \delta \cdot \gamma} \quad (13)$$

Adding and removing a part to the equation set:

$$-s\omega' = \frac{D}{\gamma} (\omega'' + \omega' \omega'' - \omega' \omega'') - \frac{(c_e - 1)}{\delta \gamma} - \frac{\omega_0}{\omega \cdot \delta \cdot \gamma} \Rightarrow -s\omega' - \frac{D}{\gamma} \left(\frac{\omega'^2}{2}\right)' + \frac{D}{\gamma} \left[\frac{(1 - \omega')^2}{2}\right]' = \frac{(1 - c_e)}{\delta \gamma} - \left(\frac{1}{\omega}\right) \left(\frac{\omega_0}{\delta \cdot \gamma}\right) \quad (14)$$

Here we introduce two dimensionless variables and parameters as follows:

Integrating from both sides yields:



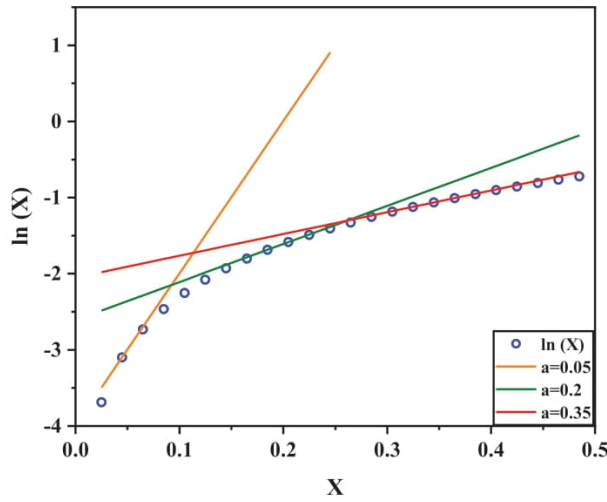


Fig. 9. Approximation of the  $\ln(X)$  function using approximate equation. The values and approximation are for arbitrary values of 'a' as in Eq. (19).

$$-s\omega + \frac{D}{2\gamma} - \frac{D}{\gamma} \omega' = \frac{(1-c_e)}{\delta\gamma} \omega - \left(\frac{\omega_0}{\delta\gamma}\right) \cdot \ln(\omega) + C_2 \quad (15)$$

The value of  $C_2$  is between two limits: the lower limit is the initial porosity ( $\omega_L = \omega_0$ ) and the higher limit is unity ( $\omega_R = 1$ ) and  $\omega'(\pm\infty) = 0$ . Then:

$$C_2 = -s + \frac{D}{2\gamma} - \frac{(1-c_e)}{\delta\gamma} \quad (16)$$

This turns Eq. (15) into:

$$\omega' = \underbrace{\left[\frac{(c_e-1)}{D\delta} + \frac{s\gamma}{D}\right]}_P \omega + \underbrace{\frac{\omega_0}{D\delta}}_Q \cdot \ln(\omega) + \underbrace{\left[\frac{s\gamma\delta + (1-c_e) - D\delta}{D\delta}\right]}_R \quad (17)$$

Rearranging and integrating again gives:

$$= y + C_3 \quad (18)$$

The integral in Eq. (18) can be solved numerically. However, our objective is to make this into an indefinite integral solution form. In this case, the approximation for  $\ln(x)$  would be helpful:

$$\ln(\omega)|_a = \ln(a) + \frac{(\omega-a)}{a} - \frac{(\omega-a)^2}{2a^2} + \frac{(\omega-a)^3}{3a^3} + \dots \quad (19)$$

In Eq. (19), 'a' is any arbitrary point between zero and one. Using the first-order approximation of Eq. (19) and ignoring higher orders, this changes Eq. (18) into:

$$= y + C_3 \Rightarrow \omega = \frac{A'}{2B'} + \frac{\sqrt{A'^2 + 4B' \cdot C'}}{2B'} \cdot \tanh\left[\frac{(y + C_3)}{2} \cdot \sqrt{A'^2 + 4B' \cdot C'}\right] \quad (20)$$

This newly proposed equation form is suggested for the first time, introducing changes in the porosity of the medium due to acid reactions on the rock surface. An approximation for the logarithmic function in the denominator of Eq. (18) is used. In the case of selecting an appropriate value for 'a' in Eq. (19), the error of this approximation would be less than 0.5% (Fig. 9). The best-suggested value would be the initial porosity ( $\omega_0$ ), as changes in porosity due to acid reaction would not be dramatic due to acid imbibition. Furthermore, the value of constant  $C_3$  can be defined based on the initial and boundary conditions.

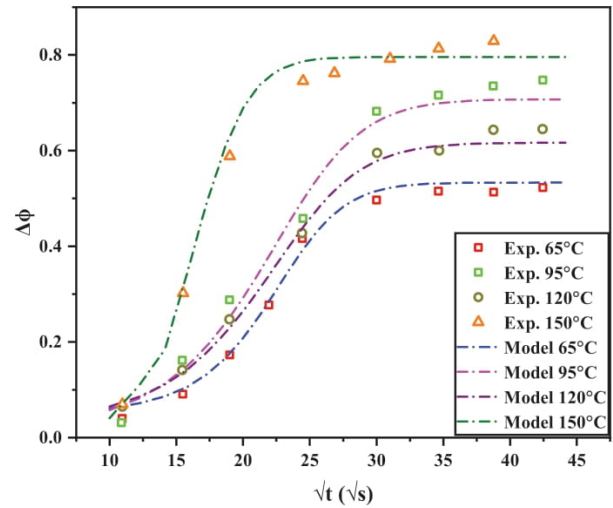


Fig. 10. Matching experimental data (Exp.) with the mathematical model (Model) proposed in this study. Data obtained from Rabie (Rabie, 2012). The mathematical model covers all experimental data points with a maximum 5% error in estimation.

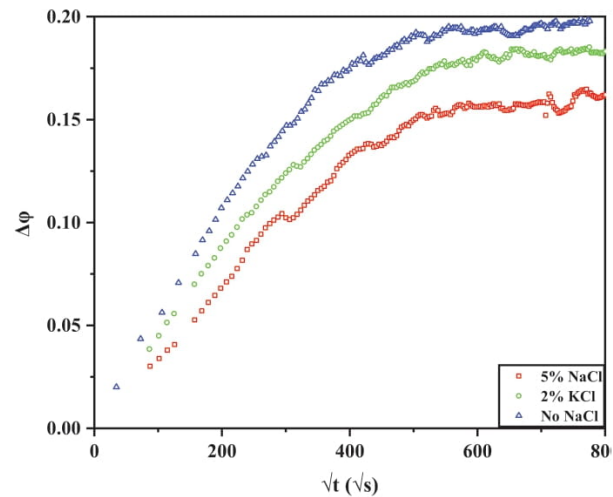


Fig. 11. Effect of additives on the acidizing efficiency of 1.5% HCl reacting on the surface of Eagle Ford shale samples.

### 5. Data matching and model validation

Matching the experimental results with the proposed analytical solution requires a broad physical understanding of the process as well as effective parameters regarding the reaction. The objective of this section is to provide a comprehensive perspective of the HCl acid reaction on the rock surface.

There are several factors influencing the acid diffusion coefficient, which can be pre-defined or uncontrollable. Some of the controllable factors are acid concentration, acid viscosity, the salinity of the solute, and the pressure and temperature conditions of the experiment. Parameters regarding rock properties are uncontrollable (e.g., porosity, permeability, and carbonate content).

The most effective parameter on the diffusion coefficient (D in Eq. (1)) is temperature (Lund et al., 1973; Wragg, 1971; Weast, 1979; Mumallah, 1991). For small temperature changes, the variation in



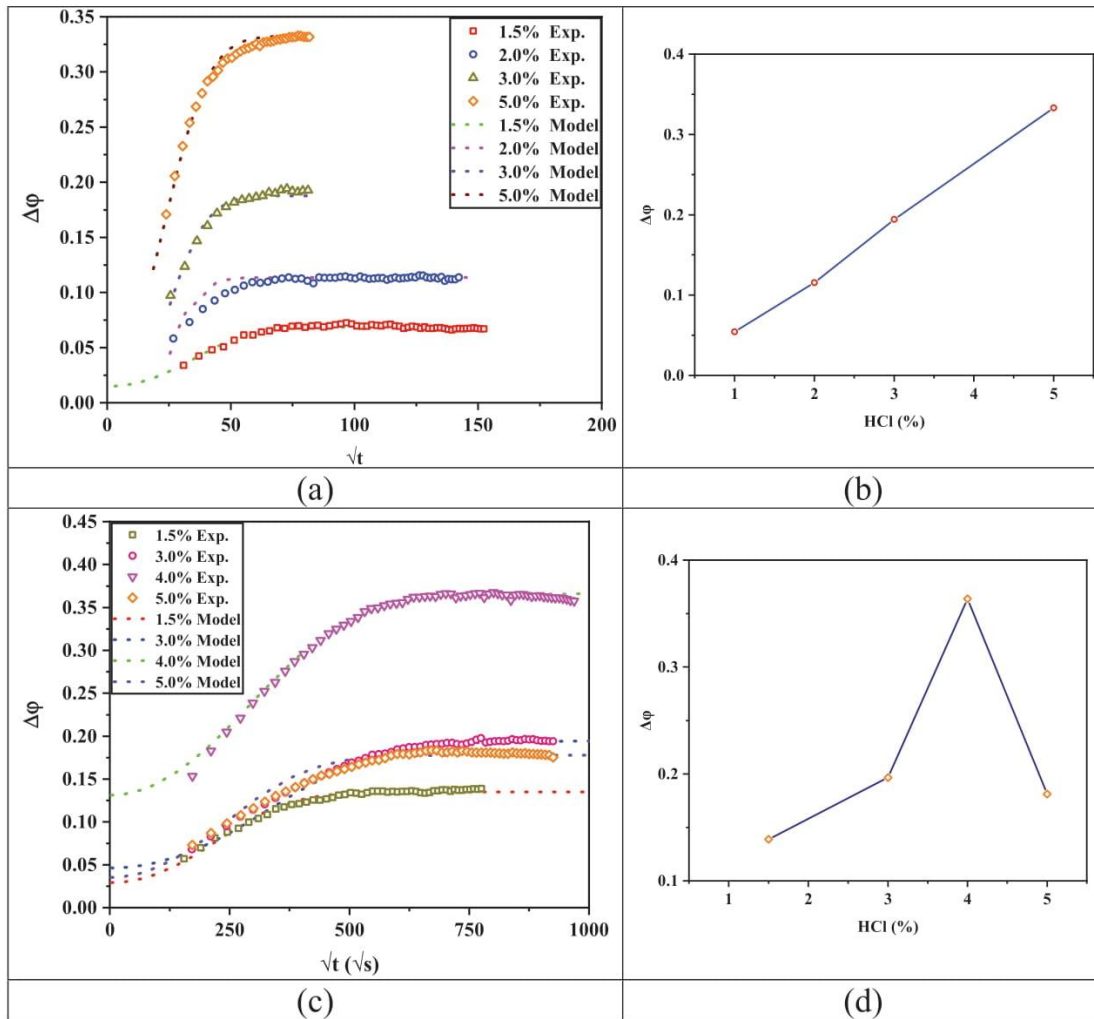


Fig. 12. Effect of HCl percentage on porosity changes of experimental samples (Exp.) as in Table 1 matched with the analytical solution (Model) a) Indiana limestone matching with the mathematical model, b) acid concentration effect on acidizing efficiency for Indiana limestone, c) Eagle Ford shale samples matching with the mathematical model, d) acid concentration effect on acidizing efficiency for Eagle Ford shale sample.

diffusion coefficient is approximated by (Cheryan, 1998):

$$\frac{D_{T_2}}{D_{T_1}} = \frac{T_2\mu_1}{T_1\mu_2} \quad (21)$$

where T is temperature and  $\mu$  is viscosity. The effect of temperature on viscosity has been fully investigated. This dependency can be achieved through the following equation (Weast, 1979):

$$\log \frac{\mu_T}{\mu_{20}} = \frac{1.3272(20 - T) - 0.001053(T - 20)^2}{T + 105} \quad (22)$$

In this study, the effect of temperature changes on the experimental results has not been highlighted, with all tests being performed under

ambient conditions. However, it has been confirmed in the literature that a temperature increase is accompanied by a rise in the value of the diffusion coefficient. Based on experimental results, Arslan et al. (2017) reported that increasing the acid temperature from 38 °C to 93 °C resulted in a 12 times increase in the diffusion coefficient value. Wang et al. (2018) measured an increase in the growth ratio by up to 4 times as the temperature was increased from 30 °C to 90 °C. Applying these variations in the values of diffusion coefficients, the mathematical model presented in this study corresponds well with that in the literature. Fig. 10 shows the model's capability in the prediction of porosity increases due to acidizing.

Due to the high reactivity of HCl acid with carbonates, sometimes it is necessary to decelerate this rate in order to control the order of

Table 3  
Involved parameters within the tests matched with experimental results.

	EF2-P1	EF2-P3	EF2-P4	EF3-P3	IL-P1	IL-P2	IL-P3	IL-P4
A (m/ $\sqrt{s}$ )	$7.15 \times 10^{-8}$	$2.61 \times 10^{-7}$	$7.80 \times 10^{-8}$	$2.10 \times 10^{-6}$	$8.30 \times 10^{-5}$	$9.30 \times 10^{-5}$	$4.50 \times 10^{-5}$	$8.00 \times 10^{-5}$
D (m <sup>2</sup> /s)	$6.70 \times 10^{-6}$	$1.70 \times 10^{-5}$	$9.50 \times 10^{-6}$	$1.95 \times 10^{-5}$	$2.80 \times 10^{-7}$	$3.05 \times 10^{-7}$	$5.00 \times 10^{-8}$	$5.80 \times 10^{-7}$
Acid (%)	1.5	3.0	5.0	4.0	1.0	3.0	5.0	2.0

reactivity. Several studies have used cross-linkers, emulsifiers and other additives to fulfill this objective as they create better wormhole propagation through a porous medium. However, their viscosity effect may lead to damage (Hoefner and Fogler, 1985, 1988; Sayed et al., 2018). For this experimental study, 5% NaCl and 2% KCl were used as additives in Eagle Ford samples to avoid shale swelling. These additives reduced the activity of the acid (1.5% HCl in these tests), with the final porosity change lower in comparison to samples without additives (Fig. 11).

Another important parameter affecting the diffusion coefficient is the pH of the solution. As different concentrations of HCl acid were used for the experimental setup, the pH of the solution changed accordingly. Changes in pH are also referred to in the literature as ionic strength.

Indiana limestone samples were prone to saturate during the test, but the reaction rate was fast enough to prevent saturation of the samples. Therefore, the reaction trend continuously increased, with high acid concentrations leading to the complete disappearance of rock samples. Fig. 12 (a) shows the weight percent changes with respect to the square root of time for the limestone samples in Table 1. The matching of the proposed mathematical model in this study is also shown. Accordingly, it can be observed that the trend of porosity increased with a higher acid percentage, where higher acid content resulted in higher efficiency of the acidizing process (Fig. 12 (b)).

For the Eagle Ford shale samples in Table 1, an optimum HCl acid concentration of close to 4% was found (Fig. 12 (c) and (d)). Higher acid concentrations led to lower acid efficiencies, as the reaction rate is faster than the diffusion of the products outwards of the interface. Figure (b) shows the matching of the experimental results with the mathematical model proposed in this study. For both matching figures, the mathematical model performed perfect matching with an error of estimation of less than 6%. The matching values of the parameters for all rock samples are presented in Table 3. As discussed earlier, the difference in the values of 'A' and 'D' was mainly related to the ionic strength (pH) of the solution and the viscosity (which is also affected by the acidity of the solution) in these series of experiments.

The mineral composition of rock in contact with acid is quite significant in the determination of the acid diffusion coefficient. Samples taken from a single rock type may even react differently in terms of the diffusion coefficient. Anderson (1991) and Taylor et al. (2004) confirmed this finding by performing experiments on different dolomite samples. Similarly, Mumallah (1998) focused on one rock type (North Sea chalk reservoir) with different properties (i.e., porosity, permeability, hardness, and acid solubility), and found that the reaction rate is highly dependent on the permeability and acid solubility, while other parameters were less critical.

Overall, an increase or decrease in the effective parameters listed above resulted in a 1–3 times alteration of the diffusion coefficient (Kadafur et al., 2020). For instance, the diffusion coefficient of HCl reaction with calcite was two times greater than that of dolomite, while all other parameters remained the same. Additionally, a diffusion coefficient at 85 °C was three orders of magnitude greater than the value at 25 °C (Al-Mutairi et al., 2009). The diffusion coefficient of Eagle Ford shale and Indiana limestone samples had the same findings, with 1–3 times alteration as illustrated in Table 3.

## 6. Conclusion

A new mathematical solution methodology has been proposed using the physical and theoretical background of acid reaction on the surface of a carbonate sample. The solution is focused on the collaborating kinetics of reaction and continuity of common ion content between a reacting fluid and rock mineral. This approach has led to the formation of a new mathematical solution, verified by experimental data. This mathematical model can be used at different scales of porous mediums (pore-scale up to reservoir scale). The derived solution is also suitable for benchmarking and calibrating numerical models.

## Declaration of competing interest

The authors declare that they have no known competing financial interests or personal relationships that could have appeared to influence the work reported in this paper.

## List of symbols

$\varphi$	porosity
$c$	concentration of ion in the fluid phase
$c_e$	concentration of ion in the solid phase
$D_e$	effective dispersion tensor, $m^2/s$
$k_c$	local mass transfer coefficient
$a_v$	interfacial area of reaction, $1/m$
$\rho$	density of the solid phase, $kg/m^3$
$\alpha$	dissolving power of acid
$\tau$	kinetic delay time, t
$R(c)$	reaction kinetics of the acid
$k_s$	surface reaction rate constant, $m/s$
$u$	Darcy velocity, $m/s$

## References

- Abass, H.H., et al., 2006. Acid fracturing or proppant fracturing in carbonate formation? A rock mechanics view. In: SPE Annual Technical Conference and Exhibition.
- Akhondzadeh, H., et al., 2021. Liquid nitrogen fracturing efficiency as a function of coal rank: a multi-scale tomographic study. *J. Nat. Gas Sci. Eng.* 95, 104177.
- Al-Mutairi, S.H., et al., 2009. Effect of droplet size on the reaction kinetics of emulsified acid with calcite. *SPE J.* 14 (4), 606–616.
- Alfarge, D., Wei, M., Bai, B., 2018. Data analysis for CO<sub>2</sub>-EOR in shale-oil reservoirs based on a laboratory database. *J. Petrol. Sci. Eng.* 162, 697–711.
- Alharthy, N.S., Teklu, T.W., Nguyen, T.N., Kazemi, H., Graves, R.M., 2016. Nanopore compositional modeling in unconventional shale reservoirs. *SPE Reservoir Eval. Eng.* 19 (3), 415–428.
- Alvarez, J.O., Schechter, D.S., 2017. Wettability alteration and spontaneous imbibition in unconventional liquid reservoirs by surfactant additives. *SPE Reservoir Eval. Eng.* 20 (1), 107–117.
- Anderson, M.S., 1991. Reactivity of san andres dolomite. *SPE Prod. Eng.* 6 (2), 227–232.
- Arslan, E., et al., 2017. Reaction Rate of a Novel In-Situ Generated HCl Acid and Calcite. *Bedrikovetsky, P., et al., 2012. Stimulation of natural cleats for gas production from coal beds by graded proppant injection. In: SPE Asia Pacific Oil and Gas Conference and Exhibition. SPE-158761-MS.*
- Boomer, D.R., McCune, C.C., Fogler, H.S., 1972. Rotating disk Apparatus for reaction rate studies in corrosive liquid environments. *Rev. Sci. Instrum.* 43 (2), 225–229.
- Cash, R., Zhu, D., Hill, A.D., 2016. Acid fracturing carbonate-rich shale: a feasibility investigation of Eagle Ford formation. In: SPE Asia Pacific Hydraulic Fracturing Conference. D031S007R002.
- Cheryan, M., 1998. Ultrafiltration and Microfiltration Handbook. CRC press.
- Deng, J., Mou, J., Hill, A.D., Zhu, D., 2012. A new correlation of acid-fracture conductivity subject to closure stress. *SPE Prod. Oper.* 27 (2), 158–169.
- Driskill, B., et al., 2013. 11 Applications of SEM Imaging to Reservoir Characterization in the Eagle Ford Shale, South Texas, USA.
- Economides, M.J., 2013. Petroleum Production Systems. Pearson Education.
- EIA, 2021. Drilling Productivity Report for Key Tight Oil and Shale Gas Regions.
- Farah, N., 2016. Flow Modelling in Low Permeability Unconventional Reservoirs.
- Farrokhrouz, M., Asef, M.R., 2010a. Simulating model to reduce detrimental acidizing in tabnak gas field. In: SPE Deep Gas Conference and Exhibition. SPE-131986-MS.
- Farrokhrouz, M., Asef, M.R., 2010b. Production enhancement via scale removal in nar formation. In: SPE Production and Operations Conference and Exhibition. SPE-135854-MS.
- Farrokhrouz, M., Taheri, A., Keshavarz, A., 2020. Numerical reactive flow transport simulation on core samples during acid fracturing in carbonaceous shale. *J. Nat. Gas Sci. Eng.* 84, 103615.
- Farrokhrouz, M., et al., 2021. Analytical exact solution for Co-current spontaneous imbibition in porous media considering early- and late-time effects. *Energy Fuels* 35 (21), 17499–17511.
- Farrokhrouz, M., Taheri, A., Iglauer, S., Keshavarz, A., 2022. Exact analytical solutions of countercurrent imbibition with both capillary and gravity effects. *Energy Fuels* 36 (3), 1457–1469.
- Gomaa, A.M.M., Nasr-El-Din, H.A.A., 2010. New insights into the viscosity of polymer-based in-situ-gelled acids. *SPE Prod. Oper.* 25 (3), 367–375.
- Gray, H.H., 1979. The Mississippian and Pennsylvanian (Carboniferous) Systems in the United States-Indiana. US Government Printing Office.
- Hoefner, M.L., Fogler, H.S., 1985. Effective matrix acidizing in carbonates using microemulsions. *Chem. Eng. Prog.* 81, 40–44.
- Hoefner, M.L., Fogler, H.S., 1988. Pore evolution and channel formation during flow and reaction in porous media. *AIChE J.* 34, 45–54.
- Kadafur, I.B., Aljawad, M.S., Mahmoud, M., 2020. Review of acid diffusion measurement methods in porous media. *Energy Fuels* 34 (10), 11916–11941.



- Keshavarz, A., et al., 2014. Enhancement of CBM well fracturing through stimulation of cleat permeability by ultra-fine particle injection. *APPEA J.* 54 (1), 155–166.
- Keshavarz, A., et al., 2018. Chapter eight - enhanced gas recovery techniques from coalbed methane reservoirs. In: Bahadori, A. (Ed.), *Fundamentals of Enhanced Oil and Gas Recovery from Conventional and Unconventional Reservoirs*. Gulf Professional Publishing, pp. 233–268.
- Li, K., Horne, R.N., 2006. Generalized scaling approach for spontaneous imbibition: an analytical model. *SPE Reservoir Eval. Eng.* 9 (3), 251–258.
- Li, J., Du, C.M., Zhang, X., 2011. Critical evaluation of shale gas reservoir simulation approaches: single-porosity and dual-porosity modeling. In: *SPE Middle East Unconventional Gas Conference and Exhibition*. SPE-141756-MS.
- Li, X., et al., 2016. The impact of water salinity/surfactant on spontaneous imbibition through capillarity and osmosis for unconventional IORURTEC-2461736-MS. In: *SPE/AAPG/SEG Unconventional Resources Technology Conference*.
- Li, L., Hao, Y., Lv, Y., Wang, C., Yao, C., Zhao, Q., Xiao, P., 2020. Experimental investigation on low-velocity seepage characteristics and influencing factors in a shale oil reservoir. *J. Petrol. Sci. Eng.* 195, 107732.
- Liu, F., et al., 2021. Acid-etched fracture length and conductivity experiments with relayed large-scale rock plates. *J. Petrol. Sci. Eng.* 196, 107978.
- Lund, K., Fogler, H.S., McCune, C.C., 1973. Acidization—I. The dissolution of dolomite in hydrochloric acid. *Chem. Eng. Sci.* 28 (3), 691–IN1.
- Ma, S., Morrow, N.R., Zhang, X., 1997. Generalized scaling of spontaneous imbibition data for strongly water-wet systems. *J. Petrol. Sci. Eng.* 18 (3), 165–178.
- MaGee, J., Buijse, M., Pongratz, R., 1997. Method for effective fluid diversion when performing a matrix acid stimulation in carbonate formations. In: *Middle East Oil Show and Conference*. OnePetro.
- McWhorter, D.B., Sunada, D.K., 1990. Exact integral solutions for two-phase flow. *Water Resour. Res.* 26 (3), 399–413.
- Mohammadzadeh Shirazi, M., Ayatollahi, S., Ghotbi, C., 2019. Damage evaluation of acid-oil emulsion and asphaltic sludge formation caused by acidizing of asphaltic oil reservoir. *J. Petrol. Sci. Eng.* 174, 880–890.
- Morsy, S., et al., 2013. Potential of improved waterflooding in acid-hydraulically-fractured shale formations. In: *SPE Annual Technical Conference and Exhibition*. D031S040R006.
- Morsy, S., Hetherington, C.J., Sheng, J.J., 2015. Effect of low-concentration HCl on the mineralogy, physical and mechanical properties, and recovery factors of some shales. *J. Unconv. Oil Gas Resour.* 9, 94–102.
- Mukhina, E., et al., 2021. Enhanced oil recovery method selection for shale oil based on numerical simulations. *ACS Omega* 6 (37), 23731–23741.
- Mumallah, N.A., 1991. Factors Influencing the Reaction Rate of Hydrochloric Acid and Carbonate Rock.
- Mumallah, N.A., 1998. Reaction rates of hydrochloric acid with chalks. *J. Petrol. Sci. Eng.* 21 (3), 165–177.
- Nasr-El-Din, H., Taylor, K., Al-Hajji, H., 2002. Propagation of cross-linkers used in in-situ gelled acids in carbonate reservoirs. In: *SPE/DOE Improved Oil Recovery Symposium*. OnePetro.
- Panga, M.K.R., Ziauddin, M., Balakotaiah, V., 2005. Two-scale continuum model for simulation of wormholes in carbonate acidization. *AIChE J.* 51 (12), 3231–3248.
- Peng, H., et al., 2022. Research and application of a proppant transport experimental device for complex fractures in the unconventional reservoir. *Geofluids* 2022, 8356470.
- Rabie, A., 2012. Reaction of Calcite and Dolomite with In-Situ Gelled Acids, Organic Acids, and Environmentally Friendly Chelating Agent. (GLDA).
- Rubin, B., 2010. Accurate simulation of non-Darcy flow in stimulated fractured shale reservoirs. In: *SPE Western Regional Meeting*. SPE-132093-MS.
- Samuel, M., et al., 1997. Polymer-free fluid for hydraulic fracturing. In: *SPE Annual Technical Conference and Exhibition*. OnePetro.
- Sanaei, A., et al., 2018. Comprehensive study of gas cycling in the Bakken shale. In: *Unconventional Resources Technology Conference*, Houston, Texas, 23–25 July 2018. Society of Exploration Geophysicists, American Association of Petroleum.
- Saneifar, M., 2012. The Effect of Acid Additives on Carbonate Rock Wettability and Spent Acid Recovery in Low Permeability Gas Carbonates. Texas A & M University.
- Sang, Q., et al., 2014. Enhanced oil recovery by branched-preformed particle gel injection in parallel-sandpack models. *Fuel* 136, 295–306.
- Santiago, C.J., Kantzas, A., 2020. On the role of molecular diffusion in modelling enhanced recovery in unconventional condensate reservoirs. In: *SPE Europec*. D021S014R004.
- Sayed, M., et al., 2018. A Low-Viscosity Retarded Acid System for Stimulation of High-Temperature Deep Wells.
- Schmid, K.S., et al., 2016. Analytical solutions for spontaneous imbibition: fractional-flow theory and experimental analysis. *SPE J.* 21 (6), 2308–2316.
- Shaffer, N.R., 2020. Indiana Limestone: America's building stone. *Geol. Soc. Lond. Spec. Publ.* 486 (1), 77–101.
- Sheng, J.J., 2015. Enhanced oil recovery in shale reservoirs by gas injection. *J. Nat. Gas Sci. Eng.* 22, 252–259.
- Sheng, J., et al., 2014. Matrix acidizing characteristics in shale formations. *J. Petrol. Environ. Biotechnol.* 5 (5).
- Suleimenova, A., 2015. Acid Fracturing Feasibility Study for Heterogeneous Carbonate Formation.
- Talabani, S., Islam, M., 1999. Diverting acid into low permeability reservoir using foam for stimulation. In: *Technical Meeting/Petroleum Conference of the South Saskatchewan Section*. OnePetro.
- Taylor, K.C., Nasr-El-Din, H.A., 2009. Measurement of acid reaction rates with the rotating disk Apparatus. *J. Can. Petrol. Technol.* 48 (6), 66–70.
- Taylor, K.C., Al-Ghamdi, A.H., Nasr-El-Din, H.A., 2004. Measurement of acid reaction rates of a deep dolomitic gas reservoir. *J. Can. Petrol. Technol.* 43 (10).
- Teklu, T.W., et al., 2014. Vanishing interfacial tension algorithm for MMP determination in unconventional reservoirs. In: *SPE Western North American and Rocky Mountain Joint Meeting*. SPE-169517-MS.
- Tripathi, D., Pournik, M., 2014. Effect of acid on productivity of fractured shale reservoirs. In: *SPE/AAPG/SEG Unconventional Resources Technology Conference*. OnePetro.
- Wang, D., et al., 2012. Wettability survey in bakken shale with surfactant-formulation imbibition. *SPE Reservoir Eval. Eng.* 15 (6), 695–705.
- Wang, S., et al., 2018. Experiment and analysis of the reaction kinetics of temperature control viscosity acids with limestone. *J. Petrol. Sci. Eng.* 165, 305–312.
- Weast, R.C., 1979. *CRC Handbook of Chemistry and Physics*.
- Williams, B.B., Gidley, J.L., Schechter, R.S., 1979. *Acidizing Fundamentals*.
- Wragg, A., 1971. Combined free and forced convective ionic mass transfer in the case of opposed flow. *Electrochim. Acta* 16 (3), 373–381.
- Wu, Y.S., Li, J., Ding, D., Wang, C., Di, Y., 2013. A generalized framework model for simulation of gas production in unconventional gas reservoirs. In: *SPE Reservoir Simulation Symposium*. SPE-163609-MS.
- Yan, B., Wang, Y., Killough, J.E., 2013. Beyond dual-porosity modeling for the simulation of complex flow mechanisms in shale reservoirs. In: *SPE Reservoir Simulation Symposium*. SPE-163651-MS.



**Chapter 6:**  
**Effect of Acidizing Propped Fracture on Productivity**  
**Optimization: Eagle Ford Case Study**

# Statement of Authorship

Title of Paper	The effect of acidizing propped fracture on productivity optimization: Eagle Ford case study
Publication Status	<input checked="" type="checkbox"/> Published <input type="checkbox"/> Accepted for Publication <input type="checkbox"/> Submitted for Publication <input type="checkbox"/> Unpublished and Unsubmitted work written in manuscript style
Publication Details	Journal of Fuel Volume 329, 125363 <a href="https://doi.org/10.1016/j.fuel.2022.125363">https://doi.org/10.1016/j.fuel.2022.125363</a>

## Principal Author

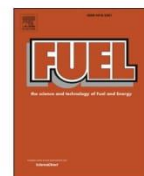
Name of Principal Author (Candidate)	Mohsen Farrokhrouz		
Contribution to the Paper	Familiarizing with new setup, Running the experiments, Acquiring Data, Checking the sensitivity analysis, Knowledge, Analysis, Drafting		
Overall percentage (%)	80%		
Certification:	This paper reports on original research I conducted during the period of my Higher Degree by Research candidature and is not subject to any obligations or contractual agreements with a third party that would constrain its inclusion in this thesis. I am the primary author of this paper.		
Signature		Date	19/03/2022

## Co-Author Contributions

By signing the Statement of Authorship, each author certifies that:

- i. the candidate's stated contribution to the publication is accurate (as detailed above);
- ii. permission is granted for the candidate to include the publication in the thesis; and
- iii. the sum of all co-author contributions is equal to 100% less the candidate's stated contribution.

Name of Co-Author	Dr Abbas Taheri		
Contribution to the Paper	Knowledge, Conception, Drafting		
Signature		Date	05/01/2022
Name of Co-Author	Dr Alireza Keshavarz		
Contribution to the Paper	Knowledge, Conception, Drafting		
Signature		Date	05/01/2022
Name of Co-Author	Prof Stefan Iglauer		
Contribution to the Paper	Knowledge, Conception, Drafting		
Signature		Date	05/01/2022



## Full Length Article

# The influence of acidizing on propped fractures for productivity enhancement: Eagle Ford laboratory study

Mohsen Farrokhrouz<sup>a,b,\*</sup>, Abbas Taheri<sup>a,c</sup>, Stefan Iglauer<sup>b</sup>, Alireza Keshavarz<sup>b</sup>

<sup>a</sup> School of Civil, Environment and Mining Engineering, The University of Adelaide, Adelaide, SA, Australia

<sup>b</sup> School of Engineering, Edith Cowan University, Perth, WA, Australia

<sup>c</sup> The Robert M. Buchan Department of Mining, Queen's University, Kingston, Ontario, Canada



## A B S T R A C T

Hydraulic fracturing of tight formations and placing proppants within induced fractures are commonly performed in unconventional shale reservoirs all over the world, especially in North America. However, the overall recovery of these oil and gas resources is very low and hence, production enhancement is inevitable.

This study investigated the acidizing of propped fractures as a recovery enhancement method in Eagle Ford shale samples. Experiments were designed using sample slabs having proppants between them. Differing parameters were examined to optimize the fracture conductivity through acidizing. For a range of confining pressures, the fracture conductivity was maximized by minimizing the proppant embedment. A higher acid injection rate was achieved with a 5 % HCl concentration. Proppant concentration and proppant size were found to affect fracture conductivity inversely. However, this trend was not observed to be monotonic. In terms of production parameters, the skin factor determined the optimized conditions at a constant confining pressure. Overall, the optimum conditions for acidizing in the propped fractures were determined while having 5 % HCl concentration, 1 lb/ft<sup>2</sup> (4.88 kg/m<sup>2</sup>) proppant concentration, 600–710 μm of proppant size and 8 ml/min acid injection rate. These findings confirmed the applicability of the method for hydraulic fracturing optimization in Eagle Ford shale samples. It can also be regarded as a primary enhancement method due to its low cost and the process simplicity in comparison to hydraulic fracturing operations. The experimental results of this study would correspondingly enlighten their potential field applications through facilitating appropriate modification with regards to specific operational conditions.

## 1. Introduction

The significance of shale in North America is growing in terms of oil and natural gas production. Statistics indicate that it will remain the primary contributor of energy in the middle of the 21st century [1]. The US alone holds around six trillion barrels of shale oil in place [2], with 495 trillion cubic feet (TCF) of shale gas [1]. Shaly formations contain less than 10 % organic content and 50 % clay, with the remainder being quartz and/or calcite [3].

The ultra-low permeability of shale formations presents a significant challenge in hydrocarbon production. The permeability in shales could span from tens to hundreds of nano-Darcy [4]. Therefore, conventional production methods do not apply to these reserves. Instead, directional drilling techniques followed by hydraulic fracturing are applied in the high permeable channels within the rock to initiate the production from fractures [5]. Hydraulic fracturing is known as a revolutionary technique for production from unconventional reservoirs [6]. Despite having expensive operations, the primary recovery of shale is less than 10 % [7].

Therefore, potential secondary recovery methods are essential to maintain production levels. Due to high capital costs within the first

stage, economic concerns are the priority. Waterflooding is the cheapest and most reasonable technology in most conventional oil reservoirs. However, in unconventional reservoirs, this practice still requires further investigation. There are only a few studies which have focused on this in pilot-scale [8] and laboratory core flooding experiments [9].

During hydraulic fracturing, different stages of the acid, pad, prop, and flush may be included within the operation. Some studies focused on engineering proppant properties, like graded proppant injection [10,11] and/or micro and nano-sized particles injection [12–14]. For shale formations, due to their diverse mineralogy, each stimulation and frac-job are tailored according to the specific reservoir. Within a typical frac-job, the fracturing fluid consists of 98 % water and proppant, with less than 2 % of the mixture having other chemicals such as friction reducers, iron stabilizers, scale inhibitors, surfactants and pH regulators [3]. There is a pre-flush stage in this process, which includes the use of an acid (HCl) to reduce the compressive strength of the formation. The acid wash removes formation damage during drilling and completion while improving the connectivity of micro-fractures via calcite removal [15].

Apart from propped fracturing, two other stimulation techniques (matrix acidizing and acid fracturing) are utilized with higher acid concentrations inside shale formations. Matrix acidizing is mostly operated in calcite at low pressures for sediment dissolution and mud

\* Corresponding author at: School of Engineering, Edith Cowan University, Perth, WA, Australia.

E-mail addresses: [mohsen.farrokhrouz@adelaide.edu.au](mailto:mohsen.farrokhrouz@adelaide.edu.au), [m.farrokhrouz@ecu.edu.au](mailto:m.farrokhrouz@ecu.edu.au) (M. Farrokhrouz).

<https://doi.org/10.1016/j.fuel.2022.125363>

Received 19 March 2022; Received in revised form 13 July 2022; Accepted 19 July 2022

Available online 29 July 2022

0016-2361/© 2022 Elsevier Ltd. All rights reserved.



Nomenclatures		Greek Symbols	
<i>English Symbols</i>		$\mu$	viscosity, Pa.s
A	section area, m <sup>2</sup>	$\pi$	Pi number, 3.141
B	formation volume factor, dimensionless	$\Pi$	productivity index, m <sup>3</sup> /Pa.s
h	proppant pack height, m	$\rho$	density, kg/m <sup>3</sup>
J	productivity ratio, dimensionless	$\varphi$	porosity, fraction
k	permeability, m <sup>2</sup>	<i>Subscripts</i>	
L	proppant pack length, m	0	initial case
N	Reynold's number, dimensionless	d	damaged
Q	flow rate, m <sup>3</sup> /s	D	dimensionless
S	skin factor, dimensionless	f	fracture
v	velocity, m/s	Re	Reynolds
w	proppant pack width, m	s	skin
		t	current case
		w	water

solids [16]. Acid fracturing is mostly utilized in dolomite formations [17–20]. In terms of operation, acid fracturing is viable in long term compared to propped fracturing and hydraulic fracturing [21].

In addition to carbonate formations, acid fracturing can also be operated with carbonaceous shale. In these types of formations, the efficiency of acid fracturing is proportional to carbonate content and the reactivity of acid/rock surfaces [22]. After hydraulic fracturing and primary recovery of the shale, a stage of matrix acidizing (and/or acid fracturing) is performed through the already propped reservoir to increase the conductivity of the fractures and extend the production life of the reservoir over time. Investigating the possibility of these forms of operation and optimizing procedures for acidizing the propped fracture is the main motive of this study. To the best of our knowledge, there is no other study implementing such experimental testing of acidizing propped fracture for Eagle Ford shale samples.

In this paper, the Eagle Ford shale sample as a typical oil shale formation was selected for propped conductivity measurement experiments. Acidization with different concentrations and injection rates were conducted through the proppant packs. During these experiments, the conductivity of the fractures was determined while considering acid and proppant different characteristics. The conductivity analysis performed on the experimental outcomes was presented and optimized conditions were proposed.

## 2. Materials and methods

In this study, fracture conductivity measurements were carried out with the API standard Fracture Conductivity System (FCS) at Edith Cowan University, using Core Lab laboratory facilities. A schematic of this system and the actual setup are shown in Fig. 1. Eagle Ford shale samples were provided by Kocurek Industries Inc. and were cut according to the Fracture Conductivity System (FCS).

### 2.1. Properties of proppants

The API standard proppant, provided by the Core Lab company was used for these experiments. Based on the company catalogue, the size of the particles ranged from 150 to 420  $\mu\text{m}$  (mesh 40/100). The proppant was sieved followed by the selection of 180–250  $\mu\text{m}$  (mesh size 60/80) range for the experiments. A 2 lb/ft<sup>2</sup> (9.76 kg/m<sup>2</sup>) of API proppant with a mesh size of 60/80 was utilized to repeat the test. An acid optimization test was also conducted by the API proppant. A ceramic proppant provided by the Schlumberger company was selected for the rest of the optimization process which had a Carbolite proppant of 420–850  $\mu\text{m}$  (mesh size 20/40) size. This proppant was sieved to produce a narrower particle size of 710–800  $\mu\text{m}$  (mesh size 22/25). Detailed properties of

the proppants are given in Table 1.

### 2.2. Core samples

The core samples were prepared in a slab shape having the dimension of 17.75 cm in length, 3.75 cm in width and 1.15 cm in thickness as per the standard for measuring the long-term conductivity of proppants [17]. The Eagle Ford shale sample is known to have carbonaceous shale with high calcite content (up to 70 %) [23,24]. The mineral composition based on the XRD test of the samples used in this study is provided in Table 2. The performed test to determine the peaks of these minerals is shown in Fig. 2. Acidizing was performed on this sample by utilizing hydrochloric acid (HCl).

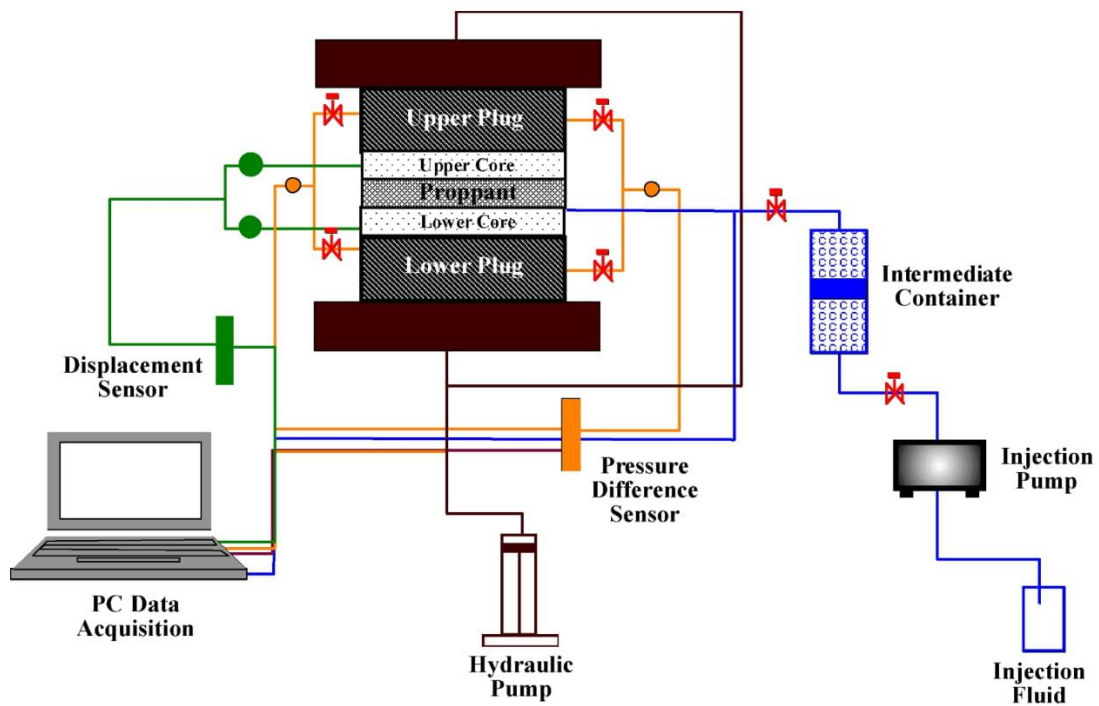
### 2.3. Experimental procedures

The test procedure is designed as preparation of a proppant pack on Eagle Ford shale samples and then inject the acid into this fractured medium. Therefore, the shale slabs were placed inside the fracture conductivity system as shown in Fig. 1. According to the ISO standard recommendation [25], 2 lb/ft<sup>2</sup> (9.76 kg/m<sup>2</sup>) proppant was placed between the samples. A pre-flush test was conducted to remove air from the proppant pack that included injecting 150 ml brine (5 % w/w NaCl in DI water) into the cell with a constant injection pressure of 140 kPa. For the matrix acidizing process, the amount and rate of acid injection should be selected appropriately which can ensure that the rock surface reacts with the acid properly and the products can be transferred easily towards the effluent. Therefore, 250 ml of 5 % HCl was injected at an 8 ml/min rate while the cell was under 3.5 MPa confining pressure. Subsequently, the acid concentration and injection rate were optimized based on several tests. Afterwards, 150 ml of the same brine was used as post-flush to remove acid from the cell and to prevent acid and rock reaction further. Conductivity measurements were carried out at different confining pressures (5 MPa–50 MPa). After repeatability tests, optimization was performed based on acid concentration, proppant type, proppant distribution, proppant particle size and acid injection rate. Data acquisition was performed automatically by the conductivity system.

## 3. Theory of acidizing in proppant pack

The principle of fluid flow through the sand pack can be described by Darcy's law:

$$k = \frac{Q\mu L}{A\Delta p} \quad (1)$$



(a)



(b)

Fig. 1. a) Schematic of the fracture conductivity system; b) Conductivity setup under confining pressure.

**Table 1**  
Properties of the proppants used in the tests.

Type of property	Ceramic proppant (Carbolite)	Sand proppant (API Standard)
Mesh Range (Mesh size)	22/25	60/80
Median Particle Diameter (µm)	730	220
Bulk Density (g/cm <sup>3</sup> )	1.57	1.60
Roundness	0.9	0.6
Sphericity	0.9	0.6
Apparent Specific Gravity	2.71	2.59
Absolute Volume (litre/kg)	0.367	0.386
Acid Solubility (%)	1.7	3.0
Crushing Rate (%)	5.2 (Effective closure Stress = 52 MPa)	9.4 (Effective Closure Stress = 40 MPa)

**Table 2**  
Properties of Eagle Ford shale slabs for the experiments (Data provided by the provider, Kocurek industries).

Mineral	Calcite	Quartz	Dolomite	Pyrite	Kaolinite	TOC*
Content (%)	70	18	2	1	9	5.5

\*TOC: Total Organic Content.

where  $k$  is the permeability of the fracture ( $\mu\text{m}^2$ ),  $Q$  is the flow rate ( $\text{cm}^3/\text{s}$ ),  $\mu$  is the viscosity of the fluid ( $\text{mPa}\cdot\text{s}$ ),  $L$  is the length of the test section ( $\text{cm}$ ),  $A$  is the area of cross-section of the fracture ( $\text{cm}^2$ ) and  $\Delta p$  is pressure differential through the test section ( $\text{atm}$ ). In an API standard conductivity cell, these parameters are already determined [25] which has a  $65 \text{ cm}^2$  test area,  $17.8 \text{ cm}$  sample length with  $3.8 \text{ cm}$  width and  $12.7 \text{ cm}$  distance between pressure ports.

Fluid flow in a porous medium can disturb or enhance the original permeability as well as the conductivity of a medium. The skin factor is one of the parameters to determine this degree of change which can be positive (formation damage), negative (stimulation), or zero (no effect on porous medium). Definition of skin factor in a skin zone is uniform, where pressure drop across this zone can be approximated by Darcy's equation [26,27]:

$$\Delta P_{skin} = \left[ \frac{Q_w B_w \mu_w}{kA} \right] S \tag{2}$$

Applying the term skin factor to Darcy's law and assuming the linear displacement of the fluid within a medium, the steady-state flow can be expressed as:

$$Q = \frac{k \cdot w_f \cdot h}{\mu} \frac{\Delta P}{L(1 + S)} \tag{3}$$

The term  $k \cdot w_f$  is known as conductivity in fractured medium and it is shown with 'C', too. The productivity index (PI) is the absolute value of the slope of an IPR straight line. Accordingly, it relates production rate to drawdown pressure:

$$\Pi = \frac{Q}{\Delta P} \tag{4}$$

The productivity ratio ( $J_D$ ) is defined as the ratio of the actual productivity index to the ideal productivity index (total skin = 0) which is a dimensionless term:

$$J_D = \frac{\Pi(t)}{\Pi(0)} \tag{5}$$

This is also called dimensionless productivity or normalized productivity index. Acidizing optimization depends on several parameters and experimental tests and hence, it should be sequentially designed. It can be used as a unique factor to investigate the effects of involved parameters on the final recovery of an acidizing process. The  $J_D$  is a good option while considering the acidizing process. It can be properly used to compare the productivity improvement after acidizing while investigating the effective parameters. The utilization of this parameter for investigating acid efficiency and comparing conductivity values has already been reported [20,22,28–30]. There are also studies available that suggest algorithms for production prediction using neural networks and history-matching field data [31].

Using Equation (3) in the productivity ratio definition (Equation (5)), results in:

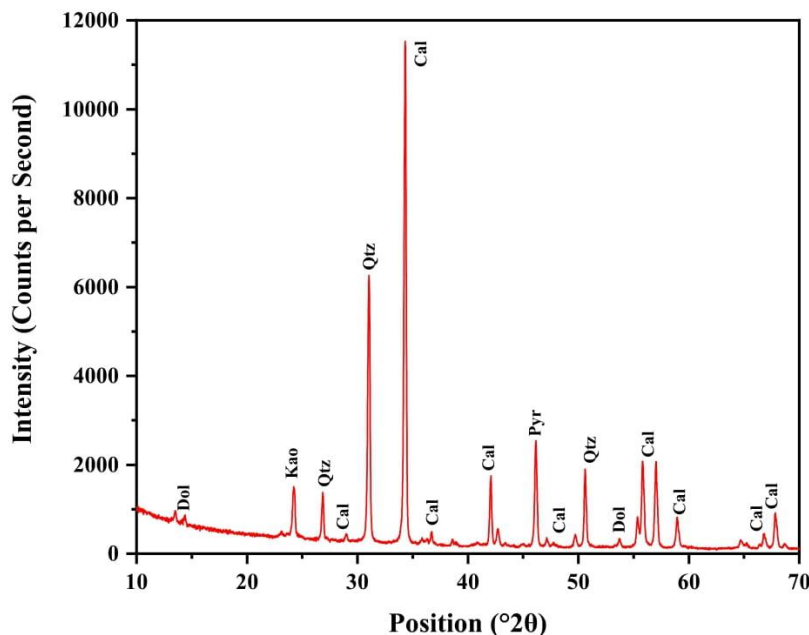


Fig. 2. Powder XRD patterns of Eagle Ford shale sample showing the peaks of minerals (Cal: Calcite, Qtz: Quartz, Dol: Dolomite, Kao: Kaolinite, Pyr: Pyrite).



$$J_D = \frac{\Pi(t)}{\Pi(0)} = \underbrace{\frac{C_r}{C_0}}_{A'} \underbrace{\frac{[1+S]_0}{[1+S]_t}}_{B'} \quad (6)$$

Parameter ‘C’ is equivalent to the term ‘kh’ which can be considered equivalent to the term ‘kw<sub>f</sub>’ called as hydraulic conductivity (w<sub>f</sub> is the width of the fracture). The J<sub>D</sub> is composed of two main terms, i.e., A’ and B’. By controlling these terms, we can verify the effect of acidizing parameters on the system. At the same time, only one of these two terms can change and the other should be kept constant.

During confining pressure alteration, the value of conductivity change ‘h’ in Equation (3) and term A’ in Equation (6) will be affected. To keep the term B’ constant, the skin factor needs to remain unchanged both in the base and the case under study. Therefore, we have performed conductivity measurements at a constant flow rate.

Sometimes, the acidizing could render a negative skin within a system, which could alter the term B’. To precisely understand the stimulation process, the effect of different rates on the term B’ needs to be verified and during these tests, the term A’ needs to be maintained as constant by conducting the tests at constant confining stress.

#### 4. Results and discussion

According to the Equation (6), a base case (Π(0)) is required. This case is considered a zero-acid case to measure the conductivity for brine flooding (5 % NaCl + 0 % HCl) with both proppant types. The repeatability of the tests can also be obtained for this case. Fig. 3 shows the change in conductivity at different confining pressures with no acid injection. Experimental results confirmed the perfect repeatability of the tests as the conductivity values fall within the 10 % error band of each other.

##### 4.1. Acid concentration effect

For investigating the acid concentration effect, three different

concentrations (5, 10 and 15 %) of HCl were used. The effect of different acid concentrations on the normalized productivity index is shown in Fig. 4. The results of these experiments demonstrated that acidizing a propped fracture increased the reservoir’s productivity at all acid concentrations. In addition, 15 % HCl showed the highest productivity between 25 and 35 MPa confining, while 10 % HCl showed the best results between 7 and 20 MPa confining pressure. For the whole range of confining pressures (7 to 40 MPa), the 5 % HCl was found to be optimum.

At the beginning of the process, the reaction of the acid with the calcite available on the rock surface is limited by the rate of mass

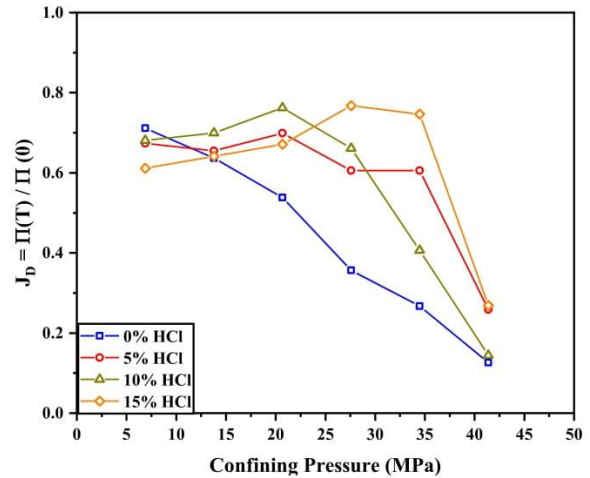


Fig. 4. Effect of acid concentration on the productivity index of Eagle Ford shale samples. The proppant used for the test was API standard with the distribution of 2 lb/ft<sup>2</sup> (9.76 kg/m<sup>2</sup>) and particle size of 180–250 μm.

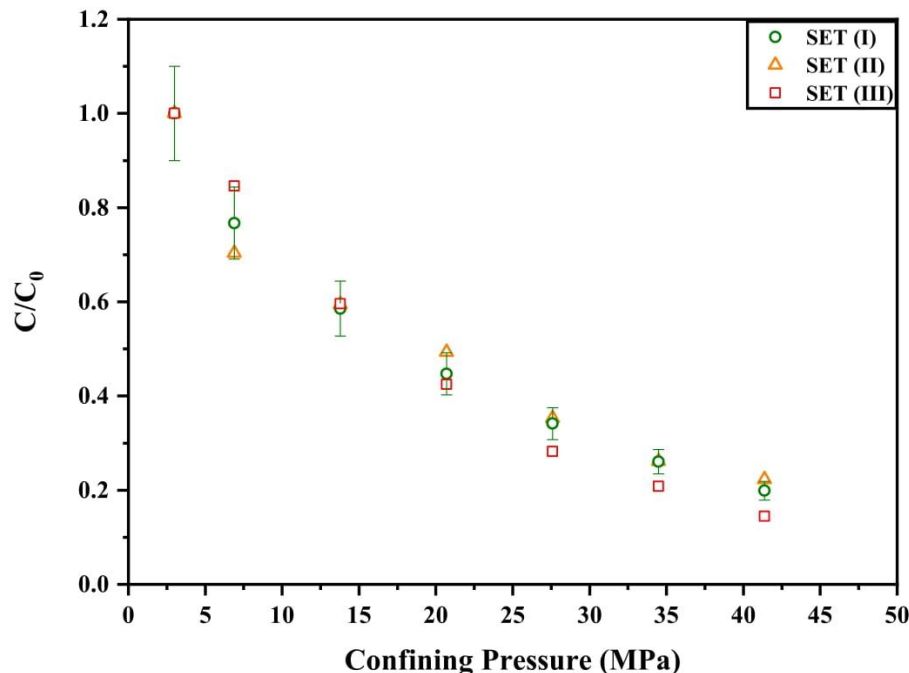


Fig. 3. Repeatability of the tests for the base case. The injected fluid is 5% w/w NaCl solution in De-Ionized (DI) water. Error bars shows 10% error in conductivity ratios.

transfer and the rate of surface reactions. At a lower concentration of acid, these products can transfer from the rock surface easily, but the number of reactions in unit time will be low. At the same time, at high acid concentration, a higher number of reactions per unit time can occur. However, the products cannot transfer towards the effluent easily and the fresh rock surface cannot be always in contact with acid. This effect of acid on the rock surface has been reported in many experimental and modelling studies [20,32–35]. It has been observed that at a certain confining pressure below 30 MPa, 10 % acid concentration is the best option, as 5 % HCl is reaction-limited and 15 % HCl is transfer-limited (Fig. 4).

The second mechanism shows up at higher confinements (more than 30 MPa). API proppants begin to crush at 25 MPa (Fig. 5), which could cause a decrease in conductivity [36–38]. Moreover, proppant embedment in rock surfaces could occur frequently in shale formations at higher confinements [39–41]. This effect is more intense for better-acidized surfaces, as the depth on embedment is likely to increase, leading to a sharp decrease in the 10 % HCl concentration trend line. Two other concentrations demonstrated a similar trend at this range of confining pressure (Fig. 4).

Considering different trends of conductivity and the whole range of confinements, 5 % HCl was selected as the optimum acid concentration for matrix acidizing through the Eagle Ford shale sample. The proppant was 180–250  $\mu\text{m}$  of API type with a concentration of 2  $\text{lb}/\text{ft}^2$  (9.76  $\text{kg}/\text{m}^2$ ).

#### 4.2. Effect of proppant concentration

In this set of experiments, the ceramic proppant displayed in Table 1 was utilized. Due to its higher resistance, the crushing rate of this proppant decreased substantially for the confining range. Ceramic proppant was selected due to its high resistance, low specific gravity, longer transport along the fracture and uniform size [42,43].

Therefore, the negative effect of crushing on the conductivity was compensated to a great extent in comparison with the API proppant. The normalized productivity index confirmed this concept (Fig. 6(a)), where the proppant size was constant during the experiments (710–800  $\mu\text{m}$ ). According to the standard [25], 2  $\text{lb}/\text{ft}^2$  (9.76  $\text{kg}/\text{m}^2$ ) was selected as the starting concentration of the proppant.

Subsequently, 1  $\text{lb}/\text{ft}^2$  (4.88  $\text{kg}/\text{m}^2$ ) as a medium concentration and 0.3  $\text{lb}/\text{ft}^2$  (1.46  $\text{kg}/\text{m}^2$ ) were selected as the mono-layer proppant distribution for this particle size. The bulk density of the proppant particles was 1.57  $\text{g}/\text{cm}^3$ . Acidizing was performed with 5 % HCl acid.

The effect of proppant concentration on normalized productivity after acidizing was shown in Fig. 6(b). As compared to Fig. 4, Fig. 6(b)

displayed little fluctuation, which could be attributed to the higher resistance of the proppant. At lower confining, higher concentrations displayed better results because higher amounts of proppant were not fully packed. With the increase in confining pressure, the jamming ratio of the proppant and embedment increased. The former affects the conductivity of higher proppant concentration and the latter the conductivity of the lower proppant concentration. Therefore, the medium range of proppant concentration produced better results for higher confinements, where this concentration was selected as the optimum condition for the rest of the experiments. This finding is also consistent with the results of previous experimental studies for shale samples [44], high-strength proppants [45] and statistical studies based on field data [46].

#### 4.3. Effect of proppant size

After optimizing the acid and proppant concentration (5 % HCl and 1  $\text{lb}/\text{ft}^2$ ), the size of the proppant was also required to be optimized for further productivity. The proppant size used at this point was 710–800  $\mu\text{m}$  (mesh size 22/25). In this section, other proppant sizes were also applied (Fig. 7). Two other sizes (+850 and 250–300  $\mu\text{m}$ ) showed lower productivity indices, while the proppant size of 600–710  $\mu\text{m}$  showed enhancement in productivity ratio. As explained earlier, for smaller proppant sizes, high confinement leads to further packing of the proppant while representing lower permeability. In contrast, a bigger proppant size at lower confinement can withstand higher pressure. After a minor breakage, redistribution of the particles could take place which could slightly increase the productivity and a constant productivity index can be achieved. However, particle embedment in the rock surface can also decrease productivity. The particle size between these two extremes (600–710  $\mu\text{m}$ ) can be termed as the optimum size with minimum embedment. If the proppant pack is compressed to a lower extent, the productivity of the medium can increase.

#### 4.4. Effect of acid injection rate

Acidizing efficiency is controlled by the rate of reaction and transfer of products. An injection acid rate of 8  $\text{ml}/\text{min}$  was selected for all the experiments. To enhance and investigate the effect of acid injection rate, the rate was subsequently decreased to 4  $\text{ml}/\text{min}$  and 2  $\text{ml}/\text{min}$ . The results of this effect were presented in Fig. 8(a). The remainder of the parameters were set at optimized conditions based on the previous tests. It can be concluded from Fig. 8(a) that at a higher acid injection rate, acid does not have enough time to react with the rock surface. Lower reactions indicate less embedment of the proppant into the rock surface. However, at lower injection rates, the acid-rock surface is mass-transfer

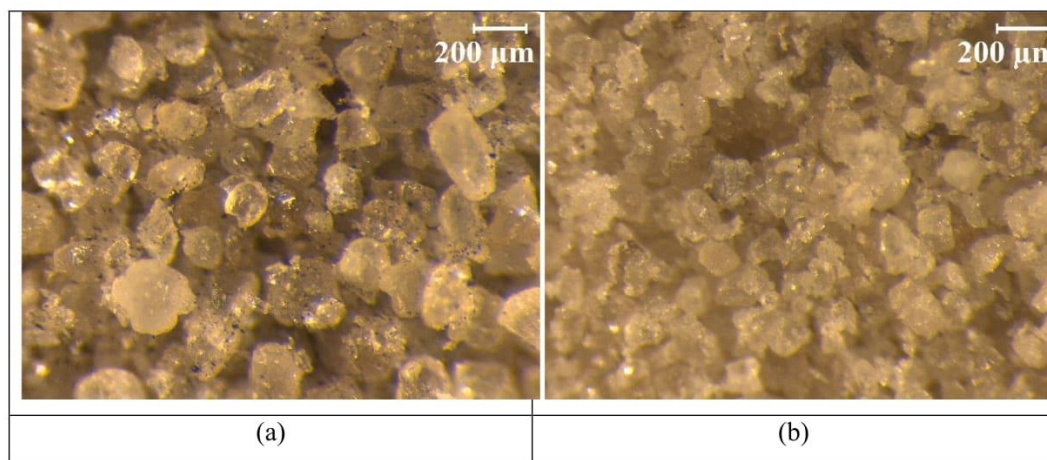
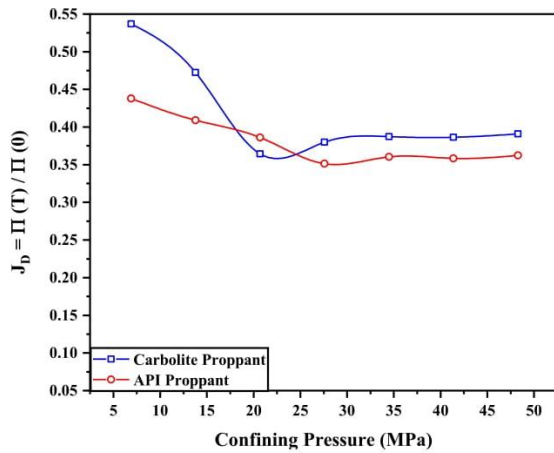
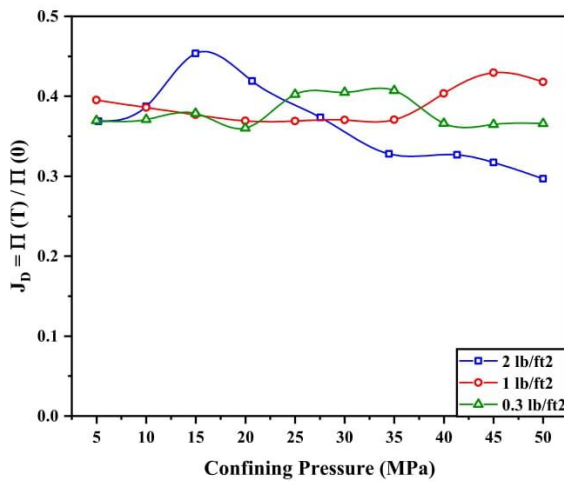


Fig. 5. The effect of confining pressure crushing the API proppant: a) after 17 MPa confinement, b) after 25 MPa confinement.





(a)



(b)

Fig. 6. Effect of proppant type and concentration on productivity ratio: a) comparison of proppant types as in Table 1; b) Effect of proppant concentration.

limited, and the acid has enough time to react with the rock surface. This leads to higher embedment of the proppant into the rock and a decrease in conductivity. Consequently, the value of the productivity index decreases. This is in good agreement with the literature, which states that after stimulation, embedment could cause a decline in conductivity and porosity of the propped fracture [47–50]. The transducers located next to the conductivity cells measured the embedment of the proppants. For a lower injection rate, the embedment was higher, leading to a lower conductivity value and productivity index (Fig. 8(b)).

4.5. Skin factor Calculation at constant confining pressure

As noted earlier, skin factor calculations should be conducted at a constant confining pressure. Based on the data in Table 1, 20 MPa was selected as the proper confining pressure that has minimum crushing of the proppants. At this specific confining pressure, the optimized condition is not necessarily the same as discussed in Sections 4.2 to 4.4.

The optimized condition was identified by the case of minimum skin factor after acidizing. The skin factor (S) in Equation (3) represents the

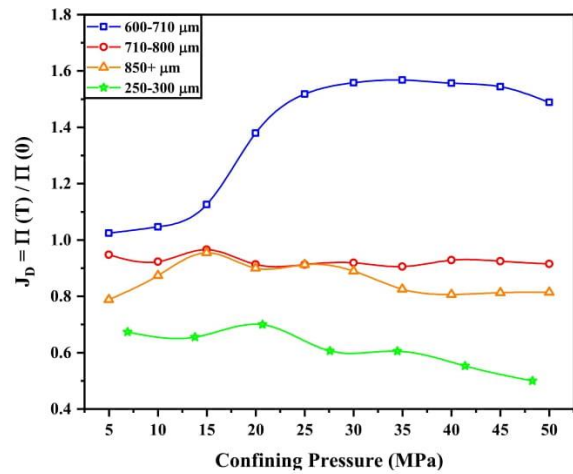


Fig. 7. Effect of proppant size on productivity index at different confining pressures.

total skin. Various types of skin factors were determined through the processes that could cause permeability impairment. These skin factors could be stress-induced skin, which was not the case in our study as we had compared all the results at one confining pressure. Other types of skin in the field are dedicated to the completion, perforation, casing, and partial penetration of the fluid into the wellbore [51]. In our experiments, we did not account for all these skins as they are field-related pseudo-skin terms.

Other skin factors are related to the geometry of the formation or fluid phases within a fractured medium [52]. For all our experiments, these parameters were either same or were not present during the tests. There is also a rate-dependent skin factor which is important in a turbulent environment. Turbulency of the fluid movement is characterized by the Reynolds number. The Reynolds number inside a porous medium can be defined by the following equation [53]:

$$N_{Re} = \frac{10}{\phi^{2.3}} \frac{\rho v}{\mu} \sqrt{k} \tag{7}$$

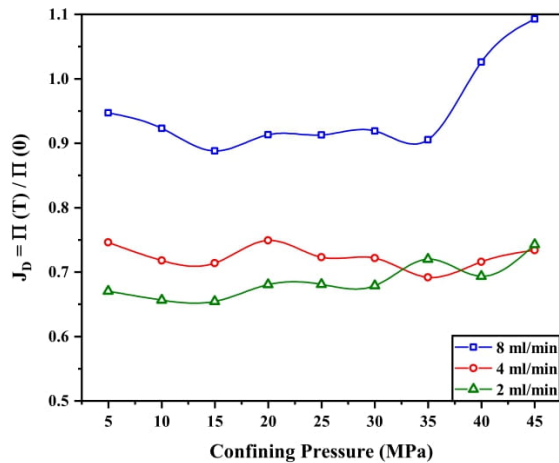
For laminar flow,  $N_{Re}$  should be less than 1. The typical values of the parameters in Equation (7) is like this: porosity in the range of 2 to 44 %, density and viscosity of 5 % NaCl solution (1038 kg/m<sup>3</sup> and 0.972 m.Pa.s) and permeability of the base case measured at the conductivity cell system (453 md at 8 ml/min brine injection). According to these values, the Reynolds number is far below 1, and the fluid flow is laminar. Therefore, non-Darcy flow and corresponding skin do not exist. However, the Reynolds number is still a function of velocity as mentioned in Equation (7). It is worth mentioning that the flow of fluid phases through the porous medium is also a function of saturation profile and there are previous studies which have suggested mathematical models for that [54,55].

The only significant skin factor that should be considered for the duration of the tests is mechanical damage pseudo-skin induced by proppant embedment. The decline in conductivity of propped fractures due to deeper embedment (the width of fracture remains constant) is already well-established within the literature [39,56–58]. According to the study conducted by Cramer [59], fracture skin ( $S_f$ ) can be estimated as:

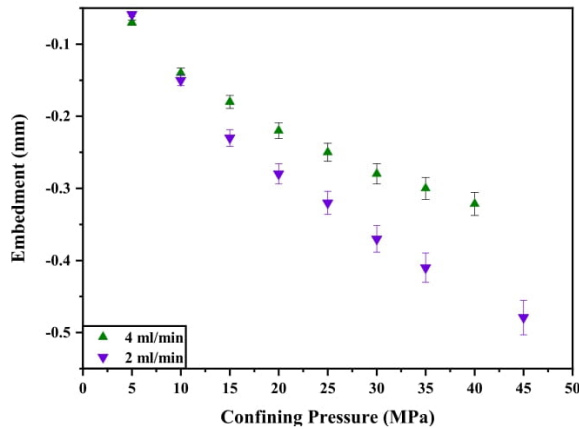
$$S_f = \frac{\pi h_d}{L_f} \left( \frac{K}{K_d} - 1 \right) \tag{8}$$

Where  $h_d$  is the width of the damaged zone on the rock surface,  $L_f$  is the fracture length, and  $K$  and  $K_d$  are the non-damaged and damaged reservoir formation permeability, respectively. Instead of permeability





(a)



(b)

Fig. 8. a) Acid injection rate effect on productivity, b) proppant embedment into the rock surface measured by the Linear Variable Differential Transformer (LVDT) sensors.

values, the ratio of conductivity values can be used in Equation (8) as they represent the same concept.

The base case data was achieved for the sample without acidizing, as illustrated in Section 4 and Fig. 3. According to Equations (3) and (4), we have obtained:

$$\Pi = \frac{Q}{\Delta P} = \frac{h}{\mu L(1+S)} k \cdot w_f \tag{9}$$

As evident, the plot of productivity index ( $\Pi$ ) versus conductivity ( $C = k \cdot w_f$ ) was a straight line (Fig. 9). The slope of this line was a constant with known parameter values and the skin factor was independent of flow rate. For this base case, the constant value was  $103.4 \text{ Pa}^{-1} \cdot \text{s}^{-1}$  which resulted in a skin factor of 1.32. This indicates that the system itself had some pseudo-skin factor that may be due to the geometry of the sand pack or mechanical skin factor due to the confinement. Comparing this base case with acidized samples and using Equation (6) the new skin can be calculated. Values smaller than 1.32 represents an enhancement in conductivity, while higher values represent the damaging effects of acidizing.

Calculation of the skin factor should be conducted at a constant

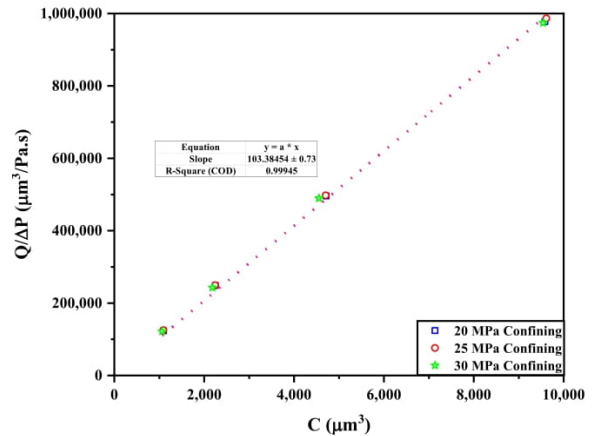


Fig. 9. Productivity index as a function of conductivity at different confining stress for the proppant pack without acid injection.

conductivity and constant confining pressure. The confining pressure was selected as 20 MPa. By changing different parameters at constant confining, the value of conductivity was measured. The parameters included proppant size, proppant concentration and acid injection rate. Fig. 10 shows the optimum conditions at this confining pressure. The green circles represented the path of optimization. In all of the cases, the skin factor was negative which demonstrated the efficiency of acidizing in comparison with non-acidizing cases. At 20 MPa confining pressure, the optimum condition was determined to be 600–710  $\mu\text{m}$  proppant size, 0.3  $\text{lb}/\text{ft}^2$  ( $1.46 \text{ kg}/\text{m}^2$ ) proppant concentration and 8  $\text{ml}/\text{min}$  acid injection rate. It should be noted that these optimum conditions are only valid for this confining pressure. For the whole range of confining pressures (5 to 50 MPa), the optimized conditions were discussed in Sections 4.1 to 4.4.

### 5. Conclusion

In this paper, acidizing as an enhancement method through propped formations has been examined through experiments. Two main categories of the parameters were investigated: the parameters that affect the conductivity of the propped fracture and those parameters that influence the skin factor of the medium. Based on this, these parameters were acid concentration, acid injection rate, proppant size and proppant concentration. Experiments were conducted to optimize these parameters one by one on Eagle Ford shale samples as an unconventional carbonaceous shale on a range of confining stresses from 5 MPa up to 50 MPa. Optimized parameters were determined by experimental results. Moreover, skin factors were checked at a constant confining pressure and optimizations were conducted.

During acidizing, effect of acid is restricted by two factors: reaction rate of the acid with the rock surface and transfer rate of the products from the rock surface. Lower acid concentrations have lower reaction rates and higher acid concentrations have lower transfer rate. Therefore there is an optimized acid concentration in between.

Another important parameter on the propped fracture conductivity is embedment of the proppants. Acidized rock surface is more susceptible to deeper particles embedment, and this leads to decrease in the rock conductivity. The size of the proppants also play role on this and again optimization should be done considering all these effects. Embedment was proportional to the proppant concentration and inversely proportional to proppant size.

Regarding acid injection rate, optimization was slightly more complex, which was dependent on the mineral distribution on the surface of the rock, reaction rate, transfer rate of the products, and proppant

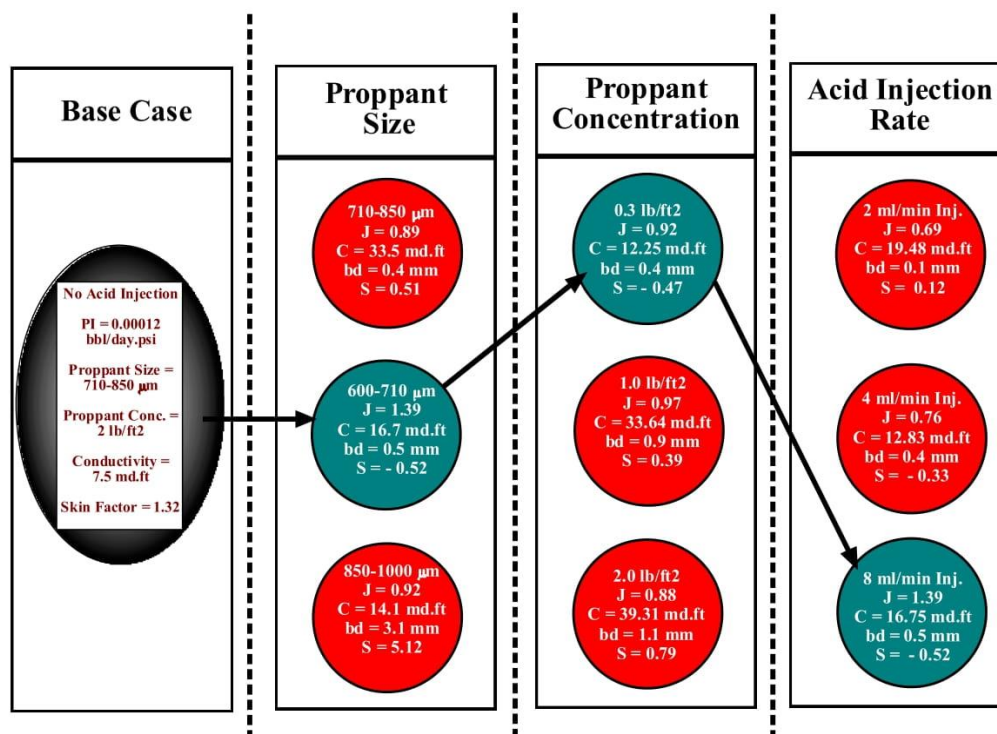


Fig. 10. Optimization pathway based on skin factor value by considering the enhancement in skin factor. The green circles show the best condition for confining stress of 20 MPa. (For interpretation of the references to colour in this figure legend, the reader is referred to the web version of this article.)

characteristics. Overall, the negative skin factor value showed enhancement in the conductivity of propped fractures. This study could be applied in unconventional reservoirs as a primary enhancement recovery method.

#### Declaration of Competing Interest

The authors declare that they have no known competing financial interests or personal relationships that could have appeared to influence the work reported in this paper.

#### Data availability

Data will be made available on request.

#### References

- [1] EIA, *Drilling Productivity Report for Key tight oil and shale gas regions*. 2020.
- [2] Killen, J.C., Biglarbigi, K., *Oil Shale Research in the United States 2011*, INTEC Inc.: US. p. 70.
- [3] Morsy S, Hetherington CJ, Sheng JJ. Effect of low-concentration HCl on the mineralogy, physical and mechanical properties, and recovery factors of some shales. *J Unconventional Oil Gas Resour* 2015;9:94–102.
- [4] Swami V, Clarkson CR, Settari A. *Non-Darcy Flow in Shale Nanopores: Do We Have a Final Answer?*, in *SPE Canadian Unconventional Resources Conference*. 2012. p. SPE-162665-MS.
- [5] Fakharoephol P, Charoenwongsa S, Kazemi H, Wu YS. *The Effect of Water-Induced Stress to Enhance Hydrocarbon Recovery in Shale Reservoirs*, in *SPE Annual Technical Conference and Exhibition*. 2012. p. SPE-158053-MS.
- [6] Su X, Li F, Su L, Wang Q. The experimental study on integrated hydraulic fracturing of coal measures gas reservoirs. *Fuel* 2020;270:117527.
- [7] Mukhina E, Cheremisin A, Khakimova L, Garipova A, Dvoretzskaya E, Zvada M, et al. Enhanced oil recovery method selection for shale oil based on numerical simulations. *ACS Omega* 2021;6(37):23731–41.
- [8] Wood T, Milne B. *Waterflood potential could unlock billions of barrels*. Crescent Point Energy 2011:12.
- [9] Wang D, Butler R, Liu H, Ahmed S. *Flow Rate Behavior and Imbibition in Shale*, in *SPE Eastern Regional Meeting*. 2010. p. SPE-138521-MS.
- [10] Keshavarz A, et al. Enhancement of CBM well fracturing through stimulation of cleat permeability by ultra-fine particle injection. *APPEA J* 2014;54(1):155–66.
- [11] Bedrikovetsky P, et al., *Stimulation of Natural Cleats for Gas Production From Coal Beds by Graded Proppant Injection*, in *SPE Asia Pacific Oil and Gas Conference and Exhibition*. 2012. p. SPE-158761-MS.
- [12] Awan F, Keshavarz A, Akhondzadeh H, Al-Anssari S, Iglauer S. A novel approach for using silica nanoparticles in a proppant pack to fixate coal fines. *APPEA J* 2020; 60(1):88–96.
- [13] Awan FUR, et al. Adsorption of nanoparticles on glass bead surface for enhancing proppant performance: a systematic experimental study. *J Mol Liq* 2021;328: 115398.
- [14] Aslannezhad M, Kalantariasl A, You Z, Iglauer S, Keshavarz A. Micro-proppant placement in hydraulic and natural fracture stimulation in unconventional reservoirs: a review. *Energy Rep* 2021;7:8997–9022.
- [15] Fontaine JS, Johnson NJ, Schoen D. Design, Execution, and Evaluation of a “Typical” Marcellus Shale Slickwater Stimulation: A Case History, in *SPE Eastern Regional/AAPG Eastern Section Joint Meeting*. 2008. p. SPE-117772-MS.
- [16] Bale A, Smith MB, Klein HH. Stimulation of Carbonates Combining Acid Fracturing With Proppant (CAPF): A Revolutionary Approach for Enhancement of Sustained Fracture Conductivity and Effective Fracture Half-length, in *SPE Annual Technical Conference and Exhibition*. 2010. p. SPE-134307-MS.
- [17] Metcalf AS, Miller HL, Weaver RT, Swain ML, Nordstog K, Fallon J. Case history: acid fracturing deep hot Ellenburger. in *Production and Operations Symposium*. 2007.
- [18] Bybee K. Acid fracturing a carbonate reservoir. *J Petrol Technol* 2004;56(07): 49–52.
- [19] Bartko KM, Nasr-El-Din HA, Rahim Z, Al-Muntasheri GA. Acid Fracturing of a Gas Carbonate Reservoir: The Impact of Acid Type and Lithology on Fracture Half Length and Width. in *SPE Annual Technical Conference and Exhibition*. 2003.
- [20] Aljawad MS, Aljulaib H, Mahmoud M, Desouky M. Integration of field, laboratory, and modeling aspects of acid fracturing: a comprehensive review. *J Petrol Sci Eng* 2019;181:106158.
- [21] Economides MJ, Nolte KG. *Reservoir stimulation*, Vol. 2. NJ: Prentice Hall Englewood Cliffs; 1989.
- [22] Aljawad MS, Schwalbert MP, Zhu D, Hill AD. Improving acid fracture design in dolomite formations utilizing a fully integrated acid fracture model. *J Petrol Sci Eng* 2020;184:106481.
- [23] Sheng JJ, Gomaa A, Soliman M. *Matrix Acidizing Characteristics in Shale Formations*, *Pet Environ Biotechnol*. Default Journal, 2014.



- [24] Fan L, Martin R, Thompson J, Atwood K, Robinson J, Lindsay G. An Integrated Approach for Understanding Oil and Gas Reserves Potential in Eagle Ford Shale Formation, in Canadian Unconventional Resources Conference. 2011. p. SPE-148751-MS.
- [25] 13503-5, I. *Petroleum and natural gas industries, Completion fluids and materials — Part 5: Procedures for measuring the long-term conductivity of proppants*, in 1st Edition. 2006, International Standard Organization (ISO): Geneva, Switzerland.
- [26] Ahmed T. *Reservoir engineering handbook*. 2018: Gulf professional publishing.
- [27] Hawkins MF. A note on the skin effect. *J Petrol Technol* 1956;8(12):65–6.
- [28] Kakkar P. *Experimental study of the effect of stress and fluid sensitivity on propped and un-propped fracture conductivity in preserved reservoir shale*. 2016.
- [29] Ghosh S, Rai CS, Sondergeld CH, Laese RE. *Experimental Investigation of Proppant Diagenesis*, in *SPE/CSUR Unconventional Resources Conference – Canada*. 2014. p. D011S003R007.
- [30] Pattamasinh P. *Fracturing Optimization Based on Dynamic Conductivity*. 2016.
- [31] Tripoppoom S, Xie J, Yong R, Wu J, Yu W, Sepehrmoori K, et al. Investigation of different production performances in shale gas wells using assisted history matching: hydraulic fractures and reservoir characterization from production data. *Fuel* 2020;267:117097.
- [32] Lund K, Fogler HS, McCune CC. Acidization—I. The dissolution of dolomite in hydrochloric acid. *Chem Eng Sci* 1973;28(3):691–IN1.
- [33] Lund K, Acidization—II, et al. The dissolution of calcite in hydrochloric acid. *Chem Eng Sci* 1975;30(8):825–35.
- [34] Farrokhrouz M, Taheri A, Keshavarz A. Numerical reactive flow transport simulation on core samples during acid fracturing in carbonaceous shale. *J Nat Gas Sci Eng* 2020;84:103615.
- [35] Farrokhrouz M, Taheri A, Iglauer S, Keshavarz A. Laboratorial and analytical study for prediction of porosity changes in carbonaceous shale coupling reactive flow and dissolution. *J Petrol Sci Eng* 2022;215:110670.
- [36] Han J, Wang JY. *Fracture conductivity decrease due to proppant deformation and crushing, a parametrical study*, in *SPE Eastern Regional Meeting*. 2014. OnePetro.
- [37] Barboza BR, Chen B, Li C. A review on proppant transport modelling. *J Petrol Sci Eng* 2021;204:108753.
- [38] Zoveidavianpoor M, Gharibi A. Characterization of agro-waste resources for potential use as proppant in hydraulic fracturing. *J Nat Gas Sci Eng* 2016;36: 679–91.
- [39] Li JH, Li B, Cheng QY, Gao Z. Characterization of the fracture compressibility and its permeability for shale under the effects of proppant embedment and compaction: a preliminary study. *Pet Sci* 2021.
- [40] Katende A, O'Connell L, Rich A, Rutqvist J, Radonjic M. A comprehensive review of proppant embedment in shale reservoirs: experimentation, modeling and future prospects. *J Nat Gas Sci Eng* 2021;95:104143.
- [41] Shi F. XFEM-based numerical modeling of well performance considering proppant transport, embedment, crushing and rock creep in shale gas reservoirs. *J Petrol Sci Eng* 2021;201:108523.
- [42] Ahamed MAA, Perera MSA, Elsworth D, Ranjith PG, Matthai SKM, Dong-yin L. *Effective application of proppants during the hydraulic fracturing of coal seam gas reservoirs: implications from laboratory testings of propped and unpropped coal fractures*. *Fuel* 2021;304:121394.
- [43] Zhang CP, et al. Combined micro-proppant and supercritical carbon dioxide (SC-CO<sub>2</sub>) fracturing in shale gas reservoirs: a review. *Fuel* 2021;305:121431.
- [44] Fredd CN, McConnell SB, Boney CL, England KW. Experimental study of fracture conductivity for water-fracturing and conventional fracturing applications. *SPE J* 2001;6(03):288–98.
- [45] Awoleke O, Romero J, Zhu D, Hill AD. Experimental Investigation of Propped Fracture Conductivity in Tight Gas Reservoirs Using Factorial Design. in *SPE Hydraulic Fracturing Technology Conference*. 2012.
- [46] Barree RD, Miskimins JL, Conway MW, Duenkel R. *Generic Correlations for Proppant Pack Conductivity*. in *SPE Hydraulic Fracturing Technology Conference*. 2016.
- [47] Wang J, Elsworth D. Role of proppant distribution on the evolution of hydraulic fracture conductivity. *J Petrol Sci Eng* 2018;166:249–62.
- [48] Hou L, Elsworth D, Geng X. Swelling and embedment induced by sub- and supercritical-CO<sub>2</sub> on the permeability of propped fractures in shale. *Int J Coal Geol* 2020; 225:103496.
- [49] Bandara KMAS, Ranjith PG, Rathnaweera TD. Laboratory-scale study on proppant behaviour in unconventional oil and gas reservoir formations. *J Nat Gas Sci Eng* 2020;78:103329.
- [50] Wang J, Elsworth D, Ma T. Conductivity Evolution of Proppant-Filled Hydraulic Fractures, in 52nd U.S. Rock Mechanics/Geomechanics Symposium. 2018. p. ARMA-2018-111.
- [51] Civan F. Chapter 21 - Determination of Formation- and Pseudodamage from Well Performance—Identification, Characterization, Evaluation, and Abatement. In: Civan F, editor. *Reservoir Formation Damage (Third Edition)*. Boston: Gulf Professional Publishing; 2016. p. 717–62.
- [52] Patel MC, Singh A. Near Wellbore Damage and Types of Skin Depending on Mechanism of Damage, in *SPE International Conference and Exhibition on Formation Damage Control*. 2016. p. D012S007R008.
- [53] Van Golf-Racht TD. *Fundamentals of Fractured Reservoir Engineering*, in *Developments in Petroleum Science*. 1982, Elsevier. p. iv.
- [54] Farrokhrouz M, Taheri A, Iglauer S, Keshavarz A. Exact analytical solutions of countercurrent imbibition with both capillary and gravity effects. *Energy Fuels* 2022;36(3):1457–69.
- [55] Farrokhrouz M, Taheri A, Iglauer S, Keshavarz A. Analytical exact solution for co-current spontaneous imbibition in porous media considering early- and late-time effects. *Energy Fuels* 2021;35(21):17499–511.
- [56] Bandara KMAS, Ranjith PG, Haque A, Wanniarachchi WAM, Zheng W, Rathnaweera TD. An experimental investigation of the effect of long-term, time-dependent proppant embedment on fracture permeability and fracture aperture reduction. *Int J Rock Mech Min Sci* 2021;144:104813.
- [57] Mittal A, Rai CS, Sondergeld CH. Proppant-conductivity testing under simulated reservoir conditions: impact of crushing, embedment, and diagenesis on long-term production in shales. *SPE J* 2018;23(04):1304–15.
- [58] Lei G, Liao Q, Patil S. A new mechanistic model for conductivity of hydraulic fractures with proppants embedment and compaction. *J Hydrol* 2021;601:126606.
- [59] Cramer DD. Fracture Skin: A Primary Cause of Stimulation Ineffectiveness in Gas Wells, in *SPE Annual Technical Conference and Exhibition*. 2005. p. SPE-96869-MS.



## **Chapter 7: Conclusion and Recommendations**

The following general conclusion can be drawn from this PhD thesis:

For the paper in **Chapter 2**, a numerical simulation model was developed and validated by experimental acidizing results through one pure carbonate fractured sample. Then, the model was reconstructed for different carbonaceous shale samples and simulation study performed. There is an optimum acid injection rate at which the required breakthrough pore volume is minimized inside the intact core sample while for fractured sample, this optimum injection rate is much lower at different carbonaceous shale samples (i.e., Eagle Ford, Cooper Basin, Sargelu, Lower Bakken and McArthur shale samples). By increasing acid concentration, the required breakthrough pore volume is reduced to a certain value (40% HCl) and then higher acid concentration has a reverse effect on acidizing efficiency as rate of product transfer controls it. Within the fractured sample, the simulation showed that at lower acid concentrations (30% HCl), breakthrough pore volume is minimum and higher acid concentrations do not have a negative or positive effect on acidizing efficiency. The effect of temperature is also totally negligible.

In **Chapter 3 and 4**, two analytical models were established for non-reacting fluid saturation movement in porous medium, and exact functional forms were suggested for co-current and counter-current movement in a porous medium. The models were also validated with experimental results and showed the functional form's accurate capability to predict saturation inside the medium. Using proposed analytical solutions, the front of the fluid within the medium can be determined precisely as a function of time and space.

The whole concept of **Chapter 5** can be divided into two disciplines. The acid reaction with the rock surface can be controlled with different parameters. Time is the most important of all. Low stagnant acid concentration (in the range of 1-5%

HCl) in long-term contact with the surface of the Eagle Ford can even induce some minor fractures and veins at a microscopic scale. The proposed mathematical model used to predict porosity alteration due to reaction with acid. The model was validated with experimental results at different acid concentrations, different brine types, and within a range of temperature changes.

**Chapter 6** is about the other effect of time on acidizing process. High concentration acid (5-15% HCl) front was injected during experimental works in this section. The efficiency of acidizing, is limited by the reaction rate or transfer rate of the products. For the propped medium, apart from acid concentration, the concentration of the proppants or the sizes of the proppants can also affect the efficiency of the acidizing operation. For the Eagle Ford shale sample in this study, the optimum condition is 5-10% HCl acid, 600-710  $\mu\text{m}$  of proppant size, 0.3  $\text{lb}/\text{ft}^2$  of proppant concentration (close to mono-layer condition), and 8  $\text{ml}/\text{min}$  injection rate of the acid. These are the optimum conditions at laboratory scale and can be modified for the field scale.

Altogether, within this study the following bullet points were covered:

- ✓ Geochemical study of the acid effect on shale rock types;
- ✓ Modelling and simulation of acidizing through the fractures using commercial software after validating the model with experimental data;
- ✓ Mathematical modelling of saturation front movement through the porous medium and introducing exact solution;
- ✓ Preparation and conducting experimental setup for investigation of long-term acid effect on shale rock types;
- ✓ Proposing new mathematical model for acid diffusion inside the porous medium and validating with experimental results.



- ✓ Suggestion of methodology for production enhancement through propped fractures and optimize the field conditions based on that.

For future works, the following goals can be examined:

- Performing experimental tests on different carbonaceous shale samples other than Eagle Ford;
- Proposing mathematical model for acid movement through the porous medium where both convection and diffusion terms are present;
- Investigation of acid application inside non-propped fractured through the standard conductivity setup;
- Long-term effect of acid on propped fractured sample to check the effect of proppant on recovery;
- Utilization of graded proppant technology to explore the effect of diffusion on oil recovery from unconventional reservoirs;